Ceramic capillary membranes with tailored pore sizes and functionalizations for virus retention

Vom Fachbereich Produktionstechnik

der

UNIVERSITÄT BREMEN

zur Erlangung des Grades

Doktor-Ingenieur

genehmigte

Dissertation

von

M. Sc. Julia Bartels

Gutachter:

Prof. Dr. Kurosch Rezwan

Prof. Dr. Andreas Dotzauer

Tag der mündlichen Prüfung: 19. Februar 2020

Für meine Familie.

Danksagung

Die vorliegende Arbeit entstand während meiner Tätigkeit als wissenschaftliche Mitarbeiterin im Fachgebiet Keramische Werkstoffe und Bauteile (Advanced Ceramics) des Fachbereiches Produktionstechnik der Universität Bremen.

Zu allererst möchte ich Herrn Prof. Dr. Kurosch Rezwan danken, nicht nur für die Möglichkeit diese Arbeit anzufertigen, sondern auch für die wissenschaftliche Weiterbildung, die konstruktive und motivierende Betreuung und die Begutachtung dieser Dissertation. Desweiteren danke ich Prof. Dr. Andreas Dotzauer für das Interesse an meiner Arbeit und die damit verbundene Tätigkeit als Zweitgutachter. Mein besonders herzlicher Dank gilt Dr. rer. nat. Stephen Kroll und Dr. rer. nat. Michael Maas, die mir mit stetiger Hilfsbereitschaft, inspirierenden wissenschaftlichen Diskussionen und wertvollen Hinweisen während der Zeit meiner Arbeit zur Seite standen.

Danken möchte ich zudem meinen Kolleginnen und Kollegen im Fachgebiet ohne die, diese Zeit sicher nicht so erfolgreich verlaufen wäre. Mir werden die angenehme Arbeitsatmosphäre, die umfangreiche Unterstützung sowie die hilfreichen wissenschaftlichen und nicht-wissenschaftlichen Gespräche immer in Erinnerung bleiben.

Weiterhin möchte ich den Studentinnen und Studenten danken, die während meiner Promotionszeit ihre Projekt-, Bachelor- oder Master-Arbeiten unter meiner Leitung mit Fleiß und Engagement durchgeführt haben.

Abschließend danke ich meiner Familie herzlichst dafür, dass sie immer da waren und immer da sein werden, wenn ich sie brauche.

Danke!

Julia

Zusammenfassung

Das Ziel dieser Arbeit ist die Entwicklung eines vielseitigen und effektiven Virusfiltrationssystems auf Keramikbasis, das sowohl einen hohe Wasserpermeatfluss als auch eine hohe Rückhaltekapazität für eine Vielzahl von Viren aufweist. Zu diesem Zweck wird ein Extrusionsprozess auf Basis von Yttrium-stabilisierten Zirkoniumoxid (YSZ) Pulvern mit Partikeldurchmessern von 30 nm, 40 nm bzw. 90 nm entwickelt, um tubulare Membranen herzustellen. Nach dem Sintern bei 1050 °C für 2 h wird eine defektfreie, homogene Struktur mit einer offenen Porosität von ca. 50 % erreicht. Es werden durchschnittliche Membranporengrößen im Bereich von 24 nm für Kapillaren basierend auf dem YSZ-30 Pulver bis hin zu 146 nm für Kapillaren basierend auf dem YSZ-90 Pulver erhalten. Eine hohe Membranporengröße führt zu einem verminderten Virenrückhaltevermögen in Kombination mit einem erhöhten Wasserpermeatfluss. Kapillaren basierend auf dem YSZ-40nm Pulver sind vielversprechend, da sie das von der Weltgesundheitsorganisation geforderte Virenfilterkriterium von 4 logarithmischen Reduktionswerten (LRVs), in Kombination mit einem relativ hohen Membranfluss von ~30 L/(m^{2}hbar), erfüllen. YSZ-90nm Kapillaren erfüllen aufgrund ihrer durchschnittlichen Porengröße von ~150 nm nicht das geforderte Virenfilterkriterium. Nichtsdestotrotz besitzen sie einen Wasserpermeatflussfluss von ~150 L/(m^{2}hbar) und können somit für Anwendungen, bei denen hohen Flussraten gefordert sind, verwendet werden, wenn eine geeignete Adsorptionskapazität für Viren durch eine Membranfunktionalisierung bereitgestellt wird. Aus diesem Grund wird eine chemische Funktionalisierungsstrategie mit Aminosilanen bestehend aus einer, zwei oder drei Aminogruppen (Aminopropyltriethoxysilan (APTES), N-(2-Aminoethyl)-3-Aminopropyltriethoxysilan (AE-APTES) und N-(3-Trimethoxysilylpropyl)diethylenetriamine (TPDA)) pro Silanmolekül angewendet. Das Zeta-Potential der Membranoberfläche wird von negativ in positiv geändert. Dadurch wird das Virenrückhaltevermögen für das Modellvirus MS2 (Durchmesser = 25 nm, isoelektrischer Punkt (IEP) = 3,9) für neutrale Viren-Ausgangslösungen (Feed-Lösungen) basierend auf einwertigen und zweiwertigen Salzen (NaCl, MgCl$_2$) signifikant von einem LRV von <0,3 für nicht-funktionalisierte Membranen zu einem LRV von 9,6 ± 0,3 für TPDA funktionalisierte Membranen, aufgrund von elektrostatischen Wechselwirkungen, erhöht. Ein geringer LRV von 6,4 wird für Feedlösungen beobachtet, die nur auf einwertigen Ionen (NaCl) basieren. Daher wird die TPDA-funktionalisierte Oberfläche auf der atomistischen Skala mit einer Molekular-Dynamiksimulation in Gegenwart von Na$^+$- oder Mg^{2+}-Ionen betrachtet. Diese zeigt, dass die Mg^{2+}-Ionen an der Membranoberfläche adsorbiert bleiben, während die Na$^+$-Ionen nur schwach mit der Oberfläche in Verbindung stehen. Aufgrund der adsorbierten Mg^{2+}-Ionen liegen die TPDA-Moleküle in einer eher aufrechten Ausrichtung an der Oberfläche vor, wohingegen die TPDA-Moleküle in Gegenwart von Na$^+$-Ionen eher geneigt sind. Dieses führt zu einer besseren Zugänglichkeit der TPDA-Moleküle für Viren und damit zu einem besseren Virusrückhaltevermögen bei der Verwendung von Feed-Lösungen basierend auf Mg^{2+}-Ionen. Die Rückhaltekapazität für das Modellvirus PhiX174 (Durchmesser = 26 nm, IEP = 6,2) kann durch TPDA-funktionalisierte Membranen aufgrund der Abstoßung zwischen den positiv geladenen Bakteriophagen und den positiv geladenen Membranen bei neutralem pH nicht erhöht werden. Aus diesem Grund wird eine hydrophobe Funktionalisierung der keramischen Membranen mit Silanen bestehend aus Kohlenstoffketten durchgeführt. Bei Kapillaren, die mit C8-Ketten (N-octyltriethoxysilan, OTS) funktionalisiert sind, steigt das Virenrückhaltevermögen am stärksten an und zeigt für beide Viren (MS2 und PhiX174) LRVs von ~9 mit Permeatdurchsätzen von bis zu ~400 L/(m²h), selbst bei der Verwendung unterschiedlicher Feed-Bedingungen. Dementsprechend sind diese hydrophoben, keramischen Membranen eine vielseitige Alternative zu herkömmlichen polymeren Membranen für Virenfiltrationsanwendungen.

Abstract

The aim of this work is the design of a versatile and effective virus filtration system based on ceramic which offers both high membrane throughput rates and high retention capacities for a wide variety of viruses. For this purpose, an extrusion process based on yttria stabilized zirconia (YSZ) powders with particle sizes of 30 nm, 40 nm or 90 nm is implemented to shape tubular membranes. After sintering at 1050 °C for 2 h a defect-free homogenous structure with open porosities of around 50 % is achieved. By increasing the initial YSZ particle size, increased average membrane pore sizes ranging from 24 nm to 146 nm are obtained. A high membrane pore size leads to reduced virus retention capacities in combination with increased water permeate fluxes. Capillaries made of YSZ-40nm are promising candidates as they fulfill the virus filter criterion of 4 log reduction values (LRVs) required by the World Health Organization in combination with a membrane flux of ~30 L/(m^{2}hbar). Capillaries made of YSZ-90nm do not fulfill the virus filter criterion due to their average pore size of ~150 nm. However, they show a membrane flux of ~150 L/(m^{2}hbar) and can therefore be used for high flux filtration applications, if an adequate adsorption capacity for viruses by a membrane surface functionalization is provided. Therefore, a straightforward chemical functionalization strategy using aminosilanes with one, two or three amino groups per silane molecule, namely 3-aminopropyltriethoxysilane (APTES), N-(2-aminoethyl)-3-aminopropyltriethoxysilane (AE-APTES) and n-(3-trimethoxysilylpropyl)diethylenetriamine (TPDA), is used. The zeta-potential of the membrane surface is converted from negative to positive. Therefore, the virus retention capacity for the model virus MS2 (diameter = 25 nm, isoelectric point (IEP) = 3.9) is significantly increased for neutral feed solutions based on monovalent and divalent salts (NaCl, MgCl$_2$) from a LRV of <0.3 for non-functionalized membranes to LRVs of up to 9.6 ± 0.3 for the TPDA functionalized capillaries due to electrostatic interactions. A lower LRV of 6.4 is observed for feed solutions which are based on only monovalent ions (NaCl). Therefore, the TPDA functionalized surface is simulated at the atomistic scale using explicit-solvent molecular dynamics in the presence of either Na$^+$ or Mg^{2+} ions. This shows that the binding free energy reveals that the Mg^{2+} ions remain adsorbed to the membrane surface, whereas Na$^+$ ions form only a weakly bound with the surface. Due to the adsorbed Mg^{2+} ions an upright orientation of the TPDA molecules and opposed to that a more tilted orientation in the presence of Na$^+$ ions is found. Therefore, a better accessibility of the TPDA molecules for the viruses and thus a better virus retention capacity is found when using feed solutions based on Mg^{2+} ions. The retention capacity for the model virus PhiX174 (diameter = 26 nm, IEP = 6.2) viruses cannot be increased by TPDA functionalized membranes due to the repulsion between the positively charged bacteriophages and the positively charged pore wall surfaces at a neutral pH. Therefore, a hydrophobic functionalization of the ceramic membranes with silanes offering carbon chains is performed. Virus retention increases most strongly for capillaries functionalized with C8-chains (n-octyltriethoxysilane, OTS), showing LRVs of ~9 for both viruses (MS2 and PhiX174) with throughput rates of up to ~400 L/(m²h) even under varying feed conditions. Accordingly, such hydrophobic ceramic membranes are a versatile alternative to conventional polymeric membranes for virus retention applications.

x

Contents

4. Production of Ceramic Membranes with Different Pore Size for Virus Retention

5. Amino-Functionalized Ceramic Capillary Membranes for Controlled Virus Retention

6. Effect of Cations on the MS2 Retention Capacity of Amino-Functionalized Ceramic Filters

7. Hydrophobic Ceramic Capillary Membranes for Versatile Virus Filtration

8. Conclusions

9. Outlook

A Appendix

Curriculum Vitae

List of Publications (peer-reviewed)

Author Contributions for the Publications Presented in this Work

List of Oral and Poster Presentations

List of Student Projects

Nomenclature

°C	grad Celsius
AE-APTES	n-2-aminoethyl-3-aminopropyltriethoxysilane
AH-AMTES	n-(6-aminohexyl)-aminomethyltriethoxysilane
APTES	3-aminopropyltriethoxysilane
APTMS	3-aminopropyltrimethoxysilane
DBP	disinfection by-product
DLVO	Derjaguin, Landau, Verwey, Overbeek Theory
DNA	deoxyribonucleic acid
ds	double stranded
DSMZ	german collection of microorganisms and cell cultures GmbH
PVA	polyvinyl alcohol
E.Coli	*Escherichia coli*
EMEA	european Medicines Agency
FDA	United States food and drug administration
Fe	iron
FSZ	fully stabilized zirconia
HIV	human immunodeficiency virus
IEP	isoelectric point
ISO	international organization for standardization
MF	microfiltration
NF	nanofiltration
POU	point-of-use
PSZ	partially stabilized zirconia
PV	pervaporation
RNA	ribonucleic acid
RO	reverse osmosis
RT	room temperature
SEM	scanning electron microscopy
ss	single stranded
SSA	specific surface area
TEM	transmission electron microscopy
TES	triethoxysilane
TGA	thermogravimetric analyses
TMS	trimethoxysilane
TPDA	n-(3-trimethoxysylilpropyl)diethylenetriamine
TSA	tryptic soy agar
TSB	tryptic soy broth
UF	ultrafiltration
USEPA	United States environmental protection agency
WHO	world health organization
XPS	x-ray photoelectron spectroscopy
YSZ	yttrium stabilized zirconia
ZrO_2	zirconia dioxide

1. Introduction and Aim of Work

1.1 General Introduction

The three main water contaminations are of chemical (e.g. heavy metals, organic and inorganic species), physical (e.g. color) and biological (e.g. bacteria and viruses) origin.[1]

Especially viruses are challenging to remove from water[2, 3] and food products[4]. Based on the guidelines from World Health Organization (WHO) and United States Environmental Protection Agency (USEPA) a log-reduction value (LRV) of at least 4 (99.99 percent removal) is required to provide safe drinking water. In biopharmacy, virus filtration is mainly used for virus clearance of plasma products and monoclonal antibodies and the purification of viral vectors and vaccines[5-7].

Conventional virus inactivation methods are heat treatment techniques, chemical treatments like the usage of free chlorine or chlorine dioxide, and the application of ozone or UV-irradiation. All these methods inactivate viruses, but have disadvantages, as high costs, the potential production of toxic disinfection by-products (DBPs) and the requirement of trained personnel.[8-12] An alternative to the physical and chemical inactivation methods is filtration. Filtration is based on size exclusion effects, where contaminants, which are larger than the membrane pore size can be retained.[13, 14] Polymeric membranes combine high water permeate fluxes and the required high virus retention level.[15, 16] In contrast to polymeric membranes, ceramic membranes offer high mechanical stabilities, therefore they can withstand high pressure loads and can consequently endure high water permeate flux rates. Due to their excellent chemical and thermal stabilities, ceramic membranes can easily be cleaned by backflushing, thermal, acidic or basic treatment without affecting the pore morphology.[17] In addition, ceramic membranes do not show any swelling behavior during water filtration maintaining their structural compactness, but are brittle and have a higher material weight.[18] The production costs of ceramic membranes, which are 3 to 5 times higher compared to polymeric membranes, can be compensated by their longer lifetime of up to ten years due to the cleaning possibilities.[19]

Viruses, which are pathogens with diameters between 20 and 300 nm[20] can be removed by ultrafiltration using pore sizes in the range between 2 and 100 nm.[21] The bacteriophages MS2 and PhiX174 are two of the most well studied viruses and are often used as model viruses in water disinfection studies, as they are considered as relevant non-pathogenic surrogates for pathogenic viruses in aqueous media.[13, 22-24] MS2 is a single-stranded RNA virus which belongs to the family *Leviviridae* showing a diameter of 25 - 27 nm[25] and an isoelectric point (IEP) of 3.5 ± 0.6[26] and PhiX174 is a single-stranded DNA virus which belongs to the family *Microviridae* showing a diameter of 26 - 32 nm[13] and an IEP of 6.2 ± 1.6[26]. Both bacteriophages are mainly hydrophilic with hydrophobic residues on the virus surface of around 10 %.[27-30]

Membranes with pores in the mesoporous and lower macroporous range lead to low water permeate fluxes.[22, 31, 32] Virus filters with pore sizes over 100 nm can be used for high flux filtration applications, if an adequate adsorption capacity is provided next to the size exclusion. But due to the structural diversity of the wide variety of viruses, virus-material interactions are complex and difficult to predict.[33] Electrostatic interactions were demonstrated to play the major role in virus-material interactions in the absence of a direct size exclusion effect.[6] As most viruses have IEPs between 3.5 and 7.0[26] and contaminated water samples usually have a neutral pH, an ideal virus adsorbent is positively charged (IEP $\geq$ 8) at acidic and neutral pH conditions. From a ceramics processing standpoint, positive membrane surfaces can be achieved with metal oxyhydroxides (e.g. $Y(OH)_x$, $Zr(OH)_x$ and $Mg(OH)_2$)[24, 34, 35], iron oxide[36] or zerovalent Fe[37] for ceramic materials by coating or doping. A positive surface charge can also be provided by chemical surface functionalization Silanization can be performed in aqueous[38, 39] or

organic solvents[40, 41] or in vapor phase[42, 43] using moderate temperatures. Silanes can be used for chemical functionalization approaches as there is a broad spectrum of silanes showing different functional groups (e.g. amino-, carboxyl- or alkyl-groups) and spacer length [44]. Silanes can be applied on almost any type of ceramic material and support and can therefore widely be used for tailored chemical surface functionalities.[44] Focusing on virus adsorption mechanisms especially amino silanes are successfully applied as they provide a positive surface charge for the adsorption of negatively charged viruses at neutral and acidic pH, respectively. As shown by several authors high virus adsorption capacities are reached by wet chemical functionalization of silica and alumina particles with aminosilanes [30, 45-47].

Electrostatic double layer forces between the membrane surface and the virus are described by the well-known DLVO theory, named after Derjaguin, Landau, Verwey and Overbeek.[48-53] But in many cases very little is known about the precise chemical environment of the functional groups on the silanized material surface and the interactions of this material surfaces with viruses in complex buffer systems. It was shown by several studies, that the addition of salts to buffer systems enhance the virus adsorption to membranes, where the presence of trivalent cations (Al^{3+}) promotes larger virus adsorption compared to divalent (Mg^{2+}) and monovalent cations (Na^+).[36-38] But generalization of this finding was disputed by Lukasik et al.[39], who showed that the effects of salt ions on virus adsorption depend on the used filter type and that under different conditions, $MgCl_2$ promoted, inhibited or had no effect on virus adsorption.

The major disadvantage of adsorption by electrostatic interaction is that it only works for viruses that are oppositely charged to the membrane surface. Beyond the classic DLVO forces, hydrophobic interactions can significantly influence the adsorption of viruses to membranes. Hydrophobic interactions can influence the adsorption even of predominantly hydrophilic viruses[33, 54, 55], as hydrophobic surfaces have a preference to associate with each other, which is caused by the high free energy of the interfacial solute layer of polar water molecules which decreases with a reduction of the water-exposed surface area.[56] Various studies reported hydrophobic interactions in virus filtration experiments especially with regard to the removal of viruses by soil passage.[33, 55] Furthermore, the significance of hydrophobic interactions for the retention of the bacteriophage MS2 were shown for hydrophobic polymer membranes, as they were a better barrier for MS2 than hydrophilic polymer membranes with the same pore size.[28, 57, 58]

1.2 Aim of Work

The major challenge of this work is the design of a versatile and effective virus filtration system based on ceramics which offers both high membrane throughput rates and high retention capacities for a wide variety of viruses. Therefore, membranes with a tailored pore size in the upper mesoporous or lower macroporous region in combination with a functionalization which adsorb viruses to the membrane surface are needed.

The importance of porous ceramic membranes is increasing in water purification, due to their excellent chemical, thermal and mechanical stabilities. For the fabrication of ceramic membranes monomodal and narrow pore size distributions in the upper meso- or lower macroporous range are required offering a reliable cut-off for viruses in combination with high open porosities and consequently high water permeate fluxes. Therefore, the preparation of tubular yttria-stabilized zirconia (YSZ) membranes by extrusion is investigated using different sized initial YSZ powders. YSZ was chosen because of its high fracture toughness and strength compared to other ceramic oxide materials (e.g. alumina) which guarantees a high mechanical stability even at high open porosities.[59] The effect of the different sized initial YSZ powders on the membrane microstructure (pore size, open porosity, specific surface area), the mechanical stability (bending strength), the water permeate flux and the virus retention capacity were analyzed in detail.

Capillaries produced with 90 nm particles (YSZ-90nm capillaries), which do not fulfill the virus filter criterion of LRV>4 due to their average pore size of 150 nm can be advantageously used for high flux filtration applications if an ideal adsorbent for viruses is applied. As most viruses have IEPs in the acidic and neutral range[26] and contaminated water samples are pH neutral, an ideal virus adsorbent is positively charged at acidic and neutral pH conditions. In this study, an adequate adsorption capacity for viruses by a membrane surface functionalization to increase the virus retention behavior by electrostatic interactions of surface and virus is examined. Therefore, a straightforward wet chemical functionalization strategy is presented where the sintered YSZ-90nm capillary membranes are activated by acidic hydroxylation with piranha solution and are functionalized with three different aminosilanes with one, two or rather three amino groups per silane molecule. 3-aminopropyltriethoxysilane (APTES), N-(2-aminoethyl)-3-aminopropyltriethoxysilane (AE-APTES) and N-(3-trimethoxysilylpropyl)di ethylenetriamine (TPDA) are used as promising candidates to generate positively charged surfaces which are able to interact with negatively charged viruses. The aminosilanization effects on the membrane microstructure, the mechanical stability, the membrane flux and the virus retention capacity are investigated in detail.

Very little is known about the precise chemical environment of the functional groups on the silanized material surface and the interactions of this material surfaces with viruses in complex buffer systems. Therefore, the virus retention behavior of YSZ-90nm capillary membranes functionalized with TPDA in the presence of mono- (Na^+) and divalent salt ions (Mg^{2+}) was investigated. Therefore, advanced-sampling molecular dynamics simulations (MD) to analyze the effects on the atomistic scale were performed and the adsorption strengths and distributions of the ions at the surface were investigated. In particular, the orientation and accessibility of the TPDA molecules on the capillary surface dependent on the used ion type (Na^+ or Mg^{2+}) is

investigated.

The major disadvantage of adsorption by electrostatic interaction with TPDA molecules is that the viruses have to be the opposite charge of the membrane surface. Therefore, another approach was investigated in this study working on hydrophobic interactions between viruses and membrane surfaces. The association of hydrophobic surfaces is caused by the high free energy of the interfacial solute layer of polar water molecules which decreases with a reduction of the water-exposed surface area.[56]

The well established YSZ-90nm capillary membranes were silanized with n-hexyltriethoxysilane (HTS) or n-octyltriethoxysilane (OTS) to generate hydrophobic surfaces which can interact with viruses. Next to the microstructure analysis, the capillaries were investigated due to their hydrophobic behavior and their water permeate flux. The capillaries were challenged at throughput rates up to 400 L/(m²hbar) under varying feed conditions to investigate the virus retention behavior of the bacteriophages MS2 and PhiX174.

References

1. A. Gadgil. "Drinking water in developing countries". *Annual Review of Energy and the Environment* 1998, 23, 253-286.
2. J. P. S. Cabral. "Water Microbiology: Bacterial Pathogens and Water". *International Journal of Environmental Research and Public Health*, 2010, 7, 3657-3703.
3. P. Reeve, et al. "Virus removal of new and aged UF membranes at full-scale in a wastewater reclamation plant". *Environmental Science: Water Research & Technology*, 2016, 2, 1014-1021.
4. M. Koopmans and E. Duizer. "Foodborne viruses: an emerging problem". *Int J Food Microbiol*, 2004, 90, 23-41.
5. P. Nestola, et al. "Improved virus purification processes for vaccines and gene therapy". *Biotechnology and Bioengineering*, 2015, 112, 843-857.
6. J. A. Redman, et al. "Filtration of Recombinant Norwalk Virus Particles and Bacteriophage MS2 in Quartz Sand: Importance of Electrostatic Interactions". *Environmental Science & Technology*, 1997,

31, 3378-3383.

7. C. Charcosset, "Membrane Processes in Biotechnology and Pharmaceutics", Elsevier, 2012.

8. T. Clasen, et al. "Cost-effectiveness of water quality interventions for preventing diarrhoeal disease in developing countries". *Journal of Water and Health*, 2007, 599-608.

9. M. A. Shannon, et al. "Science and technology for water purification in the coming decades". *Nature*, 2008, 452, 301-310.

10. H. Junli, et al. "Disinfection effect of chlorine dioxide on viruses, algae and animal planktons in water". *Water Research*, 1997, 31, 455-460.

11. W. H. Organization, ed. M. D. Sobsey, Geneva, 2002.

12. G. Ko, et al. "UV inactivation of adenovirus type 41 measured by cell culture mRNA RT-PCR". *Water Research*, 2005, 39, 3643-3649.

13. A. Duek, et al. "New and conventional pore size tests in virus-removing membranes". *Water Research*, 2012, 46, 2505-2514.

14. I. Voigt. "Nanofiltration with ceramic membranes". *Chemie Ingenieur Technik*, 2005, 77, 559-564.

15. A. M. ElHadidy, et al. "An evaluation of virus removal mechanisms by ultrafiltration membranes using MS2 and φX174 bacteriophage". *Separation and Purification Technology*, 2013, 120, 215-223.

16. J. Langlet, et al. "Efficiency of MS2 phage and Qβ phage removal by membrane filtration in water treatment: Applicability of real-time RT-PCR method". *Journal of Membrane Science*, 2009, 326, 111-116.

17. J. Finley. "Ceramic membranes: a robust filtration alternative". *Filtration & Separation*, 2005, 42, 34-37.

18. C. B. Carter and M. G. Norton, "Ceramic Materials, Science and Engineering", New York, 2007.

19. E. P. Garmash, et al. "Ceramic membranes for ultra- and microfiltration (Review)". *Glass and Ceramics*, 1995, 52, 150-152.

20. R. D. Arnone and J. P. Walling. "Waterborne pathogens in urban watersheds". *Journal of Water and Health*, 2007, 05.1, 149-162.

21. S. S. Madaeni, et al. "Virus removal from water and wastewater using membranes". *Journal of Membrane Science*, 1995, 102, 65-75.

22. S. Kroll, et al. "High virus retention mediated by zirconia microtubes with tailored porosity". *Journal of the European Ceramic Society*, 2012, 32, 4111-4120.

23. B. Michen, Dr.-Ing. doctor thesis, Technische Universität Bergakademie Freiberg, 2010.

24. M. Wegmann, et al. "Nanostructured surface modification of microporous ceramics for efficient virus filtration". *Journal of the European Ceramic Society*, 2008, 28, 1603-1612.

25. L. Gutierrez, et al. "Adsorption of rotavirus and bacteriophage MS2 using glass fiber coated with hematite nanoparticles". *Water Research*, 2009, 43, 5198-5208.

26. B. Michen and T. Graule. "Isoelectric points of viruses". *Journal of Applied Microbiology*, 2010, 109, 388-397.

27. R. Attinti, et al. "Virus' (MS2, φX174, and Aichi) Attachment on Sand Measured by Atomic Force Microscopy and Their Transport through Sand Columns". *Environmental Science & Technology*, 2010, 44, 2426-2432.

28. C. D. Lytle and L. B. Routson. "Minimized virus binding for tests of barrier materials". *Applied and Environmental Microbiology*, 1995, 61, 643-649.

29. R. M. Chaudhry, et al. "Impact of virus surface characteristics on removal mechanisms within membrane bioreactors". *Water Research*, 2015, 84, 144-152.

30. F. Meder, et al. "The role of surface functionalization of colloidal alumina particles on their controlled interactions with viruses". *Biomaterials*, 2013, 34, 4203-4213.

31. S. S. Madaeni. "The application of membrane technology for water disinfection". *Water Research*, 1999, 33, 301-308.

32. R. Aronino, et al. "Removal of viruses from surface water and secondary effluents by sand filtration". *Water Research*, 2009, 43, 87-96.

33. J. F. Schijven and S. M. Hassanizadeh. "Removal of Viruses by Soil Passage: Overview of Modeling, Processes, and Parameters". *Crit Rev Env Sci Tec*, 2000, 30, 49-127.

34. B. Michen, et al. "Improved Virus Removal in Ceramic Depth Filters Modified with MgO". *Environmental Science & Technology*, 2013, 47, 1526-1533.

35. M. Wegmann, et al. "Modification of ceramic microfilters with colloidal zirconia to promote the adsorption of viruses from water". *Water Research*, 2008, 42, 1726-1734.

36. Y. You, et al. "Removal and Inactivation of Waterborne Viruses Using Zerovalent Iron". *Environmental Science & Technology*, 2005, 39, 9263-9269.

37. C. Shi, et al. "Removal of viruses and bacteriophages from drinking water using zero-valent iron". *Separation and Purification Technology*, 2012, 84, 72-78.

38. S. Kroll, et al. "Highly Efficient Enzyme-Functionalized Porous Zirconia Microtubes for Bacteria Filtration". *Environmental Science & Technology*, 2012, 46, 8739-8747.

39. F. Meder, et al. "Protein adsorption on colloidal alumina particles functionalized with amino, carboxyl, sulfonate and phosphate groups". *Acta Biomaterialia*, 2012, 8, 1221-1229.

40. H. J. Kim, et al. "Enhancement of mechanical properties of aluminium/epoxy composites with silane functionalization of aluminium powder". *Composites Part B: Engineering*, 2012, 43, 1743-1748.

41. M. Moritz and M. Łaniecki. "SBA-15 mesoporous material modified with APTES as the carrier for 2-(3-benzoylphenyl)propionic acid". *Applied Surface Science*, 2012, 258, 7523-7529.

42. H. Weetall. "Preparation of immobilized proteins covalently coupled through silane coupling agents to inorganic supports". *Applied Biochemistry and Biotechnology*, 1993, 41, 157-188.

43. S. Fiorilli, et al. "Vapor-phase self-assembled monolayers of aminosilane on plasma-activated silicon substrates". *Journal of Colloid and Interface Science*, 2008, 321, 235-241.

44. L. Treccani, et al. "Review: Functionalized ceramics for biomedical, biotechnological and environmental applications". *Acta Biomaterialia*, 2013, 9, 7115-7150.

45. R. Cademartiri, et al. "Immobilization of bacteriophages on modified silica particles". *Biomaterials*, 2010, 31, 1904-1910.

46. Z. Chen, et al. "Capture and release of viruses using amino-functionalized silica particles". *Anal Chim Acta*, 2006, 569, 76-82.

47. K. S. Zerda, et al. "Adsorption of viruses to charge-modified silica". *Applied and Environmental Microbiology*, 1985, 49, 91-95.

48. C. P. Gerba. "Applied and Theoretical Aspects of Virus Adsorption to Surfaces". *Advances in Applied Microbiology*, 1984, 30, 133-168.

49. H. Cao, et al. "Salinity and Soluble Organic Matter on Virus Sorption in Sand and Soil Columns". *Ground Water*, 2010, 48, 42-52.

50. S. K. Dishari, et al. "Effects of solution conditions on virus retention by the Viresolve® NFP filter". *Biotechnology Progress*, 2015, 31, 1280-1286.

51. I. C. Bourg and G. Sposito. "Molecular dynamics simulations of the electrical double layer on smectite surfaces contacting concentrated mixed electrolyte (NaCl–CaCl2) solutions". *Journal of Colloid and Interface Science*, 2011, 360, 701-715.

52. H. Yu, et al. "Simulating Monovalent and Divalent Ions in Aqueous Solution Using a Drude Polarizable Force Field". *Journal of Chemical Theory and Computation*, 2010, 6, 774-786.

53. C. Bergonzo, et al. "Divalent Ion Dependent Conformational Changes in an RNA Stem-Loop Observed by Molecular Dynamics". *Journal of Chemical Theory and Computation*, 2016, 12, 3382-3389.

54. R. C. Bales, et al. "Bacteriophage adsorption during transport through porous media: chemical perturbations and reversibility". *Environmental Science & Technology*, 1991, 25, 2088-2095.

55. H. Zhang, et al. "Removal of bacteriophages MS2 and phiX174 from aqueous solutions using a red soil". *Journal of Hazardous Materials*, 2010, 180, 640-647.

56. J. N. Israelachvili, "Intermolecular and Surface Forces″, Elsevier Science, 2015.

57. E. Arkhangelsky and V. Gitis. "Effect of transmembrane pressure on rejection of viruses by ultrafiltration membranes". *Separation and Purification Technology*, 2008, 62, 619-628.

58. E. M. van Voorthuizen, et al. "Role of hydrophobic and electrostatic interactions for initial enteric virus retention by MF membranes". *Journal of Membrane Science*, 2001, 194, 69-79.

59. C. Piconi and G. Maccauro. "Zirconia as a ceramic biomaterial". *Biomaterials*, 1999, 20, 1-25.

2. Scientific Background

2.1 Viruses

In the late nineteenth century, the evidence for the existence of very small infectious agents was given by two independently working scientists. Martinus Beijerinck in the Netherland and Dimitri Ivanovski in Russia made extracts from diseased plants which they passed through fine filters and infected healthy plants with this agent. Both scientists could not cultivate any bacteria from these agents. Beijerinck named the infectious agent "virus", which is the Latin word for poison, and this term has been used ever since.[7]

2.1.1 Structure and Morphology

Viruses are classified by the International Committee on Taxonomy of Viruses (ICTV). The ICTV groups viruses in a universal hierarchical system of orders, families, subfamilies, genera and species.[2, 13] It is an ongoing classification which started in 1971 with 290 species.

Viruses are unique in nature and can infect all living organisms. They are among the smallest known pathogens ranging from 17 nm (satellite tobacco necrosis virus) to 2000 nm (citrus triesteza virus) and consist in the basic form only of nucleic acids (genome) and a protein shell (capsid).[19, 20]

The genetic information of the virus can be stored in four different forms, as:

- double-stranded DNA (dsDNA)
- single-stranded DNA (ssDNA)
- double-stranded RNA (dsRNA)
- single-stranded RNA (ssRNA)

Viruses using the dsDNA encode their genes in the same way as animals, plants, bacteria and other cellular organisms, but the other three genome types are unique to viruses. Depending on virus type, the size of the genome can vary from 10^3 (e.g. tobacco necrosis satellite virus) up to 10^6 pairs (e.g. mimivirus).[7]

The genome is enveloped in a protein coat, the so-called capsid, which protects the genome until it can be delivered into a host cell where the virus
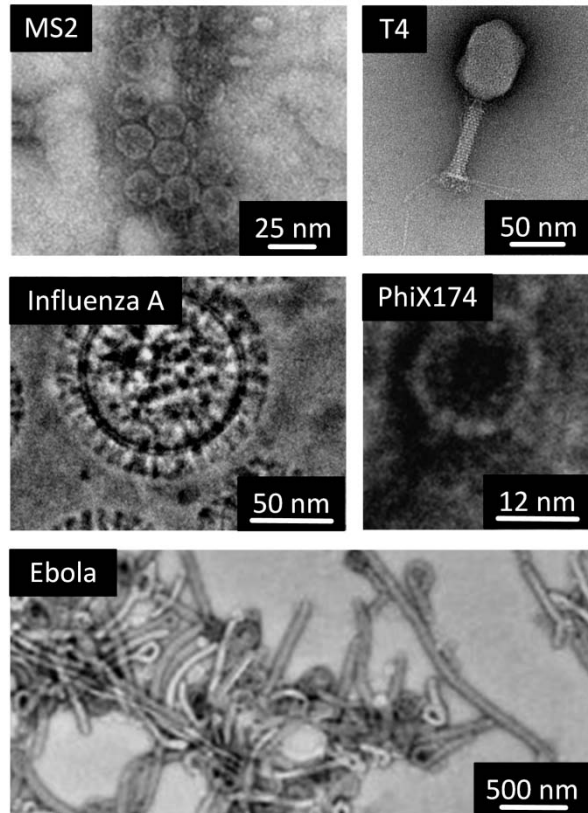
Figure 2.1. A variety of different virus structures. MS2 and PhiX174 adapted from Arkhangelsky et al.[11], T4 adapted from Knott et al.[14], Influenza A adapted from Nagayama et al.[16] and Ebola adapted from Golding et al.[21].

can replicate. Capsids can be based on only one protein species or on over 100 protein species. The individual proteins are asymmetrically organized, but the capsid itself has a symmetrical structure, which is mostly helical or icosahedral. The topography of the capsid surface varies and it can have canyons, hollows, spikes or ridges.

In general, the genome and the capsid build the whole virus, but for some viruses a lipid envelope and sometimes another layer of proteins envelopes the genome and the capsid.[7] Other viruses are constructed with a tail attached to their head with the genome. The shape of virions varies greatly, for example there are rod-shaped, filamentous, brick-shaped, bullet shaped, spherical and tadpole-shaped virions. A variety of different viruses is shown in Figure 2.1.

The complex structures of a virus is based on proteins that have a big impact on how a virus
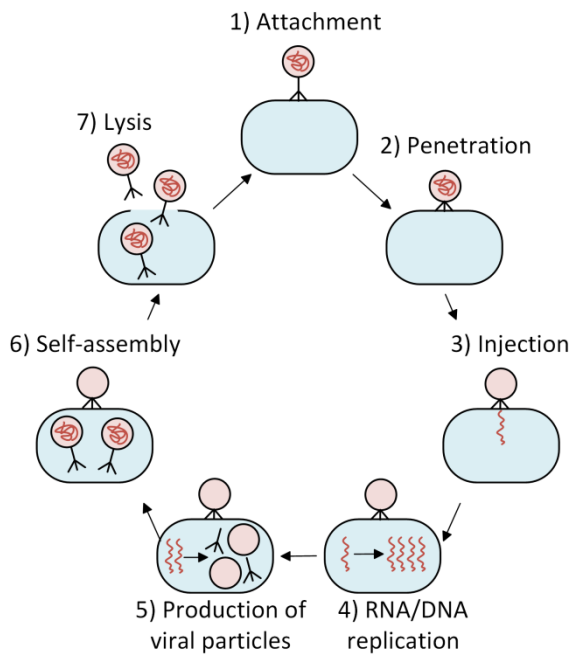
Figure 2.2. Virus replication.

interacts with its environment. Viruses have a pH-dependent surface charge in polar media. The pH value at which the net surface charge is zero is defined as the isoelectric point (IEP) and it is a characteristic parameter of the virus.[25] A review of 137 IEP values of viruses made by Michen et al. showed that viruses have IEPs in the pH range from 2.1 to 8.3 and the most frequent values appear from 3 to 7.[25] Furthermore, the specific protein sequence makes the virus surface either water-repelling (hydrophobic) or water-dissolving (hydrophilic).[28]

2.1.2 Viral "Life" Cycle

There is a debate ongoing whether viruses are living or nonliving species. On the one hand viruses have genes, which can replicate when infecting cells which can be considered as living, on the other hand viruses are very different to cellular life forms and when they are outside of their host cell they are inert and can be considered nonliving.[7]

The virus replication is based on seven steps as shown in Figure 2.2. The first step is the attachment of the virus to a host cell (1), where the virus can bind to a variety of molecules on the host's membrane. The binding can be a non-specific attachment to low-affinity sites or a

Table 2.1. ICTV Taxonomy of bacteriophages MS2 and PhiX174.[2]

	MS2	**PhiX174**
Orders	Unassigned	Unassigned
Families	Leviviridae	Microviridae
Subfamilies	Unassigned	Bullavirinae
Genera	Levivirus	PhiX174 microvirus
Species	Escherichia virus MS2	Escherichia virus PhiX174

specific binding to high affinity sites.[29] At the first stage the virus is weakly bound over one or only a few receptors, which is reversible. If the virus remains on the host, more virus receptors can attach to the host and form an irreversible bond.

After the virus attaches to the host, the virus enters the cell (2) and delivers its genetic information (RNA or DNA) by injection to the cell (3) where the virus RNA/DNA is translated to virus proteins (4) and the genome is replicated (5). During a specific time period (around 30 min for most viruses) the host produces capsids and genomes of 20 to 200 phages (burst size) which start to self-assemble into virions (6). The last step of the viral life cycle is the exit of the virions from the cell (7). This step is called burst and mostly leads to cell death of the host by breaking of the cellular membrane (lysis).[7, 20]

2.1.3 Bacteriophages MS2 and PhiX174

Bacteriophages, viruses which infect bacteria, were discovered 1915 by Frederick Twort.[7]

The bacteriophages MS2 and PhiX174 are two of the most well studied viruses. The taxonomy according to the ICTV of both bacteriophages is shown in Table 2.1.

Both viruses are coliphages and infect only one specific strain of host bacteria of the species *Escherichia coli* (*E.coli*). MS2 is a ssRNA virus with a size of 25 - 27 nm in diameter and has an isoelectric point (IEP) of 3.5 ± 0.6 and PhiX174 is a ssDNA virus with a diameter of 26 - 32 nm and an IEP of 6.2 ± 1.6.[25, 30] The bacteriophages MS2 and PhiX174 both show an excess of positively charged amino acids at pH 7.3, even if their zeta potential is negative at this pH value. This can be explained by the strong influence of

the negatively charged nucleic acid in the capsid.[31-33] Both bacteriophages are mainly hydrophilic with hydrophobic residues on the virus surface of around 10 %.[31, 34-36] The properties of both bacteriophages are given in Table 2.2.
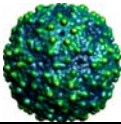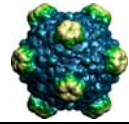
The surface structure of the bacteriophages MS2 and PhiX174 is shown in Table 2.2. MS2 has an icosahedral capsid which has around 180 copies of the coat protein and one copy of the maturation protein, which is necessary for the host infection by attaching to the sex pilus. PhiX174 has an icosahedral capsid with evenly distributed spikes on the surface which play a role in host recognition and attachment.[7]

2.2 Removal or Inactivation of Microorganisms (Viruses) from Water Sources

Today, approximately 8.5 % of the global population (605 million people), especially in developing countries, have an inadequate access to safe drinking water.[37] Water disinfection is needed in the water treatment industry where microorganisms are removed or inactivated to produce clean (drinking) water. Water should be disinfected before human consumption, as pathogens, especially viruses, are affecting the water quality and therefore the human health, as they can cause several diseases like gastroenteritis, heart anomalies and meningitis.[38] Based on the guidelines from World Health Organization (WHO) and United States Environmental Protection Agency (USEPA) a log-reduction value (LRV) of at least 4 (99.99 percent removal) is required to provide safe drinking water.[39, 40]

Furthermore, water disinfection plays an important role in the production of biopharmaceutical products which are derived from human or animal origins, where manufacturers are required to validate the virus clearance before the product is released to the market.[41] Multiple processing steps are used to ensure the removal of all viruses. Some of them are described in more detail in the following.

Table 2.2. Properties of the bacteriophages MS2 and PhiX174.

	MS2	PhiX174
Nucleic acid[1,7]	ssRNA, 3569 nucleotides	ssDNA, 5386 nucleotides
Morphology[1]	Non-enveloped, icosahedral, d = 25 - 27 nm	Non-enveloped, icosahedral, d = 26 - 32 nm
Host[15]	E.coli, F-specific	E.coli, somatic
Multiplication rate[18]	669 h^{-1}	697 h^{-1}
Molecular weight[23]	3.6 MDa	6.2 MDa
IEP[25]	3.5 ± 0.6	6.2 ± 1.6
Apperance[26]		

Heat Treatment

Heating water is the oldest disinfection method which has been used since ancient times. It is effective in killing or inactivating nearly all waterborne pathogens, as viruses, bacteria and fungi.[42] Studies show, that the inactivation of viruses was found to be faster at temperatures above 50 °C and that a temperature of 70 °C is highly effective against most bacteria types.[43, 44] Some viruses as the bacteriophages PRD1 and PhiX174 are highly resistant to temperature, therefore a heating to the boiling point is recommended to guarantee safe drinking water.

Nowadays, boiling is the most common water disinfection method in household based disinfection compared to other point-of-use (POU) treatments in developing countries.[45] One of the main drawbacks of this method is the recontamination due to a lack of residual protection and unsafe storage and handling.[45] Another disadvantage is the cost of fuel or electricity for boiling, which varies for example between 5 % and 7 % of the income in Zambia[45] and between 0.48 % and 1.04 % in rural Vietnam[46]. In some world regions the use of wood for burning is a major concern because of the loss of woodlands and the associated ecological damage.

In the water treatment industry boiling is not

preferred due to the high amounts of water which is to be decontaminated.

UV Radiation

UV radiation has initially been used in 1910 in Marseille for the disinfection of drinking water and is one of the easiest techniques for water disinfection, as only a UV lamp is needed for the production of safe water.[47] No chemicals are necessary and therefore no toxic disinfection-by-products (DBPs) are formed. UV radiation is highly effective against bacteria, but there is a lack in the inactivation of viruses, especially double-stranded DNA adenoviruses are stable against UV light.[47, 48]

One of the main disadvantages of this method is that the UV light does not provide a chemical disinfectant residual to prevent the water from recontamination. Another drawback is the required electricity to power the UV lamp, its periodically cleaning and its finite lifetime.[42]

Free Chlorine

Free chlorine (sodium hypochlorite) is the most widely used chemical in drinking water treatment industries worldwide, as it is highly effective against bacteria and most kind of viruses. The inactivation of microorganisms is greatly influenced by the pH level, the free residual chlorine concentration, the exposure time and the temperature of the water.[49] Engelbrecht et al. showed that the inactivation of enteric viruses is greater at pH 6 than at pH 10.[50] Shin et al. studied the inactivation of three different viruses at free chlorine concentrations of 1 mg/L and 5 mg/L and determined that the exposure time has to be increased for lower chlorine concentrations.[51] Generally a dose of a few mg/L and exposure times of 30 min are recommended to guarantee a >4-log inactivation of viruses and bacteria.[42]

The main drawback of the treatment with free chlorine is the formation of toxic disinfection-by-products, as trihalomethanes, haloacetic acids, halonitromethanes, haloacetonitriles, haloaldehydes, haloketones and iodo-THMs.[52] In the early 2000s many drinking water utilities started to use monochloramine next to free chlorine as a secondary disinfectant to minimize the formation of toxic DBP.[53] Other disadvantages of the treatment with free chlorine in regard to drinking water production are the influenced taste and odor of the water. Furthermore, free chlorine is not available worldwide; especially in developing countries is a lack of obtainable chemicals.[42]

Chlorine Dioxide

Chlorine dioxide (ClO_2) is a relatively strong germicide and more effective in the inactivation of viruses compared to free chorine, as the viruses are inactivated in a wider pH range with lower doses and under lower exposure times.[54] This is mainly due to the different properties of ClO_2 and free chlorine and the consequently different inactivation mechanism. For the bacteriophage MS2 it has been shown that free chlorine treatment caused a loss in the genome- and protein-mediated functions (replication and injection) whereas ClO_2 treatment is degrading the viral proteins.[55]

The major concern by using chlorine dioxide is that it is, as well as its DBPs, toxic. Therefore, special facilities and trained personnel are required to work with the hazardous chemicals.[42]

Ozone

Since the early 20th century ozone has been used for water disinfection in water supplies in developed countries as it is a strong oxidant, which can inactivate a variety of microorganisms. Viruses and bacteria are very sensitive to ozone and only low doses of ozone are required for complete inactivation.[56-59]

As ozone is a highly reactive gas it has to be generated on side with specialized equipment and trained personnel.[42] Due to the treatment with ozone a variety of DBPs is formed, e.g. low molecular weight aliphatic aldehydes (fomaldehyde, acetaldyhyde), by-products with carbonyl functionalities (glycoylic, pyruvic acid) and hydrogen peroxide.[60] Moreover, the toxic and carcinogen DBP bromate ion which is more toxic than the DBPs formed by free-chlorine is produced.[61]

Silver

Silver is known as a bacteriostatic agent since antiquity where silver vessels have been used to store water, wine or vinegar. Since the 19th century the antibacterial effect is related to silver ions.[62, 63] Nowadays, silver is used as metal, salt or nanoparticles for disinfection, as it is toxic to both aerobic and anaerobic bacteria due to the interaction of sulhydryl groups on the surface of the microorganisms.[64] Nevertheless, some bacteria strains can generate a silver resistance when excessively in contact with silver as shown by several authors.[65-67] For example, Silver et al. documented that 10 % of randomly tested enteric bacteria in the University of Illinois Chicago hospital showed genes for Ag^+ resistance.[68] Furthermore, most viruses are resistant to silver ions, only for viruses with sulfhydryl terminuses the reaction to silver is similar to that of bacteria.[69]

Silver ions have another main drawback as they can cause serious risk for the human health, therefore the World Health Organization (WHO), the National Institute for Occupational Safety Health and the European Commission set exposure limits, which vary according to the reference between 10 g intake per lifetime to 0.1 mg/L in a timeframe of 8 h.[63]

Coagulation and Flocculation

Coagulants, like vegetable substances or seeds, have been used since ancient times in water treatments. Nowadays, various salts of aluminum, iron, lime and other inorganic or organic chemicals are used to remove colloidal particles by destabilizing them and precipitating them into larger particles which can be removed by sedimentation or filtration.[42] In the flocculation process even larger particles are formed which are easier removed by sedimentation.

As the coagulation process is complex depending on microorganism, pH, coagulant dose and coagulant time, trained personnel and specialized facilities are necessary to guarantee optimal working conditions to reduce microorganisms to 90 % and up to 99 %.[42, 70-72] This are rather small reduction rates compared to the previously
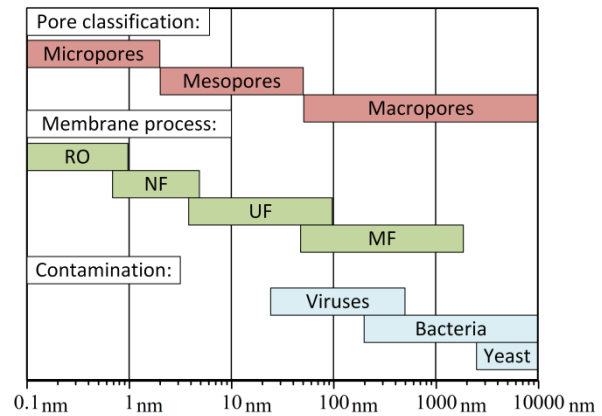
Figure 2.3. Overview of the pore classification, the separation range of pressure driven membranes and the dimensions of microorganisms (adapted from Lutz et al.[4]).

discussed water disinfection methods, therefore coagulation is mostly combined with filtration.[71-76] Other disadvantages are the relatively high costs and the limited availability of alum and ferric salts.

Combinations

Combined applications of several water disinfection methods are often used to produce water that meets the national and international standards for microbial quality. Therefore several authors showed different combination possibilities as UV/free chlorine[61], ozone/free chlorine[77], free chlorine/silver[78], UV/silver[79] and filtration/UV[80].

Water Filtration

Water filtration is the act of separating water and contaminations in a physical process which generally uses filters or membranes.[81] The word membrane has its origin from the Latin word *membrana* which means "skin". Membranes are a barrier which separate two phases in a selective way by size exclusion principle. In water filtration the solvent passes the membrane but retains the particles above a particular size, the pore size.

Membrane processes can be classified depending on the driving force that is used to separate the two phases in the following groups[82]:
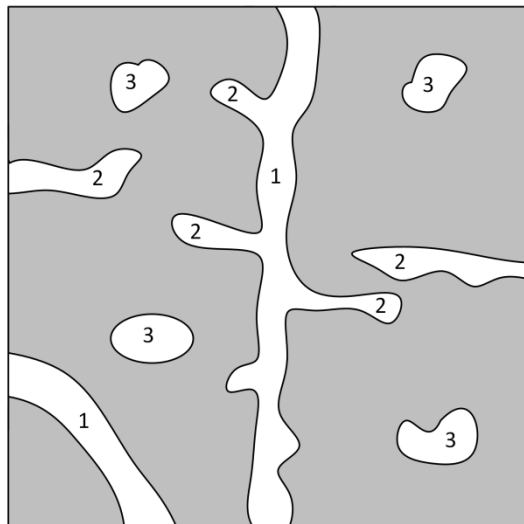
1: Open and flow-through pores
2: Open and non flow-through pores
3: Closed pores

Figure 2.4. Sketch of open and closed pores in a material (adapted from Elssner et al.[5]).

1. Pressure driven membrane processes
   - Reverse osmosis (RO)
   - Nanofiltration (NF)
   - Ultrafiltration (UF)
   - Microfiltration (MF)
   - Pervaporation (PV)
2. Concentration gradient driven membrane processes
   - Dialysis
   - Membrane extraction
2. Electrical potential driven membrane processes
   - Electrodialysis

The most relevant filtration processes in industry are pressure driven processes, therefore, the separation range of different pressure driven membranes are shown in Figure 2.3. Pressure driven membranes can have open pores which are connected to the external surface and which are responsible for the filtration mechanism and closed pores which are not connected to the external surface and thus isolated (Figure 2.4). Pores larger than 50 nm are classified as macropores, pores between 2 and 50 nm as mesopores and pores smaller than 2 nm as micropores.[82] Pressure driven membranes are divided in symmetric or in asymmetric porous

12

Table 2.3. Advantages and disadvantages of polymeric and ceramic membranes in different geometries (adapted from Ohlrogge et al.[6]).

	Tubular polymer membrane	Flat ceramic membrane	Tubular ceramic membrane
Chemical resistance	-	++	++
Thermal resistance	-	++	++
Mechanical resistance	-	++	++
Back-flushing	-	++	++
Surface area to volume ratio	++	--	++
Material weight	++	--	+
Material costs	++	--	+
Production costs	++	--	+
Market share	++	--	- → +

structures. Symmetric membranes have a homogenous pore structure while asymmetric membranes are based on a macroporous support structure with thin layers deposited on top of it, which provide the desired retention. Asymmetrical membranes are advantageous to reduce the pressure drop due to their macroporous substrate structure during filtration, as a smaller pore size leads to a higher pressure drop.[6]

The two standard membrane operation modes are dead-end and cross-flow filtration (Figure 2.5). In dead-end filtration the liquid is forced through the membrane pores during the filtration process by a pressure which is applied on the feed side. In contrast to that, in cross-flow filtration the feed flows parallel to the membrane and some liquid permeates through the membrane because of a pressure difference.[41] For both application modes, membranes can be fabricated in a wide range of forms and structures, but the main forms are flat sheet or tubular membranes, which are compared in Table 2.3. The main advantage of tubular membranes compared to flat sheet membranes is the higher surface area to volume ratio and the associated lower material weight [6].

Membranes for filtration, especially virus filtration, can be fabricated from organic or inorganic materials. Common polymers which are used in commercial applications are cellulose

and regenerated cellulose, polyethersulfone and polyvinylidence fluoride, whereas inorganic membranes are fabricated from metallic oxides (alumina, titania, zirconia), carbon or silica.[41] The advantages and disadvantages of polymeric and ceramic membranes are shown in Table 2.3. Ceramic membranes show excellent chemical, thermal and mechanical stability compared to polymeric membranes and therefore can be cleaned with aggressive chemicals, organic solvents or hot water.[6, 83] Because of their high mechanical strength, ceramic membranes can endure high pressures and thus high water permeate fluxes. They can easily be cleaned by back-flushing, thermal, acidic or basic treatment without affecting the pore morphology, even when the pores are blocked by foulants.[84, 85] In contrast to polymeric membranes, ceramic membranes do not show any swelling behavior during water filtration. In contrast to polymeric membranes, ceramic membranes are usually more expensive (3 up to 5 times higher costs), but this can be compensated by their longer lifetime of up to ten years instead of one year for polymeric membranes.[86] Further disadvantages of ceramic membranes are the vulnerability to brittle failure and the higher material weight compared to polymeric membranes.[87]

Membranes can remove viruses and bacteria from water samples if the membrane pore size is well adjusted to the contamination size.[88] Bacteria can effectively be retained by microfiltration membranes as shown by several authors.[89-96] Viruses are among the smallest waterborne pathogens with diameters of 25 nm and therefore the most difficult to remove by size exclusion principle as the pore size of the membrane has to be reduced to approximately 20 nm to guarantee an effective removal.[42, 97] Nevertheless other authors showed that the pore size of a membrane can be 2 to 3 times greater than the size of the contamination to ensure a significant retention due to adsorption effects.[27, 98]

Membranes are used in water purification for drinking water production, effluent polishing, ultrapure water production for industrial and pharmaceutical applications.[88]

Virus filtration is used in a wide range of
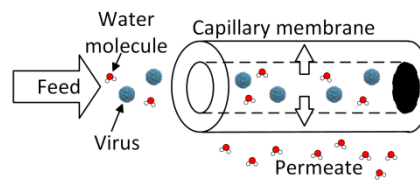
Figure 2.5. Principle of virus dead-end and cross-flow filtration with capillary membranes.

biopharmaceutic applications as overall viral clearance strategy. Guidelines for ensuring the safety of biological products are given by the European Medicines Agency (EMEA) or the US Food and Drug Administration (FDA).[99] In the early 1990s the virus filtration of plasma products has been implemented to improve the safety against non-enveloped viruses.[100] Filtration is the only possibility to remove viruses efficiently (more than 4 to 6 logs) and to recover 90 - 95 % of the protein activity.[100] Therefore, many of the licensed plasma products are filtered as it is a simple manufacturing step which guarantees a reliable virus reduction which eliminates the risk of transmission with human immunodeficiency virus (HIV), hepatitis B and C viruses by any plasma-derived products. Another, biopharmaceutical application of filtration is the production of monoclonal antibodies, as they have emerged as a valuable class of therapeutic products for the treatment of cancer and diseases like rheumatoid arthritis, allergic asthma and multiple sclerosis.[101, 102] For an effective use of virus filtration the conditions of antibody solution as ionic strength, pH, concentration and buffer composition play an major role as shown by Hongo-Hirasaki et al.[103]

The removal of microorganisms by filtration is not only important in biopharmaceutical applications but also for drinking water providers worldwide to ensure the public health and to meet the water quality regulations. A log reduction value of 4 is required through drinking

water treatment by the guidelines from WHO and United States Environmental Protection Agency (USEPA) to provide safe water. Membranes were used in drinking water treatments since World War II were the Germans started to check their drinking water after bombardments.[88]

Nowadays, in developing regions like Oceania or Sub-Saharan Africa were the lack of safe drinking water is the highest, sand, cotton or linen filters and clay-based filters are used which reduce the number of viruses in drinking water, but do not guarantee a complete removal.[42, 104, 105] Besides the effect of simple size exclusion, new membrane types are developed using preferential adsorption of the viruses on the membrane surface. El Hadidy et al. used a commercially available hollow fiber UF membrane made from modified polyvinylidene difluoride (PVDF) and showed that size exclusion is the main removal mechanisms but that electrostatic repulsion is contributing to the virus removal.[106] Other authors used oxyhydroxides as $Y(OH)_x$, $Zr(OH)_x$ and $Mg(OH)_2$ to coat or dope membranes to enhance the virus retention by adsorption.[107-109]

The main advantage of water filtration regarding the other water disinfection methods is the treatment in a one-stage process without any chemicals.[110] The main drawback in the use of membranes is fouling, which is the growing of a filter cake accompanied by pore blocking by physical or chemical interaction between the membrane and contaminations in the feed. Due to pore blocking, the water flux is decreasing and therefore a cleaning or replacement of the membrane is required. Fouling prevention is achieved due to regular cleaning steps when the water flux decreased below a certain acceptable level.[41] The cleaning step can be realized by backflushing (physical removal of the foulant) and/or chemical cleaning.[41, 110]

2.3 Ceramic Processing

2.3.1 General Physico-Chemical Properties of ZrO₂

Zirconia (ZrO_2) was identified in 1789 by the German chemist Martin Heinrich Klaproth who obtained the reaction product after heating gems.[111] In 1975, Garvie et al.[112] considered zirconia a ceramic analogue to steel, after improving the mechanical strength and toughness and implemented the name "ceramic steel". Since then this material has been used for innumerable applications.

Zirconia is inert, features high corrosion resistance and has mechanical properties better than other oxide ceramic materials (e.g. twice the flexural strength of alumina).[111] Zirconia is a polymorphic material that occurs in three temperature-dependent forms: monoclinic (room temperature to 1170 °C), tetragonal (1170 to 2370 °C) and cubic (2370 to 2700 °C). To retain the tetragonal phase in a metastable condition at RT, stabilizing agents, for example yttria (Y_2O_3), magnesia (MgO), ceria (CeO_2) or calcium (CaO) can be added to zirconia to generate multiphase materials known as partially stabilized zirconia (PSZ) or fully stabilized zirconia (FSZ).[111, 113] These precipitates can exist at the grain boundaries or inside the cubic matrix grains.

2.3.2 Shaping Strategies

The shaping strategies of ceramics differ from that of other material classes (e.g. polymers or metals), as ceramics cannot be shaped in the molten state or be formed under heat treatment. A wide variety of substrate morphologies with different sizes, shapes, complexities and microstructures is available due to advanced processing and manufacturing technologies for ceramics.

A: Dry pressing (uniaxial)

B: Slip casting

C:Extrusion (with a ram extruder)
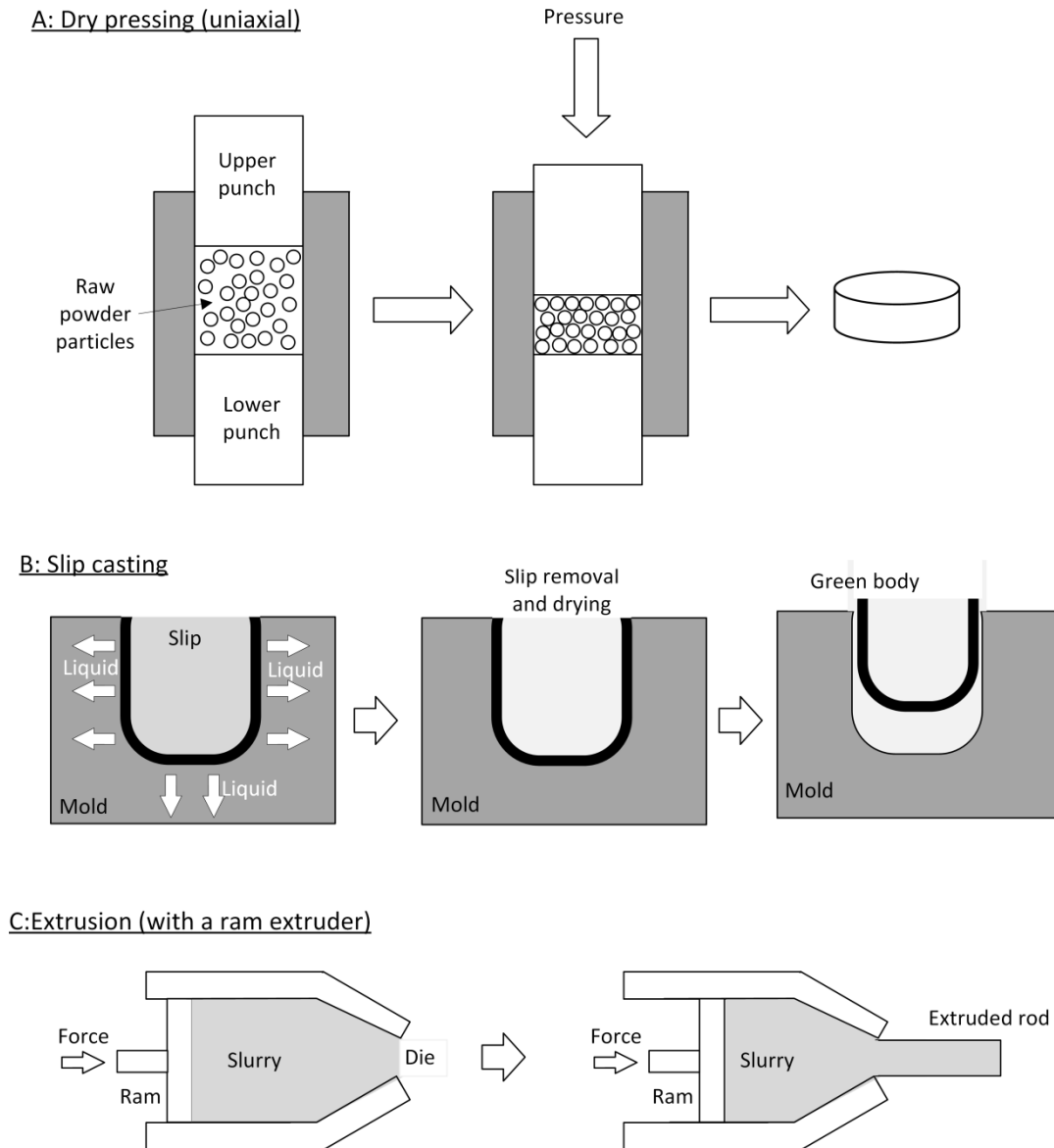
Figure 2.6. Principle of uniaxial dry pressing, slip casting and extrusion with a ram extruder.

In general five steps need to be conducted for the processing of ceramics.[9, 114] In the first step the ceramic powder is mixed with solvents and additives to achieve the so called "slurry". The slurry is shaped in the second step. Based on the desired material and the structural characteristics, the shaping method of choice is selected. The most widely used production methods for shaping ceramic materials are dry pressing, slip casting and extrusion (Figure 2.6).[115] All three shaping strategies are described in this chapter in more detail. The shaped but non-fired ceramic body is called green body. In the third step the solvent is removed from the body by drying the green body at a specific temperature over a specific time. The dried green body is sintered in the fourth step. The drying and sintering process is described in chapter 2.3.3. The achieved body can be post-treated in the fifth step, but as ceramic bodies are very brittle no reshaping is possible in this state.[3] All five processing steps are of great importance for the final product, therefore each step has to be carried out carefully with regard to the required final product characteristics.

Dry Pressing

Dry pressing is used for the production of simple solid shapes e.g. it is used for the production of ceramic tiles, seal rings, nozzles and plates.[87] Dry pressing is based on three basic steps, which are demonstrated in Figure 2.6 A. It is one of the most popular shaping techniques, as it involves a simple technology and high production rates.[116]

First the mold, called die, is filled with a ceramic powder which contains 0 to 7 wt% of a binder.[115] A ceramic particle size distribution between 20 and 200 μm is preferred. In the second step the powder is compacted with a pressure load. The powder can be pressed either uniaxial (from one end) or biaxial (from both ends) at defined pressures of up to 300 MPa.[87] The pressure is depending upon the material and the used press type. During the pressing process it is necessary that the powder particles "flow" between the closing punches to fill the spaces in the tile uniformly. The stages during the pressing process are sliding and rearrangement of the particles, particle fragmentation and the elimination of the pores in the solid. The third step is the ejecting of the pressed solid tile.[87] Due to the low moisture content a drying step is not needed.

Slip Casting

The word slip comes from an old English word and can be translated with cream.[87] In ceramic processing the word means a liquid ceramic mass. A ceramic slip, also called slurry, mainly consists of a solvent, usually water, and ceramic powder. The solid content in this method is up to 60 vol%.[87] Additives can be used to increase the particle and slurry stability (dispersants), the viscosity and the green body strength.[115]

Slip casting is a low cost way to produce complex shapes as teapots, wash-hand basins or gas-turbine rotors.[87]

Slip casting is based on introducing a clay/ceramic slurry (slip) into a plaster mould. The mould is oversized as the model shrinks during the drying and sintering process to its actual size. The actual size is around 25 % smaller than the mould size depending on the solvent content of the slurry and the sintering temperature used.[115] A certain amount of water

from the slurry is adsorbed by the plaster mould which force the powder particles of the slurry towards the mould walls. When the particle layer has its desired thickness, the slip is removed and the mould is dried for several days until the shaped piece can be removed and sintered.[115] The principle is shown in Figure 2.6 B.

Extrusion

Extrusion is used to produce ceramic components which have a uniform cross section and a large length-to-diameter ration e.g. ceramic tubes or rods.[87]

Extrusion is the pressing of a ceramic mass through a shaped opening, the so called die, which is shown in Figure 2.6 C.[115] The die can have the shape of rods, mono- or multichannel tubes as well as honeycomb structures. The shaped ceramic mass flows out the die with a constant speed and is cut at the required length to the angles to the direction of outflow to obtain ceramic pieces.[115]

The processing principle of extrusion is simple, but there are various extrusion units available which can be divided by their design relevant features. The most common used extruder units are the screw and the ram extruder. The screw extruder uses a screw to force the ceramic mass through the product forming mould.[117] It is used for horizontal continuous processing and can be used for large-scale production. Typically screw extruders have a mixing section, where the slurry is prepared, prior to the extrusion section.[117] The ram extruder is equipped with a hydraulically activated ram, which forces the ceramic mass through the product forming die.[117] It is used batchwise with already prepared slurries. In this thesis a self-made ram extruder is used for the fabrication of the capillaries due to the possibility to use only small feedstocks of ceramic mass. The used extruder consist of a spindle drive with shaft joint which is connected to a press ram, a convenient vessel for the slurry uptake, an extrusion die with integrated pin and a conveyor band for depositing the extruded capillaries.

Pure ceramic powder cannot be processed by extrusion, as ceramic particles itself show no plasticity or slip properties. Due to the high

melting point of ceramic powders it is not possible to use them in the molten state as it is done for the extrusion of polymers. Therefore additives, such as binders, surfactants or plasticizers have to be added to create a plastic mass. In aqueous systems polyvinyl alcohol (PVA), polyethylene glycols with a high molecular weight or cellulose derivates can be used as binders.[118] The moisture content in the ceramic mass is relevant to provide the ceramic body with enough cohesion to equilibrate the attrition forces with the extruder walls and the extrusion die.[115] If the moisture content of the slurry is too low, small cracks crossways to the extrusion direction are formed[115] and if the moisture content of the slurry is too high, the ceramic mass is not retaining its shape after extrusion.

2.3.3 Drying and Sintering

Drying

Drying of a green body is a highly sensitive step, as the formation of cracks can occur when the drying conditions (humidity and temperature) are not well adjusted. Drying starts, when the green body is exposed to an atmosphere with a lower water-vapor partial pressure as compared to the water inside the green body.[3]

Each ceramic particle in a green body is enveloped in moisture. The drying process can be divided in two parts. The first part of the drying process is the constant drying, where the ceramic particles move towards each other because of capillary forces which arise during the water evaporation. The green body shrinks due to the particle movement and obtains a higher mechanical strength. Cracks can occur due to inner tensions, as different moisture contents on the surface and in the inner of the green body are present.[3] The water content on the surface of the green body is evaporating first, therefore the shrinkage process occurs there first. The surface is thus under tension, which can result in cracks. In the end of the constant drying period the ceramic particles of the green body touches each other and the shrinkage ends.

The second drying part has a decreasing drying rate, where water adsorbed to the particle surface
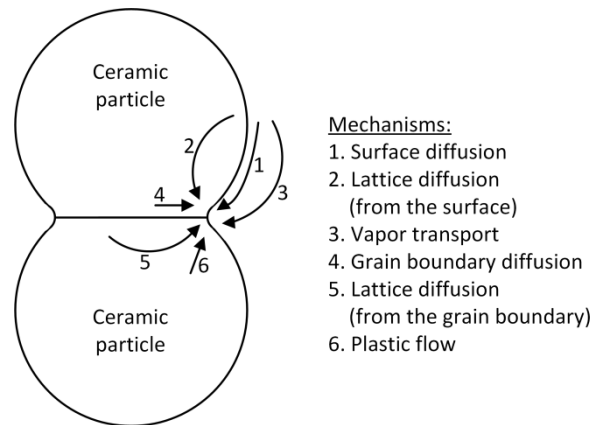
Figure 2.7. A two particle model of the mass transport mechanisms in the initial stage of sintering (adapted from Reitz et al.[9]).

and water which is remaining in small pores is removed from the green body by further evaporation.

In general the drying of green bodies is the most time consuming step in ceramic processing. An increase of the drying velocity due to the use of higher temperatures or lower humidity rates is often restricted, as cracks would occur due to inner tensions.[3]

Sintering

Sintering is the transformation of a powder compact (green body) into a solid body at high temperatures without melting the material, where the driving force is the aspiration of a system to achieve the lowest free enthalpy.[3] Powder particles have a large surface area and thus a high surface energy. The sintering reduces the surface energy and therefore the interfacial energies by grain growth due to atomic movements (Figure 2.7). The temperature which is needed to induce the atomic motion depends on the material and the particle size of the ceramic powder.[119] In general, the ideal sintering temperature to achieve a densification of bulk ceramics is between 0.7 to 0.8 of the melting temperature.[3] Even if the peak temperature is the most important sintering parameter, there are several other adjustable parameters which have an impact on sintering and are crucial for the ceramic end product, as the material, the particle size, the green density, the heating rate and the holding time during sintering.[119]

17
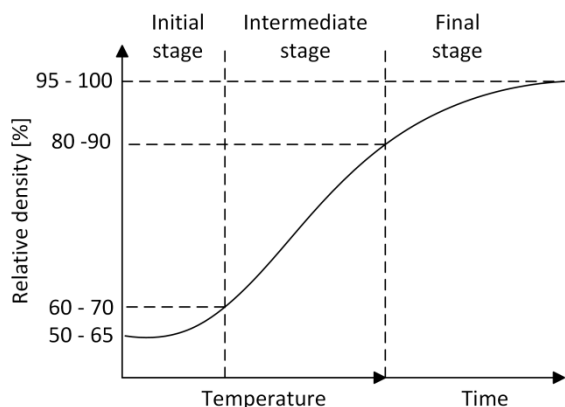
Figure 2.8. Density progress during the three stages of sintering (adapted from Salmang et al.[3]).

The densification of the ceramic is caused by a transport of mass towards the intermediate area (pores) between the ceramic particles., where the main driving force is the reduction of the Gibbs free energy of the system.[3] The rearrangement of the particles during the sintering process is caused by diffusion, crystallization and chemical reactions, in which diffusion is the main driving force as it is responsible for the mass transport and the densification. The diffusion of ions is caused by vacancies in the lattice or interstitial sites and by site changes in a solid lattice, therefore lattice-, surface- and interfacial-diffusion are existing. The diffusion velocity is depending on the temperature, the size of the diffusion species, the accessibility of the diffusion path and the charge of the diffusing species.[3]

Sintering can be divided into three stages of densification, the initial, intermediate and final stage, as shown in Figure 2.8.[120]

The first stage is characterized by a neck formation between initial particles, where a atomic diffusion from the particle surface to the neck region of two particles takes place (arrow 1 in Figure 2.7). The most dominant mechanism in this stage is the so-called surface diffusion, as the surface diffusion activation energy is lower compared to the other mass transport processes during sintering and the surface atoms start moving at lower temperatures compared to interior atoms.[119] An atom breaks an existing bond with the surface and tumbles across the

18

pore surface via random motion until it attaches at a new surface site at a surface vacancy or kink.[119] This occurs due to a gradient of vacancies, which is based on the high concentration of lattice defects at the surface and the different curvatures of the particle (convex) and the neck (concave). In general, atoms tend to migrate from convex to concave surfaces, hence from surface to neck.[119] The sample volume and the pore content is only little changed by the neck formation in the first stage, as it is only a repositioning of the atoms to create a smooth surface.[121] Therefore, there is hardly any shrinkage visible in the initial sintering stage (<5 %) and if the sintering would have stopped at the end of the first stage, a porous ceramic body with nearly the same porosity and pore size as the green body would have been created.[3]

When the sintering progresses to the intermediate stage, in general powder particles move further to each other, which is essential for the densification of the material. Predominantly volume and grain boundary diffusion occur in this stage.

The junction of two grains is defined as grain boundary. This is defective in bonding and providing a pathway for the diffusion process. Atoms which move across a grain boundary are responsible for grain size changes whereas atoms moving along the boundary are responsible for the densification of the ceramic body.[119] The grain boundary diffusion is symbolized as arrow 4 in Figure 2.7. The grain boundary diffusion depends on the grain boundary area per unit volume.[119] As surface area is decreasing and grain boundaries are increasing during the intermediate sintering stage, the role of grain boundary diffusion is increasing during this stage.

Volume diffusion or lattice diffusion occurs only at high temperatures and is responsible for the bulk transport processes. The heat application induces the atomic motion. The result is a position change of atoms and vacancies. Pores in the ceramic structure are defined as large vacancy clusters.[119] There are two types of lattice diffusion. One is from the surface through the particle interior to the particle surface (arrow 2,

in Figure 2.7), where no densification or shrinkage occurs as it is a transport from surface to surface. The second one is a bulk transport process where vacancies flow to the grain boundary and mass is transported from the grain boundary to the pore (arrow 5, in Figure 2.7).[119] This mechanism lead to a densification and shrinkage, as layers of atoms are repositioned on a pore surface. In the intermediate stage, the grain boundaries start to grow and the porosity of the structure decreases to values between 5 and 10 %.[120]

The third (final) stage is driven by volume diffusion, which is relatively slow, as curvature gradients and the surface energy are already highly reduced. In this stage the final pore elimination and grain growth occur. Smaller pores are eliminated, while larger pores grow. The number of neighboring grains define whether a grain grows or is consumed. A grain with six or less neighbors has a convex structure and gets consumed by grains with a concave structure.[87] A dense body is formed due to the grain growth.[121]

2.3.4 Processing Strategies for Porous Ceramics

There is a large number of processing strategies to produce porous ceramics. Each method has its own characteristic pore structure and porosity, as can be seen in Figure 2.9.

Freeze-Casting

Freeze-casting is based on freezing a liquid suspension, which is sublimated under reduced pressure to the solidified phase from the solid to the gas state.[10] Afterwards the green body can be sintered to consolidate and densify the structure. The pores are a replica of the solvent (mostly water) crystals and can be adjusted by the freezing conditions and the solvent content.[10]

Direct Foaming

Direct foaming is based on the introduction of gas bubbles e.g. from an alkane phase to an suspension.[122] An open-cell microstructure with pore sizes from the μm- to mm-scale is obtained. The microstructure can be adjusted via the alkane content and the applied stirring velocity during emulsification.[17, 123] The green foams are dried
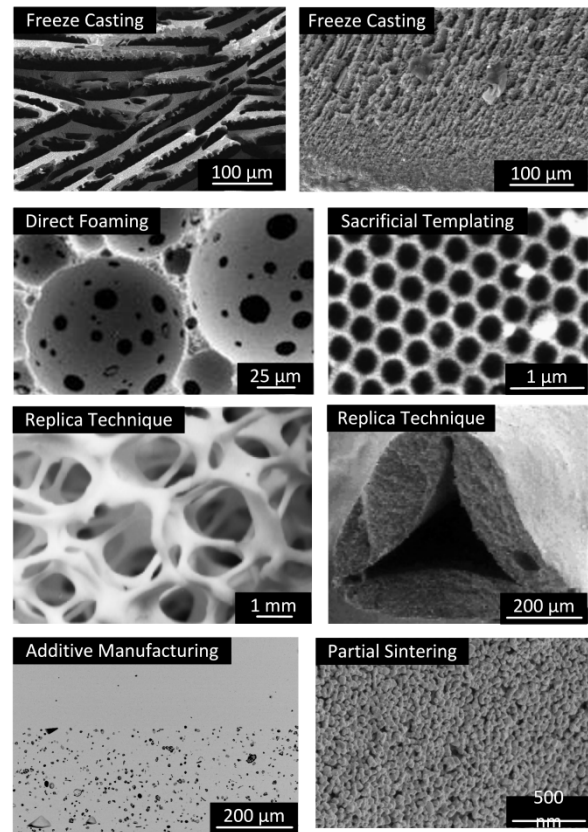
Figure 2.9. Pore structures developed by different processing strategies. Freeze casting structure adapted from Deville[10,13], direct foaming structures adapted from Kroll et al.[17], sacrificial templating and replica structures adapted from Studart et al.[22], additive manufacturing structure adapted from Scheithauer et al.[24] and partial sintering structures adapted from Werner et al.[27].

and finally sintered.

Sacrificial Templating

A sacrificial material e.g. styrofoam, wax or polymer, is incorporated in the ceramic slurry and is acting as a placeholder. During the sintering process the placeholder is evaporated resulting in empty pores.[22] The porous structure created with sacrificial templating depends on the size and the amount of placeholders as it displays a negative replica of the original sacrificial template.[22]

Replica Technique

The replica method is based on the infiltration of a cellular structure which can be synthetic or

Partial sintering
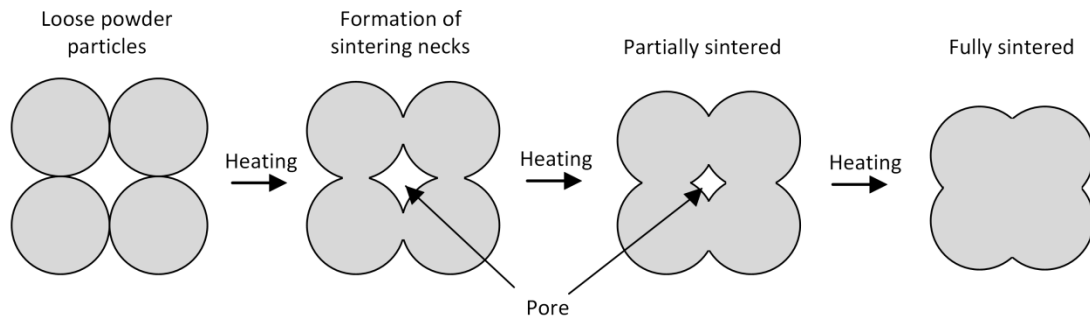
Figure 2.10. Principal of partial sintering.
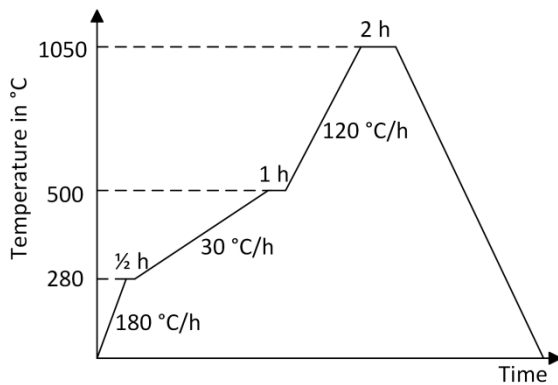
Figure 2.11. Sintering profile of porous ceramic capillary membranes in this study.

natural, with a ceramic suspension.[22] After drying, the sample is sintered and the cellular structure is burned out leaving a ceramic material with the same morphology as the original porous material.[22]

Additive Manufacturing (Rapid Prototyping)

A three-dimensional object is modeled on a computer and afterwards built up layer-by-layer in a rapid prototyping machine.[124] The structure is determined during modeling, but limited due to the process parameters.

Partial Sintering

The most common used technique to prepare a homogeneous symmetrical structure is the formation of a uniform particle network with partial sintering.[125] The pore sizes of this structure is mainly determined by the used particle size, as the network is built up by inter particle pores and the degree of partial sintering (Figure 2.10).[126] The material is only partially

20

sintered by terminating the heat treatment in the intermediate stage of the sintering process, when sinter necks are already formed and the porosity is high. Porosity decreases with sintering temperature and time and is mainly below 50 %.[125] The mechanical properties depend largely on the degree of the neck growth during the sintering process.

The sintering profile with temperatures, heating rates and holding times used to prepare porous ceramic capillary membranes in this work is shown in Figure 2.11.

2.4 Tailored Surface Functionalization of Ceramics

2.4.1 Surface Activation by Hydroxylation Methods

Ceramic surfaces are generally inert, therefore activation is a method to prepare a metal oxide surface prior to the functionalization step.

Activation means the formation of hydroxyl groups (-OH) on the surface of the oxide ceramic as these groups can be used as binding partners for functional groups. Different activation strategies were investigated by several authors ranging from physical to chemical treatments, namely the hydrothermal activation, the oxygen plasma activation and the wet chemical hydroxylation method.

Hydrothermal Activation

One way to activate the surface is hydrothermal activation which is based on the principal of water adsorption. Surface hydroxyl groups are

formed by dissociative adsorption of water molecules which bind strongly to the surface.[127] This mechanism occurs when a oxide ceramic sample is exposed to water or water vapor under high temperatures and pressures.[128] Therefore the samples are generally incubated in an autoclave under defined conditions, where the loading capacity can be influenced by incubation pressure, time and temperature.[129-131] It was shown by Kroll et al. that the hydrothermal activation of zirconia microtubes is not as effective regarding the loading capacity of hydroxyl groups on the surface when compared to other activation methods.[132]

Oxygen Plasma Treatment

Another way to generate hydroxyl groups on ceramic surfaces is plasma treatment, which can be divided in atmospheric pressure plasma and low pressure plasma activation.[133-136] Gas atoms, often oxygen, become excited by energy input to higher energy states and are ionized by introducing a large amount of energy. Due to chemical reactions the ionized gas is reacting chemically with the ceramic surface.[137] The hydroxyl loading capacity is based on the power, the pressure/ flow rate and the exposure time to the plasma. In general, room temperature, low pressures (0.01 to 1 mbar) and relatively short exposure times of 1 to 20 min are used to generate OH-ions on the ceramic surface.[138] To ensure a homogeneous plasma spraying the samples have to rearranged and turned over during the plasma process.

The oxygen plasma treatment offers many advantages, as it is environmentally friendly, easily controlled without danger and no liquid waste is produced. The major disadvantage of this method is the penetration depth of approximately 5 nm to 50 nm, where the inner of a structure is not activated at all.[17]

Wet Chemical Hydroxylation

The direct binding of hydroxyl groups (-OH) onto the inert ceramic surface is achieved by acidic as well as basic hydroxylation. Next to the concentration of the acid/base, the incubation time and temperature are crucial for the loading capacity of the hydroxyl groups. In general, by using stronger acid/base, longer incubation time and higher temperature (< 150 °C), a higher surface activation is obtained.[139]

For basic hydroxylation the most commonly used base is sodium hydroxide (NaOH) which is used generally at temperatures around 100 °C, high concentrations ranging from 1 M up to 15 M and incubation times longer than 24 h.[140, 141] An acidic hydroxylation can be accomplished with hydrogen chloride (HCl)[142-144], phosphoric acid (H_3PO_4)[141], nitric acid (HNO_3)[145, 146], hydrogen peroxide (H_2O_2)[146] or sulfuric acid (H_2SO_4)[143, 145]. High OH-loading capacities were achieved using Piranha solution, a mixture of three parts concentrated H_2SO_4 and one part 30-35 % H_2O_2.[128, 132, 141] The activation with Piranha solution is used in this work to activate the ceramic capillary membranes prior to the functionalization process. The solution is prepared by adding the hydrogen peroxide in the sulfuric acid which causes an exothermic reaction leading to a solution temperatures up to 100 °C, if the hydrogen peroxide is added too fast. Furthermore an incubation time of 30 min is sufficient and a prolongation did not further improve the OH-ions on the surface, as shown by Kroll et al.[132] Wet chemical activations are flexible and simple and therefore widely used. Nevertheless, they reveal some disadvantages like time-consuming sample washing for neutralization and high safety precautions.

2.4.2 Surface Functionalization Methods

Surface functionalization methods allow covalent immobilization of specific functional groups to an oxide ceramic surface and therefore tailoring of the surface chemistry. As a consequence, the surface functionalization is a wide research area where innumerable materials and commercial products are available.[147] Furthermore, there is a wide variety of functionalization strategies described in literature. The basis for the functionalization process is the reaction with surface hydroxyl groups which can be generated with the surface activation methods described previously.

A: General structure of silanes:

Functional or reactive group → R — (CH₂)ₙ — Si — X
Silicon atom
Hydrolyzable groups
Alkyl chain

B: Examples of silanes:

3-aminopropyltriethoxysilane (APTES)

n-2-aminoethyl-3-aminopropyltriethoxysilane (AE-APTES)

n-(3-trimethoxysylilpropyl) diethylenetriamine (TPDA)

n-hexyltriethoxysilane (HTS)

n-octyltriethoxysilane (OTS)

hexadecyltrimethoxysilane

phenyltrimethoxysilane

3-(chloropropyl)triethoxysilane
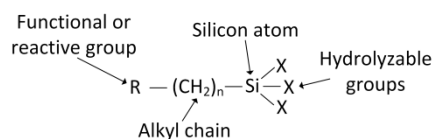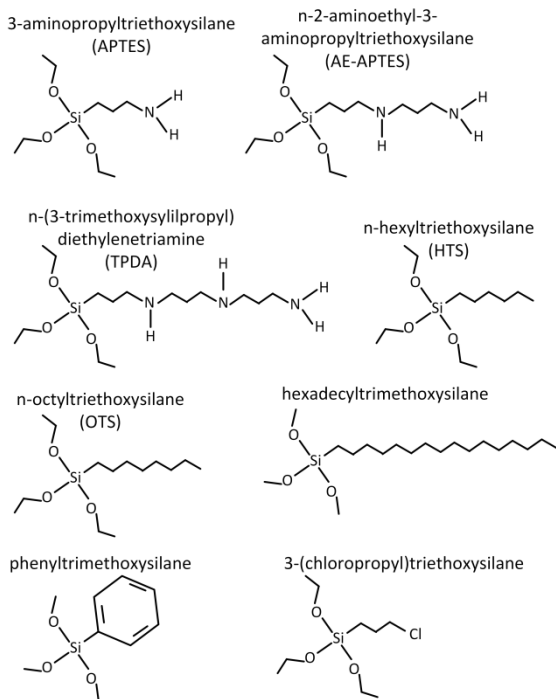
Figure 2.12. General structure of a silane coupling agent (A) (adapted from Hermanson et al.[8]) and examples of silane molecules with varying functional groups (B).

Silanization

Silanization is the most applied and versatile wet-chemical surface functionalization, as it is applicable to any type of oxide ceramic material and support. A silane compound is a monomeric silicon-based molecule which contains four components and is able to form covalent bonds with four other atoms.[8] The general structure of a silane coupling agent is presented in Figure 2.12A and contains a functional or reactive group at the end of an organic spacer. An alkyl chain is attached to the central silcon atom, which is connected to up to three hydrolyzable groups.

Silanes containing one carbon-silicon bond (CH_3) are called an organosilane. Oxide ceramics can be modified by functional groups as amino-groups [148-150], sulphonate-groups [151], alkyl-groups [152, 153], carboxyl-groups[154, 155] or fluorinated
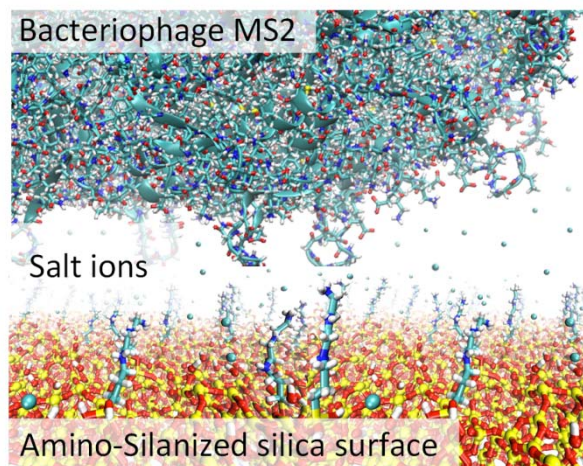
Figure 2.13. Simulated silica surface functionalized with the aminosilane TPDA used for the adsorption of bacteriophages MS2.[12]

groups [156] which are all available with a variety of spacer lengths.[147] Chemical spacers consist of carbon atoms and the spacer length is in a range between C3 (propyl) and C18 (octadecyl). Trimethoxysilanes (TMS) and triethoxysilanes (TES) are both used for silanization with methoxy and ethoxy groups as leaving groups.

Among the most commonly used silanes are aminosilanes, in particular 3-aminopropyltrimethoxysilane (APTMS) and 3-aminopropyltriethoxysilane (APTES), which have been studied for various applications, like protein adsorption[151], enzyme immobilization[132] or virus adsorption[31]. In the last years, aminosilanes with a more complex structure have been studied, for example n-2-aminoethyl-3-aminopropyltriethoxysilane (AE-APTES) with two amino-groups and a 7-atom spacer, n-(6-aminohexyl)-amniomethyltriethoxysilane (AH-AMTES) with two amino-groups and a 9-atom spacer or n-(3-trimethoxysylilpropyl)diethylenetriamine (TPDA) with three amino-groups and a 10-atom spacer. Examples of silanes are shown in Figure 2.12B. Furthermore, a simulated silica surface functionalized with the aminosilane TPDA used for the adsorption of bacteriophages is shown in Figure 2.13.

The silanization process is based on the hydrolysis-condensation reaction as shown in Figure 2.14. There are two main procedures for

the silanization of ceramic material. The first method, referred to as liquid phase method, is the immersion of the ceramic into a silane solution which can be based on aqueous media[132, 151] or organic solvents (e.g. ethanol, toluene, chloroform, acetone or xylene)[17, 157-159]. In the second procedure the ceramic is placed in a silane which is in the vapor phase.[160, 161] The choice of the reaction strategy is made by the ceramic type, the reactive group of the silane and the desired loading capacity. The method used in this study is the liquid phase method in an aqueous media.

The hydrolyzable alkoxy group of the silane molecule react with water, forming silanol groups (Si-OH) and alcohol molecules as byproduct. This activation by hydrolysis is carried out in presence of water, therefore when using an organic solvent for silanization it is mostly mixed with a small amount of water (1:5 to 1:10 vol.%). Some groups describe a silanization in water-free organic solvents as anhydrous toluene.[149, 162]

The silanol molecule condensates to a hydroxyl-activated surface bonding and water is released as a byproduct. A hydrogen bond (intermediate state) between the silanol molecule and the surface is formed. A condensation reaction, which usually requires heat or vacuum to remove water, results in a covalent bond of the silanes to the substrate surface.[8] One silane molecule is able to bond to one, two or even three hydroxyl groups on the ceramic surface under optimal conditions (no sterical hindering). Silanes can form a monolayer on the surface or they crosslink with already bound silanes and form multilayers.[163] Next to the solvent in which the silanization is carried out, the silane layer can be influenced by silane concentration, incubation time and temperature.[149] In general, higher incubation temperatures and longer incubation times result in a higher loading capacity. Temperature limits are given by the evaporation of the solvent and the stability of the silane, therefore temperatures in the range from RT to 90 °C are often used. After a certain point of time the silanization is completed and no further molecules can attach to the surface. Often, this saturation is achieved after 24 h of reaction
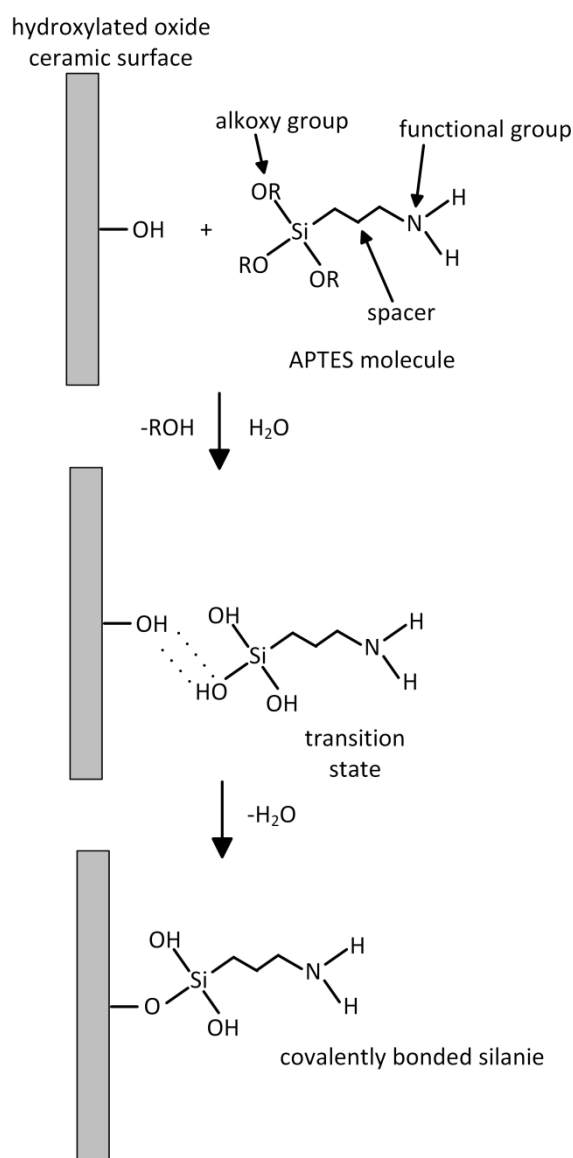
Figure 2.14. Hydrolysis-condensation reaction.

time.[149] The bond between the ceramic substrate and the silane layer can be strengthened by post-silanization heat-treatment.[164] Nevertheless, some studies show that there is a lack of stability of silanized surfaces under different conditions, in different aqueous media or over long time periods.[150, 162]

The loading capacity of functional groups on the ceramic surface can be analyzed by different analytical methods and measurement techniques. The most used methods for quantification are specific photometric assays like the acid-orange assay for the detection of amino groups[132, 165, 166], the thermogravimetric analysis (TGA)[167, 168] and

the X-ray photoelectron spectroscopy (XPS)[169, 170]. Methods which are used to estimate the loading capacity are IR spectroscopy[171, 172] or zeta potential/streaming potential measurements [151, 173]. Further information on characterization methods can be found in Chapter 3.

Non-Silane Functionalization

Next to silanization, even though less characterized and less widely applied, the functionalization with organophosphonates and phosphonates became of great interest for the modification of metal oxides in the last couple of years[174, 175]. Mono-, bi-, tri- or multidentate anchorages of phosphonates on the ceramic surface are possible. Compared to silanes, the condensation between the precursor molecules is significantly lower. Therefore, no cross-linking between individual phosphonate molecules occurs and homogenous monolayers are achieved.[176, 177]

The wide variety of organophosphonates with heteroatoms as fluorine, sulfur and chlorine is existing, therefore it is a versatile tool for functionalization. Functionalization with phosphonates are generally carried out in a wet-chemical process with water as a solvent or at low acid concentrations at temperatures around 100 °C for a few hours. The resulting bonds are more stable towards hydrolysis over a large pH range compared to those created by silanization, therefore phosphonates are a valuable alternative to silanes.[178] A disadvantage of phosphonates is that their stability depends on the metal oxide substrate structure, where it was shown that it is highly stable on alumina and zirconia and less stable on silica surfaces.[176, 179]

2.5 Virus Adsorption Mechanisms

Due to the high structural complexity of viruses, the understanding of virus-material interactions is challenging and not yet completely understood.[180]
The most important factors of virus adsorption to membranes are the chemical composition of the membrane surface, the ratio of membrane pore diameter to virus size, as well as the hydrophobic and electrostatic interactions.[181, 182] Additional forces based on e.g. viral shape, specific viral

24

surface properties or the conformation of the capsid were shown to only play a limited role in their adsorption behavior.[183, 184]

2.5.1 Electrostatic Interaction

Electrostatic interactions were demonstrated to play a dominant role in virus-material interactions.[182] At a neutral pH, most viruses are negatively charged as they show IEPs between 3.0 and 7.0 and are therefore able to adsorb to a positively charged membrane surface (IEP > 8).[108, 109, 185, 186] The thickness of the electrostatic double layer of both the virus particle and the membrane surface as described by the DLVO theory[187-190] is of importance for the adsorption behavior and can be influenced by pH or salt concentration. Lukasik et al.[191] showed that salt ions like $MgCl_2$ can promote, inhibit or have no effect on virus adsorption under different circumstances e.g. the filter type and the filtration conditions.

An improved virus removal can be provided by materials which show a positive surface charge at neutral pH. Ceramic materials can be modified by coating, doping or chemical surface functionalization. Metal oxyhydroxides e.g. $Y(OH)_x$, $Zr(OH)_x$ and $Mg(OH)_2$ are coated or doped on membranes to adjust the surface charge.[107-109] Surface modifications with iron oxide or zerovalent Fe is used to adsorb viruses.[186, 192, 193] Chemical functionalization approaches, especially with amino groups as accessible chemical surface functionalities are shown to provide a positive surface charge on silica and alumina particles for the adsorption of negatively charged viruses at neutral and acidic pH, respectively.[31, 194-196]

2.5.2 Hydrophobic Interaction

Hydrophobic interactions have a major influence on the adsorption of viruses. Hydrophobic surfaces have a preference to associate with each other in aqueous media, which is due to the high free energy of the interfacial solute layer of polar water molecules which are decreasing with a reduction of the water-exposed surface area.[197] Hydrophobic interactions are reported by several studies which investigated the virus filtration by

soil passages.[180, 198] For the retention of the bacteriophage MS2, the hydrophobic interactions play an important role as hydrophobic polymer membranes were found to be a better barrier than hydrophilic polymer membranes.[11, 35, 199] Even for relatively hydrophilic viruses like MS2 and PhiX174, the hydrophobic effect is important for adsorption.[200] Additionally, some salts can improve the effect on virus removal due to a better ordering of the water molecules and the promotion of the sequestering of the hydrophobic entities.[187]

References

1. ICTV. "ICTV 8th Report".
2. ICTV, Taxonomy Release History, Accessed 10.07.2017.
3. H. Salmang and H. Scholze, "Keramik", Springer, 2006.
4. H. Lutz, "Ultrafiltration for Bioprocessing", 2015.
5. G. Elssner, et al., "Ceramics and Ceramic Composites: Materialographic Preparation", Elsevier Science, 1999.
6. K. Ohlrogge and K. Ebert, in *Membranen; Grundlagen, Verfahren und industrielle Anwendungen*, ed. W.-V. V. G. C. KGaA, Weinheim, 2006.
7. J. Carter and V. Saunders, "Virology, Principles and Applications", 2007.
8. G. T. Hermanson, in *Bioconjugate Techniques (Second Edition)*, ed. G. T. Hermanson, Academic Press, New York, 2008, pp. 562-581.
9. W. Reitz. "Ceramic Processing and Sintering by M. N. Rahaman". *Mater Manuf Process*, 1997, 12, 555-556.
10. S. Deville. "Freeze-Casting of Porous Ceramics: A Review of Current Achievements and Issues". *Advanced Engineering Materials*, 2008, 10, 155-169.
11. E. Arkhangelsky and V. Gitis. "Effect of transmembrane pressure on rejection of viruses by ultrafiltration membranes". *Separation and Purification Technology*, 2008, 62, 619-628.
12. J. Bartels, et al. "Effect of divalent versus monovalent cations on the MS2 retention capacity of amino-functionalized ceramic filters". *Phys Chem Chem Phys*, 2018, 11215-11223.
13. S. Deville. "Freeze-Casting of Porous Biomaterials: Structure, Properties and Opportunities". *Materials*, 2010, 3, 1913.
14. G. Knott and C. Genoud. "Is EM dead?".

15. H. Leclerc, et al. "Bacteriophages as indicators of enteric viruses and public health risk in groundwaters". *Journal of Applied Microbiology*, 2000, 88, 5-21.
16. K. Nagayama and R. Danev. "Phase contrast electron microscopy: development of thin-film phase plates and biological applications". *Philosophical Transactions of the Royal Society B: Biological Sciences*, 2008, 363, 2153-2162.
17. S. Kroll, et al. "Colored ceramic foams with tailored pore size and surface functionalization used as spawning plates for fish breeding". *Ceramics International*, 2014, 40, 15763-15773.
18. M. De Paepe and F. Taddei. "Viruses' Life History: Towards a Mechanistic Basis of a Trade-Off between Survival and Reproduction among Phages". *Plos Biol*, 2006, 4, e193.
19. B. N. Fields, et al., "Fields' Virology", Wolters Kluwer Health/Lippincott Williams & Wilkins, 2007.
20. H. Cypionka, "Grundlagen der Mikrobiologie", Springer Berlin Heidelberg, 2010.
21. C. G. Golding, et al. "The scanning electron microscope in microbiology and diagnosis of infectious disease". *Sci Rep-Uk*, 2016, 6, 26516.
22. A. R. Studart, et al. "Processing Routes to Macroporous Ceramics: A Review". *Journal of the American Ceramic Society*, 2006, 89, 1771-1789.
23. L. R. Overby, et al. "Comparison of Two Serologically Distinct Ribonucleic Acid Bacteriophages I. Properties of the Viral Particles". *J Bacteriol*, 1966, 91, 442-448.
24. U. Scheithauer, et al. "Ceramic-Based 4D Components: Additive Manufacturing (AM) of Ceramic-Based Functionally Graded Materials (FGM) by Thermoplastic 3D Printing (T3DP)". *Materials*, 2017, 10, 1368.
25. B. Michen and T. Graule. "Isoelectric points of viruses". *Journal of Applied Microbiology*, 2010, 109, 388-397.
26. VIperdb.
27. J. Werner, et al. "Production of ceramic membranes with different pore sizes for virus retention". *Journal of Water Process Engineering*, 2014, 4, 201-211.
28. C. L. Heldt, et al. "Experimental and computational surface hydrophobicity analysis of a non-enveloped virus and proteins". *Colloids and Surfaces B: Biointerfaces*, 2017, 153, 77-84.
29. R. A. Villanueva, et al. "Interactions Between

Virus Proteins and Host Cell Membranes During the Viral Life Cycle". *International Review of Cytology*, 2005, 245, 171-244.

30. A. Duek, et al. "New and conventional pore size tests in virus-removing membranes". *Water Research*, 2012, 46, 2505-2514.

31. F. Meder, et al. "The role of surface functionalization of colloidal alumina particles on their controlled interactions with viruses". *Biomaterials*, 2013, 34, 4203-4213.

32. C. Dika, et al. "Impact of Internal RNA on Aggregation and Electrokinetics of Viruses: Comparison between MS2 Phage and Corresponding Virus-Like Particles". *Applied and Environmental Microbiology*, 2011, 77, 4939-4948.

33. C. M. Schaldach, et al. "The influence of ionic strength on the interaction of viruses with charged surfaces under environmental conditions". *Journal of Colloid and Interface Science*, 2006, 294, 1-10.

34. R. Attinti, et al. "Virus' (MS2, φX174, and Aichi) Attachment on Sand Measured by Atomic Force Microscopy and Their Transport through Sand Columns". *Environmental Science & Technology*, 2010, 44, 2426-2432.

35. C. D. Lytle and L. B. Routson. "Minimized virus binding for tests of barrier materials". *Applied and Environmental Microbiology*, 1995, 61, 643-649.

36. R. M. Chaudhry, et al. "Impact of virus surface characteristics on removal mechanisms within membrane bioreactors". *Water Research*, 2015, 84, 144-152.

37. U. Nations, ed. U. Nations, New York, 2012.

38. R. D. Arnone and J. P. Walling. "Waterborne pathogens in urban watersheds". *Journal of Water and Health*, 2007, 05.1, 149-162.

39. A. Bennett. "Maintaining the integrity of filtration systems". *Filtration & Separation*, 2005, 42, 30-33.

40. J. J. Simonis, et al. "Removal of microbes to World Health Organization requirements using a locally developed, low cost, micro-porous, ceramic water filter". *Journal of Water, Sanitation and Hygiene for Development*, 2014, 4, 620-624.

41. C. Charcosset, "Membrane Processes in Biotechnology and Pharmaceutics*"*, Elsevier, 2012.

42. W. H. Organization, ed. M. D. Sobsey, Geneva, 2002.

43. I. Bertrand, et al. "The impact of temperature on the inactivation of enteric viruses in food and water: a review". *Journal of Applied Microbiology*, 2012, 112, 1059-1074.

44. Y. Iijima, et al. "Prevention of Bacterial Diarrhea by Pasteurization of Drinking Water in Kenya". *Microbiol Immunol*, 2001, 45, 413-416.

45. R. Psutka, et al. "Assessing the Microbiological Performance and Potential Cost of Boiling Drinking Water in Urban Zambia". *Environmental Science & Technology*, 2011, 45, 6095-6101.

46. T. F. Clasen, et al. "Microbiological Effectiveness and Cost of Boiling to Disinfect Drinking Water in Rural Vietnam". *Environmental Science & Technology*, 2008, 42, 4255-4260.

47. W. A. M. Hijnen, et al. "Inactivation credit of UV radiation for viruses, bacteria and protozoan (oo)cysts in water: A review". *Water Research*, 2006, 40, 3-22.

48. Q. S. Meng and C. P. Gerba. "Comparative inactivation of enteric adenoviruses, poliovirus and coliphages by ultraviolet irradiation". *Water Research*, 1996, 30, 2665-2668.

49. S. Kelly and W. W. Sanderson. "The effect of chlorine in water on enteric viruses". *American Journal of Public Health*, 1958, 48, 1323-1334.

50. R. S. Engelbrecht, et al. "Comparative inactivation of viruses by chlorine". *Applied and Environmental Microbiology*, 1980, 40, 249-256.

51. G.-A. Shin and M. D. Sobsey. "Inactivation of norovirus by chlorine disinfection of water". *Water Research*, 2008, 42, 4562-4568.

52. C. M. M. Bougeard, et al. "Comparison of the disinfection by-product formation potential of treated waters exposed to chlorine and monochloramine". *Water Research*, 2010, 44, 729-740.

53. T. L. Cromeans, et al. "Inactivation of Adenoviruses, Enteroviruses, and Murine Norovirus in Water by Free Chlorine and Monochloramine". *Applied and Environmental Microbiology*, 2010, 76, 1028-1033.

54. H. Junli, et al. "Disinfection effect of chlorine dioxide on viruses, algae and animal planktons in water". *Water Research*, 1997, 31, 455-460.

55. K. R. Wigginton, et al. "Virus Inactivation Mechanisms: Impact of Disinfectants on Virus Function and Structural Integrity". *Environmental Science & Technology*, 2012, 46, 12069-12078.

56. K. Herbold, et al. "Comparison of ozone inactivation, in flowing water, of hepatitis A virus, poliovirus 1, and indicator organisms". *Applied and Environmental Microbiology*, 1989, 55, 2949-2953.

57. P. Xu, et al. "Wastewater disinfection by

ozone: main parameters for process design". *Water Research*, 2002, 36, 1043-1055.

58. G.-A. Shin and M. D. Sobsey. "Reduction of Norwalk Virus, Poliovirus 1, and Bacteriophage MS2 by Ozone Disinfection of Water". *Applied and Environmental Microbiology*, 2003, 69, 3975-3978.

59. H. Liltved, et al. "Inactivation of bacterial and viral fish pathogens by ozonation or UV irradiation in water of different salinity". *Aquacult Eng*, 1995, 14, 107-122.

60. H. S. Weinberg and W. H. Glaze. "An overview of ozonation disinfection by-products". *CRC Press*, 1996, 165-186.

61. M. A. Shannon, et al. "Science and technology for water purification in the coming decades". *Nature*, 2008, 452, 301-310.

62. S. Chernousova and M. Epple. "Silver as Antibacterial Agent: Ion, Nanoparticle, and Metal". *Angewandte Chemie International Edition*, 2013, 52, 1636-1653.

63. K. Mijnendonckx, et al. "Antimicrobial silver: uses, toxicity and potential for resistance". *Biometals*, 2013, 26, 609-621.

64. C. Marambio-Jones and E. M. V. Hoek. "A review of the antibacterial effects of silver nanomaterials and potential implications for human health and the environment". *J Nanopart Res*, 2010, 12, 1531-1551.

65. A. N. Kremer and H. Hoffmann. "Subtractive Hybridization Yields a Silver Resistance Determinant Unique to Nosocomial Pathogens in the Enterobacter cloacae Complex". *Journal of Clinical Microbiology*, 2012, 50, 3249-3257.

66. I. J. Davis, et al. "Isolation of silver- and antibiotic-resistant Enterobacter cloacae from teeth". *Oral Microbiology and Immunology*, 2005, 20, 191-194.

67. G. Larkin Mchugh, et al. "Salmonella typhimurium to silver nitrate, chloramphenicol, and ampicillin: a new threat in burn units?". *The Lancet*, 1975, 305, 235-240.

68. S. Silver. "Bacterial silver resistance: molecular biology and uses and misuses of silver compounds". *Fems Microbiol Rev*, 2003, 27, 341-353.

69. R. L. Davies and S. F. Etris. "The development and functions of silver in water purification and disease control". *Catalysis Today*, 1997, 36, 107-114.

70. N. Shirasaki, et al. "Comparison of behaviors of two surrogates for pathogenic waterborne viruses, bacteriophages Qβ and MS2, during the aluminum coagulation process". *Water Research*, 2009, 43, 605-612.

71. T. Matsushita, et al. "Effect of membrane pore size, coagulation time, and coagulant dose on virus removal by a coagulation-ceramic microfiltration hybrid system". *Desalination*, 2005, 178, 21-26.

72. T. Meyn, et al. "MS2 removal from high NOM content surface water by coagulation - ceramic microfiltration, for potable water production". *AIChE Journal*, 2012, 58, 2270-2281.

73. B. Zhu, et al. "Virus removal by iron coagulation–microfiltration". *Water Research*, 2005, 39, 5153-5161.

74. N. Shirasaki, et al. "Comparison of removal performance of two surrogates for pathogenic waterborne viruses, bacteriophage Qβ and MS2, in a coagulation–ceramic microfiltration system". *Journal of Membrane Science*, 2009, 326, 564-571.

75. C. T. Tanneru and S. Chellam. "Mechanisms of virus control during iron electrocoagulation – Microfiltration of surface water". *Water Research*, 2012, 46, 2111-2120.

76. B. Zhu, et al. "Comparison of electrocoagulation and chemical coagulation pretreatment for enhanced virus removal using microfiltration membranes". *Water Research*, 2005, 39, 3098-3108.

77. S. A. Tyrrell, et al. "Inactivation of bacterial and viral indicators in secondary sewage effluents, using chlorine and ozone". *Water Research*, 1995, 29, 2483-2490.

78. F. X. Abad, et al. "Disinfection of human enteric viruses in water by copper and silver in combination with low levels of chlorine". *Applied and Environmental Microbiology*, 1994, 60, 2377-2383.

79. J. Y. Kim, et al. "Enhanced inactivation of E. coli and MS-2 phage by silver ions combined with UV-A and visible light irradiation". *Water Research*, 2008, 42, 356-362.

80. B. Guo, et al. "Virus removal and inactivation in a hybrid microfiltration–UV process with a photocatalytic membrane". *Separation and Purification Technology*, 2015, 149, 245-254.

81. K. Sutherland, "Filters and Filtration Handbook (Fifth edition)″, 2008.

82. K. Nath, "Membrane separation processes″, New Delhi, 2008.

83. R. Sondhi, et al. "Applications and benefits of ceramic membranes". *Membrane Technology*, 2003, 2003, 5-8.

84. J. Finley. "Ceramic membranes: a robust filtration alternative". *Filtration & Separation*, 2005, 42, 34-37.

85. T. Melin and R. Rautenbach, "Membranverfahren, Grundlagen der Modul- und Anlagenauslegung″, 2007.

86. E. P. Garmash, et al. "Ceramic membranes for ultra- and microfiltration (Review)". *Glass and Ceramics*, 1995, 52, 150-152.

87. C. B. Carter and M. G. Norton, "Ceramic Materials, Science and Engineering*"*, New York, 2007.

88. S. S. Madaeni. "The application of membrane technology for water disinfection". *Water Research*, 1999, 33, 301-308.

89. S. J. Judd and S. W. Till. "Bacterial rejection in crossflow microfiltration of sewage". *Desalination*, 2000, 127, 251-260.

90. R. Wang, et al. "Nanofibrous microfiltration membranes capable of removing bacteria, viruses and heavy metal ions". *Journal of Membrane Science*, 2013, 446, 376-382.

91. Y. Wang, et al. "Quantification of the Filterability of Freshwater Bacteria through 0.45, 0.22, and 0.1 μm Pore Size Filters and Shape-Dependent Enrichment of Filterable Bacterial Communities". *Environmental Science & Technology*, 2007, 41, 7080-7086.

92. N. Muhammad, et al. "Ceramic Filter for Small System Drinking Water Treatment: Evaluation of Membrane Pore Size and Importance of Integrity Monitoring". *J Environ Eng*, 2009, 135, 1181-1191.

93. A. R. Bielefeldt, et al. "Bacterial treatment effectiveness of point-of-use ceramic water filters". *Water Research*, 2009, 43, 3559-3565.

94. S. M. Kumar and S. Roy. "Recovery of Water from Sewage Effluents using Alumina Ceramic Microfiltration Membranes". *Sep Sci Technol*, 2008, 43, 1034-1064.

95. J. J. Simonis and A. K. Basson. "Manufacturing a low-cost ceramic water filter and filter system for the elimination of common pathogenic bacteria". *Physics and Chemistry of the Earth, Parts A/B/C*, 2012, 50–52, 269-276.

96. T. Kristian Stevik, et al. "Retention and removal of pathogenic bacteria in wastewater percolating through porous media: a review". *Water Research*, 2004, 38, 1355-1367.

97. T. Urase, et al. "Effect of pore structure of membranes and module configuration on virus retention". *Journal of Membrane Science*, 1996, 115, 21-29.

98. S. M. Krivobok, et al. "Disinfecting water by means of microfiltration membranes". *Soviet Journal of Wtaer Chemistry and Technology*, 1986, 8 (4), 112-115.

99. T. A. Grein, et al. "Membrane Supported Virus Separation from Biological Solutions". *Chemie Ingenieur Technik*, 2013, 85, 1183-1192.

100. T. Burnouf and M. Radosevich. "Nanofiltration of plasma-derived biopharmaceutical products". *Haemophilia*, 2003, 9, 24-37.

101. B. F. Marques, et al. "Virus filtration of high-concentration monoclonal antibody solutions". *Biotechnology Progress*, 2009, 25, 483-491.

102. G. Walsh. "Biopharmaceutical benchmarks 2010". *Nat Biotech*, 2010, 28, 917-924.

103. T. Hongo-Hirasaki, et al. "Effect of antibody solution conditions on filter performance for virus removal filter Planova™ 20N". *Biotechnology Progress*, 2010, 26, 1080-1087.

104. R. Aronino, et al. "Removal of viruses from surface water and secondary effluents by sand filtration". *Water Research*, 2009, 43, 87-96.

105. M. D. Sobsey, et al. "Point of Use Household Drinking Water Filtration: A Practical, Effective Solution for Providing Sustained Access to Safe Drinking Water in the Developing World". *Environmental Science & Technology*, 2008, 42, 4261-4267.

106. A. M. ElHadidy, et al. "An evaluation of virus removal mechanisms by ultrafiltration membranes using MS2 and φX174 bacteriophage". *Separation and Purification Technology*, 2013, 120, 215-223.

107. M. Wegmann, et al. "Nanostructured surface modification of microporous ceramics for efficient virus filtration". *Journal of the European Ceramic Society*, 2008, 28, 1603-1612.

108. M. Wegmann, et al. "Modification of ceramic microfilters with colloidal zirconia to promote the adsorption of viruses from water". *Water Research*, 2008, 42, 1726-1734.

109. B. Michen, et al. "Improved Virus Removal in Ceramic Depth Filters Modified with MgO". *Environmental Science & Technology*, 2013, 47, 1526-1533.

110. M. Peter-Varbanets, et al. "Decentralized systems for potable water and the potential of membrane technology". *Water Research*, 2009, 43, 245-265.

111. C. Piconi and G. Maccauro. "Zirconia as a ceramic biomaterial". *Biomaterials*, 1999, 20, 1-25.

112. R. C. Garvie, et al. "Ceramic steel?". *Nature*, 1975, 258, 703-704.

113. J. Chevalier, et al. "Critical effect of cubic phase on aging in 3 mol% yttria-stabilized zirconia ceramics for hip replacement prosthesis". *Biomaterials*, 2004, 25, 5539-5545.

114. M. V. Swain. "Processing of ceramics, Parts I and II. edited by R. J. Brook, Volume 17 of materials science and technology-A

comprehensive treatment, edited by R. W. Cahn, P. Haasen, E. J. Kramer, VCH, Weinheim 1996, Volume 17A, xix, 405 pp., hardcover, DM 380.00, ISBN 3-527-26830-8; Volume 17B, xix, 378 pp., hardcover, DM 380.00, ISBN 3-527-29356-6". *Advanced Materials*, 1997, 9, 442-443.

115. F. Händle, "Extrusion in Ceramics″, Springer Berlin Heidelberg, 2007.

116. D. Bortzmeyer, in *Ceramic Processing*, eds. R. A. Terpstra, P. P. A. C. Pex and A. H. de Vries, Springer Netherlands, Dordrecht, 1995, pp. 102-146.

117. R. W. Rice, "Ceramic Fabrication Technology″, CRC Press, 2002.

118. P. Boch and J. C. Nièpce, "Ceramic Materials: Processes, Properties, and Applications″, Wiley, 2010.

119. R. M. German, in *Sintering: from Empirical Observations to Scientific Principles*, ed. R. M. German, Butterworth-Heinemann, Boston, 2014, pp. 183-226.

120. S. Somiya, et al., "Handbook of Advanced Ceramics: Materials, Applications, Processing and Properties″, Elsevier Science, 2003.

121. R. Riedel and I. W. Chen, "Ceramics Science and Technology, Volume 3: Synthesis and Processing″, Wiley, 2008.

122. S. Barg, et al. "Cellular Ceramics by Direct Foaming of Emulsified Ceramic Powder Suspensions". *Journal of the American Ceramic Society*, 2008, 91, 2823-2829.

123. S. Barg, et al. "New cellular ceramics from high alkane phase emulsified suspensions (HAPES)". *Journal of the European Ceramic Society*, 2009, 2439-2446.

124. J. P. Kruth, et al. "Progress in Additive Manufacturing and Rapid Prototyping". *CIRP Annals*, 1998, 47, 525-540.

125. T. Ohji and M. Fukushima. "Macro-porous ceramics: processing and properties". *International Materials Reviews*, 2012, 57, 115-131.

126. K. Gotoh, et al. "Pore size distributions in random assemblies of equal spheres". *The Journal of Chemical Physics*, 1986, 85, 3078-3080.

127. H. Tamura, et al. "Mechanism of Hydroxylation of Metal Oxide Surfaces". *Journal of Colloid and Interface Science*, 2001, 243, 202-207.

128. V. Dugas and Y. Chevalier. "Surface hydroxylation and silane grafting on fumed and thermal silica". *Journal of Colloid and Interface Science*, 2003, 264, 354-361.

129. N. Eils, et al. "High-Temperature Hydroxylation and Surface Corrosion of 2/1-Mullite Single Crystals in Water Vapor Environments". *Journal of the American Ceramic Society*, 2006, 89, 2887-2894.

130. R. Leboda, et al. "Peculiarities of steam-phase hydrothermal modification of pyrogenic silicium dioxide". *Colloids and Surfaces A: Physicochemical and Engineering Aspects*, 1998, 135, 253-265.

131. E. M. Moser, et al. "Surface analytical study of hydrothermally treated zirconia ceramics". *Fresenius' Journal of Analytical Chemistry*, 1993, 346, 255-260.

132. S. Kroll, et al. "Highly Efficient Enzyme-Functionalized Porous Zirconia Microtubes for Bacteria Filtration". *Environmental Science & Technology*, 2012, 46, 8739-8747.

133. L. Bónová, et al. "Atmospheric pressure plasma treatment of flat aluminum surface". *Applied Surface Science*, 2015, 331, 79-86.

134. C. Tendero, et al. "Atmospheric pressure plasmas: A review". *Spectrochimica Acta Part B: Atomic Spectroscopy*, 2006, 61, 2-30.

135. D. M. Mattox. "Surface cleaning in thin film technology". *Thin Solid Films*, 1978, 53, 81-96.

136. H. Steffen, et al. "Process control of RF plasma assisted surface cleaning". *Thin Solid Films*, 1996, 283, 158-164.

137. A. N. Rider, et al. "Low-power r.f. plasma oxidation of aluminium". *Surface and Interface Analysis*, 2001, 31, 302-312.

138. J. F. O'Hanlon. "Factors Affecting the Growth Rate of Plasma A nodi zed Al2 O 3". *Journal of The Electrochemical Society*, 1971, 118, 270-273.

139. J. M. Kim, et al. "Control of hydroxyl group content in silica particle synthesized by the sol-precipitation process". *Ceramics International*, 2009, 35, 1015-1019.

140. H. Fischer, et al. "Bioactivation of inert alumina ceramics by hydroxylation". *Biomaterials*, 2005, 26, 6151-6157.

141. U. Lohbauer, et al. "Hydroxylation of dental zirconia surfaces: Characterization and bonding potential". *Journal of Biomedical Materials Research Part B: Applied Biomaterials*, 2008, 87B, 461-467.

142. C.-C. Li, et al. "Efficient hydroxylation of BaTiO3 nanoparticles by using hydrogen peroxide". *Colloids and Surfaces A: Physicochemical and Engineering Aspects*, 2010, 361, 143-149.

143. X. Zhao, et al. "Acid-induced bioactive titania surface". *J Biomed Mater Res A*, 2005, 75A, 888-894.

144. R. E. Black, et al. "Where and why are 10 million children dying every year?". *The Lancet*, 2003, 361, 2226-2234.

145. K. K. Unger, et al. "Impact of acidic/hydrothermal treatment on pore

structural and chromatographic properties of porous silicas". *Journal of Chromatography A*, 1991, 556, 395-406.

146. C. Y. K. Lung, et al. "Surface modification of silica-coated zirconia by chemical treatments". *Applied Surface Science*, 2010, 257, 1228-1235.

147. L. Treccani, et al. "Review: Functionalized ceramics for biomedical, biotechnological and environmental applications". *Acta Biomaterialia*, 2013, 9, 7115-7150.

148. S. Kroll, et al. "Development and characterisation of functionalised ceramic microtubes for bacteria filtration". *Journal of Membrane Science*, 2010, 365, 447-455.

149. J. A. Howarter and J. P. Youngblood. "Optimization of Silica Silanization by 3-Aminopropyltriethoxysilane". *Langmuir*, 2006, 22, 11142-11147.

150. E. Asenath Smith and W. Chen. "How To Prevent the Loss of Surface Functionality Derived from Aminosilanes". *Langmuir*, 2008, 24, 12405-12409.

151. F. Meder, et al. "Protein adsorption on colloidal alumina particles functionalized with amino, carboxyl, sulfonate and phosphate groups". *Acta Biomaterialia*, 2012, 8, 1221-1229.

152. A. Y. Ku, et al. "Evidence of Ion Transport through Surface Conduction in Alkylsilane-Functionalized Nanoporous Ceramic Membranes". *Langmuir*, 2006, 22, 8277-8280.

153. J. R. Stephens, et al. "Diffusive flux of nanoparticles through chemically modified alumina membranes". *Analyst*, 2011, 136, 3797-3802.

154. G. K. Toworfe, et al. "Nucleation and growth of calcium phosphate on amine-, carboxyl- and hydroxyl-silane self-assembled monolayers". *Biomaterials*, 2006, 27, 631-642.

155. F. Meder, et al. "Controlling Mixed-Protein Adsorption Layers on Colloidal Alumina Particles by Tailoring Carboxyl and Hydroxyl Surface Group Densities". *Langmuir*, 2013, 29, 12502-12510.

156. G. D. Bothun, et al. "Role of tail chemistry on liquid and gas transport through organosilane-modified mesoporous ceramic membranes". *Journal of Membrane Science*, 2007, 301, 162-170.

157. H. J. Kim, et al. "Enhancement of mechanical properties of aluminium/epoxy composites with silane functionalization of aluminium powder". *Composites Part B: Engineering*, 2012, 43, 1743-1748.

158. M. Moritz and M. Łaniecki. "SBA-15 mesoporous material modified with APTES

as the carrier for 2-(3-benzoylphenyl)propionic acid". *Applied Surface Science*, 2012, 258, 7523-7529.

159. L. A. S. A. Prado, et al. "Surface modification of alumina nanoparticles with silane coupling agents". *Journal of the Brazilian Chemical Society*, 2010, 21, 2238-2245.

160. H. Weetall. "Preparation of immobilized proteins covalently coupled through silane coupling agents to inorganic supports". *Applied Biochemistry and Biotechnology*, 1993, 41, 157-188.

161. S. Fiorilli, et al. "Vapor-phase self-assembled monolayers of aminosilane on plasma-activated silicon substrates". *Journal of Colloid and Interface Science*, 2008, 321, 235-241.

162. M. Zhu, et al. "How To Prepare Reproducible, Homogeneous, and Hydrolytically Stable Aminosilane-Derived Layers on Silica". *Langmuir*, 2012, 28, 416-423.

163. M. D. K. Ingall, et al. "Surface Functionalization and Imaging Using Monolayers and Surface-Grafted Polymer Layers". *Journal of the American Chemical Society*, 1999, 121, 3607-3613.

164. P. H. Corazza, et al. "Effect of Post-silanization Heat Treatments of Silanized Feldspathic Ceramic on Adhesion to Resin Cement". *Journal of Adhesive Dentistry*, 2013, 15(5), 473-479.

165. A. Andrzejewska, et al. "Adsorption of organic dyes on the aminosilane modified TiO2 surface". *Dyes and Pigments*, 2004, 62, 121-130.

166. A. M. Donia, et al. "Effect of structural properties of acid dyes on their adsorption behaviour from aqueous solutions by amine modified silica". *Journal of Hazardous Materials*, 2009, 161, 1544-1550.

167. V. Cauda, et al. "Bio-degradation study of colloidal mesoporous silica nanoparticles: Effect of surface functionalization with organo-silanes and poly(ethylene glycol)". *Microporous and Mesoporous Materials*, 2010, 132, 60-71.

168. B. Besser, et al. "A comparative experimental study on the deviation of the ideal selectivity in HDTMS-functionalized and untreated ceramic structures with pores in the upper mesoporous range". *Microporous and Mesoporous Materials*, 2015, 217, 253-261.

169. C. Picard, et al. "Characterisation of hydrophilic ceramic membranes modified by fluoroalkylsilanes into hydrophobic membranes". *Solid State Sciences*, 2004, 6, 605-612.

170. T. Yokoi, et al. "Amino-functionalized mesoporous silica as base catalyst and adsorbent". *Applied Catalysis A: General*, 2012, 421–422, 14-37.

171. V. Sunkara and Y.-K. Cho. "Aminosilane layers on the plasma activated thermoplastics: Influence of solvent on its structure and morphology". *Journal of Colloid and Interface Science*, 2013, 411, 122-128.

172. N. A. Ahmad, et al. "Membranes with Great Hydrophobicity: A Review on Preparation and Characterization". *Separation & Purification Reviews*, 2015, 44, 109-134.

173. E. Soto-Cantu, et al. "Synthesis and Rapid Characterization of Amine-Functionalized Silica". *Langmuir*, 2012, 28, 5562-5569.

174. D. Carrière, et al. "Modification of the Surface Properties of Porous Nanometric Zirconia Particles by Covalent Grafting". *Langmuir*, 2004, 20, 3449-3455.

175. E. J. Juárez-Pérez, et al. "Anchoring of Phosphorus-Containing Cobaltabisdicarbollide Derivatives to Titania Surface". *Langmuir*, 2010, 26, 12185-12189.

176. M.-A. Neouze and U. Schubert. "Surface Modification and Functionalization of Metal and Metal Oxide Nanoparticles by Organic Ligands". *Monatshefte für Chemie - Chemical Monthly*, 2008, 139, 183-195.

177. S. Pawsey, et al. "Self-Assembly of Carboxyalkylphosphonic Acids on Metal Oxide Powders". *Langmuir*, 2002, 18, 5205-5212.

178. N. Adden, et al. "Phosphonic Acid Monolayers for Binding of Bioactive Molecules to Titanium Surfaces". *Langmuir*, 2006, 22, 8197-8204.

179. P. H. Mutin, et al. "Hybrid materials from organophosphorus coupling molecules". *Journal of Materials Chemistry*, 2005, 15, 3761-3768.

180. J. F. Schijven and S. M. Hassanizadeh. "Removal of Viruses by Soil Passage: Overview of Modeling, Processes, and Parameters". *Crit Rev Env Sci Tec*, 2000, 30, 49-127.

181. S. S. Madaeni, et al. "Virus removal from water and wastewater using membranes". *Journal of Membrane Science*, 1995, 102, 65-75.

182. J. A. Redman, et al. "Filtration of Recombinant Norwalk Virus Particles and Bacteriophage MS2 in Quartz Sand: Importance of Electrostatic Interactions". *Environmental Science & Technology*, 1997, 31, 3378-3383.

183. C. V. Chrysikopoulos and V. I. Syngouna. "Attachment of bacteriophages MS2 and ΦX174 onto kaolinite and montmorillonite: Extended-DLVO interactions". *Colloids and Surfaces B: Biointerfaces*, 2012, 92, 74-83.

184. S. Chattopadhyay and R. W. Puls. "Forces dictating colloidal interactions between viruses and soil". *Chemosphere*, 2000, 41, 1279-1286.

185. J. Bartels, et al. "Amino-Functionalized Ceramic Capillary Membranes for Controlled Virus Retention". *Environmental Science & Technology*, 2016.

186. I. Bradley, et al. "Iron oxide amended biosand filters for virus removal". *Water Research*, 2011, 45, 4501-4510.

187. C. P. Gerba. "Applied and Theoretical Aspects of Virus Adsorption to Surfaces". *Advances in Applied Microbiology*, 1984, 30, 133-168.

188. H. Cao, et al. "Salinity and Soluble Organic Matter on Virus Sorption in Sand and Soil Columns". *Ground Water*, 2010, 48, 42-52.

189. S. K. Dishari, et al. "Effects of solution conditions on virus retention by the Viresolve® NFP filter". *Biotechnology Progress*, 2015, 31, 1280-1286.

190. I. C. Bourg and G. Sposito. "Molecular dynamics simulations of the electrical double layer on smectite surfaces contacting concentrated mixed electrolyte (NaCl–CaCl2) solutions". *Journal of Colloid and Interface Science*, 2011, 360, 701-715.

191. J. Lukasik, et al. "Influence of Salts on Virus Adsorption to Microporous Filters". *Applied and Environmental Microbiology*, 2000, 66, 2914-2920.

192. Y. You, et al. "Removal and Inactivation of Waterborne Viruses Using Zerovalent Iron". *Environmental Science & Technology*, 2005, 39, 9263-9269.

193. C. Shi, et al. "Removal of viruses and bacteriophages from drinking water using zero-valent iron". *Separation and Purification Technology*, 2012, 84, 72-78.

194. R. Cademartiri, et al. "Immobilization of bacteriophages on modified silica particles". *Biomaterials*, 2010, 31, 1904-1910.

195. Z. Chen, et al. "Capture and release of viruses using amino-functionalized silica particles". *Anal Chim Acta*, 2006, 569, 76-82.

196. K. S. Zerda, et al. "Adsorption of viruses to charge-modified silica". *Applied and Environmental Microbiology*, 1985, 49, 91-95.

197. J. N. Israelachvili, "Intermolecular and Surface Forces", Elsevier Science, 2015.

198. H. Zhang, et al. "Removal of bacteriophages MS2 and phiX174 from aqueous solutions using a red soil". *Journal of Hazardous Materials*, 2010, 180, 640-647.

199.   E. M. van Voorthuizen, et al. "Role of hydrophobic and electrostatic interactions for initial enteric virus retention by MF membranes". *Journal of Membrane Science*, 2001, 194, 69-79.

200.   R. C. Bales, et al. "Bacteriophage adsorption during transport through porous media: chemical perturbations and reversibility". *Environmental Science & Technology*, 1991, 25, 2088-2095.

3. Experimental Methods and Principles

In Table 3.1 is an overview of the characterization methods used in this work. Furthermore, it shows the chapter where to find the results of a characterization method for a specific sample types.

3.1 Helium Pycnometry

The true or real density (δ) is defined as the mass (m) divided by the volume of the sample (V_{sample})[1]:

$$\delta = \frac{m}{V_{sample}}$$ (3.1)

The helium pycnometer can measure the true density by fluid displacement of a solid.[3] A pycnometer consists of two measurement chambers with defined volume. The first chamber (V_1) is the sample holder and the second chamber (V_2) serves as reference. First, the chambers were evacuated and a defined helium pressure (p_1) is applied to the sample chamber. Helium is used as gas, as it is inert and due to its small size it can even enter the smallest pores of a sample. A pressure balance (p_2) occurs and the equilibrium pressure between the sample and the reference chamber is determined. The sample volume can be calculated by the following equation:

$$V_{sample} = V_1 - V_2 \cdot \frac{p_2}{p_1 - p_2}$$ (3.2)

In this work the measurements are performed with Pycnomatic ATC (Thermo Scientific, Italy) at 20 °C ± 0.01 °C. According to the manufacturer the accuracy and reproducibility is better than 0.01 % on the sample volume.[4]

3.2 Acoustic Spectroscopy

The methods for the determination of the particle size distribution and the average particle size (d_{50}-values) of a powder can be divided into three groups.
In the first group the particle size is determined by the separate counting of single particles for example in microscopic image analysis, where every single particle is measured and therefore the particle size distribution can only be determined when analyzing a high count of particles. The second group of methods fractionates the particles, for example by sieving which is not suitable for particles in the nm range. The third group determines the particle size indirectly for example by light scattering or acoustic spectroscopy. The acoustic spectroscopy is used in this work for evaluating the powder size and therefore described in detail in the following section.

Acoustic spectroscopy uses ultra sound waves of frequencies typically between 1 and 150 MHz which are applied to a solution containing the to be measured particles. The solid content of the solution can vary between 0.5 and 50 vol.%.[5] An ultrasonic transducer transmitted the sound waves through the concentrated suspension and another transducer receives the attenuated waves. The attenuation happens because of the wave interaction with the liquid medium and the dispersed particles. Each particle is responsible for discontinuities by diffraction and reflection or thermal and viscous effects which are caused by the pulsation and oscillation of particles.[6] The ultra sound attenuation spectrum is determined and can be fitted to a particular theoretical model when the physical properties of the system are known. The particle size can be evaluated from this fit.[7] Particle sizes between 0.01 and 1000 μm can be determined by acoustic spectroscopy in relatively short times (typically a few minutes).[5]
In this work, particle size distributions and average particle sizes were determined by using the DT 1200 (Dispersion Technology Inc., USA). A ceramic suspensions containing 1 vol.% particles at pH 3 was used to ensure a stable suspension, due to the IEP of ~7-9 for YSZ.[8] Before the acoustic spectroscopy, an ultrasonic treatment was applied to the ceramic suspension for 10 min at 240 W with a pulse rate of 0.5 s (ultrasonic finger, Branson Sonifier 450, Heinemann, Germany) to deagglomerate the powder.

Table 3.1. Overview of the characterization methods and their characteristics used for specific sample types. The results are presented in the named chapters.

Characterization method	Characteristic	Sample type and chapter				
		YSZ powder	Sintered capillary	Activated capillary	Aminosilanized capillary	Hydrophobic capillary
Helium pycnometry	Density	4	4			
Acoustic spectroscopy	Particle size	4				
Nitrogen adsorption/desorption - BET	Specific surface area	4	4	5	5	7
Zeta-Potential measurement	Isoelectric point Electrokinetic potential	4	5	5	5	7
Transmission electron microscopy - TEM	Particle visualization	4, A1				
Optical microscopy	Shrinkage determination		4			
Mercury Intrusion Porosimetry	Average pore size Porosity Pore size distribution		4	5	5	7
Scanning electron microscopy - SEM	Microstructure visualization		4	5, A2	5, A2	7
3-point bending test	Bending strength Weibull modulus		4	5	5	7
Membrane flux measurement	Water permeate flux		4	5	5	7
Virus retention test in dead-end mode	Virus retention		4	5	5	7
Pressure: 0.5 bar Feed: 0.02 M $MgCl_2$/0.15 M NaCl, pH 5.8 Permeate volume: 15 mL Phage: MS2 ($\sim10^9$ PFU/mL)			4	5	5	7
Pressure: 0.5 bar Feed: 0.02 M $MgCl_2$/0.15 M NaCl, pH 5.8 Permeate volume: 15 mL Phage: Phix174 ($\sim10^9$ PFU/mL)			4			7
Pressure: 0.5 bar Feed: 0.02 M $MgCl_2$/0.15 M NaCl, pH 5.8 Filtration time: 14 days Phage: MS2 ($\sim10^9$ PFU/mL)			4			

|				
Particularities: with backflushing				
Pressure: 0.5 bar Feed: 0.02 M $MgCl_2$/0.15 M NaCl, pH 5.8 Filtration time: 4 days Phage: MS2 ($\sim 10^9$ PFU/mL) Particularities: with membrane regeneration			5	
Pressure: 0.5 bar Feed: based on different salt solutions, pH 5.8 Permeate volume: 15 mL Phage: MS2 ($\sim 10^9$ PFU/mL)			6	7
Pressure: 0.5 bar Feed: based on different salt solutions, pH 5.8 Permeate volume: 15 mL Phage: PhiX174 ($\sim 10^9$ PFU/mL)				7
Pressure: 0.5 bar Feed: 0.02 M $MgCl_2$/0.15 M NaCl, pH 3 - 12 Permeate volume: 15 mL Phage: MS2 and PhiX174 ($\sim 10^9$ PFU/mL)				7
Pressure: 0.5 - 2.5 bar Feed: 0.02 M $MgCl_2$/0.15 M NaCl, pH 5.8 Permeate volume: 15 mL Bacteriophage: MS2 and PhiX174 ($\sim 10^9$ PFU/mL)				7
Acid Orange II Assay	Quantification of silane loading		5	
Leaching test	Silane stability		5	7
Molecular dynamic simulations	Atomistic scale analysis		6	
Water contact angle	Wettability	7		7
Thermogravimetric analysis	Quantification of silane loading	7		7
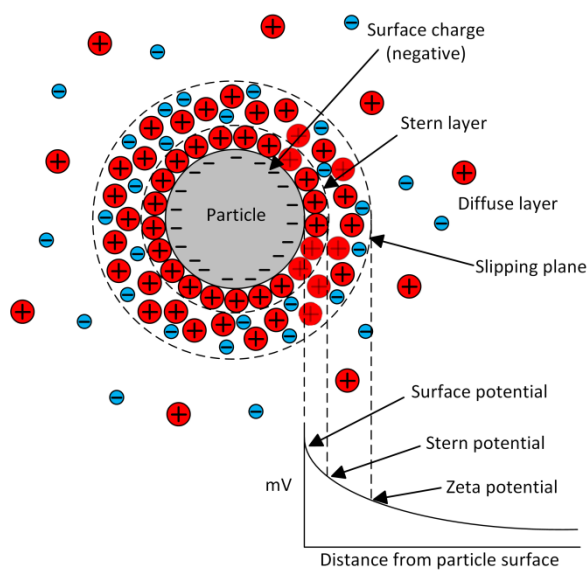
Figure 3.1. Model of the electric double layer of a charged colloidal particle in an aqueous media.

3.3 Nitrogen Adsorption/Desorption - BET Method

The specific surface area (SSA) defines the surface area of the pores in a porous material and is based on the mass (S) or the bulk volume (S_{bulk}). To determine the SSA, a nitrogen adsorption measurement has to be performed and the data have to be analyzed by the BET method. The BET method is named after Stephen Brunauer, Paul Hugh Emmett and Edward Teller who published the theory in 1938.[9]

BET is a technique where gaseous nitrogen is adsorbed and desorbed on a solid material at very low temperatures. The gas adsorption can be determined either gravimetrically or volumetrically. The solid material is cooled down to -196 °C in liquid nitrogen, while the pressure is reduced. To record the adsorption isotherm, nitrogen gas is stepwise filled into the sample chamber. The gas pressure is stepwise increased to the saturation vapor pressure of 103 kPa (1 atm). At each measuring step, the adsorbed amount of gas on the sample is measured by the gas which was filled into the sample cell and the amount of unadsorbed gas. In the equilibrium state, nitrogen molecules adsorb to the solid material proportional to the gas pressure.[10] Therefore, the obtained isotherms show the

36

adsorbed nitrogen depending on the nitrogen pressure at a standard temperature (77K - boiling temperature of nitrogen) and standard pressure (101.3 kPa - vapor pressure of nitrogen at -196 °C).[11] For the desorption isotherm, the pressure of the gas in the sample cell is stepwise reduced. To determine the SSA from a measured nitrogen adsorption isotherm the BET method is the standard approach.

The adsorbed gas can be calculated by the following equation:

$$S_{BET} = \frac{V_m N_A a \rho}{M}$$

(3.3)

The BET surface area (S_{BET}) is the product of the volume of nitrogen molecules forming a monolayer (V_m), the Avogadro constant ($N_A=6.022\cdot 10^{23}$ mol^{-1})[10], the required space of a nitrogen molecule ($a=0.162$ nm²), the ratio of density (ρ) and the molecular weight of the adsorbate (M).[1]

In this work, the specific surface area of samples was determined by nitrogen adsorption with a BELSORP-mini II (Bel Japan Inc., Japan) according to BET method after degassing the capillaries for at least 3 h at 120 °C and reduced pressure (< 2 Pa) followed by cooling to RT under argon for 30 min. The measurement was carried out at liquid nitrogen temperature in a standard sample cell with around 1.8 cm³ of volume. The adsorption was performed until a set point for the relative pressure (p/p_0) of 0.6 was reached. The minimum relative set pressure for desorption was 0.3. The first measurement point was around 60 Pa. The resolution of the pressure sensors is ~4 Pa and the accuracy is 0.25 %.[12] The device is suitable for materials with specific surface areas >0.01 m²/g.

3.4 Zeta Potential Measurement

The surface charge of particles creates an electric field in an aqueous medium (see Figure 3.1), which attracts a layer of oppositely charged counter-ions around the particle. This is called the electric double layer, which compensates the particles' surface charge.[13] The first layer, the Stern or Helmholtz layer, is based on counter-

ions which are adsorbed on the particle surface, but do not entirely neutralize the charge of the colloid.[14] The excess charge gives rise to the second layer, the diffuse layer or Gouy-Chapman layer, which is based on mobile counter- and co-ions.[14, 15] The ion concentration is maximal on the particle surface and decays linearly in the Stern layer and exponentially in the diffuse layer. The zeta potential is the potential at the shear plane at the outer periphery of the Stern layer and is a function of the pH of the medium.[14] The pH at which the zeta potential of a colloidal particle is zero, is called the isoelectric point (IEP).

In this work, zeta potential measurements with suspensions containing 1 vol.% particles were performed with DT 1200 (Dispersion Technology Inc., USA) to determine the IEPs of the YSZ powders. The pH titration was carried out with an integrated titration unit using 1 M HCl or 1 M KOH. A zeta potential probe of the DT1200 transmits an acoustic wave (typical between 2 and 10 MHz) into a stirred particle suspension, which leads to a particle motion relative to the liquid medium.[16] The particle motion causes a rearrangement of the double layer which surrounds the particle and induces a dipole moment and an electric field. An electric current is generated by the sum of the electric fields of all particles in the suspension, the so-called colloidal vibration current (CVI).[16] A transducer in the zeta potential probe receives the CVI. Based on the known particle concentration, the size, the density and the properties of the liquid medium the zeta potential can be calculated from the measured CVI.

The surface properties of the sintered, activated and amino-silanized capillary membranes were examined with a self-made streaming potential equipment at the Institute of Electronic- and Sensor-Materials at the TU Bergakademie Freiberg, Germany. For the measurement a gear pump transported a KCl electrolyte solution with molarities between 10 and 3 M (25 °C) from a beaker to the measuring cell. The conductivity, the temperature and the pH of the solution is measured. The pH is adjusted from pH 9 to pH 3 automatically with either 0.05 M KOH or HCl. The pressure difference and the potential

difference is measured along (overflow measurement) or across (throughflow measurement) the capillaries. Therefore Ag/AgCl-electrodes are placed at the inlet and the outlet of the electrolyte flow inside the capillary. A third electrode is placed into the permeate. The applied pressure was increased from 0 bar to a differential pressure of 0.5 bar for the overflow measurements and to a trans-capillary pressure difference of 1.2 bar for the throughflow measurements. After the pressure increase (upward measurement) and a plateau measurement at 0.5 or 1.2 bar, the pressure was reduced again (downward measurement) under streaming potential measurement. The streaming potential coefficient ($\Delta U/\Delta p$) was calculated by the slope of the linear pressure.

The zeta potential (ζ-potential) of the capillary surface is calculated by the Helmholtz-Smoluchowski equation

$$\xi = \frac{\Delta U}{\Delta p}\left(\frac{\eta}{\varepsilon_0 \varepsilon_r}\right)\kappa$$

(3.4)

where Δp is the hydraulic pressure, ε_0 is the permittivity of vacuum, ε_r is the relative permittivity of the solvent, η is the viscosity of the solution and κ is the conductivity of the solution.

The surface properties of the hydrophobic capillary membranes were analyzed by a SurPASS apparatus (Anton Paar, Germany) under the same measuring conditions used for the capillaries measured at the TU Bergakademie Freiberg. The main difference is the usage of crushed capillaries, therefore no overflow and throughflow mode was measured.

3.5 Microscopy Techniques

Microscopy is used to view objects or areas of objects, respectively, that cannot be seen by the human eye. Electromagnetic radiation or electron beams can interact with a ceramic sample in many ways, e.g. by reflection, absorption, refraction or diffraction.[17] The image is e.g. created by collecting the scattered radiation.

Visible-light microscopy, often referred to as optical microscopy, is used since the 18th century

and is still in use today. Visible light is transmitted or reflected from the sample surface and passed through a single lens or a multi lenses system to see a magnification of the sample. The magnification of this microscopic technique can range up to 50.000x with a resolution up to 250 nm, when using a high-tech device.[17] In this work the sintering shrinkage was determined by measuring the outer and inner diameter of the capillary membranes by optical microscopy (VHX-600DSO, Keyence). For each capillary type ten samples were tested for statistical significance.

Scanning electron microcopy (SEM) is capable of imaging details of a sample in the sub-nanometer range by scanning the surface with a focused beam of electrons.[18] Electrons that strike a sample surface can produce a wide range of interactions which causes various charged particles and photons.[18] The emitted ones can be collected and used to form an image of the surface topography. The resolution of a SEM is around 2.5 nm[17], which is much higher compared to the visible-light microscopy. Another advantage of the SEM is, that it has a much greater depth of field, which let images appear more three-dimensional.[17] The capillaries were analyzed by SEM (Field-emission SEM SUPRA 40, Zeiss, Germany) to visualize the microstructure of the outer capillary surface and to check the presence of potential macro- and microdefects.

Transmission electron microscopy (TEM) is a microscopy technique where an electron beam is transmitted through an ultrathin ("transparent") sample (< 100 nm).[19] Both techniques, SEM and TEM, are based on electron beams, but SEM uses scattered electrons, whereas TEM is based on transmitted electrons. The image of the TEM is formed by the electrons that pass through the sample, as they can illuminate the image. The resolution of a TEM is determined by the energy of the electrons, the thickness of the sample, the distance between sample and lens and the inherent quality of the lens.[17] The best TEMs have resolutions of 0.05 nm, which is much better compared to the SEM.[17] In this work, the morphology of the YSZ powders were analyzed

with a TEM (FEI Titan 80/300, Netherlands) which was equipped with a Cs corrector for the imaging lens using a 300 keV electron beam and a vacuum of $1.3 \cdot 10^{-7}$ mbar. A 200-mesh cupper grid S162 covered with a formvar film (Plano GmbH, Germany) were used as sample holder.

3.6 Mercury Intrusion Porosimetry

Mercury intrusion porosimetry (Hg-porosimetry) is an analytical method to measure precisely the porosity, the pore size distribution and the average pore size of a sample. Pores in the range between 0.03 and 200 µm can be determined.[20] Mercury has a high surface tension (480 mN/m at 20 °C under vacuum) and is non-wetting to most materials.[21] Mercury has a mean contact angle of ~140° on ceramic materials.[11] Therefore, it cannot be adsorbed by the pores of a sample spontaneously, but must be forced into the pores by pressure.[21] The extent of pressure which needs to be applied depends on the pores size. The pore size can be calculated by the Washburn equation[22] (3.5) based on the external pressure which is required to fill a pore:

$$r_p = -\frac{2\gamma\cos(\phi)}{\Delta p} \qquad (3.5)$$

In this equation r_p is the pore radius, γ is the surface tension, ϕ is the contact angle and p is the used pressure.

In this work, the pore size distribution, the average pore size (d_{50}) and the open porosity of the sintered samples were analyzed by mercury intrusion porosimetry (Mercury Porosimeter Pascal 140 and 440, POROTEC GmbH). The measurements were performed in a pressure range between 0.1 and 400 kPa with an accuracy of <0.25 %. All measurements are carried out according to DIN 66133. An empty measurement is performed as a blank correction.

In addition to the experimental determination of the pore size, the d_{50} pore size (d_{pore50}) assuming a random dense packing (3.6) and a random loose packing (3.7) of processed ceramic particles was calculated for the sintered capillaries based on the simulation of Gotoh et al.,[23] where a_{50} is the particle size:

$$d_{pore50} = 0.46 \cdot a_{50} \qquad (3.6)$$

$$d_{pore50} = 0.48 \cdot a_{50} \qquad (3.7)$$

3.7 3-Point Bending Test

The mechanical strength of the sintered capillaries was measured by 3-point bending tests (Figure 3.2) according to DIN EN 843-1 (Roell Z005, Zwick). The testing machine was equipped with a load cell for up to 5 kN. The applied velocity was 0.4 mm/min. A capillary with a length of 12 mm was placed in the centre of the sample holder and tested. The distance between the sample holder and the support rollers (L) was 8 mm. To calculate the bending strength σ_F, the following equation was used:

$$\sigma_F = \frac{8 \cdot F \cdot L \cdot OD}{\pi \cdot (OD^4 - ID^4)} \qquad (3.8)$$

In this equation, F is the measured force at which fracture takes place; OD is the outer and ID the inner diameter of the capillary. For each sintered capillary type 30 samples were tested for statistical significance. The statistical analysis was based on the maximum-likelihood method.

3.8 Quantification of Aminosilane loading: Acid-Orange II Assay

The amount of accessible amino groups on capillaries after aminosilanization was quantified by acid orange II assay as described by Kroll et al.[24], where a set of two capillaries with an individual length of 2.5 cm was incubated in 1.75 mL acid orange II reagent (0.5 mM orange II sodium salt, product number, 75370, in HCl, product number 35328, both from Sigma-Aldrich Chemie GmbH, Germany) at pH 3 for 24 h at RT and 300 rpm (ThermoMixer C, Eppendorf). Next, the incubated membranes were washed with 10 mL HCl (pH 3) three times to remove unbound acid orange II molecules from the surface. Each membrane was placed in 2 mL NaOH (product number 71692, Sigma-Aldrich Chemie GmbH, Germany) solution (pH 12) for 15 min at RT and 300 rpm where the acid orange II molecules desorb from the sample. The
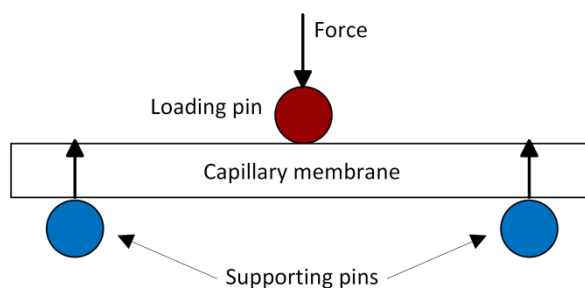

Figure 3.2. Principle of 3-point bending test.

supernatants were photometrically analyzed at 483 nm (Multiskan Go, Thermo Scientific, Germany) where NaOH (pH 12) served as blank sample. Hydroxyl-activated samples served as references and the photometrical measured values were subtracted from the sample measurements. With a calibration curve the amount of accessible amino groups per surface area (amino groups/nm^2) was calculated. For each membrane type, four individual capillaries were tested.

3.9 Thermogravimetric Analysis (TGA)

The thermogravimetric analysis (TGA) is a measurement technique where the change of a sample weight is monitored during a heating and cooling process.[25] Therefore, two crucibles are placed on a balance which is located in a furnace. One crucible is used to carry the sample and the other is empty and used as a reference. The furnace is heated up and the temperature, the weight change of the sample and the weight difference between the two crucibles holders are monitored. The relative weight change of the sample in relation to the temperature change is analyzed.

Thermogravimetric analysis (STA503, Bähr-Thermoanalyse GmbH, Hüllhorst, Germany) was performed with the capillary membranes in a temperature range between 40 °C and 900 °C with a heating rate of 10 K/min under 2 L/h flowing air. The STA503 has a temperature resolution of 0.01 °C with an accuracy of ± 0.1 °C and a weight resolution of 1 µg.

3.10 Propagation and Enumeration of Bacteriophages

The propagation and the enumeration of bacteriophages is based on standard methods of the International Organization for Standardization (ISO) for the enumeration of F-specific and somatic coliphages (ISO 19705-1/2). All used media and instruments were autoclaved before usage to avoid contaminations.

3.10.1 Propagation of the Bacteriophages

Bacteriophages can only propagate in growing bacterial cells (exponential phase of bacterial culture). Therefore, a commercially available complex medium, tryptic soy broth (TSB, product number 22091, Sigma-Aldrich Chemie GmbH, Germany), is used to cover the demands of the bacteria. The bacteria were grown in 50 mL of a sterile 30 g/L TSB medium at 37 °C in an incubator shaker (Inkubator 1000/Unimax 1010, Heidolph) at 150 rpm for 16 h (overnight culture). Two different *E.coli* strains were used depending on the virus. All microorganisms were purchased from the German Collection of Microorganisms and Cell Cultures (DSMZ). For the virus MS2 (DSM Cat. No. 13767) the *E.Coli* strain with the DSM Cat. No. 5210 and for the virus PhiX174 (DSZ Cat No. 4497) the *E.Coli* strain with the DSM Cat. No. 13127 were used. 200 µL of the overnight bacteria culture was inoculated in 50 mL of a sterile 30 g/L TSB medium at 37 °C on an incubator shaker (Inkubator 1000/Unimax 1010, Heidolph) at 150 rpm for 4 h to obtain bacteria in an exponential growth phase (4-h culture).

After this, an optional washing step may be added to remove the agents from the TSB medium. Therefore, the bacteria culture was centrifuged at 3000 g for 10 min, the supernatant was removed and the bacteria were resuspended in 50 mL of a salt solution containing 0.02 M $MgCl_2$ (product number M2670, Sigma-Aldrich Chemie GmbH, Germany) and 0.15 M NaCl. (product number S7653, Sigma-Aldrich Chemie GmbH, Germany) The solution is then placed back at the incubation shaker and heated up to 37 °C.

In 50 mL of the bacteria host culture 1 mL of the bacteriophages stock suspension (prepared according to suppliers information) were added and incubated at 37 °C at 100 rpm for 20 h. When using the unwashed bacteria culture 0.125 mL of 4 M $MgCl_2$ solution was added to adjust the $MgCl_2$ concentration to 0.02 M. After the incubation time of 20 h the bacteria have to be removed from the solution to obtain a pure virus solution. Therefore, the culture was centrifuged at 3000 g for 30 min at RT and the supernatant which contains the viruses was additionally cleared of bacterial debris through sterile 0.2 µm syringe filters.

To further purify the bacteriophages from residues of the propagation process an optional washing step can be added. To this end, the suspension is transferred to an ultrafiltration spin column (Vivaspin 15, Sartorius Stedim Biotech GmbH) with a 100 kDa molecular weight cut-off (MWCO). The suspension was centrifuged for 10 min at 3000 g at RT. The bacteriophages were collected in the spin column. 15 mL of sterile 0.15 M NaCl solution was added to the spin column and centrifuged for 10 min at 3000 g at RT. This step is repeated 5 times.

The virus stock solution was stored at 4 °C in the fridge.

3.10.2 Enumeration of the Bacteriophages - Plaque Assay

The enumeration of the bacteriophages was carried out with the plaque assay where a single infectious bacteriophage gives rise to a macroscopic area of cythopathology on a monolayer of bacteria cells that were grown in a petri dish. More precisely, a single bacteria cell in a monolayer of cultured cells is infected with a single virus. New viruses are propagated by the bacteria cell and can infect surrounding bacteria cells, which as well propagate new viruses which infect the surrounding cells. After a period of hours or days (depending on the virus) the initial infection produced a macroscopic area of cythopathology, called a plaque.[26] A semisolid nutrient medium prevents the formation of secondary plaques through diffusion of viruses and restricts the plaque. The plaque assay is a
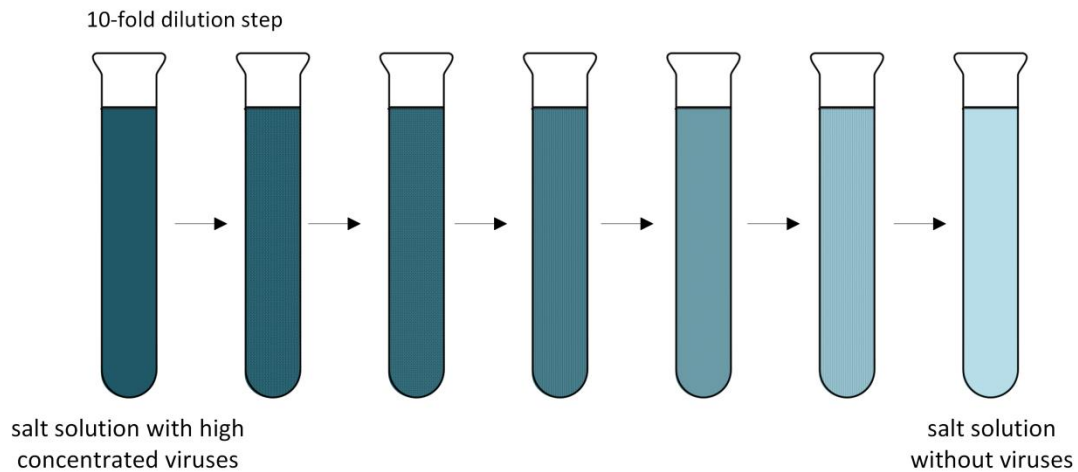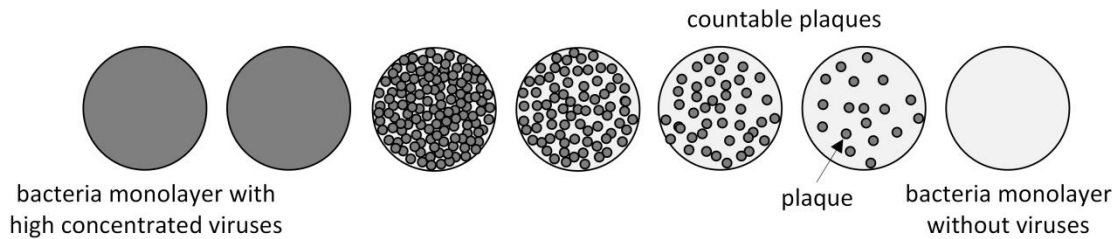
Dilution row

10-fold dilution step

salt solution with high
concentrated viruses

salt solution
without viruses

Plaque assay

countable plaques

bacteria monolayer with
high concentrated viruses

plaque

bacteria monolayer
without viruses

Figure 3.3. Principle of the plaque assay for the enumeration of bacteriophages.

most quantitative and relatively simple biological assay for viruses which was developed in the early 1900s by d'Herelle.

A sample of unknown virus concentration is diluted in 10-fold steps in a salt solution containing 0.02 M $MgCl_2$ and 0.15 M NaCl at RT (dilution row - see Figure 3.3). The sample volume of 1.8 mL (MS2) or 4.5 mL (PhiX174) were mixed with 0.2 mL or 0.5 mL, respectively, of the 4-h phage-specific host culture. Afterwards, around 3 mL or 5 mL of a sterile phage-specific agar which was heated to 50 °C was added to the suspension. The agar is based on commercially available complex media consisting of 15 g/L tryptic soy broth and 40 g/L tryptic soy agar (TSA, product number 22091, Sigma-Aldrich Chemie GmbH, Germany). Phages, bacteria and agar were mixed and poured into a petri dish (6 cm in diameter for MS2 and 9.2 cm in diameter for PhiX174). Different sizes of petri dishes were used as MS2 forms small plaques with a diameter of 1 mm and in comparison to that PhiX174 forms large plaques with a diameter of 5 mm. After incubating the petri dishes for 16 hours at 37 °C the plaques are visible. The goal of the assay is to find the dilution of viruses that leads to the formation of countable (20 - 100) plaques on a single petri dish. This number is on the one hand statistically significant and on the other hand individual plaques can be distinguished. Low virus dilution have only dead bacteria cells and/or too many plaques (> 100) to count and high virus dilutions have very few (< 20) or no plaques (see Figure 3.3). The petri dish with countable plaques is used to calculate the virus titer by taking the serial dilution into account. Retention of microorganisms is expressed in the log-reduction value (LRV), which is defined as the logarithm to base 10 of the ratio of viral concentrations in the feed to those in the permeate.[27] The titer is expressed in plaque-forming units per mL (PFU/mL).

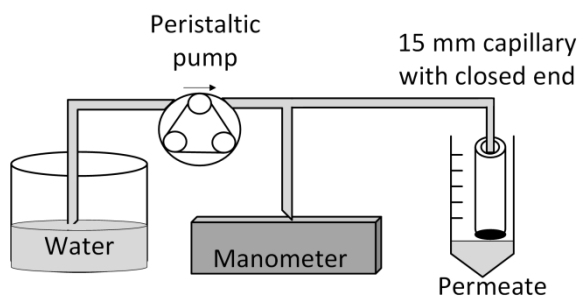Titers derived by serial dilution have high errors

Figure 3.4. Experimental set-up of the water permeate flux test (adapted from Werner et al)[2].

due to the pipetting steps, therefore errors of up to a factor of 2 are normal and satisfactory for the most purposes. For each virus sample three dilution series of Plaque Assays were carried out.[28]

3.11 Filtration Experiments

3.11.1 Water Permeate Flux

The water permeate flux of the sintered YSZ capillaries was determined by intracapillary water feeding operating in dead-end mode where double-deionized water served as feed solution. The set-up is shown in Figure 3.4. Intracapillary water feeding was achieved by a peristaltic pump (BVP Standard, Ismatec) applying different pressures in the range between 25 and 500 mbar to force the water through the membrane. Therefore, one end of the capillary was sealed with silicon (Wirosil Dublier-Silikon, BEGO Medical GmbH) and the other end was connected with a convenient silicon tubing to a peristaltic pump. The applied pressures was monitored with a manometer (C9500, COMARK). Three individual capillaries with a length of 1.5 cm or 5 cm were tested operating in vertical orientation. The applied operating time for membrane samples varied depending on the pore size of the capillary between 5 min and 24 h. The permeated water volumes were obtained by weight measurements (ABJ, Kern & Sohn GmbH). Each measurement was performed in triplicate.

The membrane flux for 1 bar was calculated by linear regression and flux values were given in L/(m²hbar). The error due to water evaporation

during gravimetric measurements at RT was 0.8 ± 0.2 % for filtration times of 30 min and 14.7 ± 4.6 % for filtration times of 24 h.

3.11.2 Virus Retention Test

The virus retention of the capillary membranes was tested using two small bacteriophages which served as surrogates for human pathogenic viruses: MS2 and PhiX174. MS2 is a single-stranded RNA virus with a diameter of 25-27 nm and an IEP of 3.9 [29, 30]. PhiX174 is a single-stranded DNA virus with a diameter of 26-32 nm and an IEP of 6.6 [29, 30]. For more information regarding the viruses see chapter 2.1.3. These viruses belong to the smallest viruses and therefore, filtration based on size exclusion principle can be ideally investigated.

A virus containing saline solutions (0.02 M $MgCl_2$/0.15 M NaCl) at pH 5.8 served as viral feed solution showing initial virus concentrations of around 10^9 PFU/mL.

Virus filtration tests were performed using the experimental set-up as shown in Figure 3.4 with the exception that a virus containing solution instead of water served as feed. The virus retention test was performed in dead-end mode and virus containing solutions were intracapillary fed to single capillary membranes with an accessible length of 1.5 cm or 5 cm. For each filtration test, new single capillary membranes were used and intracapillary virus feeding was performed at an applied pressure of 500 mbar (if not stated different) until a permeate volume of 15 mL was reached. For each membrane type, three individual capillary membranes were tested in parallel (triplicate determination).

The bacteriophages in the feed solution and permeate were enumerated using the plaque-forming-unit (PFU) method according to the procedure as described in chapter 3.3.2.

References

1. S. Lowell, et al., "Characterization of Porous Solids and Powders: Surface Area, Pore Size and Density″, Springer Netherlands, 2012.
2. J. Werner, et al. "Production of ceramic membranes with different pore sizes for virus retention". *Journal of Water Process Engineering*, 2014, 4, 201-211.

3.   J. Rouquerol, et al., in *Pure Appl Chem*, 1994, vol. 66, p. 1739.

4.   P. A. A. T. C. I. Manual. *Thermo Electron S.p.A. Strada Rivoltana, 20090 Rodano-Milan, Italy*, 2004.

5.   R. Xu, "Particle Characterization: Light Scattering Methods″, Springer Netherlands, 2006.

6.   E. Tsotsas and A. S. Mujumdar, "Modern Drying Technology, Experimental Techniques″, Wiley, 2011.

7.   E. D. Shchukin, et al., "Colloid and Surface Chemistry″, Elsevier Science 2001.

8.   A. R. Hanifi, et al. "Effects of calcination and milling on surface properties, rheological behaviour and microstructure of 8mol% yttria-stabilised zirconia (8 YSZ)". *Powder Technology*, 2012, 231, 35-43.

9.   S. Brunauer, et al. "Adsorption of Gases in Multimolecular Layers". *Journal of the American Chemical Society*, 1938, 60, 309-319.

10.   K. Sing. "The use of nitrogen adsorption for the characterisation of porous materials". *Colloids and Surfaces A: Physicochemical and Engineering Aspects*, 2001, 187, 3-9.

11.   H. Salmang and H. Scholze, "Keramik″, Springer, 2006.

12.   B.-m. Technical specification BELSORP series. *BEL Japan, Inc. 1-Chrome, Haradanaka, Toyonaka-City, Osaka, Japan*, 2009.

13.   L. Albright, "Albright's Chemical Engineering Handbook″, Taylor & Francis, 2008.

14.   Woodard and I. Curran, "Industrial Waste Treatment Handbook″, Elsevier Science, 2011.

15.   R. J. Hunter, et al., "Zeta Potential in Colloid Science: Principles and Applications″, Elsevier Science, 2013.

16.   A. S. Dukhin and P. J. Goetz, "Characterization of Liquids, Nano- and Microparticulates, and Porous Bodies using Ultrasound″, Elsevier Science, 2002.

17.   C. B. Carter and M. G. Norton, "Ceramic Materials, Science and Engineering″, New York, 2007.

18.   D. Stokes, "Principles and Practice of Variable Pressure/Environmental Scanning Electron Microscopy (VP-ESEM)″, 2008.

19.   A. C. McLaren, "Transmission Electron Microscopy of Minerals and Rocks″, Cambridge University Press, 2005.

20.   S. Sahin and S. G. Sumnu, "Physical Properties of Foods″, Springer New York, 2007.

21.   J. Park and R. S. Lakes, "Biomaterials: An Introduction″, Springer New York, 2007.

22.   E. W. Washburn. "The Dynamics of Capillary Flow". *Physical Review*, 1921, 17, 273-283.

23.   K. Gotoh, et al. "Pore size distributions in random assemblies of equal spheres". *The Journal of Chemical Physics*, 1986, 85, 3078-3080.

24.   S. Kroll, et al. "Development and characterisation of functionalised ceramic microtubes for bacteria filtration". *Journal of Membrane Science*, 2010, 365, 447-455.

25.   P. J. Haines, et al., "Principles of Thermal Analysis and Calorimetry″, Royal Society of Chemistry, 2002.

26.   B. N. Fields, et al., "Fields' Virology″, Wolters Kluwer Health/Lippincott Williams & Wilkins, 2007.

27.   S. Kroll, et al. "High virus retention mediated by zirconia microtubes with tailored porosity". *Journal of the European Ceramic Society*, 2012, 32, 4111-4120.

28.   J. Carter and V. Saunders, "Virology, Principles and Applications″, 2007.

29.   B. Michen and T. Graule. "Isoelectric points of viruses". *Journal of Applied Microbiology*, 2010, 109, 388-397.

30.   A. Duek, et al. "New and conventional pore size tests in virus-removing membranes". *Water Research*, 2012, 46, 2505-2514.

4. Production of Ceramic Membranes with Different Pore Size for Virus Retention

Adapted from

Published in

Authors

Julia Werner, Benjamin Besser, Christoph Brandes, Stephen Kroll, Kurosch Rezwan

Advanced Ceramics, University of Bremen, Am Biologischen Garten 2, 28359 Bremen, Germany

Abstract

Porous ceramic capillary membranes made of yttria-stabilized zirconia (YSZ) are presented, which are conditioned for virus filtration by varying the initial YSZ particle size. Compared to polymeric membranes, ceramic membranes offer remarkable advantages for filtration processes as they show excellent chemical, thermal and mechanical stability and can easily be cleaned by backflushing. YSZ powders with different particle sizes (30 nm, 40 nm and 90 nm) are individually and mixed processed by extrusion, dried and finally sintered at 1050 °C for 2 h. The sintered YSZ capillaries are characterized by microstructural analysis including Hg-porosimetry, BET analysis and 3-point bending tests. By increasing the initial YSZ particle size, increased average membrane pore sizes ranging from 24 nm to 146 nm are obtained. Mechanically stable membranes are provided showing high open porosities of ~45 % and ~36 % for capillaries composed of single and mixed YSZ powders, respectively. By increasing the membrane pore size, reduced virus retention capacities in combination with increased water permeate fluxes are achieved. Capillaries made of YSZ-40nm ensure both, log reduction values (LRV) ≥ 4 for small model bacteriophages MS2 and PhiX174 and high water permeate fluxes (~30 L/(m^{2}hbar)), being suitable for sustainable virus filtration as requested by the World Health Organization (WHO) and the United States Environmental Protection Agency (USEPA). Due to long-term virus filtration for two weeks, membrane pore plugging is successfully avoided by iterative backflushing and relatively high membrane fluxes in combination with requested LRV 4 level fulfilling the virus filter criterion are achieved.

4.1 Introduction

Water is essential to life, but today, 783 million people still have an inadequate access to clean drinking water.[2] Especially in developing countries, an access to safe drinking water and sanitation is not ensured, e.g. for 46 % of the population in Oceania and 39 % of the population in Sub-Sahara Africa.[2, 3] According to the World Health Organization (WHO), 1.8 million people die annually from diseases such as diarrhoea, cholera and dysentery transmitted through polluted water.[4, 5]

The three main contaminations for water pollution are of chemical (e.g. heavy metals, organic and inorganic species), physical (e.g. color) and biological (e.g. bacteria and viruses) origin.[6] The biological pollutants are the most frequent and deadly contaminations in the drinking water of developing countries, because waterborne diseases are mainly caused by viruses (e.g. adenovirus, enterovirus, rotaviruses, hepatitis A and E virus) and bacteria (e.g. Vibrio cholerae, Escherichia coli, Salmonella enterica).[3, 6, 7]

Nowadays, water disinfection methods to inactivate viruses are based on physical or chemical processes. Conventional methods to inactivate viruses in water are heat treatment techniques, chemical treatments using free chlorine or chlorine dioxide, and the application of ozone or UV-irradiation. Especially for heat and chemical treatments, a virus inactivation can be achieved, but high costs and the potential production of toxic disinfection by-products (DBPs) are given at the same time. Ozone treatments and UV-irradiations can induce virus inactivation, but high investment costs and trained personal are required.[8-12]

A promising alternative for water disinfection is the filtration which is based on removing suspended solids from a fluid by passing it through a permeable fabric (e.g. membranes). Filtration is based on size exclusion effects and therefore, contaminants which are larger than the membrane pore size can be effectively retained.[13, 14] A virus removal using ceramic filters made of raw materials (e.g. diatomaceous earth) or chemically synthesized ceramics (e.g. zirconia) is possible as shown by several authors.[15-17] To ensure a high virus removal even for pore sizes larger than the viruses a pretreatment by coagulation/flocculation was performed by other authors.[18-21] Beside size exclusion methods particularly functionalized ceramic particles (e.g. amino-silanized) and ceramic components (e.g. MgO-doped, colloidal zirconia) are applied for virus adsorption to enhance the virus titer reduction.[22-24]

Today, polymeric membranes possess high water permeate fluxes combined with required high virus retention levels.[25, 26] Compared to polymeric membranes, ceramic membranes show excellent chemical, thermal and mechanical stability. The importance of porous ceramic membranes is increasing in water purification, because monomodal and narrow pore size distributions in the meso- and macroporous range can be tailored depending on applied processing parameters (e.g. initial ceramic particle size, shaping technique, drying and sintering conditions). Because of their high mechanical strength ceramic membranes can withstand high pressure loads and therefore, they are able to endure high water permeate flux rates. Another advantage of ceramic membranes is that they can easily be cleaned by backflushing, thermal, acidic or basic treatment without affecting the pore morphology.[27] In addition, ceramic membranes do not show any swelling behavior during water filtration maintaining their structural compactness. In contrast to polymeric membranes, the production costs of ceramic membranes are 3 up to 5 times higher, but this can be compensated by their longer lifetime of up to ten years instead of one year for polymeric membranes.[28] Further disadvantages of ceramic membranes are their brittle behavior and higher material weight compared to polymeric membranes.[29]

For a highly efficient virus filtration it is necessary that a reliable pore size of the membrane of less than or equal to virus size is provided to act as a mechanical filter based on size exclusion principle. Viruses are the smallest pathogens and have diameters between 20 and 300 nm.[7] Therefore, virus removal can be attained by ultrafiltration showing pore sizes in

the range between 2 and 100 nm, i.e. mesoporous and lower macroporous range.[30] To ensure high virus removal capacities, pore sizes less than the virus are preferred leading to low water permeate fluxes.[16, 31, 32] Based on the guidelines from WHO and United States Environmental Protection Agency (USEPA) a log-reduction value of 4 (i.e. at least 99.99 percent (4-log) removal) is required to fulfill the virus filter criterion providing safe and clean drinking water. The generation of tubular ceramic membranes offering both, a reliable cut-off for virus retention in combination with high open porosities and water permeate fluxes, is challenging and requires in-depth knowledge of the whole processing route.

The aim of this work is to extrude yttria-stabilized zirconia (YSZ) capillaries for virus filtration that feature ideally pore sizes and porosities for realizing high virus retention capacities of LRV ≥ 4 in combination with high permeate fluxes. YSZ was chosen because of its high fracture toughness and strength compared to other ceramic oxide materials (e.g. alumina). The effect of initial YSZ powders showing different particle sizes on the membrane microstructure (pore size, open porosity, specific surface area), mechanical stability (bending strength) and water permeate flux were analyzed in detail. Virus retention capacities of the extruded and finally sintered capillary membranes were determined by virus filtration tests in dead-end mode using two small bacteriophages, MS2 and PhiX174, which served as surrogates for human pathogenic viruses. Finally, long-term virus filtration tests for two weeks were performed applying iterative backflushing to control the membrane fouling.

4.2 Materials and Methods

4.2.1 Materials

The yttria-stabilized zirconia (YSZ) powders and reagents were purchased from commercial sources and used as received. Three different YSZ powders were used: VP Zirkonoxid 3-YSZ (YSZ-30nm, Lot. 3157061469, specific surface area = 40 ± 15 m^2/g, particle size < 30 nm) was purchased from Evonik Industries, Germany, TZ-3Y-E (YSZ-40nm, Lot. Z302131P, specific

surface area = 16 ± 3 m^2/g, particle size = 40 nm) and TZ-3YS-E (YSZ-90nm, Lot. S300886P, specific surface area = 7 ± 2 m^2/g, particle size = 90 nm) were obtained from Krahn Chemie GmbH, Germany.

3-Aminopropyltriethoxysilane (APTES, 99 %, product number 440140, Lot. SHBC8357V), magnesium chloride hexahydrate (MgCl2, product number M2670, Lot. BCBJ3659V), polyvinyl alcohol (PVA, fully hydrolysed, product number P1763, Lot. SLBC9027V), sodium chloride (NaCl, product number S7653, Lot. SZBC2560V), tryptic soy agar (TSA, product number 22091, Lot. BCBG4777V) and culture media tryptic soy broth (TSB, product number T8907, Lot. 109K0165) were obtained from Sigma-Aldrich Chemie GmbH, Germany.

For virus retention tests we used the bacteriophage MS2 (DSM Cat. No. 13767) and its host bacteria E. coli (DSM Cat. No. 5210) as well as the bacteriophage PhiX174 (DSM Cat. No. 4497) and its host bacteria E. coli (DSM Cat. No. 13127) from German Collection of Microorganisms and Cell Cultures (DSMZ), Germany.

All experiments were carried out using double-deionised water with an electrical resistance of 18 MΩ, which was obtained from a Synergy® apparatus (Millipore, Germany).

4.2.2 Characterization of YSZ Powders

The particle properties of three different YSZ powders, namely VP Zirkonoxid 3-YSZ (YSZ-30nm), TZ-3Y-E (YSZ-40nm) and TZ-3YS-E (YSZ-90nm), were characterized determining the particle size distribution, density, specific surface area and zeta-potential. Particle size distributions and average particle sizes (d_{50}-values) were determined by acoustic spectroscopy (DT 1200, Dispersion Technology) using ceramic suspensions containing 1 vol.% particles. An ultrasonic treatment was applied for 10 min at 240 W with a pulse rate of 0.5 s (ultrasonic finger, Branson Sonifier 450, Heinemann, Germany) to deagglomerate the YSZ powders before the measurement. The acoustic spectroscopy was taken out at pH 3 to ensure a particle rejection, because YSZ has an isoelectric
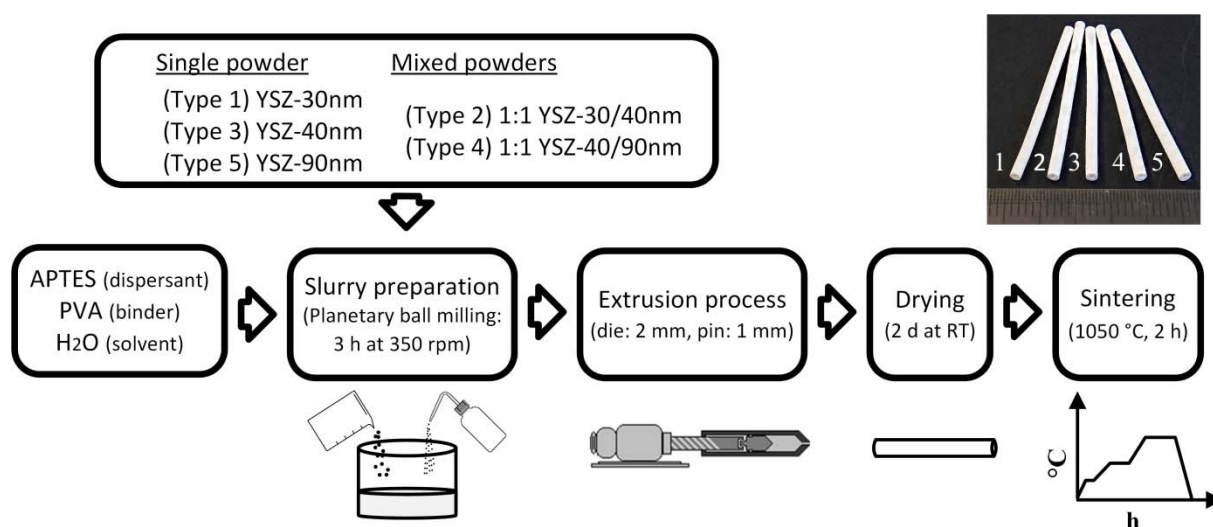
Figure 4.1. Processing route for the fabrication of porous YSZ capillaries sintered at 1050 °C for virus filtration based on initial YSZ powders with different particle sizes.

point (IEP) in the neutral to low basic pH range (IEP$_{YSZ}$ = ~7-9).[33]

Additionally, transmission electron microscopy (TEM, FEI Titan 80/300) was performed to estimate the particle size and morphology. The density of the three different YSZ powders was analyzed by helium pycnometry (Pyconmatic ATC, Porotec). The specific surface area was obtained by nitrogen adsorption according to BET method (BELSORB-Mini, BEL Japan Inc.) after degassing the YSZ powders using argon for at least 3 h at 120 °C followed by flushing with dry argon. Zeta-potential measurements (DT 1200, Dispersion Technology) with suspensions containing 1 vol.% particles were performed to determine the IEPs of the YSZ powders. The pH titration was carried out with an integrated titration unit using 1 M HCl or 1 M KOH.

4.2.3 Fabrication of YSZ Capillaries by Extrusion

Figure 4.1 shows the processing route for the fabrication of YSZ capillaries by extrusion. The fabrication is divided into four main parts involving slurry preparation, shaping by extrusion process, drying of the extruded capillaries and finally, sintering of the obtained green capillaries.

4.2.3.1 Slurry Preparation

As shown in Figure 4.1, four components were used to prepare the ceramic slurry: YSZ powder as ceramic material, APTES as dispersant, PVA as binder and double-deionized water as solvent. As already described by Qui et al., PVA was used because of the low risk of crack-formation during the drying of extruded capillaries made of YSZ.[34] Based on the manufacturer data, the primary particle size of the used YSZ powders ranged from 30 nm to 90 nm. Five different types of capillaries were prepared. Three capillary types were all based on one YSZ powder, namely Type 1 (made of YSZ-30nm), Type 3 (made of YSZ-40nm) and Type 5 (made of YSZ-90nm), respectively. The two other capillary types were composed of two of the three YSZ powders. The powders were mixed in a ratio of 1:1 (w/w) and the capillaries were named Type 2 (based on YSZ-30nm and YSZ-40nm powder) and Type 4 (based on YSZ-40nm and YSZ-90nm powder), respectively. To create extrudable slurries showing different initial particle sizes, individual slurry compositions for each YSZ particle type were used. For one batch (i.e. one grinding vessel of the planetary ball mill), the amount of YSZ powder as well as the amount of the binder (PVA) was kept constant at 132 g and 8 g, respectively. To provide stabilized and homogeneous YSZ slurries for the extrusion

process following slurry compositions were used: For the preparation of Type 1 capillaries, 44.4 g water and 7.4 g APTES for the preparation of Type 2 capillaries, 38 g water and 5.7 g APTES and for the preparation of Type 3, Type 4 and Type 5 capillaries 33 g water and 4 g APTES were used. The solid contents of the prepared feedstocks were then 72.9 wt.% (Type 1), 76.2 wt.% (Type 2) and, 79.1 wt.% (Type 3-5), respectively.

The preparation of the slurry in the planetary ball mill (PM400, Retsch) was performed in the same way for each YSZ powder. Each of two grinding vessels was filled with the reagents (YSZ powder, PVA, APTES and water) and 50 alumina grinding balls with a diameter of 10 mm. The slurry was milled for 3 h at 350 rpm changing the rotation direction every 5 min. Afterwards, the grinding balls were removed from the slurry and the slurry was transferred to the extruder.

4.2.3.2 Extrusion Process

The extrusion was carried out with a self-made laboratory extruder as described in our previous works.[16, 35] The extruder consisted of a spindle drive with shaft joint which was connected to a press ram, a convenient vessel for the slurry uptake, an extrusion die with integrated pin and a conveyor band for depositing the extruded capillaries. The extruder was equipped with an extrusion die of 2.0 mm diameter and an integrated pin with 1.0 mm diameter.

4.2.3.3 Drying and Sintering

The extruded capillaries were dried for at least two days at RT to remove residual solvents. Afterwards, these green capillaries were sintered for 2 h at 1050 °C with preceding dwell times at 280 °C and 500 °C to remove the dispersant (APTES) and binder (PVA) molecules, respectively (Nabertherm, Germany). According to our previous studies based on YSZ, a moderate sintering temperature of 1050 °C for 2 h was chosen to obtain capillary membranes showing both, relatively high open porosities in combination with a sufficient mechanical stability.[16, 36] After sintering, the capillaries were

ready for characterization.

4.2.4 Characterization of Extruded Green and Sintered YSZ Capillaries

4.2.4.1 Structural and Mechanical Membrane Properties

The sintering shrinkage was determined by measuring the outer and inner diameter of the sintered (1050 °C for 2 h) capillary membranes by optical microscopy (VHX-600DSO, Keyence). For each capillary type ten samples were tested for statistical significance. The pore size distribution, the average pore size (d_{50}) and the open porosity of the sintered samples were analyzed by Hg-porosimetry (Mercury Porosimeter Pascal 140 and 440, POROTEC GmbH). In addition to the experimental determination of the pore size, the d_{50} pore size (d_{pore50}) assuming a random dense packing (4.1) and a random loose packing (4.2) of processed ceramic particles was calculated based on the simulation of Gotoh et al.[1] where a_{50} is the particle size:

$$d_{pore50} = 0.46 \cdot a_{50} \qquad (4.1)$$
$$d_{pore50} = 0.48 \cdot a_{50} \qquad (4.2)$$

The specific surface area of the sintered capillaries was determined by nitrogen adsorption according to BET method after degassing the capillaries for at least 3 h at 120 °C using argon. Furthermore, the sintered capillaries were analyzed by scanning electron microscopy (SEM, Field-emission SEM SUPRA 40, Zeiss) to visualize the microstructure of the outer capillary surface and to check the presence of potential macro- and microdefects.

The mechanical strength of the sintered capillaries was measured by 3-point bending tests according to DIN EN 843-1 (Roell Z005, Zwick). The testing machine was equipped with a load cell for 5 kN. The applied velocity was 0.4 mm/min. A capillary with a length of 12 mm was placed in the centre of the sample holder and tested. The distance between the sample holder and the support rollers (L) was 8 mm. To calculate the bending strength σ_F, the following equation was used:
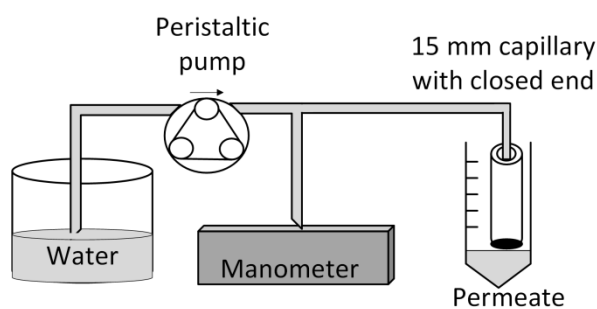
Figure 4.2. Experimental set-up of the water permeate flux test.

$$\sigma_F = \frac{8 \cdot F \cdot L \cdot OD}{\pi \cdot (OD^4 - ID^4)} \qquad (4.3)$$

In this equation, F is the measured force at which fracture takes place; OD is the outer and ID the inner diameter of the capillary. For each sintered capillary type 30 samples were tested for statistical significance. The statistical analysis was based on the maximum-likelihood method.

4.2.4.2 Water Permeate Flux

The water permeate flux of the sintered YSZ capillaries was determined by intracapillary water feeding operating in dead-end mode where double-deionized water served as feed solution. Intracapillary water feeding was achieved by a peristaltic pump (BVP Standard, Ismatec) applying different pressures in the range between 25 and 500 mbar to force the water through the membrane. Therefore, one end of the capillary was sealed with silicon (Wirosil Dublier-Silikon, BEGO Medical GmbH) and the other end was connected with a convenient silicon tubing to the peristaltic pump (Figure 4.2). Based on adjustable flow rates mediated by the peristaltic pump a manometer was used to determine the applied pressures (C9500, COMARK). For each membrane type (Type 1-5), three individual capillaries with a length of 1.5 cm were tested operating in vertical orientation. The active filtering area of the sintered capillaries is 0.40 cm^2. The applied filtration time for membrane samples fabricated with YSZ-40nm and YSZ-90nm was 30 min for each applied pressure (Type 3, Type 4 and Type 5). Due to low water permeate fluxes of capillary membranes derived from capillaries based on YSZ-30nm powder (Type 1 and Type 2) filtration times up to one day were applied. The permeated water volumes were obtained by weight measurement (ABJ, Kern & Sohn GmbH). Each measurement was performed in triplicate.

The error due to water evaporation during gravimetric measurements at RT was 0.8 ± 0.2 % for membranes made of YSZ-40nm as well as YSZ-90nm (30 min filtration time) and 14.7 ± 4.6 % for membranes consisting of YSZ-30nm (24 h filtration time).

4.2.4.3 Virus Retention Test

The virus retention of the sintered capillaries was tested using two small bacteriophages which served as surrogates for human pathogenic viruses: MS2 and PhiX174. MS2 is a single-stranded RNA virus with a diameter of 25-27 nm and an IEP of 3.9.[13, 37] PhiX174 is a single-stranded DNA virus with a diameter of 26-32 nm and an IEP of 6.6.[13, 37] These viruses belong to the smallest viruses and therefore, filtrations based on size exclusion principle can be ideally investigated.

The virus retention test was performed as described in our previous study[16] with slight modifications. In short, the preparation of the virus feed solutions was done by virus propagation for MS2 and PhiX174, respectively, and the bacteriophages were separately propagated in their specific host bacteria (E. coli). Virus containing saline solutions (0.02 M MgCl$_2$/0.15 M NaCl) at pH 5.8 served as viral feed solution showing initial virus concentrations of around 10^9 PFU/mL.
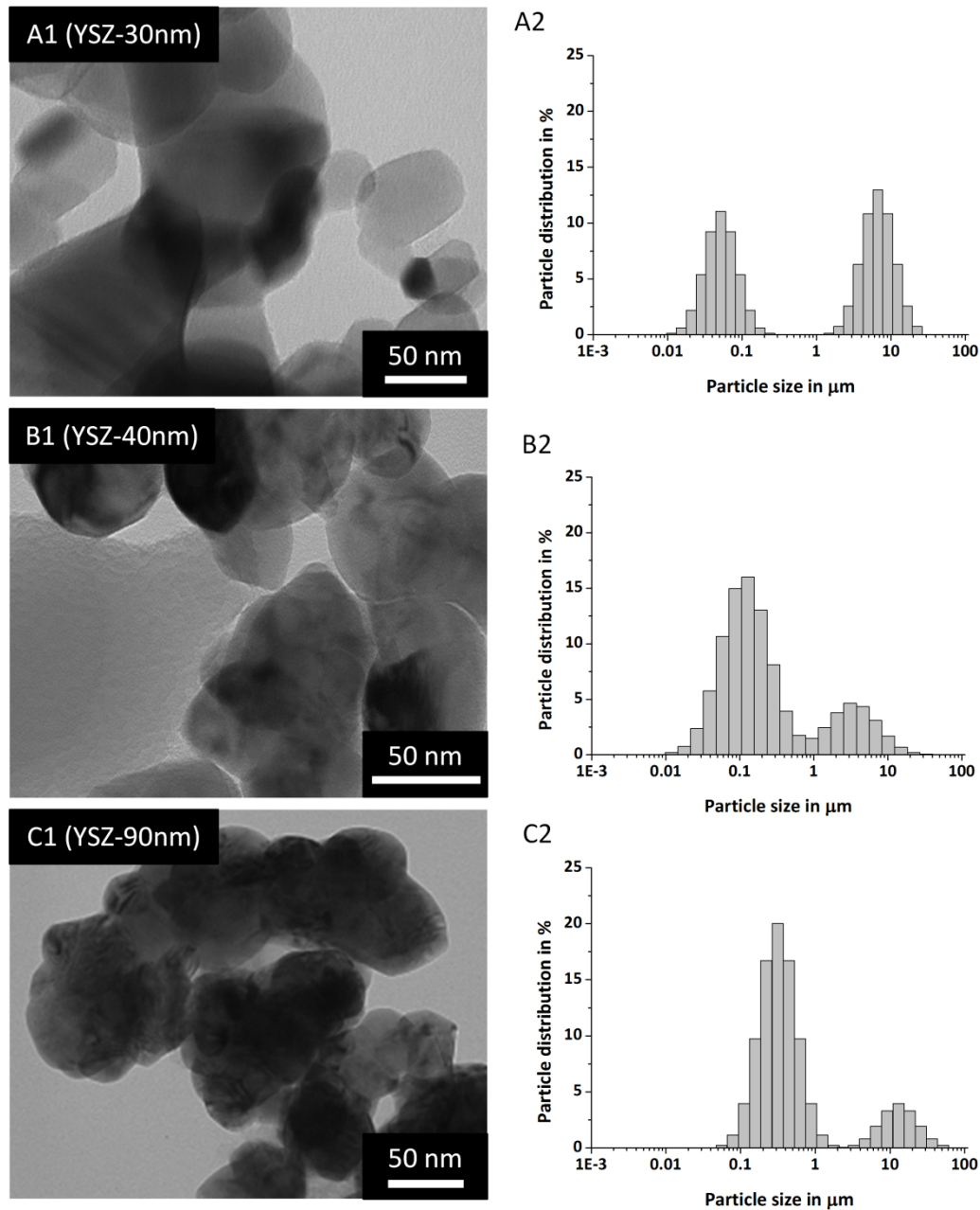
Figure 4.3. TEM images (1) and particle size distributions (2) obtained by acoustic spectroscopy for A = YSZ-30nm powder, B = YSZ-40nm powder and C = YSZ-90nm powder.

The virus retention test was performed in dead-end mode and virus containing solutions were intracapillary fed to single capillary membranes with an accessible length of 1.5 cm. For each filtration test, new single sintered capillary membranes were used (Type 1-5) and intracapillary virus feeding was performed at an applied pressure of 500 mbar until a permeate volume of 15 mL was reached. For each membrane type, three individual capillary membranes were tested in parallel (triplicate determination).

The bacteriophages in the feed solution and permeate were enumerated using the plaque-forming-unit (PFU) method according to the procedure as described in our previous work.[16] The PFU method was performed using 5 mL feed and permeate solution, respectively, and virus quantification was done in triplicate. The dosage of bacteriophage stocks was aimed to reach a final concentration of 10^9 PFU/mL and therefore, theoretically detectable virus retention was LRV of 9 which is equivalent to a percental value of 99.9999999 %.

Long-term virus filtration tests for a period of two weeks were performed using the experimental set-up as shown in Figure 4.2 with the exception that a virus containing solution instead of water served as feed. The long-term filtration test was performed in dead-end mode and a MS2 containing solution with a concentration of 10^9 PFU/mL was intracapillary fed at an applied pressure of 500 mbar to a single capillary membrane (Type 3) with a length of 1.5 cm. For statistical significance four individual capillary membranes were used in parallel (fourfold determination). Every day (i.e. after a filtration time of 24 h) the water permeate flux and the transmembrane pressure were determined and the virus retention capacity of each capillary was analyzed by plaque test. Backflushing was applied after the membrane flux reached a threshold level less than $5 \, \mathrm{L/(m^2 hbar)}$. Therefore, a pulsating backflush was performed for a period of 3 h using a $MgCl_2$ (pH 5.8) solution. The capillary was therefore alternating backflushed at an applied pressure of 1000 mbar for 20 min and flushed forward at an applied pressure of 500 mbar for 2 min. The capillary was finally backflushed for 21 h at an applied pressure of 1000 mbar being ready for a new filtration cycle. The virus feed solution was replaced after each backflushing cycle by a new prepared MS2 solution showing a concentration of 10^9 PFU/mL. The long-term virus filtration experiment was performed for two weeks and three backflushing cycles for membrane cleaning were applied (after day 4, 8 and 12, respectively).

4.3 Results and Discussion

4.3.1 Properties of YSZ Powders

TEM was performed to analyse the size, surface and morphology of used YSZ particles and the results are shown in Figure 4.3 presenting TEM images of YSZ-30nm (A1), YSZ-40nm (B1) and YSZ-90nm (C1). According to the manufacturer data, the specified primary particle sizes of < 30 nm, 40 nm and 90 nm can be confirmed by TEM analyses. All YSZ particles have a spherical shape and the tendency to form agglomerates.

In addition to TEM measurements, particle size distributions and average particle sizes (d_{50}-values) of the YSZ powders were quantified by acoustic spectroscopy. These quantitative results are shown in Figure 4.3 for the different powders in form of YSZ-30nm (A2), YSZ-40nm (B2) and YSZ-90nm (C2). All powders have a bimodal particle size distribution where the first peak at lower particle sizes < 1 µm represents the primary particle size and possible small agglomerations, respectively. The second peak at particle sizes > 1 µm indicates larger agglomerations composed of several YSZ particles. In agreement with the manufacturer data, increased particle sizes in the following order were obtained: YSZ-30nm < YSZ-40nm < YSZ-90nm. The determined average particle sizes (d_{50}) in relation to first peaks were 55 nm, 122 nm and 310 nm, respectively. Compared to specified primary YSZ particle sizes of the manufacturers, increased d_{50}-values (first peaks) by factor 1.7-3.4 were obtained assuming particle aggregation which can be confirmed by TEM analyzes (Figure 4.3, A1-C1).

The second peak of the bimodal particle size distributions is attributed to greater agglomerates > 1 µm. Figure 4.3 shows, that the tendency to form agglomerates decreases with increasing YSZ particle sizes. Hence, the intensity of the second peaks decreases in the following order: YSZ-30nm > YSZ-40nm > YSZ-90nm. However, under consideration of agglomeration, the YSZ particle sizes specified by the manufacturers can

be confirmed by qualitative TEM analyses and quantitative acoustic spectroscopy measurements. Table 1 summarizes the results of the acoustic spectroscopy measurements for the powders YSZ-30nm (VP Zirkonoxid 3-YSZ, Evonik Industries), YSZ-40nm (TZ-3Y-E, Krahn Chemie GmbH) and YSZ-90nm (TZ-3YS-E, Krahn Chemie GmbH) in comparison to the manufacturer data. In addition, the density, specific surface area and IEPs of YSZ powders are given.

Table 4.1.   Properties of used YSZ powders (YSZ-30nm, YSZ-40nm and YSZ-90nm powder).

		VP Zirkonoxid 3-YSZ	TZ-3Y-E	TZ-3YS-E
	Product name	Evonik Industries	Tosoh Corporation[a]	Tosoh Corporation[a]
	Company	YSZ-30nm	YSZ-40nm	YSZ-90nm
	Abbreviations of YSZ powder types			
Manufacturer's data	Primary particle size (nm)	<30	40	90
	Density (g/cm^3)	n/a	6.1	6.1
	Specific surface area (m²/g)	40 ± 15	16 ± 3	7 ± 2
	IEP (-)	7.1	8.6	8.5
Measurements	Particle size (nm) (bimodal distribution): peak 1; peak 2	55; 6700	122; 3080	310; 13000
	Density (g/cm^3)	5.7	5.8	5.8
	Specific surface area (m²/g)	39.4 ± 0.8	14.4 ± 0.2	6.6 ± 0.1
	IEP (-)	7.3	9.0	8.2

[a] YSZ powders were produced from Tosoh Coorperation, Inc. (Japan) and sold by Krahn Chemie GmbH (Germany)

The density of the powders YSZ-30nm, YSZ-40nm and YSZ-90nm which was measured by helium pycnometry is 5.7 g/cm³ and 5.8 g/cm³, respectively, and these values are in agreement with the density of 3 mol% (~5 wt%) YSZ powders indicated by the manufacturer. As expected, YSZ powders with increasing particle sizes show decreased specific surface areas and determined values of 39.4 ± 0.8 m²/g (YSZ-30nm), 14.4 ± 0.2 m²/g (YSZ-40nm) and 6.6 ± 0.1 m²/g (YSZ-90nm) are in accordance with the information specified by the manufacturers. Based on zeta potential measurements the IEPs of YSZ-30nm, YSZ-40nm and YSZ-90nm are 7.3, 9.0 and 8.2, respectively, and thus, IEPs of YSZ powders at neutral or rather slight basic pH values are obtained which is as expected for YSZ particles doped with 3 mol% yttria.

4.3.2 Properties of Extruded YSZ Capillaries
4.3.2.1 Sintering Shrinkage
The outer diameter (OD) and inner diameter (ID) of the sintered (1050 °C for 2 h) capillaries were measured by optical microscopy. The initial size of the capillaries after the extrusion was equal to the dimensions of used extrusion die (2.0 mm

diameter) and integrated pin (1.0 mm diameter). Figure S1 (Supplementary information) compares the measured outer and inner diameters of the capillaries in the sintered state made of different YSZ powders varying in their particle size. The sintering shrinkage implies the shrinkage after drying and sintering and therefore, it is equal to the total shrinkage. As expected, all capillary types shrink during drying as well as during sintering. The highest shrinkage is detected for the Type 1 and Type 2 capillaries which were based on the lowest YSZ particle size (YSZ-30nm or rather a mixture of YSZ-30nm and YSZ-40nm), because relatively high specific surface areas of around 39.4 m²/g and 14.4 m²/g (Tab. 1) are responsible for the induction of increased particle-particle-contacts and for the driving force during sintering. The outer as well as the inner diameter were reduced to around 80 % of their initial size due to applied sintering at 1050 °C for 2 h. The outer diameter of both capillary types is 1.65 ± 0.04 mm and the inner diameter changed to 0.8 ± 0.04 mm. In contrast to the capillaries made of YSZ-40nm and YSZ-90nm (Type 3-5), no difference between the shrinkage of the outer and inner diameter was determined.
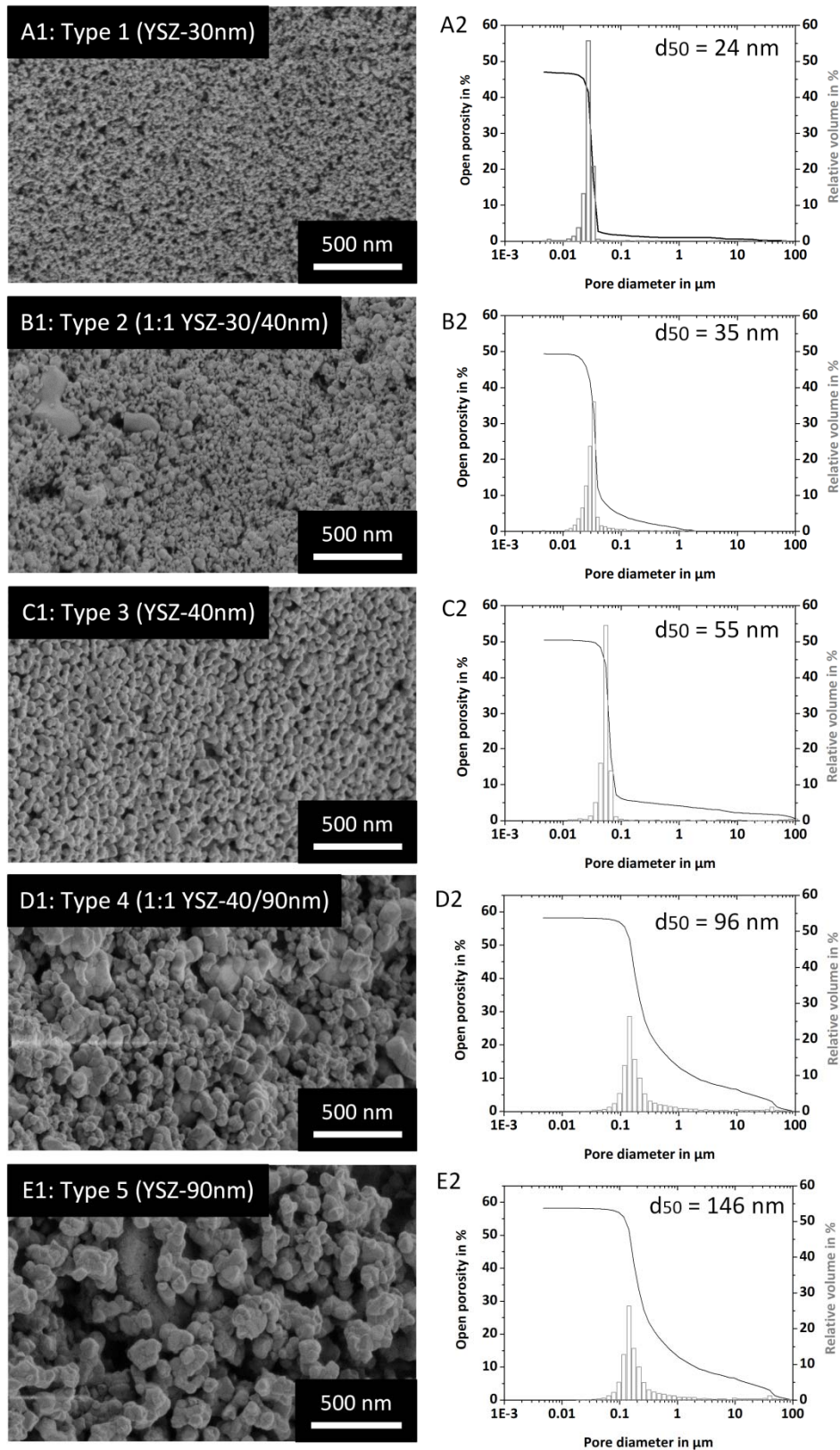
Figure 4.4. Microstructures of the outer capillary surface (1) and pore size distributions as well as open porosities (2) of YSZ capillaries sintered at 1050 °C for 2 h based on different initial YSZ powders. A = YSZ-30nm capillary, B = capillary made of YSZ-30nm and YSZ-40nm, C = YSZ-40nm capillary, D = capillary made of YSZ-40nm and YSZ-90nm and E = YSZ-90nm capillary.

Table 4.2. Membrane properties of YSZ capillaries sintered at 1050 °C based on different initial YSZ powders

Parameter	YSZ capillary type				
	Type 1 (YSZ-30nm)	Type 2 (1:1 YSZ-30/40nm)	Type 3 (YSZ-40nm)	Type 4 (1:1 YSZ-40/90nm)	Type 5 (YSZ-90nm)
Hg-porosimetry					
Pore diameter (nm)	10 - 40	10 - 50	20 - 100	20 - 300	50 - 500
Measured d_{50} (nm)	24.0 ± 2.6	35.0 ± 1.0	55.3 ± 3.2	96.0 ± 2.6	146.0 ± 4.4
Calculated d_{50} based on random close packing (nm)[a]	25.3	n.d.	56.1	n.d.	142.6
Calculated d_{50} based on random loose packing (nm)[b]	26.4	n.d.	58.6	n.d.	148.8
Open porosity (%)[c]	42.8 ± 2.6	35.6 ± 1.7	42.1 ± 3.0	34.1 ± 2.6	45.4 ± 2.7
BET method					
Specific surface area (m²/g)	21.9 ± 2.6	16.3 ± 0.1	10.0 ± 0.4	8.4 ± 0.1	5.5 ± 0.0
3-point bending test					
Bending strength (MPa)	38.0	28.1	26.3	12.9	9.2
Weibull modulus m (-)	6.2	6.6	8.2	6.1	5.2

[a] Average pore diameters for capillaries made of single YSZ powders are calculated according to Eq. (1) based on the work from Gotoh et al.[1]

[b] Average pore diameters for capillaries made of single YSZ powders are calculated according to Eq. (2) based on the work from Gotoh et al.[1]

[c] Based on the intruded Hg volume the determined open porosity is related to the pore size range representing exclusively the pores in the membrane (<0.5 μm)

Compared to capillaries made of YSZ-30nm (Type 1), samples based on only YSZ-40nm (Type 3) or only YSZ-90nm (Type 5) show significantly reduced shrinkage values. These two capillary membranes show a similar shrinkage behavior. After sintering at 1050 °C for 2 h, the capillaries made of YSZ-40nm (Type 3) and YSZ-90nm (Type 5) have an outer diameter of approximately 92 - 95 % and an inner diameter of approximately 84-89 % compared to their initial geometrical dimensions. The Type 4 capillaries which are based on both, YSZ-40nm and YSZ-90nm powder, show a higher shrinkage in comparison to the capillaries based on only one of these powders, but a lower shrinkage compared to the capillaries based on YSZ-30nm powder (Type 1 and Type 2). The shrinkage after sintering is 86 % for the outer diameter and around 80 % for the inner diameter.

4.3.2.2 Pore Size Distribution and Open Porosity

Ceramic capillary membranes were fabricated using initial YSZ powders differing in their particle size (YSZ-30nm, YSZ-40nm and YSZ-90nm) and both individual and mixed YSZ powders were used for membrane fabrication resulting in sintered capillaries with high contour accuracy (Figure 4.1). In addition to the macroscopic overview, Figure 4.4 presents the microstructures of the outer capillary surface obtained by SEM (A1-E1). Here, the pores are uniformly distributed within the YSZ matrix and as expected, increased pore sizes are achieved by the processing of YSZ powders with increased particle sizes (Type 1 < Type 2 < Type 3 < Type 4 < Type 5). Quantification of the pore size distribution, average pore diameter (d_{50}) and open porosity for all capillary types 1-5 was achieved by Hg-porosimetry as shown in parts A2-E2 of Figure 4.4. The sintered capillary membranes based on both single YSZ powders (Type 1, 3 and 5) and mixed YSZ powders (Type 2 and 4) show monomodal pore size distributions.

According to SEM analyses, increasing the initial YSZ particle size led to increased pore sizes of the capillary membrane. In relation to used YSZ

powders in form of YSZ-30nm (Type 1), 1:1 YSZ-30/YSZ-40nm (Type 2), YSZ-40nm (Type 3), 1:1 YSZ-40/YSZ-90nm (Type 4) and YSZ-90nm (Type 5) pore size distributions are obtained from 10 to 40 nm (A2), 10 to 60 nm (B2), 20 to 100 nm (C2), 20 to 500 nm (D2) and 50 to 500 nm (E2). The determined average pore diameters were 24 nm, 35 nm, 57 nm, 96 nm and 146 nm, respectively, which can be attributed to the mesoporous and lower macroporous range.

Parts A2-E2 of Figure 4.4 show that the open porosity of the capillary membranes made of single and mixed YSZ powders is in a similar range of around 47-55 %. Thereby, a relatively high content of the open porosity up to 11 % can be attributed to pore sizes > 0.1 μm (A2, B2, C2) and > 0.5 μm (D2, E2), respectively. The intruded Hg volume representing this porosity content can be related to surface inhomogeneities of the capillary membrane and the inner channel of the capillary (lumen). Thus, the open porosity which exclusively represents the pore sizes of the apillary membranes composed of individual YSZ powders (Type 1, 3 and 5, respectively) is approximately 42-45 %. Here, the initial particle size has no significant influence on the membrane open porosity because of the random arrangement of uniform YSZ particles during processing (YSZ-30nm, YSZ-40nm and YSZ-90nm, respectively). In contrast, the capillary membranes composed of mixed YSZ powders (Type 2 and 4) show lower open porosities of around 36 % considering relevant pore sizes < 0.5 μm. This reduction of the open porosity can be attributed to a higher particle packing density where smaller particles can fill the 'gaps' (i.e. pores) between bigger particles. The tendency to form high particle densities is further strengthened by capillary membranes made of YSZ-30nm and YSZ-90nm where pore sizes are mesoporous and low open porosities of ~30 %

are evident, being not suitable for the application of high performance membranes for virus filtrations (data not shown).

Table 2 summarizes the results achieved by Hg-porosimetry compared to calculated average membrane pore sizes which show a good matching with the measured ones. Additionally, the specific surface areas obtained by BET analyses and bending strengths obtained by 3-point bending tests are presented. In agreement with determined pore sizes, the specific surface area of the capillary membranes significantly decreased with increasing pore sizes from values of 21.87 ± 2.57 m^2/g (Type 1) to 5.51 ± 0.01 m^2/g (Type 5). Here, an increase of the average pore size from 24 nm to 146 nm (factor ~6) results in a decrease of the specific surface area of the capillaries by a factor of ~4. As expected, the bending strength of the YSZ capillary membranes strongly decreased with increasing membrane pore sizes. Bending strength values for σ_0 from 38.0 MPa (Type 1) to 9.2 MPa (Type 5) were determined. A moderate sintering temperature of 1050 °C for 2 h was chosen to achieve ceramic capillary membranes showing both, high open porosities > ~35 % which are necessary for high performance filtration applications and sufficient mechanical stabilities to endure high pressure loads during filtration. To obtain the highest possible strength level for porous ceramic oxide membranes yttria-stabilized zirconia (YSZ) was used even if it is more expensive compared to alumina. As written by Park[38] the strength of ceramics depends on the porosity as shown in the following equation (Ryshkewitch's equation[39]):

$$\sigma = \sigma_0 e^{-np} \qquad (4.4)$$

where σ is the strength of a porous material, σ_0 is the pore free strength, p is the volume fraction of porosity and n is an integer (n = 4~7).
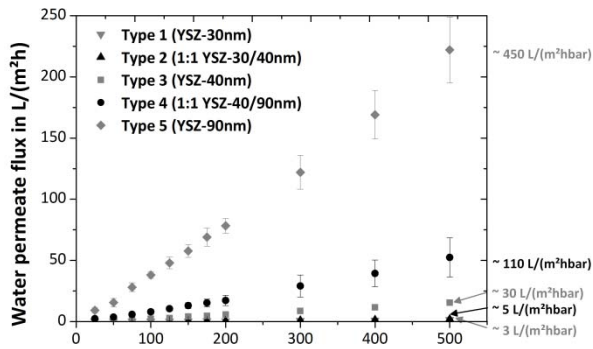
Figure 4.5. Determination of water permeate flux at different applied pressures using YSZ capillaries sintered at 1050 °C based on different initial YSZ powders.

Figure 4.6. Retention of two small bacteriophages in form of MS2 and PhiX174 mediated by YSZ capillaries sintered at 1050 ºC based on different initial YSZ powders. Virus feed concentrations were 10^9 PFU/mL.

As specified by the manufacturers the used YSZ powders have a bending strength of 1200 MPa for dense sintered bodies. The bending strength for dense sintered alumina is around 500 MPa [38]. Considering the Ryshkewitch's equation this higher bending strength by a factor of 2.4 for nonporous YSZ will have an influence on the strength of the porous body. The Weibull modulus m is in a range between 8.2 and 5.2 which is a value quite normal for porous structures compared to other authors who worked with porous ceramic materials.[40-42] Based on capillary membranes showing the highest average pore size of 146 nm in combination with an open porosity of approximately 45 %, the bending strength reached nearly 10 MPa, being already suitable for sample handling and filtration applications.

4.3.2.3 Water Permeate Flux

Figure 4.5 presents the water permeate fluxes of all YSZ capillary membrane types (Type 1-5) as a function of applied pressure. As expected, water permeate fluxes are increased with increasing applied pressures for all YSZ capillary membranes. In agreement with determined pore sizes and open porosities of the capillaries (Figure 4.4, Tab. 2), water permeate fluxes are
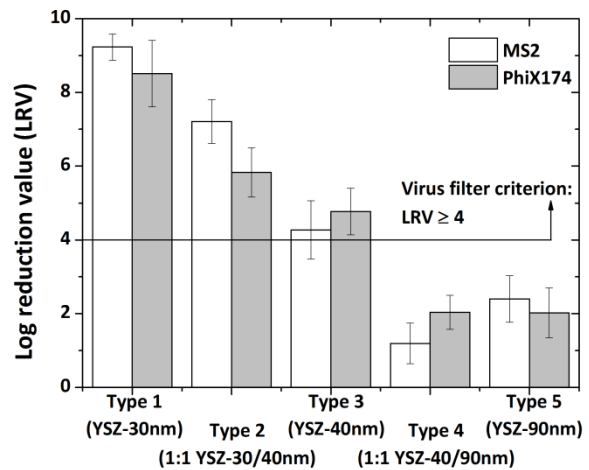
increased in the following order: Type 5 ($\sim$450 L/(m^{2}hbar)) > Type 4 ($\sim$110 L/(m^{2}hbar)) > Type 3 ($\sim$30 L/(m^{2}hbar)) > Type 2 ($\sim$5 L/(m^{2}hbar)) > Type 1 ($\sim$3 L/(m^{2}hbar)). Compared to the capillary membrane made of YSZ-30nm (Type 1) considerable higher water permeate fluxes by a factor of around 150 are achieved for the capillaries made of YSZ-90nm (Type 5). To realize both high water permeate fluxes and a performance reliability during virus filtration operating in dead-end mode an adequate pressure of 500 mbar was applied for all membrane types.

4.3.2.4 Virus Retention

Two small bacteriophages, namely MS2 (25-27 nm) and PhiX174 (26-32 nm), were used to quantify the virus retention capacity of the YSZ capillaries sintered at 1050 °C for 2 h. The virus filtration was performed in dead-end mode by intracapillary virus feeding.
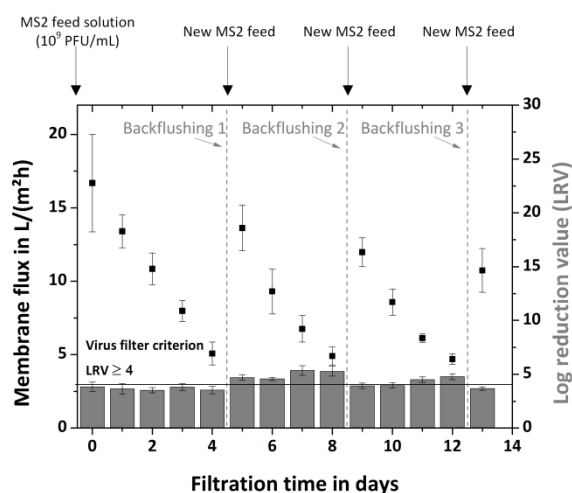
Figure 4.7. Long-term virus filtration with capillary membranes made of YSZ-40nm (Type 3) determining both the water permeate flux and the virus retention capacity as a function of the filtration time. MS2 was used as model virus showing feed concentrations of 10^9 PFU/mL and applied transmembrane pressures were 500 mbar.

Figure 4.6 shows the results of the virus retention performance. As expected, each type of the YSZ capillary membranes (Type 1-5) show a similar retention behaviour for MS2 and PhiX174, because these viruses have nearly the same size. The capillary made of YSZ-30nm (Type 1) shows a LRV of 9.2 ± 0.4 for MS2 and 8.5 ± 0.9 for PhiX174 fulfilling the virus filter criterion (LRV ≥ 4). Based on the mesoporous membrane structure featuring an average pore diameter of 24 nm and an open porosity of 45 % (Figure 4.4/A2) the viruses can be efficiently retained by size exclusion. By increasing the membrane pore size reduced virus retention capacities are obtained resulting in LRVs of around 6-7 (Type 2), 4.5 (Type 3) and 2 (Type 4 and 5, respectively). The processing of powder mixtures of YSZ-40nm and YSZ-90nm (Type 4) as well as the single YSZ-90nm powder (Type 5) results in macroporous membranes with average pore diameters of
96 nm and 146 nm (Figure 4.4/D2 and E2), respectively, which are nearly four and six times higher than the virus diameters. Therefore, these capillary membranes cannot fulfill the virus filter criterion of LRV ≥ 4, being not suitable for virus
58

filtration applications. However, based on used capillaries made of YSZ-40nm (Type 3) both the required LRV of at least 4 is fulfilled for MS2 (4.3 ± 0.8) and PhiX174 (4.8 ± 0.6) and relatively high water permeate fluxes of ~30 L/(m²hbar) (Figure 4.5) are achieved providing a promising candidate for long-term virus filtration. Compared to the Type 5 capillaries (450 L/(m²hbar)) the Type 3 capillaries show reduced water permeate flux values by a factor of 15, but the virus retention capacity of the membrane is fulfilled (LRV ≥ 4). The Type 5 capillaries made of YSZ-90nm are promising membrane candidates due to their high flux properties if the membrane surface characteristics are adequately adjusted for virus adsorption (e.g. wet-chemical aminosilanization, membrane doping with metal oxides (MgO)).

Today, polymer membranes (e.g. PVDF) as presented in the study by El Hadidy et al.[25] show both a high virus retention capacity combined with a high water permeate flux. However, compared to ceramic membranes polymeric membranes show no high chemical, thermal and mechanical stability. Therefore, ceramic membranes can easily be cleaned by backflushing (where high pressure loads are applied), thermal, acidic or basic treatment without affecting the pore morphology.[27] Consequently, cleaned ceramic capillary membranes maintain their integrity and they can be used for a high number of filtration cycles without losing their membrane performance. In contrast to polymeric membranes, the production costs of ceramic membranes are 3 up to 5 times higher, but this can be compensated by their longer lifetime of up to ten years instead of one year for polymeric membranes.[28]

4.3.2.5 Long-Term Virus Filtration Test
Figure 4.7 shows the results of the long-term virus filtration test for two weeks using Type 3 capillaries (YSZ-40nm) and the bacteriophage MS2 to analyze the pore blocking behavior during filtration (membrane fouling) and the membrane regeneration potential mediated by backflushing. In agreement with determined water permeate fluxes at an applied pressure of

500 mbar for capillary membranes made of YSZ-40nm (Figure 4.5/Type 3) an initial membrane flux of 16.7 L/(m^{2}h) (day 0) is obtained. By virus filtration for four days the membrane flux is stepwise reduced to 5 L/(m^{2}h) (factor ~3) whereas LRVs of around 4 were evident during filtration (after day 1, day 2, day 3 and day 4, respectively) ensuring a reliable virus retention by size exclusion. Backflushing was applied after four filtration days resulting in a membrane flux value of 13.6 L/(m^{2}h) which is marginally lower compared to the initial membrane flux (day 0). However, retained viruses at the membrane surface which were responsible for pore plugging can be successfully removed by backflushing and cleaned capillary membranes are provided for a new virus filtration cycle. Due to the second and third filtration cycle from day 4-8 and day 8-12, respectively, the membrane fluxes are decreased with increasing filtration times and the membrane virus retention capacities are slightly increased of around 11 % and 19 %, respectively, based on membrane fouling and the associated pore plugging by retained viruses. The fouled capillary membranes can be regenerated by applied backflushing steps. Membrane fluxes of 12.0 L/(m^{2}h) and 10.7 L/(m^{2}h) are obtained after second and third backflushing procedure, respectively, while the virus retention capacities of the capillary membranes are not really affected by both increased filtration times and backflushing showing LRVs of around 4. Compared to the initial membrane flux (day 0) a flux reduction of 36 % is obtained after the third backflushing step (day 13) still fulfilling the virus filter criterion after a filtration time of nearly two weeks which is required by WHO and USEPA to guarantee save drinking water.

4.4 Conclusion

This study demonstrates the possibility to fabricate YSZ capillary membranes with adjustable pore size by extrusion for controlled virus retention. The effect of the initial YSZ particle size on the capillary properties was analyzed in detail focusing on the macro- and microstructure. Based on the achieved results the YSZ-phase and the pores were uniformly distributed forming two interpenetrating networks with the individuals (particles and pores). Increasing the initial YSZ particle size led to an increased pore size of the capillary membrane. By utilization of different YSZ powders (single versus mixed powders) showing primary particle sizes of 30 nm, 40 nm and 90 nm, average pore sizes of the capillary membranes of 24 nm (Type 1 made of YSZ-30nm), 35 nm (Type 2 made of YSZ mixture of YSZ-30nm/40nm), 55 nm (Type 3 made of YSZ-40nm), 96 nm (Type 4 made of YSZ mixture of YSZ-40/90nm) and 146 nm (Type 5 made of YSZ-90nm) were generated. A sintering at moderate temperatures of 1050 °C for 2 h induced the formation of sintering necks between single YSZ particles generating capillary microstructures with relatively high open porosities of ~45 % for capillary membranes made of single YSZ powders and ~36 % for capillary membranes made of mixed YSZ powders in combination with a sufficient mechanical stability for filtration applications.

Based on adjustable membrane pore sizes in the meso- and lower macroporous range, the virus filtration efficiency can be controlled where increased pore sizes led to higher permeate fluxes, but at the same time to reduced virus retention capacities. Fulfilling the virus filter criterion of at least 4 LRV level in combination with high flow capacities, capillaries made of YSZ-40nm (Type 3) are promising candidates for sustainable virus filter systems. Here, small bacteriophages in form of MS2 and PhiX174 were efficiently retained (LRV of 4.3 and 4.8, respectively) and water permeate fluxes of around 30 L/(m^{2}hbar) were obtained. Under consideration of the initial particle size of the used ceramic powder, the presented processing route represents a versatile tool for the fabrication of tubular ceramic membranes with reliable cut-offs for virus filtration applications.

However, the capillaries made of a mixture of YSZ-40/90nm and YSZ-90nm (Type 4 and Type 5), respectively, which do not fulfill the virus filter criterion can be advantageously used for high flux filtration applications if an adequate adsorption capacity for viruses by a membrane

surface functionalization is provided. Beside conventional chemical membrane functionalization strategies (e.g. silanizations) the direct integration of metal oxides (e.g. FeO, MgO) during slurry preparation can open up new perspectives on analyzing the interactions between viruses and modified ceramic surfaces under flow conditions. A long-term virus filtration test for two weeks using Type 3 capillaries (YSZ-40nm) showed that a membrane regeneration can be successfully applied by backflushing maintaining relatively high membrane fluxes in combination with requested LRV 4 level by WHO and USEPA fulfilling the virus filter criterion.

Acknowledgements

References

1. K. Gotoh, et al. "Pore size distributions in random assemblies of equal spheres". *The Journal of Chemical Physics*, 1986, 85, 3078-3080.
2. U. Nations, ed. U. Nations, New York, 2012.
3. J. P. S. Cabral. "Water Microbiology: Bacterial Pathogens and Water". *International Journal of Environmental Research and Public Health*, 2010, 7, 3657-3703.
4. W. H. Organization, WHO Press, Geneva, 2005.
5. K. Onda, et al. "Global Access to Safe Water: Accounting for Water Quality and the Resulting Impact on MDG Progress". *International Journal of Environmental Research and Public Health*, 2012, 9, 880-894.
6. A. Gadgil. "Drinking water in developing countries". *Annual Review of Energy and the Environment* 1998, 23, 253-286.
7. R. D. Arnone and J. P. Walling. "Waterborne pathogens in urban watersheds". *Journal of Water and Health*, 2007, 05.1, 149-162.
8. T. Clasen, et al. "Cost-effectiveness of water quality interventions for preventing diarrhoeal disease in developing countries". *Journal of Water and Health*, 2007, 599-608.
9. M. A. Shannon, et al. "Science and technology for water purification in the coming decades". *Nature*, 2008, 452, 301-310.
10. H. Junli, et al. "Disinfection effect of chlorine dioxide on viruses, algae and animal planktons in water". *Water Research*, 1997, 31, 455-460.
11. W. H. Organization, ed. M. D. Sobsey, Geneva, 2002.
12. G. Ko, et al. "UV inactivation of adenovirus type 41 measured by cell culture mRNA RT-PCR". *Water Research*, 2005, 39, 3643-3649.
13. A. Duek, et al. "New and conventional pore size tests in virus-removing membranes". *Water Research*, 2012, 46, 2505-2514.
14. I. Voigt. "Nanofiltration with ceramic membranes". *Chemie Ingenieur Technik*, 2005, 77, 559-564.
15. B. Michen, et al. "Virus Removal in Ceramic Depth Filters Based on Diatomaceous Earth". *Environmental Science & Technology*, 2011, 46, 1170-1177.
16. S. Kroll, et al. "High virus retention mediated by zirconia microtubes with tailored porosity". *Journal of the European Ceramic Society*, 2012, 32, 4111-4120.
17. N. Muhammad, et al. "Ceramic Filter for Small System Drinking Water Treatment: Evaluation of Membrane Pore Size and Importance of Integrity Monitoring". *J Environ Eng*, 2009, 135, 1181-1191.
18. T. Meyn, et al. "MS2 removal from high NOM content surface water by coagulation - ceramic microfiltration, for potable water production". *AIChE Journal*, 2012, 58, 2270-2281.
19. B. Zhu, et al. "Virus removal by iron coagulation–microfiltration". *Water Research*, 2005, 39, 5153-5161.
20. L. Fiksdal and T. Leiknes. "The effect of coagulation with MF/UF membrane filtration for the removal of virus in drinking water". *Journal of Membrane Science*, 2006, 279, 364-371.
21. N. Shirasaki, et al. "Comparison of removal performance of two surrogates for pathogenic waterborne viruses, bacteriophage Qβ and MS2, in a coagulation–ceramic microfiltration system". *Journal of Membrane Science*, 2009, 326, 564-571.
22. F. Meder, et al. "The role of surface functionalization of colloidal alumina particles on their controlled interactions with viruses". *Biomaterials*.
23. B. Michen, et al. "Improved Virus Removal

in Ceramic Depth Filters Modified with MgO". *Environmental Science & Technology*, 2013, 47, 1526-1533.

24. M. Wegmann, et al. "Modification of ceramic microfilters with colloidal zirconia to promote the adsorption of viruses from water". *Water Research*, 2008, 42, 1726-1734.

25. A. M. ElHadidy, et al. "An evaluation of virus removal mechanisms by ultrafiltration membranes using MS2 and φX174 bacteriophage". *Separation and Purification Technology*, 2013, 120, 215-223.

26. J. Langlet, et al. "Efficiency of MS2 phage and Qβ phage removal by membrane filtration in water treatment: Applicability of real-time RT-PCR method". *Journal of Membrane Science*, 2009, 326, 111-116.

27. J. Finley. "Ceramic membranes: a robust filtration alternative". *Filtration & Separation*, 2005, 42, 34-37.

28. E. P. Garmash, et al. "Ceramic membranes for ultra- and microfiltration (Review)". *Glass and Ceramics*, 1995, 52, 150-152.

29. C. B. Carter and M. G. Norton, "Ceramic Materials, Science and Engineering", New York, 2007.

30. S. S. Madaeni, et al. "Virus removal from water and wastewater using membranes". *Journal of Membrane Science*, 1995, 102, 65-75.

31. S. S. Madaeni. "The application of membrane technology for water disinfection". *Water Research*, 1999, 33, 301-308.

32. R. Aronino, et al. "Removal of viruses from surface water and secondary effluents by sand filtration". *Water Research*, 2009, 43, 87-96.

33. A. R. Hanifi, et al. "Effects of calcination and milling on surface properties, rheological behaviour and microstructure of 8mol% yttria-stabilised zirconia (8 YSZ)". *Powder Technology*, 2012, 231, 35-43.

34. M. Qiu, et al. "Preparation of supported zirconia ultrafiltration membranes with the aid of polymeric additives". *Journal of Membrane Science*, 2010, 348, 252-259.

35. S. Kroll, et al. "Development and characterisation of functionalised ceramic microtubes for bacteria filtration". *Journal of Membrane Science*, 2010, 365, 447-455.

36. S. Kroll, et al. "Highly Efficient Enzyme-Functionalized Porous Zirconia Microtubes for Bacteria Filtration". *Environmental Science & Technology*, 2012, 46, 8739-8747.

37. B. Michen and T. Graule. "Isoelectric points of viruses". *Journal of Applied Microbiology*, 2010, 109, 388-397.

38. J. Park, "Bioceramics; Properties, Characterization and Apllications", Springer Science and Business Media, LLC, New York, USA, 2008.

39. E. Ryshkewitch. "Compression Strength of Porous Sintered Alumina and Zirconia". *Journal of the American Ceramic Society*, 1953, 36, 65-68.

40. T. Isobe, et al. "Gas permeability and mechanical properties of porous alumina ceramics with unidirectionally aligned pores". *Journal of the European Ceramic Society*, 2007, 27, 53-59.

41. A. Atkinson and A. Selçuk. "Mechanical behaviour of ceramic oxygen ion-conducting membranes". *Solid State Ionics*, 2000, 134, 59-66.

42. C. Brandes, et al. "Gel Casting of Free-Shapeable Ceramic Membranes with Adjustable Pore Size for Ultra- and Microfiltration". *Journal of the American Ceramic Society*, 2014, 97, 1393-1401.

5. Amino-Functionalized Ceramic Capillary Membranes for Controlled Virus Retention

Adapted from

Amino-Functionalized Ceramic Capillary Membranes for Controlled Virus Retention

Authors

Julia Bartels[1], Marina N. Souza[1], Amelie Schaper[1], Pál Árki[2], Stephen Kroll[1,3], Kurosch Rezwan[1,3]

[1]Advanced Ceramics, University of Bremen, Am Biologischen Garten 2, 28359 Bremen, Germany

[2]Institute of Electronic- and Sensor-Materials, Technical University (TU) Bergakademie Freiberg, Gustav-Zeuner Str. 3, 09599Freiberg, Germany

[3]MAPEX - Center for Materials and Processes, University of Bremen, Am Fallturm 1, 28359 Bremen, Germany

Abstract

A straightforward chemical functionalization strategy using aminosilanes for high-flux yttria-stabilized zirconia capillary membranes (YSZ-90nm) is presented to apply an adequete adsoprtion capacity for viruses (macroporous, d_{50} = 144 nm, open porosity = 49 %, membrane flux ~150 L/(m^{2}hbar)). As shown in chapter 4, the unfunctionalized YSZ-90nm capillaries do not fulfill the virus filter criterion of at least 4 LRV level, but do show a high water perrmeate flux. Therefore, three different aminosilanes with one, two or three amino groups per silane molecule, namely 3-aminopropyltriethoxysilane (APTES), N-(2-aminoethyl)-3-aminopropyltriethoxysilane (AE-APTES) and N-(3-trimethoxysilylpropyl)diethylenetriamine (TPDA), are used to generate the amino-functionalized membranes. With a higher number of amino groups per silane molecule increased loading capacities between 0.44-1.01 accessible amino groups/nm^2 membrane are achieved. Streaming potential measurements confirm that the zeta-potential of the membrane surface is converted from negative (non-functionalized) to positive (amino-functionalized). By operation in dead-end filtration mode using the model virus MS2 (diameter = 25 nm, IEP = 3.9) the virus retention capacity of the amino-functionalized membranes is significantly increased and log reduction values (LRVs) of up to 9.6 ± 0.3 (TPDA) are obtained whereas a LRV < 0.3 is provided by the non-functionalized membranes. Long-term dead-end filtration experiments for one week reveal a high stability of immobilized aminosilanes (TPDA), being robust against leaching. By iterative backflushing with desorption buffer MS2-loaded membranes are successfully regenerated being reusable for a new filtration cycle. The presented functionalization platform is highly promising for controlled virus retention.

5.1 Introduction

Filtration technologies are used to purify liquids from contaminations made of chemical (e.g. organic and inorganic species), physical (e.g. color) and biological (e.g. bacteria and viruses) origin.[1] Especially, biological contaminations based on viruses can cause harmful and debilitating diseases and they are one of the most challenging contaminations in water supplies[2], food products[3] or biopharmaceutics[4] which have to be controllable eliminated to ensure the protection of public health. The interest in virus adsorption mechanisms is not only limited to contamination removal, but also for virus concentration to overcome detection limits in liquid samples[5] or for the preparation of inactivated viral vaccines for e.g. influenza control[6]. The major challenge for contamination removal is to provide membrane systems showing high membrane fluxes in combination with high retention capacities to guarantee a highly effective filtration performance. Today, polymeric membranes combine both requirements for virus filtration[7, 8], but compared to ceramic membrane applications limitations are given due to reduced chemical, thermal and mechanical stabilities. Furthermore, ceramic membranes show no swelling behavior preserving their integrity, the adjustment of nano-scaled narrow pore size distributions is feasible and cleaning by backflushing, thermal, acidic or basic treatment can be successfully performed for membrane regeneration.[9, 10] All in all, the higher material and fabrication costs for ceramic membranes can be compensated by their longer service life of up to ten years.[10]

Due to the fact that most viruses show isoelectric points (IEPs) between 3.5 and 7.0[11] and the pH of contaminated water samples is often attributed to the neutral pH-regime, an ideal adsorbent with high application potential has an IEP $\geq$ 8, i.e. being positively charged at acidic and neutral pH conditions. The often used model bacteriophage MS2 is a single-stranded RNA virus which belongs to the family Leviviridae showing a diameter of 25 - 27 nm[12] and an IEP of 3.9[11]. An improved virus removal has been reported by several authors for materials which provide a positive surface charge at neutral pH, which can be achieved for ceramic materials by coating, doping or chemical surface functionalization. Metal oxyhydroxides such as $Y(OH)_x$, $Zr(OH)_x$ and $Mg(OH)_2$ are used to coat or dope membranes for enhancing the virus retention capacity.[13-15] Iron oxide is added to a biosand filter to reach a higher adsorption capacity[16] as well as zerovalent Fe is used to adsorb viruses from liquid samples.[17, 18] Silanes can be beneficially used for chemical functionalization approaches as there is a broad spectrum of available silanes showing different functional groups (e.g. amino-, carboxyl- or alkyl-groups) and spacer length.[19] Silanization can be performed at moderate temperatures in aqueous[20, 21] and organic solvents[22, 23], respectively, or in vapor phase[24, 25] on almost any type of material and support being widely used for tailored chemical surface functionalities[19]. Focusing on virus adsorption especially amino groups as accessible chemical surface functionalities are successfully applied as they provide a positive surface charge for the adsorption of negatively charged viruses at neutral and acidic pH, respectively. Therefore, different authors determined high virus adsorption capacities by wet chemical functionalization of silica and alumina particles with aminosilanes.[26-29]

The aim of this work is to generate amino-silanized yttria-stabilized zirconia (YSZ) capillary membranes for controlled virus retention which combine a high membrane flux with a high virus adsorption capacity. Therefore, a straightforward wet chemical functionalization strategy is presented where the sintered inert YSZ capillary membranes are firstly activated by acidic hydroxylation followed by aminosilanization for membrane derivatization. Three different aminosilanes with one, two or rather three amino groups per silane molecule, namely 3-aminopropyltriethoxysilane (APTES), N-(2-aminoethyl)-3-aminopropyltriethoxysilane (AE-APTES) and N-(3-trimethoxysilylpropyl)diethylenetriamine (TPDA), are used to generate the amino-functionalized capillary membranes. The aminosilanization effects on the membrane

64

microstructure (pore size, open porosity, specific surface area), mechanical stability (3-point bending strength), membrane flux as well as the virus retention capacity are investigated in detail. Furthermore, the long-term stability of immobilized aminosilanes (TPDA) on the capillary surface is analyzed during a one week dead-end filtration experiment. Finally, a virus filtration test for four days is performed with and without iterative backflushing to show that membrane fouling can be avoided by regular cleaning cycles.

5.2 Materials and Methods

5.2.1 Materials

The yttria-stabilized zirconia (YSZ) powder and reagents were purchased from commercial sources and used without further purification. The YSZ powder TZ-3YS-E (YSZ-90nm, Lot. S304599P, specific surface area = $7 \pm 2 \ m^2/g$, particle size = 90 nm) was obtained from Krahn Chemie GmbH, Germany.

3-aminopropyltriethoxysilane (APTES, 99 %, product number 440140, Lot. SHBD4935V), hydrogen peroxide solution (purum p.a. $\geq$ 35 %, product number 95299, Lot. BCBH5638V), magnesium chloride hexahydrate ($MgCl_2$, product number M2670, Lot. BCBJ3659V), polyvinyl alcohol (PVA, fully hydrolyzed, product number P1763, Lot. SLBC9027V), sodium chloride (NaCl, product number S7653, Lot. SZBC2560V), sulfuric acid (95 - 97 %, product number 30743, Lot. SZBC1390V), tryptic soy agar (TSA, product number 22091, Lot. BCBG4777V), culture media tryptic soy broth (TSB, product number T8907, Lot.

109K0165), N-(3-trimethoxysilylpropyl)diethylenetriamine (TPDA, product number 413348, Lot. MKBQ6059V), orange II sodium salt (product number 75370, Lot. WE304250/1), hydrochloric acid solution (HCl, product number 35328, Lot. SZBD2670V) and sodium hydroxide (NaOH, product number 71692, Lot. SZB82950) were purchased from Sigma-Aldrich Chemie GmbH, Germany. N-(2-aminoethyl)-3-aminopropyltriethoxysilane (AE-APTES, 95 %, product number AB153226, Lot. 1191275) and 3-(trihydroxysilyl)-1-propanesulfonic acid (HSPSA, 30-35 %, product number AB130830, Lot. 1246512) were obtained from abcr GmbH & Co. KG, Germany.

For virus retention tests the bacteriophage MS2 was used serving as small model virus (DSM Cat. No. 13767) and its host bacteria E. coli (DSM Cat. No. 5210) was used for virus propagation, both purchased from German Collection of Microorganisms and Cell Cultures (DSMZ), Germany.

Three commercially available polymeric membranes with different pore sizes were obtained from Sartorius, Germany, namely Minisart® 0.2 µm (Product number 16534, Lot. 50320103), Minisart® 0.1 µm (Product number 16553, Lot. 41281103) and Virosart® CPV (Product number 545VI MOB, Lot. 48017133) serving as membrane references.

Double-deionized water with an electrical resistance of 18 MΩ, which was obtained from a Synergy® apparatus (Millipore, Germany), was used for all experiments.
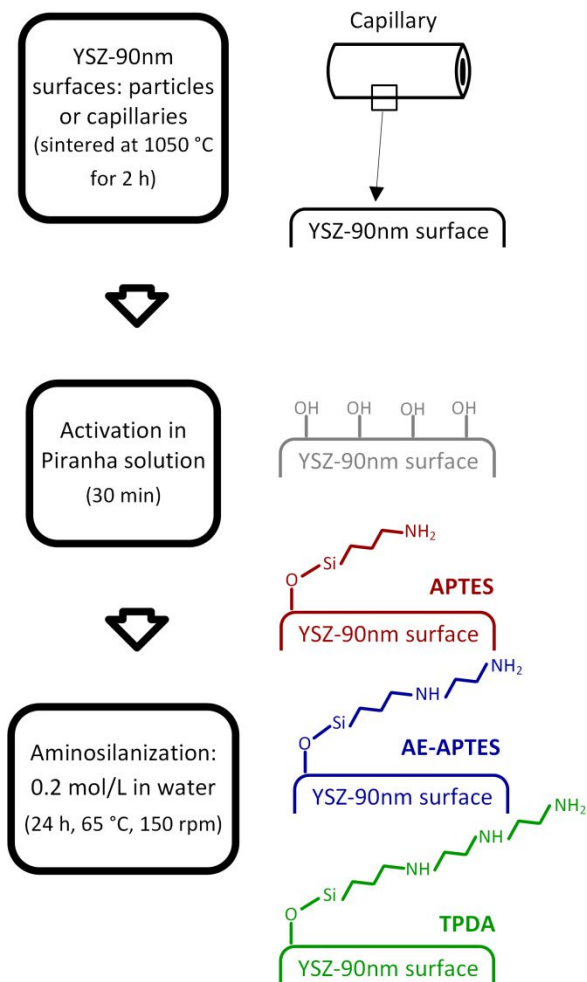
Figure 5.1. Functionalization strategy for aminosilanization of sintered YSZ capillary membranes. APTES = 3-aminopropyltriethoxy silane, AE-APTES = N-(2-aminoethyl)-3-aminopropyltriethoxysilane, TPDA = N-3-(trimethoxysilylpropyl)diethylenetriamine.

5.2.2 Fabrication of YSZ Capillary Membranes by Extrusion

The fabrication of YSZ capillary membranes by extrusion was performed as described in our previous study[30] with slight modifications using a different type of PVA (binder) to obtain both narrower pore size distributions and increased mechanical stabilities of the membranes. For the preparation of the ceramic slurry 132 g YSZ powder (YSZ-90nm) as ceramic material, 4 g APTES acting as dispersant, 20 g PVA-water solution (25 wt.%) serving as binder according to Besser et al.[31] and 13.5 g double-deionized water used as solvent were previously mixed and then

66

milled using 50 alumina grinding balls (diameter = 10 mm) in a planetary ball mill (PM400, Retsch) for 3 h at 350 rpm changing the rotation direction every 5 min. Afterwards, the stabilized and homogeneous slurry was transferred to a self-made laboratory extruder equipped with a die of 2.0 mm in diameter and an integrated pin of 1.0 mm in diameter. To realize a defect-free extrusion of the capillaries both the press capacity and the speed of the conveyor band were optimally coordinated resulting in a constant extrusion speed of 50 cm/min. The extruded capillaries were dried for at least two days at RT (20 °C, relative humidity ~50 %) and finally sintered for 2 h at 1050 °C with dwell times at 280 °C (0.5 h) and 500 °C (1 h) for removing the binder (Nabertherm, Germany).

5.2.3 Chemical Functionalization of YSZ Membrane Surfaces: Activation by Hydroxylation Followed by Aminosilanization

The preparation of amino-functionalized YSZ capillary membranes was performed as shown in Figure 5.1. The sintered YSZ capillary membranes were activated by acidic hydroxylation using Piranha solution (97 % H_2SO_4 : 35 % H_2O_2, 3:1 (v/v)) for 30 min at RT to generate hydroxyl groups on the surfaces of the capillaries. Afterwards the capillaries were rinsed with water until the effluents achieved a neutral pH followed by drying at 70 °C for 16 h. Subsequently, the activated capillaries were silanized with three different aminosilanes showing a different number of amino groups per silane molecule, i.e. APTES providing one primary amino group, AE-APTES providing one primary and one secondary amino group, and TDPA shows one primary and two secondary amino groups. Assuming no inter- and intramolecular cross-linking the total spacer lengths on the YSZ surfaces include 6 (APTES), 9 (AE-APTES) or rather 12 (TPDA) atoms. Five capillary membranes with an individual length of 6 cm were incubated with 10 mL aminosilane solution showing a concentration of 0.2 mol/L. The aminosilane solutions (APTES, AE-APTES and TPDA, respectively) were prepared by dilution with water (pH not adjusted) and the

incubation was carried out at 65 °C under slight shaking at 150 rpm (Inkubator 1000/Unimax 1010, Heidolph) for 24 h. After aminosilanization, the capillaries were washed until the effluents had a neutral pH and finally dried at 70 °C for 16 h (UT6120, Heraeus). Activated capillary membranes were functionalized in the same way as described for amino-silanes with 3-(trihydroxysilyl)-1-propanesulfonic acid (HSPSA) serving as reference. HSPSA molecules show sulfonate groups and are known to be oppositely charged compared to silanes with amino groups, being an ideal candidate as negative control for the virus adsorption experiments.

5.2.4 Characterization of Functionalized YSZ Capillary Membranes

5.2.4.1 Structural and Mechanical Properties

The determination of structural and mechanical properties of the functionalized YSZ capillary membranes was carried out according to our previous study.[30] Hg-porosimetry (Mercury Porosimeter Pascal 140 and 440, POROTEC GmbH) was used to evaluate the pore size distribution, the average pore size (d_{50}) and the open porosity of the capillary membranes. The microstructure of the outer capillary surface was analyzed by scanning electron microscopy (SEM, Field-emission SEM SUPRA 40, Zeiss). The specific surface area was obtained by nitrogen adsorption according to BET method (Gemini, Micromeritics) after degassing the capillaries at 120 °C for at least 3 h with argon. 3-point bending tests were performed according to DIN EN 843-1 (Roell Z005, Zwick) to determine the flexural strength and Weibull modulus.

5.2.4.2 Streaming Potential Measurements

The surface properties of the sintered (non-functionalized), activated, HSPSA-functionalized and aminosilanized capillary membranes were examined with a self-made streaming potential equipment at the Institute of Electronic- and Sensor-Materials at the TU Bergakademie Freiberg, Germany. A gear pump transported a KCl electrolyte solution (10-3 M) from a beaker

tempered at 25 °C through the measuring cell, while measuring the conductivity, the temperature and the pH. The pH is adjusted with either 0.05 M KOH or HCl using an automatic titration unit, starting at pH 9 followed by an acidification to pH 3. The pressure difference and the potential difference is measured either along (overflow measurement) or across (throughflow measurement) the capillary membrane with two Ag/AgCl-electrodes placed at the inlet and the outlet of the electrolyte flow inside the capillary and a third electrode is placed into the permeate. The applied pressure was increased during measurement from 0 bar to a maximum differential pressure of 0.5 bar for the overflow measurements and a trans-capillary pressure difference of 1.2 bar for the throughflow measurements, respectively. After pressure increase (upward measurement) and holding the pressure at 0.5 or rather 1.2 bar (plateau measurement), the pressure was reduced again (downward measurement) while measuring the streaming potentials. The streaming potential coefficient ($\Delta U/\Delta p$) was calculated by the slope of the linear pressure - streaming potential curve. All generated data are transmitted to the process control system. The zeta-potential (ζ-potential) of the capillary surface is calculated from the streaming potential (ΔU) using the Helmholtz-Smoluchowski equation

$$\xi = \frac{\Delta U}{\Delta p}\left(\frac{\eta}{\varepsilon_0 \varepsilon_r}\right)\kappa$$

(5.1)

where Δp is the hydraulic pressure, ε_0 is the permittivity of vacuum, ε_r is the relative permittivity of the solvent, η is the viscosity of the solution and κ is the conductivity of the solution.

5.2.4.3 Quantification of the Aminosilane Loading

The amount of accessible amino groups was quantified by acid orange II assay as described by Kroll et al.[32] with slight modifications. A set of two capillaries with an individual length of 2.5 cm was incubated in 1.75 mL acid orange II reagent (0.5 mM orange II sodium salt in HCl,

pH 3) for 24 h at RT and 300 rpm. Afterwards, the capillary membranes were washed three times with 10 mL HCl (pH 3) to remove unbound and weakly bound acid orange II molecules from the surface. The bound acid orange II dyes were removed by pH-shift adding 2 mL NaOH solution (pH 12) followed by incubation for 15 min at RT and 300 rpm (ThermoMixer C, Eppendorf). After desorption of acid orange II dye, the supernatants were photometrically analyzed at 483 nm (Multiskan Go, Thermo Scientific) where NaOH (pH 12) served as blank sample (triplicate determination). To consider unspecific binding hydroxyl-activated samples served as references and photometrical measured values were subtracted from sample measurements (aminosilanized capillary membranes). A calibration curve of various concentrations of acid orange II dye in NaOH was used to quantify the amount of accessible amino groups per surface area (amino groups/nm^2). For each membrane type, four individual capillaries were tested.

5.2.4.4 Membrane Flux Measurements

Based on our previous work[30], membrane flux measurements of the sintered (non-functionalized), hydroxyl-activated, HSPSA-functionalized and aminosilanized YSZ capillaries were performed by intracapillary water feeding with a peristaltic pump (BVP Standard, Ismatec) operating in dead-end mode using pressures between 100 and 500 mbar (C9500, COMARK). Double-deionized water served as feed solution. For each membrane type, three individual capillaries with a length of 5 cm were tested for 5 min operating in vertical orientation. The membrane flux for 1 bar was calculated by linear regression and flux values were given in L/(m²hbar).

5.2.4.5 Virus Retention Test

The virus retention test for sintered (non-functionalized), hydroxyl-activated, HSPSA-functionalized and aminosilanized capillaries was performed as described in our previous study.[30] In short, a saline solution (0.02 M MgCl$_2$/0.15 M NaCl) at pH 5.8 containing MS2 bacteriophages

served as viral feed solution showing initial virus concentrations between 10^9 and 10^{10} Plaque Forming Units (PFU)/mL. The virus retention test was performed by intracapillary virus feeding in dead-end mode at an applied pressure of 500 mbar until a permeate volume of 15 mL was filtrated. For each membrane type, three individual capillary membranes with a length of 5 cm were tested. The bacteriophages in the feed solution and permeate were enumerated using the PFU method. For the PFU method dilution series of the MS2 feed solution and permeate were performed in 0.02 M MgCl$_2$/0.15 M NaCl solution using 10-fold steps. A sample volume of 1.8 mL of undiluted or rather diluted phage suspension was mixed with 0.2 mL of the host bacteria and 5 mL agar. After pouring the mixture in a Petri dish followed by incubation for 16 h at 37 °C the formed plaques were counted and the Log reduction value (LRV) was calculated as shown by Kroll et al..[33]

As references the virus retention efficiency of three commercial available polymeric membranes (Minisart® 0.2 µm, Minisart® 0.1 µm and Virosart® CPV, Sartorius, Germany) was determined.

5.2.4.6 Leaching of Immobilized Aminosilanes: TPDA Stability

To analyze the wash-out effects of TPDA-functionalized capillaries, the capillaries were intracapillary fed with a saline solution (0.02 M MgCl2/0.15 M NaCl) at pH 5.8 and RT applying a pressure of 500 mbar for up to 7 days using the same experimental setup as for the membrane flux measurements (chapter 5.2.4.4) and virus retention tests (chapter 5.2.4.5). The capillaries were dried at RT after the flushing and an acid orange II test for quantification of the amino group loading was performed as described previously (chapter 5.2.4.3).

5.2.4.7 Virus Filtration Followed by Membrane Regeneration with Desorption Buffer

Mid-term virus filtration tests for a period of four days were performed in dead-end mode and a MS2 containing solution with a concentration of ~10^9 PFU/mL was intracapillary fed at an

Table 5.1. Membrane properties of YSZ-90nm capillary membranes: non-functionalized, activated and functionalized with HSPSA, APTES, AE-APTES and TPDA.

	Hg-porosimetry			BET method	3-point bending test	
Membrane-functionalization	Pore size range in nm	d_{50} in nm	Open porosity in%	Specific surface area in m²/g	Bending strength in MPa	Weibull modulus m
non-functionalized	5-200	144	49.3	5.4 ± 0.0	30.7	8.0
activated	10-200	133	51.8	5.9 ± 0.3	31.1	6.7
HSPSA	5-200	153	46.6	5.9 ± 0.2	26.7	5.5
APTES	8-200	145	48.9	5.4 ± 0.1	28.1	5.1
AE-APTES	5-200	152	47.9	5.2 ± 0.1	29.2	4.4
TPDA	6-200	149	48.3	5.6 ± 0.1	26.9	6.5

applied pressure of 500 mbar to a single capillary membrane functionalized with TPDA showing a length of 5 cm. For statistical significance four individual capillary membranes were used in parallel (fourfold determination). The experiment was performed with and without cleaning cycles with desorption buffer. For the experiment without cleaning cycles, every 24 h the membrane flux was determined and the virus retention capacity of each capillary was analyzed by PFU test. Afterwards, the virus feed solution was replaced by a new prepared MS2 solution showing a concentration of ~10^9 PFU/mL. For the experiment with cleaning cycles, every 22 h the membrane flux was determined and the virus retention capacity of each capillary was analyzed by PFU test and a pulsating backflush was performed after 22 h for a period of 100 min using a saline solution (0.02 M $MgCl_2$/0.15 M NaCl) which was adjusted to pH 3 with HCl (desorption buffer). The capillary was therefore alternating backflushed at an applied pressure of 1000 mbar for 10 min and flushed forward at an applied pressure of 500 mbar for 2 min. The capillary was finally backflushed for 20 minutes at an applied pressure of 1000 mbar with a saline solution (0.02 M $MgCl_2$/0.15 M NaCl) of pH 5.8, being ready for a new filtration cycle. The virus feed solution was replaced after each backflushing cycle by a new prepared MS2 solution showing a concentration of ~10^9 PFU/mL.

5.3 Results and Discussion

5.3.1 Structural and Mechanical Properties

As described in our previous study[30] macroporous YSZ capillary membranes showing a high membrane flux (Type 5) are produced by extrusion with YSZ-90nm powder (TZ-3YS-E). In this study, we slightly changed the recipe for the slurry preparation using liquid PVA instead of powdery PVA as binder to ensure a complete and more homogeneous distribution of the binder molecules within the YSZ-containing slurry.

YSZ capillary membranes with a defect-free and homogeneous membrane surface where the pores are uniformly distributed are produced (photograph and SEM micrograph are shown in the supplementary Figure S2). The membrane microstructure is not affected by treating the capillary membrane with Piranha solution for activation and aminosilane solution for functionalization (SEM micrographs are shown in the supplementary Figure S3). According to the results of Hg-porosimetry the average membrane pore size (d_{50}) of the non-functionalized capillary membrane is 144 nm featuring a pore size distribution in the range of 5 to 200 nm combined with a relatively high open porosity of 49.3 % (part C of Figure S2). In comparison to our previous study [32] the average pore size and the open porosity is not influenced by the new processing route, but advantageously the pore size range became narrower.
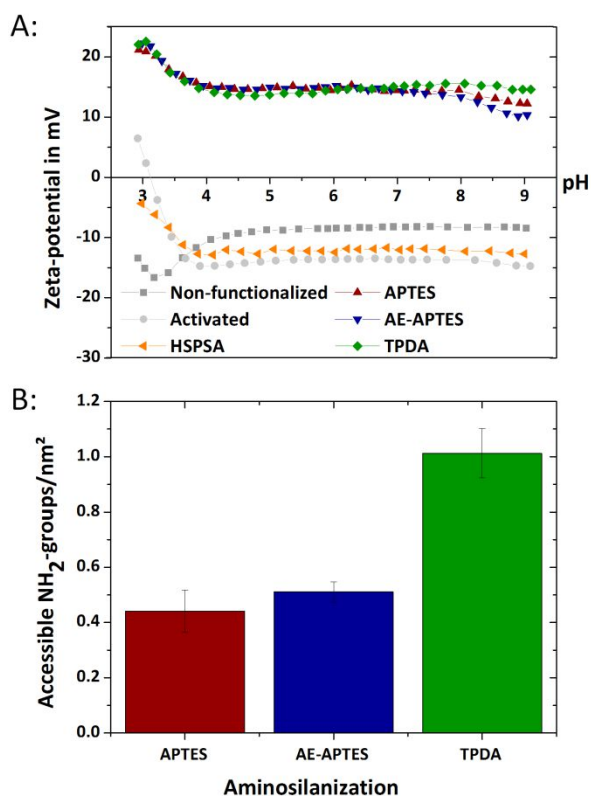
A:

B:

Figure 5.2. A: Zeta-potential of non-functionalized, activated, HSPSA-functionalized and aminosilanized YSZ capillaries measured in throughflow mode, B: Loading capacities of accessible amino groups on capillaries functionalized with APTES, AE-APTES and TPDA.

Table 5.1 summarizes the results obtained by Hg-porosimetry (pore size range, d_{50} and open porosity), BET method (specific surface area) and 3-point bending tests (bending strength, Weibull modulus) for the non-functionalized, activated, HSPSA-functionalized and aminosilanized membranes. After activation, HSPSA-functionalization and aminosilanization no change in the pore size range, the average pore size and the open porosity is detected compared to the non-functionalized capillaries. Furthermore, the specific surface area of all capillary membrane types is in the range between 5.2 and 5.9 m²/g indicating a similar surface area level for the envisaged virus adsorption. The mechanical stability of the non-functionalized capillary membranes is not influenced by the membrane activation and aminosilanization

maintaining a bending strength of around 30 MPa whereas the Weibull moduli are slightly decreased. Compared to our previous study[30] where a bending strength of 9.2 was achieved an increase in the bending strength by a factor of 3 is obtained by adapting the slurry recipe. Both the higher flexural strength and the adjustment of narrower pore size distributions widen the application ranges if high pressures and more reliable membrane cut-offs are needed.

5.3.2 Zeta-Potential and Aminosilane Loading
For the analysis of the surface charge of the capillary membranes streaming potential measurements are performed from pH 9 to 3 and corresponding zeta-potential values are obtained using the Helmholtz-Smoluchowski equation (section 5.2.4.2). Part A of Figure 5.2 shows the zeta-potentials as a function of pH of the non-functionalized, activated, HSPSA-functionalized and aminosilanized YSZ capillary membranes measured in throughflow mode (dead-end mode, inside-out). The zeta-potential results of the overflow measurements (inner capillary channel) are shown in the supplementary (Figure S4). Both measurement methods (throughflow versus overflow) show no significant differences and confirm that the zeta-potential of the membrane surface is converted from negative (non-functionalized and activated capillaries) to positive (amino-functionalized capillaries). The zeta-potential measurements of the non-functionalized and activated YSZ capillaries obtained IEPs ≤ 3. This detected low IEP is based on the utilization of APTES as dispersant during slurry preparation resulting in a modification of an initial YSZ surface to a silica-like surface. For the aminosilanized membranes the calculated zeta-potential is continuously positive in relation to applied pH range assuming IEPs > 9, most likely in the range between ~10-11. The HSPSA-functionalized capillary membrane which serves as a reference is negatively charged over the applied pH range of 3 to 9 showing similar zeta-potential curves compared to the untreated and activated capillaries where IEPs ≤ 3 are determined.
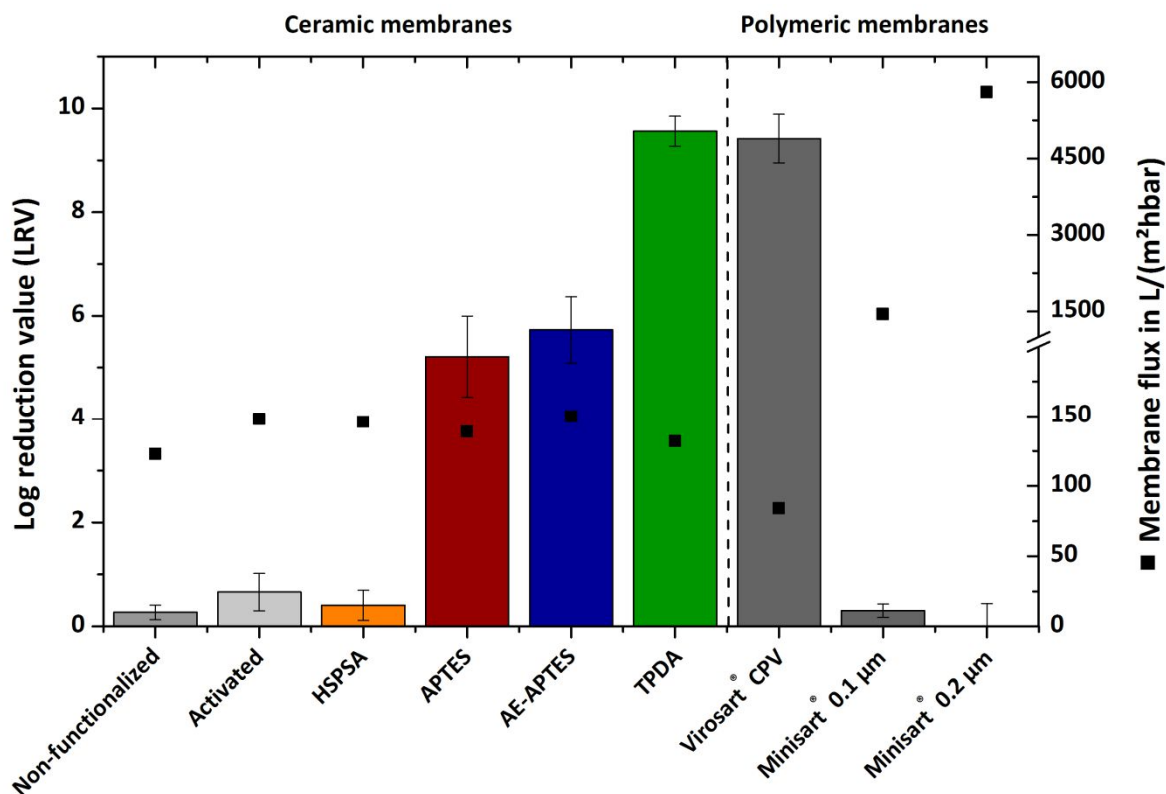
Figure 5.3. Membrane flux and retention of the model virus MS2 mediated by non-functionalized, activated, HSPSA-functionalized and aminosilanized ceramic capillaries using a viral feed concentration of $\sim 10^9$-10^{10} PFU/mL. Virus filtration tests are performed in dead-end filtration mode where commercially available polymeric membranes (Sartorius, Germany) served as references. The permeate (15 mL) of the ceramic membranes (active filtering area = 1.4 cm²) was obtained after a filtration time of ~85 min and for the polymeric membranes after a filtration time of ~45 min (Virosart® CPV; active filtering area = 5 cm²), ~2 min (Minisart® 0.1 μm, active filtering area = 6.2 cm²) and ~0.5 min (Minisart® 0.2 μm, active filtering area = 6.2 cm²), respectively.

Part B of Figure 5.2 presents the results of the photometrical acid-orange-II assay indicating the accessible NH_2-groups/nm² on the capillary membrane for APTES-, AE-APTES- and TPDA-functionalized membranes. With an increased number of amino groups per silane molecule increased loading capacities on the membrane surface are determined (TPDA > AE-APTES > APTES). Thus, the highest loading of accessible NH_2-groups is found for TPDA-functionalized capillary membranes showing 1.01 ± 0.09 NH_2-groups/nm². AE-APTES- and APTES-functionalized capillary membranes have significant lower concentrations by a factor of ~2 resulting in 0.51 ± 0.04 NH_2-groups/nm² and 0.44 ± 0.08 NH_2-groups/nm², respectively. Based on the number of provided OH-groups by activation and the degree of inter- and intramolecular crosslinking steric orientation of immobilized aminosilanes and therefore the accessibility of primary or rather secondary amino groups is affected. The used capillary membranes with pore sizes ranging from 5 - 200 nm and high open porosities of 49 % (Table 5.1) offer a good substrate structure for wet chemical aminosilanization where silane coating thickness are referred to a few nanometers.

5.3.3 Membrane Flux and Virus Retention

Figure 5.3 shows the membrane flux and the virus retention capacity for the bacteriophage MS2 of the non-functionalized, hydroxyl-activated, HSPSA-functionalized and aminosilanized ceramic capillary membranes, as well as the filtration efficiency of three commercially available polymeric membranes

obtained from Sartorius (Germany), namely Virosart® CPV, Minisart® 0.1 µm and Minisart® 0.2 µm. Photographs of the filter modules, SEM micrographs of the membrane surface as well as pore size distributions and open porosities of the polymeric reference membranes are shown in the supplementary (Figure S5).

The membrane flux of the non-functionalized, activated, HSPSA-functionalized and aminosilanized (APTES, AE-APTES and TPDA) ceramic capillary membranes is nearly in the same range (123 - 150 $L/(m^2hbar)$), because both the membrane pore size and the open porosity did not significantly change after activation and silanization, respectively (Table 5.1). Due to processing optimization changing the kind of binder addition (powdery vs. liquid PVA) the narrowing of the pore size distribution from 50-500 nm^{32} to 5-200 nm (part C of Figure S2 in the supplementary) resulted in lower membrane fluxes by a factor of around 3, but more reliable membrane cut-offs and a 3 times higher mechanical stability are provided. In agreement with the determined zeta-potential (part A of Figure 5.2) the non-functionalized, activated and HSPSA-functionalized capillary membranes show relatively low virus retention capacities of LRVs of 0.3 ± 0.1, 0.7 ± 0.4 and 0.4 ± 0.3, respectively, being the result of a repulsion between negatively charged MS2 viruses and negatively charged pore wall surfaces. In contrast, the virus retention capacities are significantly increased for all aminosilanized capillary types showing LRVs of 5.2 ± 0.8 (APTES), 5.7 ± 0.6 (AE-APTES) and 9.6 ± 0.3 (TPDA), respectively. Due to the positive membrane surface charge of around 20 mV at the applied pH of 5.8 (part A of Figure 5.2) negatively charged MS2 viruses (IEP = 3.9) can adsorb on the functionalized pore walls of the membrane under throughflow conditions. Using relatively high MS2 feed concentrations of $\sim 10^9$ $-\sim 10^{10}$ PFU/mL complete virus removal is solely obtained by TPDA-functionalized ceramic capillary membranes because they provide a high content of accessible amino groups (~ 1 NH_2-group/nm^2) being the anchor points responsible for virus adsorption. Compared to the non-functionalized ceramic capillary membrane an increase in LRV by a factor of ~9 (i.e. $\sim 10^9$ times higher in relation to non-logarithmic data) is given. Reaching such high LRV levels of 9 without post-chemical functionalization is only possible by the utilization of membranes with significantly smaller pore sizes in the range of the viral target (d_{50} = ~25 nm) associated with an enormous decrease in membrane flux (factor 45) to values of around 3 $L/(m^2hbar)$ as shown in our previous work[32]. Therefore, TPDA-functionalization is a quite promising wet chemical functionalization approach for ceramic virus filtration membranes as they provide high LRVs in combination with relatively high membrane fluxes.

Compared to the ceramic capillary membranes commercially available polymeric membranes obtained from Sartorius, Germany, are probed for their MS2 retention capacity and in agreement with determined pore size distributions (Figure S5) LRVs of 9.4 ± 0.5 (Virosart® CPV), 0.3 ± 0.1 (Minisart® 0.1 µm) and 0.00 ± 0.44 (Minisart® 0.2 µm) are achieved. Compared to TPDA-functionalized ceramic membranes the polymeric Virosart® CPV membrane reached the same high virus retention level (LRVs of ~9), but in accordance with the manufacturer data slightly lower membrane fluxes are applicable (~ 84 $L/(m^2hbar)$) for the polymeric membrane maintaining their integrity under applied pressure. As expected, the Minisart® 0.1 µm and 0.2 µm membranes show low or rather no MS2 retention due to their larger pore sizes of $\geq$ ~100 nm and $\geq$ ~200 nm, respectively, resulting in one order of magnitude higher flux values. In this study, these polymeric membranes served as negative controls for virus filtration being the membranes of choice for e.g. bacterial filtration applications.

5.3.4 Leaching of Immobilized Aminosilanes: TPDA Stability

To evaluate the stability of immobilized aminosilanes onto ceramic membranes and to determine wash-out effects under filtration conditions TPDA-functionalized capillary

membranes were used as they show the best virus retention capacities (Figure 5.3). The capillary membranes were intracapillary fed with a saline solution (pH 5.8) at RT applying a pressure of 500 mbar for up to 7 days (dead-end filtration mode) and the quantity of immobilized TPDA-molecules indicated as accessible NH_2-groups/nm^2 membrane was daily determined by photometrical acid-orange-II assay. As shown in Figure 5.4, no wash-out effects for a time period of 7 days are determined resulting in a stable bonding of TPDA onto the membrane surface. The loading capacities of TPDA-functionalized samples are ranged between 0.9 and 1.0 accessible NH_2-groups/nm^2 and no significant difference is obvious. Therefore, a stable bond formation of TPDA onto the hydroxyl-activated membrane surface via hydrolysis-condensation reaction is assumed providing sufficient amino groups for virus adsorption even under throughflow filtration conditions.

5.3.5 Virus Filtration Followed by Membrane Regeneration with Desorption Buffer

Mid-term virus filtration tests for a period of four days were performed using TPDA-functionalized membranes in dead-end mode without (part A of Figure 5.5) and with backflushing (part B of Figure 5.5) applied after each filtration day. Backflushing is performed for 2 h at pH 3 inducing MS2 desorption from the membrane surface by its change in zeta-potential from negative to positive. In accordance with the high stability of immobilized TPDA (Figure 5.4), the LRVs for both filtration experiments are around 8 based on applied feed stocks after 24 h ($\sim 10^8$ PFU/mL). After each filtration day nearly all viruses can be successfully removed from the feed solution during the whole experimental period. Furthermore, the membrane regeneration by a daily cleaning with desorption buffer (pH 3) has no negative effect on the filter performance ensuring high log levels for virus retention.

For virus filtration experiments performed without membrane regeneration (part A of Figure 5.5) the membrane flux significantly decreased
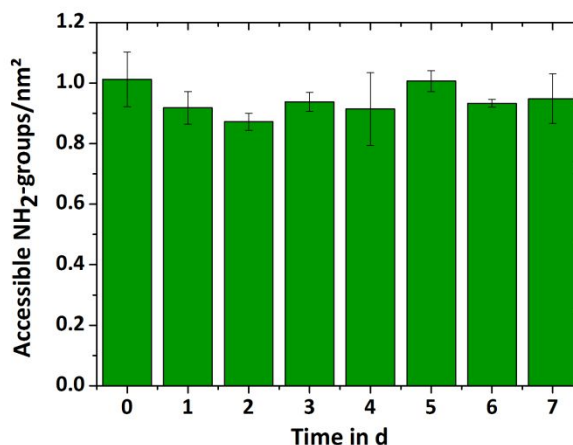

Figure 5.4. Long-term stability of TPDA on functionalized capillaries after dead-end filtration with adsorption buffer (0.02 M $MgCl_2$, 0.15 M NaCl, pH 5.8) for 7 days.

with increasing filtration time from ~ 130 L/(m^2hbar) after day 1 to ~ 50 L/(m^2hbar) after day 4. This reduction of the filter performance of 70 % can be attributed to an enhanced virus adsorption on TPDA-functionalized pore walls leading to pore narrowing or even pore blocking if virus assemblies or clusters are build up. In contrast, by membrane regeneration applying cleaning cycles at pH 3 for MS2 desorption (part B of Figure 5.5) the initial membrane flux is only reduced by 15 % after a four day filtration period. Therefore, regular cleaning cycles by pH-shift can prevent pore blocking by viruses and prolong the service life of TPDA-functionalized ceramic capillary membranes.

In summary, this study demonstrates the possibility to enhance the filter performance for virus filtration by wet chemical aminosilanization approaches based on membrane post-functionalization. Especially, high-flux membranes showing larger pore sizes than the viral target and high open porosities (correlating with high specific surface areas) are ideal candidates for such aminosilanizations, if a sufficient amount of accessible amino groups is provided on the pore walls of the membrane for virus adsorption.
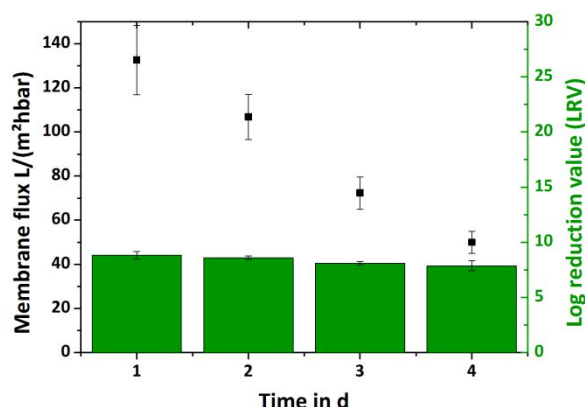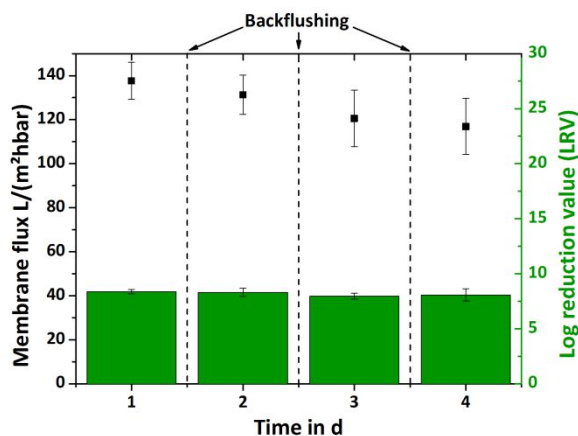
Figure 5.5. Retention of the model virus MS2 mediated by TPDA-functionalized ceramic capillaries using a viral feed concentration of 10^8 PFU/mL operating in dead-end filtration mode for 4 filtration days. A: without backflushing, B: with backflushing for virus desorption after day 1, 2 and 3 using a desorption buffer at pH 3 ensuring the repulsion between positively charged MS2 and positively charged TPDA-membranes (0.02 M $MgCl_2$, 0.15 M NaCl, pH 3).

In our studies, YSZ capillary membranes showing average pore sizes of ~150 nm (approximately 6 times larger than MS2 with a diameter of ~25 nm) and high open porosities of ~50 % which result in relatively high membrane fluxes of ~150 L/(m²hbar) are successfully functionalized with different types of aminosilanes. Especially, the functionalization with TPDA as an aminosilane with three amino groups per silane molecule resulted in a relatively high amount of ~1 accessible NH_2-groups/nm² membrane which can be beneficially utilized for virus adsorption if the environmental pH is right adjusted ($IEP_{Virus} < pH < IEP_{Membrane}$). Such TPDA-functionalized ceramic membranes show a high LRV of 9.6 ± 0.3 for the model virus MS2, being competitive against commercially available polymeric virus filtration membranes. The higher applicable pressures for ceramic compared to polymeric membranes resulted in higher flux values and a higher filter performance, maybe compensating their higher production costs. Both the long-term stability of immobilized TPDA under throughflow conditions and the possibility to simply regenerate virus loaded membranes by pH-shift open up promising perspectives for either virus removal or virus concentration. For virus concentration the trapped viruses in the membrane after filtration can be concentrated by back-flushing with either an acidic solution or a basic solution (depending on the stability of the virus) to cause a virus desorption from the membrane surface. In this study the virus retention was performed with a highly purified feed, where the only contaminants are the viral targets (bacteriophage MS2). For the water purification approach a potentially significant disadvantage for virus removal is membrane fouling by organic matter in water (e.g. humic and fulvic acids) which are negatively charged and therefore able to adsorb to the positively charged membrane surface. Further studies with especially TPDA-functionalized capillaries are necessary to examine the approach of virus removal with real water samples. To cover a wide spectrum of not only ceramic but also polymeric or composite membranes, these straightforward aminosilanizations may also be transferred to other oxide ceramic membranes (e.g. alumina, titania) or polymeric ones (e.g. poly(ether)sulfone, cellulose acetate) for generating highly affine viral adsorbents.

Acknowledgements

Supporting Information

In the supporting information SEM micrographs of the non-functionalized capillary membrane (S1), as well as of the activated and aminosilanized capillary membranes (S2) are presented. Furthermore, the zeta-potential measurements of all capillary types in overflow mode (S3) and photographs, SEM micrographs and data determined by Hg-porosimetry (pore size distribution, open porosity) for the polymeric membranes (S4) are shown.

References

1. A. Gadgil. "Drinking water in developing countries". *Annual Review of Energy and the Environment* 1998, 23, 253-286.
2. J. P. S. Cabral. "Water Microbiology: Bacterial Pathogens and Water". *International Journal of Environmental Research and Public Health*, 2010, 7, 3657-3703.
3. M. Koopmans and E. Duizer. "Foodborne viruses: an emerging problem". *Int J Food Microbiol*, 2004, 90, 23-41.
4. G. Miesegaes, et al. "Analysis of viral clearance unit operations for monoclonal antibodies". *Biotechnology and Bioengineering*, 2010, 106, 238-246.
5. M. D. Sobsey and B. L. Jones. "Concentration of poliovirus from tap water using positively charged microporous filters". *Applied and Environmental Microbiology*, 1979, 37, 588-595.
6. B. Kalbfuss, et al. "Harvesting and Concentration of Human Influenza A Virus Produced in Serum-Free Mammalian Cell Culture for the Production of Vaccines". *Biotechnology and Bioengineering*, 2007, 97, 73-85.
7. A. M. ElHadidy, et al. "An evaluation of virus removal mechanisms by ultrafiltration membranes using MS2 and φX174 bacteriophage". *Separation and Purification Technology*, 2013, 120, 215-223.
8. J. Langlet, et al. "Efficiency of MS2 phage and Qβ phage removal by membrane filtration in water treatment: Applicability of real-time RT-PCR method". *Journal of Membrane Science*, 2009, 326, 111-116.
9. J. Finley. "Ceramic membranes: a robust filtration alternative". *Filtration & Separation*, 2005, 42, 34-37.
10. E. P. Garmash, et al. "Ceramic membranes for ultra- and microfiltration (Review)". *Glass and Ceramics*, 1995, 52, 150-152.
11. B. Michen and T. Graule. "Isoelectric points of viruses". *Journal of Applied Microbiology*, 2010, 109, 388-397.
12. L. Gutierrez, et al. "Adsorption of rotavirus and bacteriophage MS2 using glass fiber coated with hematite nanoparticles". *Water Research*, 2009, 43, 5198-5208.
13. B. Michen, et al. "Improved Virus Removal in Ceramic Depth Filters Modified with MgO". *Environmental Science & Technology*, 2013, 47, 1526-1533.
14. M. Wegmann, et al. "Modification of ceramic microfilters with colloidal zirconia to promote the adsorption of viruses from water". *Water Research*, 2008, 42, 1726-1734.
15. M. Wegmann, et al. "Nanostructured surface modification of microporous ceramics for efficient virus filtration". *Journal of the European Ceramic Society*, 2008, 28, 1603-1612.
16. I. Bradley, et al. "Iron oxide amended biosand filters for virus removal". *Water Research*, 2011, 45, 4501-4510.
17. Y. You, et al. "Removal and Inactivation of Waterborne Viruses Using Zerovalent Iron". *Environmental Science & Technology*, 2005, 39, 9263-9269.
18. C. Shi, et al. "Removal of viruses and bacteriophages from drinking water using zero-valent iron". *Separation and Purification Technology*, 2012, 84, 72-78.
19. L. Treccani, et al. "Review: Functionalized ceramics for biomedical, biotechnological and environmental applications". *Acta Biomaterialia*, 2013, 9, 7115-7150.
20. S. Kroll, et al. "Highly Efficient Enzyme-Functionalized Porous Zirconia Microtubes for Bacteria Filtration". *Environmental Science & Technology*, 2012, 46, 8739-8747.
21. F. Meder, et al. "Protein adsorption on colloidal alumina particles functionalized with amino, carboxyl, sulfonate and phosphate groups". *Acta Biomaterialia*, 2012, 8, 1221-1229.

22.   H. J. Kim, et al. "Enhancement of mechanical properties of aluminium/epoxy composites with silane functionalization of aluminium powder". *Composites Part B: Engineering*, 2012, 43, 1743-1748.

23.   M. Moritz and M. Łaniecki. "SBA-15 mesoporous material modified with APTES as the carrier for 2-(3-benzoylphenyl)propionic acid". *Applied Surface Science*, 2012, 258, 7523-7529.

24.   H. Weetall. "Preparation of immobilized proteins covalently coupled through silane coupling agents to inorganic supports". *Applied Biochemistry and Biotechnology*, 1993, 41, 157-188.

25.   S. Fiorilli, et al. "Vapor-phase self-assembled monolayers of aminosilane on plasma-activated silicon substrates". *Journal of Colloid and Interface Science*, 2008, 321, 235-241.

26.   F. Meder, et al. "The role of surface functionalization of colloidal alumina particles on their controlled interactions with viruses". *Biomaterials*, 2013, 34, 4203-4213.

27.   R. Cademartiri, et al. "Immobilization of bacteriophages on modified silica particles". *Biomaterials*, 2010, 31, 1904-1910.

28.   Z. Chen, et al. "Capture and release of viruses using amino-functionalized silica particles". *Anal Chim Acta*, 2006, 569, 76-82.

29.   K. S. Zerda, et al. "Adsorption of viruses to charge-modified silica". *Applied and Environmental Microbiology*, 1985, 49, 91-95.

30.   J. Werner, et al. "Production of ceramic membranes with different pore sizes for virus retention". *Journal of Water Process Engineering*, 2014, 4, 201-211.

31.   B. Besser, et al. "A comparative experimental study on the deviation of the ideal selectivity in HDTMS-functionalized and untreated ceramic structures with pores in the upper mesoporous range". *Microporous and Mesoporous Materials*, 2015, 217, 253-261.

32.   S. Kroll, et al. "Development and characterisation of functionalised ceramic microtubes for bacteria filtration". *Journal of Membrane Science*, 2010, 365, 447-455.

33.   S. Kroll, et al. "High virus retention mediated by zirconia microtubes with tailored porosity". *Journal of the European Ceramic Society*, 2012, 32, 4111-4120.

6. Effect of Cations on the MS2 Retention Capacity of Amino-Functionalized Ceramic Filters

Authors

Julia Bartels[1]*, Nils Hildebrand[2,3]*, Marcin Nawrocki[1], Stephen Kroll[1,4], Michael Maas[1,5], Lucio Colombi Ciacchi[2,5], Kurosch Rezwan[1,5]

* These authors contributed equally to this work and are co-first authors.

[1]*Advanced Ceramics, University of Bremen, Am Biologischen Garten 2, 28359 Bremen, Germany*

[2] *Hybrid Materials Interfaces Group, Faculty of Production Engineering and Center for Environmental Research and Sustainable Technology (UFT), University of Bremen, Am Fallturm 1, 28359 Bremen, Germany*

[3] *Faserinstitut Bremen e. V. – FIBRE, Am Biologischen Garten 2, 28359 Bremen, Germany*

[4] *IfBB – Institute for Bioplastics and Biocomposites, Hochschule Hannover, University of Applied Sciences and Arts, Heisterbergallee 10A, 30453 Hannover,Germany*

[5] *MAPEX Center for Materials and Processes, University of Bremen, Am Fallturm 1,28359 Bremen, Germany*

Abstract

Ceramic capillary membranes (YSZ-90nm) conditioned for virus filtration via functionalization with n-(3-trimethoxysilylpropyl)diethylenetriamine (TPDA) as shown in chapter 5 are analyzed with respect to their virus retention capacity when using feed solutions based on monovalent and divalent salts (NaCl, $MgCl_2$). The log reduction value (LRV) by operating in dead-end mode using the model bacteriophage MS2 with a diameter of 25 nm and an IEP of 3.9 is as high as 9.6 when using feeds containing $MgCl_2$. In contrast, a lesser LRV of 6.4 is observed for feed solutions based on NaCl. The TPDA functionalized surface is simulated at the atomistic scale using explicit-solvent molecular dynamics in the presence of either Na^+ or Mg^{2+} ions. Computational prediction of the binding free energy reveals that the Mg^{2+} ions remain preferentially adsorbed at the surface, whereas Na^+ ions form a weakly bound dissolved ionic layer. The charge shielding between surface and amino groups by the adsorbed Mg^{2+} ions leads to an upright orientation of the TPDA molecules as opposed to a more tilted orientation in the presence of Na^+ ions. The resulting better accessibility of the TPDA molecules is very likely responsible for the enhanced virus retention capacity using a feed solution with Mg^{2+} ions.

6.1 Introduction

Viruses are among the most challenging biological contaminations in water[1, 2], food products[3] and biopharmaceuticals[4]. The contamination amount can be greatly reduced by selective virus filtration methods. These are also of interest for detecting and quantifying small virus concentrations[5] or for preparing inactivated viral vaccines[6]. Filtration and elimination of virus contaminations can be performed by ceramic capillary membranes specifically designed for virus adsorption via specific pore design[7] and surface functionalization[8]. As viruses generally present isoelectric points (IEPs) between 3.5 and 7.0,[9] materials which provide a positive surface potential at neutral pH are suitable for virus retention via adsorption.[10] From a ceramics processing standpoint, a positive surface charge can be obtained via various methods, including coating,[11, 12] doping[13] or chemical functionalization[14-17]. Chemical functionalization with silanes is an especially versatile tool as it allows the covalent immobilization of specific functional groups to any oxide ceramic surface, thereby tailoring the surface chemistry for specific applications. Silanization proceeds via a hydrolysis-condensation reaction which can be performed in aqueous media,[18, 19] organic solvents (e.g. ethanol, toluene, chloroform, acetone or xylene)[20-23] or in the vapor phase[24, 25]. Consequently, surface functionalization of ceramic materials is a broad and well-established research area[26] with innumerable materials and commercial products available, including a multitude of silanes with different functional groups (e.g. alkyl-,[27, 28] amino-,[29, 30] carboxyl-[31, 32] or sulphonate-groups[19]) and with a variety of spacer lengths[26]. Recent studies have demonstrated that tailoring the surface chemistry of materials shows great potential for interactions with specific viruses, proteins and other biomacromolecules.[14, 33-35] Especially amino groups, which are positively charged at neutral and acidic pH, can be used for the adsorption of negatively charged viruses.[14-17] Despite the ubiquity of such functionalization approaches, in many cases very little is known about the precise chemical environment of the functional groups on the silanized material surface, especially considering interactions with biological entities in complex buffer systems. In early studies, researchers concluded that the addition of salts to buffer systems enhance the virus adsorption to membranes. It was shown that the presence of trivalent cations (Al^{3+}) promotes larger virus adsorption compared to divalent (Mg^{2+}) and monovalent cations (Na^+).[36-38] Generalization of this finding was disputed by Lukasik et al.[39], who demonstrated that the effects of salt ions depend on the filter type. They found that for different types of membranes and under different conditions, $MgCl_2$ promoted, inhibited or had no effect on virus adsorption. Typically, these effects may be explained by DLVO-theory in terms of the influence of the ionic strength on the double-layer interaction.[40-44] Already at this level, monovalent and divalent ions behave quite differently; for instance the Debye length, calculated as $1/\kappa = 0.3 / \sqrt{[NaCl]}$ and $1/\kappa = 0.18 / \sqrt{[MgCl_2]}$, is reduced by about a factor of two for divalent ions with respect to monovalent ions.[45] Moreover, especially for divalent or trivalent ions, non-DLVO effects may dominate their behaviour in the very proximity of a solid surface.[45] Here, the adsorption of the ions at charged surface sites is strongly mediated by the mutual overlap of their hydration shells and is therefore both entropically and electrostatically driven.

In our previous work, we presented a straightforward chemical functionalization strategy for high-flux yttria-stabilized zirconia (YSZ) capillary membranes using n-(3-trimethoxysilylpropyl)diethylenetriamine (TPDA), which converted the membrane surface potential from negative to positive.[8] The non-functionalized capillary membranes showed IEPs < 3 which is similar to a silica surface due to the 3-aminopropyltriethoxysilane (APTES) which was used as dispersant during capillary production. In this procedure, APTES coats the YSZ particles in the slurry and is still present at the surface of the ceramic material after sintering. After functionalization, IEPs > 9 were achieved.[8] The virus retention capacity using the model virus MS2 in saline buffer solution (0.02 M

MgCl$_2$, 0.15 M NaCl) increased from a log reduction value (LRV) of < 0.3 for the non-functionalized membrane to a value of 9.6 ± 0.3 for the amino-functionalized membrane.[8]

The aim of the present work is to investigate the effects on the virus filtration efficiency of TPDA functionalized YSZ capillary membranes in the presence of mono- and divalent salts (NaCl, MgCl$_2$). Based on our previous work, we have used the model bacteriophage MS2, which is a single-stranded RNA virus with a diameter of about 26 nm[46] and an IEP of 3.9,[9] and TPDA functionalized YSZ capillary membranes with an average pore size (d$_{50}$) of 149 nm and an open porosity of ~48 %.[8] MS2 is considered a relevant non-pathogenic surrogate for pathogenic viruses in aqueous media.[47-49] The capillary membrane processing[8, 50] allows for a wet chemical functionalization without a meaningful effect on the accessible pore size. The virus retention capacities, and with that the filtration efficiencies, have been determined by virus filtration experiments in dead-end mode.

We assume that the filtration efficiency of the investigated membranes might directly depend on the accessibility of the terminal TPDA molecules, which in turn might be influenced by ion adsorption at the surface. To elucidate this effect, we have performed advanced-sampling molecular dynamics simulations (MD) to analyze the effects on the atomistic scale and investigated the adsorption strengths and distributions of the ions at the surface. In our simulations, both the enthalpic and the entropic effects of ions and the water distributions formed at the surface and around the ions are accurately accounted for. In particular, our approach is designed to examine the orientation and accessibility of the TPDA functionalization dependent on the used ion type and correlate the results with the experimental findings.

6.2 Experimental Section

6.2.1 Materials

All reagents were purchased from commercial sources and used without further purification.

The YSZ powder TZ-3YS-E (YSZ-90nm, Lot. S305635P) was purchased from Krahn Chemie

GmbH, Germany. 3-aminopropyltriethoxysilane (APTES, 99 %, product number 440140, Lot. SHBD4935V), hydrogen peroxide solution (purum p.a. ≥ 35 %, product number 95299, Lot. BCBH5638V), magnesium chloride hexahydrate (MgCl$_2$, product number M2670, Lot. BCBP4439V), polyvinyl alcohol (PVA, fully hydrolyzed, product number P1763, Lot. SLBC9027V), sodium chloride (NaCl, product number S7653, Lot. SZBF0350V), sulfuric acid (95 - 97 %, product number 30743, Lot. SZBF0330V), tryptic soy agar (TSA, product number 22091, Lot. BCBR8554V), culture media tryptic soy broth (TSB, product number T8907, Lot. SLBL1497V) and N-(3-trimethoxysilylpropyl)diethylenetriamine (TPDA, product number 413348, Lot. MKBW1074V) were obtained from Sigma-Aldrich Chemie GmbH, Germany. The virus retention tests were performed with the bacteriophage MS2 (DSM Cat. No. 13767) and its host bacteria E. coli (DSM Cat. No. 5210) were used for virus propagation, both purchased from German Collection of Microorganisms and Cell Cultures (DSMZ), Germany.

Double-deionized water with an electrical resistance of 18 MΩ, which was obtained from a Synergy® apparatus (Millipore), was used for all experiments.

6.2.2 Fabrication of Functionalized YSZ Ceramic Capillary Membranes

The fabrication of functionalized YSZ capillary membranes by extrusion and wet chemical post-functionalization was performed as described in our previous studies.[7, 8, 50]

In short, a ceramic slurry was prepared by milling 132 g YSZ powder (YSZ-90nm) as ceramic material, 4 g APTES as dispersant, 20 g polyvinyl alcohol (PVA) - water solution (25 wt.%) as binder and 13.5 g double-deionized water as solvent with 50 alumina grinding balls (diameter = 10 mm) in a planetary ball mill (PM400, Retsch, Haan, Germany) for 3 h at 350 rpm changing the rotation direction every 5 min. A self-made laboratory extruder equipped with a nozzle (d=2.0 mm) and an integrated pin (d=1.0 mm) was used to fabricate the capillaries
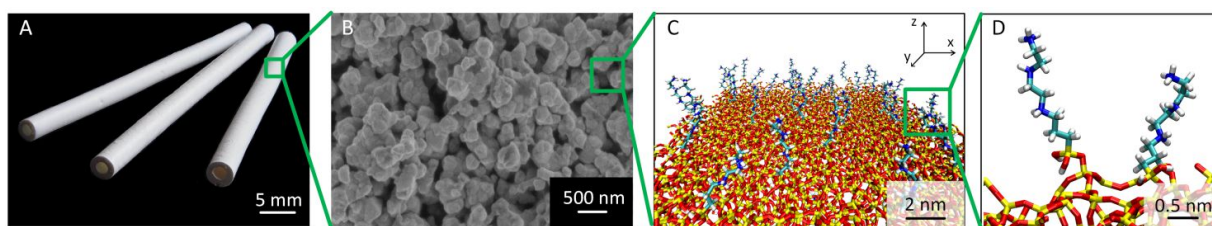
Figure 6.1. Photography of TPDA functionalized zirconia tubular membrane filters (A), microstructure of the outer capillary surface (B), simulated atomistic view on a 9 x 9 nm² part of a TPDA-functionalized surface (C) and two TPDA molecules bound to the ceramic surface (D).
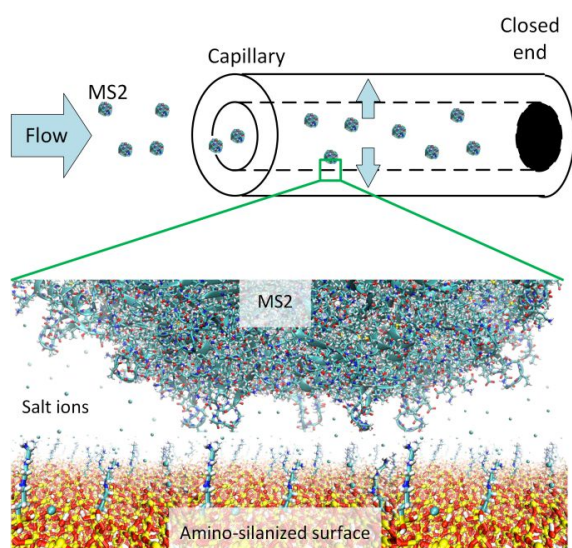

Figure 6.2. Sketch illustration of the principle of dead-end filtration with ceramic capillary membranes and the bacteriophage MS2.

with a speed of 50 cm/min. Afterwards, the extruded capillaries were dried for two days at RT and a humidity of about 50 % and finally sintered in an oven (HT40/17, Nabertherm, Lilienthal, Germany) for 2 h at 1050 °C with dwell times at 280 °C (0.5 h) and 500 °C (1 h).

The sintered capillaries were activated by acidic hydroxylation with Piranha solution (97 % H_2SO_4 : 35 % H_2O_2, 3:1 (v/v)) for 30 min at RT, followed by washing with water until the effluents reached a neutral pH, and final drying at 70 °C for 16 h (UT6120, Heraeus, Hanau, Germany). Five capillaries with an individual length of 6 cm were incubated with 10 mL TPDA-water solution (0.2 mol/L) at 65 °C under slight shaking at 150 rpm (Inkubator 1000/Unimax 1010, Heidolph, Schwabach, Germany) for 24 h. Finally, the capillaries were

washed until the effluents reached a neutral pH and dried at 70 °C for 16 h (UT6120, Heraeus, Hanau, Germany). A photography of the tubular membrane filter (A), a SEM micrograph (B), and the simulated atomistic view of the TPDA functionalized capillary membranes (C, D) are shown in Figure 1.

6.2.3 Virus Test

Sterile saline solutions with different concentrations of either $MgCl_2$, NaCl, or both, containing around 10^9-10^{10} Plaque Forming Units (PFU) per mL of MS2 bacteriophages were incubated for 2 h at RT under slight shaking at 100 rpm (Inkubator 1000/Unimax 1010, Heidolph, Schwabach, Germany). The bacteriophages were enumerated by the PFU method at the start of the incubation and after 2 h incubation time. The pH of the salt solutions was measured with a pH meter (FE20 FiveEasy, Mettler Toledo, Gießen, Germany).

The PFU method (plaque assay) which is the most quantitative and useful biological assay for viruses is based on the ability of a single virus to give rise to a macroscopic area of cythopathology on a monolayer of bacteria cells.[51] Therefore, the MS2 samples were diluted in logarithmic concentration series in a salt solution (0.02 M $MgCl_2$ and 0.15 M NaCl). For each virus sample, three dilution series of Plaque Assays were carried out. A virus sample volume of 1.8 mL was mixed with 0.2 mL of the host bacteria and 3 mL agar and poured in a Petri dish. After an incubation time of 16 h at 37 °C (UN30, Memmert, Schwabach, Germany) the plaques were visible and were counted. The goal of the assay is to find the dilution of viruses that leads to the formation of countable (20 - 100) plaques

on a Petri dish. This number is on one hand statistically significant and on the other hand individual plaques can be distinguished. Low virus dilutions (high virus concentrations) show only dead bacteria cells or too many plaques which cannot be distinguished from each other (> 100) and high virus dilutions (low virus concentrations) have very few (< 20) or no plaques. The Log reduction value (LRV) was then calculated from the counted plaques.[52]

The virus retention test was performed as described in our previous studies,[7, 8] with slight modifications. In short, a saline solution with different concentrations of either $MgCl_2$, NaCl, or both salts, containing MS2 bacteriophages in a concentration of around 10^9-10^{10} PFU/mL, served as viral feed solution. The virus retention test was performed in dead-end mode, which implies that one end of the capillary was sealed with silicone (Wirosil Dublier-Silikon, Bego Medical GmbH, Bremen, Germany) and the other end was connected to a peristaltic pump (BVP Standard, Ismatec, Wertheim, Germany). The feed was filtrated at an applied pressure of 500 mbar until a permeate volume of 15 mL was obtained. The pressure was determined with a manometer (C9500, Comark, Mörfelden-Walldorf, Germany). Three individual capillary membranes with an accessible length of 5 cm were tested for each salt concentration in the feed solution. The bacteriophages MS2 were enumerated using the PFU method. When no viruses (plaques) could be detected on both the diluted and the undiluted permeate sample, the LRV is calculated from the viral feed concentration. Therefore, the highest detectable LRVs are between 9 and 10 based on the feed concentration which varies between 10^9 and 10^{10} PFU/mL.

A sketch of the principle of the virus filtration test using TPDA functionalized capillaries is shown in Figure 2.

The hydrodynamic diameter of the bacteriophage MS2 was measured via dynamic light scattering (Malvern Instruments, Zetasizer Nano ZSP). The results were number weighted.
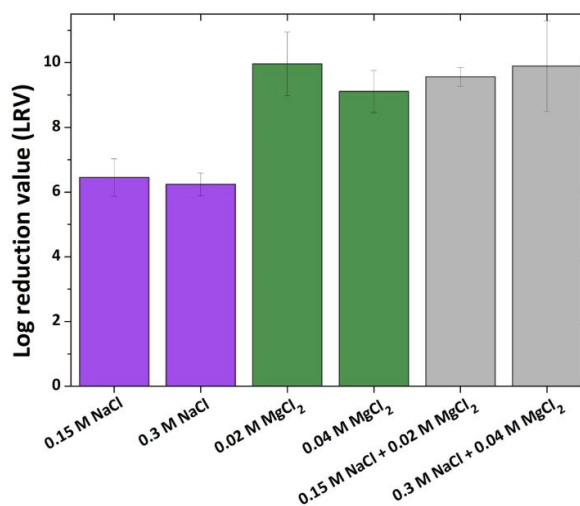

Figure 6.3. Retention of the model virus MS2 mediated by TPDA functionalized capillaries using feeds based on different salt solutions (NaCl, $MgCl_2$ and NaCl+$MgCl_2$) with varying molarities and viral concentrations of $\sim 10^9$-10^{10} PFU/mL.

Table 6.1. Characteristic properties of TPDA functionalized ceramic capillary membranes.

Hg-porosimetry	
pore size range	6-200 nm
d_{50}	149 ± 5 nm
open porosity	48.3 ± 2.7 %
BET method	
specific surface area	5.6 ± 0.1 m²/g
Streaming potential method	
isoelectric point	> 9 mV
Acid Orange II test	
accessible TPDA loading	1.01 ± 0.09 NH_2-groups/nm²

6.2.4 Molecular Dynamics Simulations

The atomic structure of the amorphous silica surface (9 x 9 nm²) is derived from Cole et al.[53] and described by the force-field MD parameters from Butenuth et al.[54] The primary and the two secondary amino groups of TPDA are protonated in the simulations performed at pH 6 in line with the experiment. The TPDA molecules were tethered to the surface via Si-O-Si bridges to deprotonated surface silanol groups, after removing the methyl groups from the Si central atom of each molecule and terminating the dangling Si-O- bonds with H atoms (see Figure
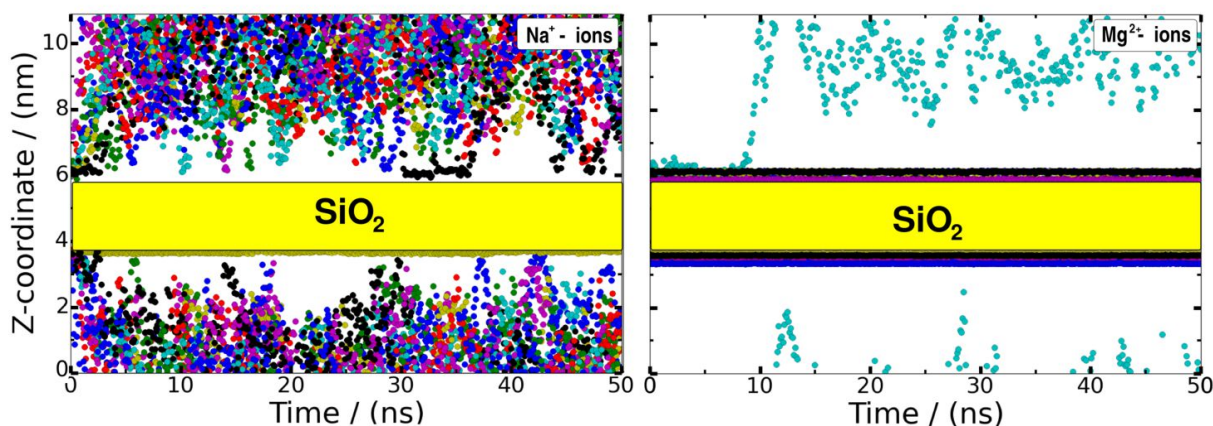
Figure 6.4. Distance of the ions to the membrane surface in the surface normal direction during 50 ns all-atom explicit solvent MD simulations. The yellow bars represent the dimension of the silica surface. After initial adsorption in the start configuration, most of the Na^+ ions (left) diffuse almost freely above the surface, whereas most of the Mg^{2+} ions (right) remain tightly adsorbed at the surface/water interface. Both systems are simulated with a concentration of the corresponding ions of 35 mM. The positions of the ions are drawn each 100 ps in a different color per ion.
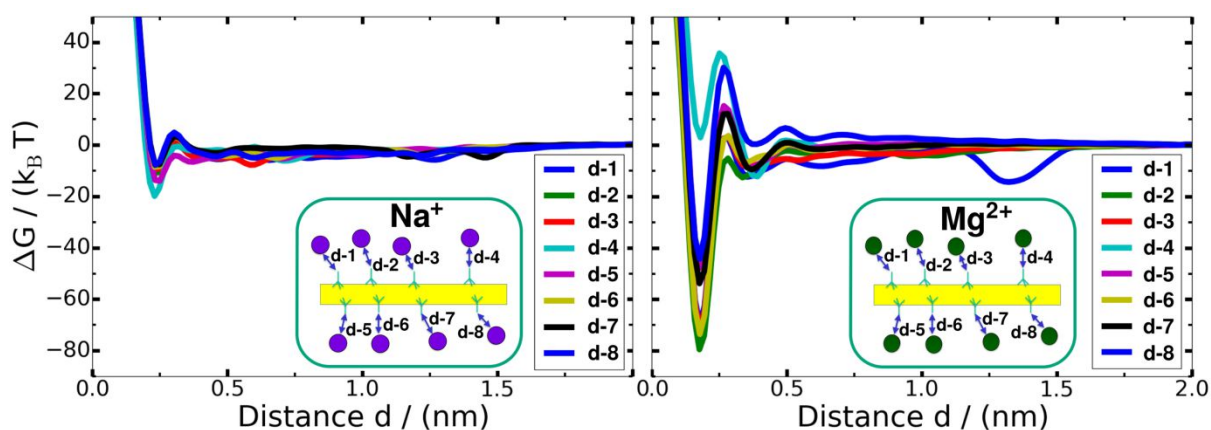

Figure 6.5. Relative adsorption free energy (ΔG) profile of Na^+ (left) and Mg^{2+} ions (right) over the silanol groups of the silica surface calculated by a Well-Tempered Metadynamics simulation using the distance to the deprotonated silanol groups as a collective variable. Eight individual Metadynamics simulations are performed in one system to increase the sampling efficiency. Mg^{2+} ions show a highly increased adsorption free energy.

6.1 D).

The MD potential parameters for the TPDA molecules were taken from the AMBER GAFF force field[55] using the semi-empirical (AM1) bond charge correction (bcc) method[56] to address the molecule charges, as included in antechamber module[57] of the AMBER 14 MD simulation package[58]. We used the default pre-set parameters to reproduce the HF/6-31G* electrostatic potential (ESP) of the molecule. Test simulations (not reported here) were performed to ensure that the resulting TPDA parameterization was fully compatible with the

AMBER99SB force field. Water was described by the TIP3P model.[59] The parameters of the Na^+ and Cl^- ions were taken from the AMBER99SB force field.[58] The parameters of the Mg^{2+} ions were taken from Li et al.[60] The terminal silanol groups at the silica surface were protonated in accordance to pH 6 based on experimental findings as described in Hildebrand et al.[61] All used force fields parameterizations (Butenuth, GAFF, AMBER99SB, TIP3P) are based on identical force field equations and combination rules, and thus combinable with each other.[54, 55, 58] The MD simulations were performed with the
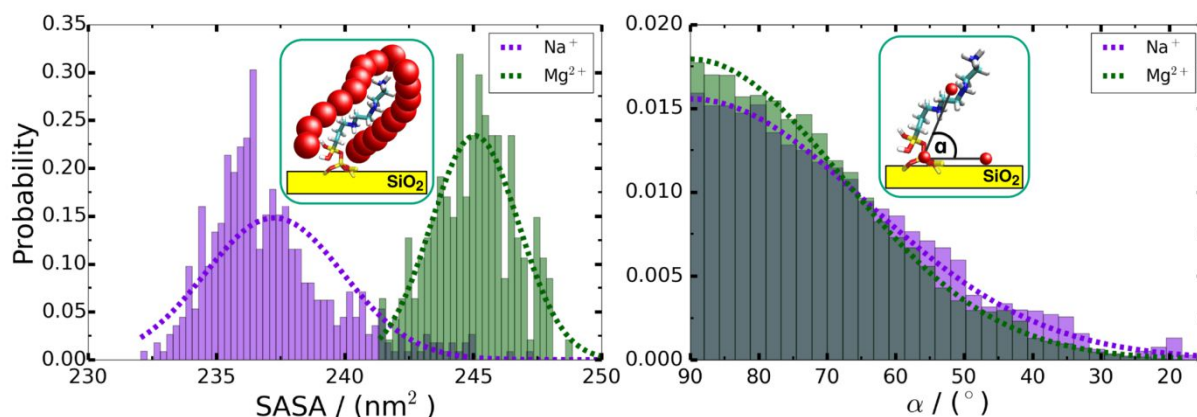
Figure 6.6. Normalized histograms of the solvent accessible surface area (SASA) around the TPDA molecules using a probe radius of 1.4 Å of the two simulated systems (left). Normalized histograms of the angle alpha between a reference molecule parallel to the surface, the central silicon atom and the center of mass of the three amino groups of the TPDA molecule. The histograms are fitted with a normal probability density function (right).

GROMACS simulation package v4.6.7., using a timestep of 2 fs.[62] The TIP3P explicit solvent systems were carefully relaxed and equilibrated first in an NVT and then in a NPT ensemble using periodic boundary conditions. Hydrogen atoms were constrained with the LINCS algorithm.[63] All surface atoms except the TPDA molecules and silanol hydrogen atoms were kept fixed. The solvent density was adjusted to the TIP3P density at 1 bar and 300 K according to our previous work.[61] After equilibration, the production simulations were performed in a NVT ensemble with a modified Berendsen thermostat with a coupling constant of 0.1 ps.[64] Long-range electrostatics was treated within periodic boundary conditions with the smooth Particle-Mesh Ewald (SPME) method[65] using a Fourier spacing of 0.16 nm and an interpolation order of 4. A cut-off of 1.2 nm was applied for the calculation of non-bonded interaction, the neighbour-list update and the real part of the Ewald sum. Visualizations and analysis of the simulations were performed with VMD.[66]

6.2.5 Metadynamics Molecular Dynamics Simulations

Metadynamics simulations were performed in explicit solvent for systems including solvated ions in proximity of the silica surface (3 x 3 nm²), without the TPDA molecules. The distances between the ions and the deprotonated silanol
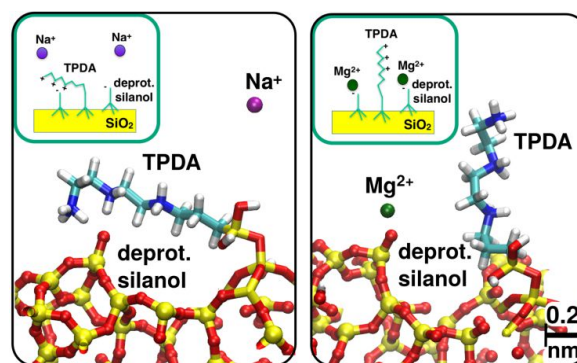

Figure 6.7. Snapshots of the Molecular Dynamics (MD) simulation of two systems containing the TPDA functionalized silica surface. Deprotonated silanol groups at the surface representing a realistic pH 6 condition (left). Additional Na$^+$ ions are added to the system. Mg^{2+} ions replace the Na$^+$ ions for a direct comparison of both ion types (right).

groups of the surface were chosen as collective variables for well-tempered Metadynamics simulations.[67] The surface contained 8 deprotonated silanol groups (-8e), which were partnered with either 8 Na$^+$ or 8 Mg^{2+} ions and 8 Cl$^-$ ions to keep the system in each case neutral. Therefore, each system included 8 parallel Metadynamics simulations. This approach is comparable to a multiple walker simulation[68], whereas each walker has its own bias potential. A repulsive wall at distances larger than 2.5 nm built with an harmonic restraint with a force

constant of 150 kJ/(mol·nm^2) was used to avoid interaction of the ions with the periodically repeated image of the surface slab. In addition, the ions were restrained with a weak force constant of 10 kJ/(mol·nm^2) in x and y directions, whereas the surface normal is oriented in z direction. This restrain guides the adsorption of each single ion on only one silanol group. The simulations were performed with the PLUMED v2 patch on GROMACS.[62, 69] For the well-tempered Metadynamics we have used a hills width of 0.05 nm, a bias factor of 10, a tau parameter of 3 and a deposition frequency of 1/ps.

6.3 Results and Discussion

YSZ capillary membranes with a defect-free and homogeneous membrane surface were activated and silanized with TPDA, as shown in our previous study.[8] The functionalized membranes show an average membrane pore size (d_{50}) of 149 nm combined with a relatively high open porosity of 48 %, which leads to a membrane flux of 150 L/(m²hbar) in dead-end mode.[8] The functionalization density on the surface of the TPDA-coated capillary membranes is roughly one accessible NH^{3+}-group per nm², as determined by photometrical acid-orange-II assay.[8] The characteristic properties of TPDA functionalized ceramic capillary membranes are listed in Table 6.1.

Figure 6.3 shows the virus retention capacity of TPDA functionalized capillaries using salt solutions with NaCl, MgCl$_2$ or a mixture of both salts in different concentrations. The virus retention capacity of TPDA functionalized membranes in feed solution containing 0.15 M NaCl (pH 6.3) shows a LRV of 6.5 ± 0.6 and in feed solution with 0.3 M NaCl (pH 6.3) shows a LRV of 6.2 ± 0.4, respectively. In the presence of only divalent cations (Mg_{2+}) in the feed solution the virus retention is increased to about 9 for both used concentrations and a nearly complete virus removal is achieved. In our previous study,[8] a complete virus removal was obtained by filtrating the feed based on 0.15 M NaCl + 0.02 M MgCl$_2$ solution with 10^9-10^{10} PFU/mL of MS2 phages. By comparison, the retention capacity did not

significantly change when a stock solution with the same salt mixture at a different ion concentration (0.3 M NaCl + 0.04 M MgCl$_2$) was used. The adsorption of the virus at the filter surface occurs due to the positive membrane surface potential of TPDA functionalized capillary membranes and the overall negative surface potential of MS2 phages at the pH of 5.9. Apparently, the presence of MgCl$_2$ instead of (or concomitantly with) NaCl enhances the virus adsorption capability to the TPDA groups, which likely serve as the anchoring points at the ceramic surface. We can thus assume that Mg^{2+} and Na^+ ions affect the accessibility of the tethered TPDA molecules in different ways, leading to different virus retention properties.

To exclude any influence of the salt on the virus itself, the quantity of infectious phages in sterile saline solutions containing around 10^9 PFU/mL of MS2 was analyzed by means of PFU tests after an incubation time of 2 h. The incubation time was chosen in accordance with the filtration time of around 1.5 h in the virus retention tests. Additionally, the colloidal stability of the virus particles was investigated via dynamic light scattering during this time frame. All six different salt solutions were considered. The number of MS2 phages remained stable over a time period of 2 h in all used feed solutions and no loss in activity could be observed. The number weighted hydrodynamic radius of the virus particles was constant at around 30 ± 5 nm over this time period, which indicates that the different buffers do not promote aggregation of the MS2 particles. Additionally, filtration experiments with non-functionalized capillaries (pore diameter 149 ± 5 nm) showed nearly no virus retention (LRV ~ 0.3), even in the presence of Mg^{2+}. The agglomeration behaviour was also studied by Pham et al.[70] who measured the hydrodynamic diameter of MS2 by dynamic light scattering for Mg^{2+} concentrations between 0.1 and 1 mM. They found hydrodynamic diameters in the range between 30 and 36 nm which is slightly larger than the dimensions of each individual MS2 particle in dry state as observed with transmission electron microscopy (25-29 nm), but showed that the viruses were still monodisperse and not

agglomerated. These results demonstrate that the observed virus reduction during the filtration experiment with YSZ capillaries functionalized with TPDA can be attributed to virus-membrane-feed interactions and is not significantly altered by virus inactivity or aggregation resulting from the elevated salt concentrations.

In the MD simulations we directly compare the influence of Na^+ and Mg^{2+} ions on the orientation of the TPDA functionalization to understand the interactions of the membrane with the feed. Two systems are prepared including the positively charged TPDA molecules and negatively charged silanol groups at pH 6, in agreement with the experiments. The surface density of TPDA molecules is adjusted to the experimental measured surface charge of about 1 e/nm², as measured in our recent report.[8] Both types of ions are placed at a distance of 1.8 Å over a deprotonated silanol group. Already within 200 ps simulation time do the Na^+ ions diffuse away from the surface towards the solvent bulk, whereas the Mg^{2+} ions remain at the deprotonated silanol surface groups for the whole simulation time of 50 ns (Figure 6.4). To exclude the effect of a faster diffusion of the lighter Na^+ ions we have performed an unphysical simulation giving the Mg^{2+} ions the mass of sodium, and have found no differences in the observed dynamics.

Further, the free energy adsorption profiles of the two ions on the silanol groups of silica are computed by means of Metadynamics (Figure 6.5). As collective variables we have chosen the distances of each ion to the deprotonated silanol surface sites (see Methods). The obtained free energy profiles after a simulation time of 300 ns are shown in Figure 6.5. A relative energy of zero is arbitrarily set to the free energy at a distance of 2.0 nm away from the oxygen atom of the silanol group. The minimum energy basin (-11 +/- 4 vs -54 +/- 26 kBT) as well as the energy barrier before adsorption (1 +/- 3 vs 12 +/- 14 kBT) are much stronger in the case of the Mg^{2+} with respect to the Na^+ ions, which explains why the former could not and the latter could readily desorb from the surface during the standard MD simulations (Figure 6.4). We note that the strong Mg^{2+}

adsorption at the surface hinders a homogeneous sampling across the collective variable, so that the presented profiles are most probably not fully converged. Nevertheless, the large difference in adsorption affinity between the two ion types is evident. The single, smaller energy basin for Mg^{2+} at a distance of 1.4 nm (shown in blue in Figure 6.5) corresponds to an ion adsorbed next to a respective silanol group assigned with the distance collective variable and can be ignored. For both ion types oscillation of the free energy profiles close to the surfaces are visible, which originate from the overlap of the hydration shells of the ions and the surface's silanol groups.

The orientation of the TPDA molecules is quantitatively analyzed through calculation of both the solvent accessible surface area (SASA) and the geometric orientation of the TPDA molecule on the surface (Figure 6.6) during the standard MD simulations (Figure 6.4). The SASA of the functionalized surface is calculated by using a probe with a radius of 1.4 Å in VMD.[66] A clear difference of both systems can be observed, which points towards an increased accessibility of the TPDA molecules in the case of Mg^{2+}. Furthermore, the distribution of the angle between the amino groups of TPDA and the surface along the MD trajectory (Figure 6.6, right) is shifted more towards flat angles for Na+ with respect to Mg^{2+}. This suggests that the presence of strongly adsorbed Mg^{2+} ions hinder, to a certain extent, the ionic interaction between the positive TPDA molecules and the negative, deprotonated silanol terminal groups. However, since there are many more TPDA molecules (36) than deprotonated silanols (8) on our 9x9 nm² surface slab, the shift of the angle distribution is only minor, despite the larger differences of the SASA values (at pH 6). In typical trajectory snapshots, we have observed that about 5 TPDA molecules, on average, lie flat on the surface in the presence of Na^+ ions; whereas all molecules remain upright in the presence of Mg^{2+} ions.

6.4 Conclusions

In summary, our simulations suggest that different types of cations present remarkably different adsorption strengths and thus residence

times on silica surfaces at neutral pH. Divalent Mg^{2+} ions effectively invert the sign of the surface potential, while Na^+ ions merely build a diffuse layer. Therefore, in the presence of only monovalent salt at low concentrations, the protonated TPDA molecules are strongly attracted by the silica surface and can assume a less accessible, rather flat orientation. When divalent cations are present (alone or in mixtures), not only is the overall surface potential more positive, but the TPDA molecules are also more upright and thus more accessible to potential binding partners, such as viruses with an overall negative surface potential (see scheme in Figure 6.7). This, finally, explains why the virus retention capacity (Figure 6.3) is higher for the feed solutions which contain $MgCl_2$ than for the feed solution containing just NaCl.

Acknowledgements

References

1. J. P. S. Cabral. "Water Microbiology: Bacterial Pathogens and Water". *International Journal of Environmental Research and Public Health*, 2010, 7, 3657-3703.
2. P. Reeve, et al. "Virus removal of new and aged UF membranes at full-scale in a wastewater reclamation plant". *Environmental Science: Water Research & Technology*, 2016, 2, 1014-1021.
3. M. Koopmans and E. Duizer. "Foodborne viruses: an emerging problem". *Int J Food Microbiol*, 2004, 90, 23-41.
4. G. Miesegaes, et al. "Analysis of viral clearance unit operations for monoclonal antibodies". *Biotechnology and Bioengineering*, 2010, 106, 238-246.
5. M. D. Sobsey and B. L. Jones. "Concentration of poliovirus from tap water using positively charged microporous filters". *Applied and Environmental Microbiology*, 1979, 37, 588-595.
6. P. Nestola, et al. "Improved virus purification processes for vaccines and gene therapy". *Biotechnology and Bioengineering*, 2015, 112, 843-857.
7. J. Werner, et al. "Production of ceramic membranes with different pore sizes for virus retention". *Journal of Water Process Engineering*, 2014, 4, 201-211.
8. J. Bartels, et al. "Amino-Functionalized Ceramic Capillary Membranes for Controlled Virus Retention". *Environmental Science & Technology*, 2016.
9. B. Michen and T. Graule. "Isoelectric points of viruses". *Journal of Applied Microbiology*, 2010, 109, 388-397.
10. N. Kattamuri, et al. "Development and surface characterization of positively charged filters". *Journal of Materials Science*, 2005, 40, 4531-4539.
11. M. Wegmann, et al. "Nanostructured surface modification of microporous ceramics for efficient virus filtration". *Journal of the European Ceramic Society*, 2008, 28, 1603-1612.
12. M. Wegmann, et al. "Modification of ceramic microfilters with colloidal zirconia to promote the adsorption of viruses from water". *Water Research*, 2008, 42, 1726-1734.
13. B. Michen, et al. "Improved Virus Removal in Ceramic Depth Filters Modified with MgO". *Environmental Science & Technology*, 2013, 47, 1526-1533.
14. F. Meder, et al. "The role of surface functionalization of colloidal alumina particles on their controlled interactions with viruses". *Biomaterials*, 2013, 34, 4203-4213.
15. R. Cademartiri, et al. "Immobilization of bacteriophages on modified silica particles". *Biomaterials*, 2010, 31, 1904-1910.
16. Z. Chen, et al. "Capture and release of viruses using amino-functionalized silica particles". *Anal Chim Acta*, 2006, 569, 76-82.
17. K. S. Zerda, et al. "Adsorption of viruses to charge-modified silica". *Applied and Environmental Microbiology*, 1985, 49, 91-95.
18. S. Kroll, et al. "Highly Efficient Enzyme-Functionalized Porous Zirconia Microtubes for Bacteria Filtration". *Environmental Science & Technology*, 2012, 46, 8739-8747.
19. F. Meder, et al. "Controlling protein–particle adsorption by surface tailoring colloidal alumina particles with sulfonate groups". *Acta Biomaterialia*, 2012, 9, 5780-5787.
20. S. Kroll, et al. "Colored ceramic foams with tailored pore size and surface functionalization used as spawning plates for fish breeding". *Ceramics International*, 2014, 40, 15763-15773.
21. H. J. Kim, et al. "Enhancement of mechanical

properties of aluminium/epoxy composites with silane functionalization of aluminium powder". *Composites Part B: Engineering*, 2012, 43, 1743-1748.

22. M. Moritz and M. Łaniecki. "SBA-15 mesoporous material modified with APTES as the carrier for 2-(3-benzoylphenyl)propionic acid". *Applied Surface Science*, 2012, 258, 7523-7529.

23. L. A. S. A. Prado, et al. "Surface modification of alumina nanoparticles with silane coupling agents". *Journal of the Brazilian Chemical Society*, 2010, 21, 2238-2245.

24. H. Weetall. "Preparation of immobilized proteins covalently coupled through silane coupling agents to inorganic supports". *Applied Biochemistry and Biotechnology*, 1993, 41, 157-188.

25. S. Fiorilli, et al. "Vapor-phase self-assembled monolayers of aminosilane on plasma-activated silicon substrates". *Journal of Colloid and Interface Science*, 2008, 321, 235-241.

26. L. Treccani, et al. "Review: Functionalized ceramics for biomedical, biotechnological and environmental applications". *Acta Biomaterialia*, 2013, 9, 7115-7150.

27. A. Y. Ku, et al. "Evidence of Ion Transport through Surface Conduction in Alkylsilane-Functionalized Nanoporous Ceramic Membranes". *Langmuir*, 2006, 22, 8277-8280.

28. J. R. Stephens, et al. "Diffusive flux of nanoparticles through chemically modified alumina membranes". *Analyst*, 2011, 136, 3797-3802.

29. S. Kroll, et al. "Development and characterisation of functionalised ceramic microtubes for bacteria filtration". *Journal of Membrane Science*, 2010, 365, 447-455.

30. J. A. Howarter and J. P. Youngblood. "Optimization of Silica Silanization by 3-Aminopropyltriethoxysilane". *Langmuir*, 2006, 22, 11142-11147.

31. F. Meder, et al. "Controlling Mixed-Protein Adsorption Layers on Colloidal Alumina Particles by Tailoring Carboxyl and Hydroxyl Surface Group Densities". *Langmuir*, 2013, 29, 12502-12510.

32. G. K. Toworfe, et al. "Nucleation and growth of calcium phosphate on amine-, carboxyl- and hydroxyl-silane self-assembled monolayers". *Biomaterials*, 2006, 27, 631-642.

33. M. P. Calatayud, et al. "The effect of surface charge of functionalized Fe3O4 nanoparticles on protein adsorption and cell uptake". *Biomaterials*, 2014, 35, 6389-6399.

34. G. Hollermann, et al. "Functionalized porous ceramic microbeads as carriers in enzymatic tandem systems". *Biochem Eng J*, 2017, 126, 30-39.

35. P. Maffre, et al. "Effects of surface functionalization on the adsorption of human serum albumin onto nanoparticles – a fluorescence correlation spectroscopy study". *Beilstein Journal of Nanotechnology*, 2014, 5, 2036-2047.

36. C. Wallis, et al. "Concentration of viruses from water by membrane chromatography". *Annual Reviews in Microbiology*, 1979, 33, 413-437.

37. C. Wallis, et al. "Enterovirus Concentration on Cellulose Membranes". *Applied Microbiology*, 1972, 23, 476-480.

38. C. P. Gerba. "Applied and Theoretical Aspects of Virus Adsorption to Surfaces". *Advances in Applied Microbiology*, 1984, 30, 133-168.

39. J. Lukasik, et al. "Influence of Salts on Virus Adsorption to Microporous Filters". *Applied and Environmental Microbiology*, 2000, 66, 2914-2920.

40. H. Yu, et al. "Simulating Monovalent and Divalent Ions in Aqueous Solution Using a Drude Polarizable Force Field". *Journal of Chemical Theory and Computation*, 2010, 6, 774-786.

41. C. Bergonzo, et al. "Divalent Ion Dependent Conformational Changes in an RNA Stem-Loop Observed by Molecular Dynamics". *Journal of Chemical Theory and Computation*, 2016, 12, 3382-3389.

42. I. C. Bourg and G. Sposito. "Molecular dynamics simulations of the electrical double layer on smectite surfaces contacting concentrated mixed electrolyte (NaCl–CaCl2) solutions". *Journal of Colloid and Interface Science*, 2011, 360, 701-715.

43. H. Cao, et al. "Salinity and Soluble Organic Matter on Virus Sorption in Sand and Soil Columns". *Ground Water*, 2010, 48, 42-52.

44. S. K. Dishari, et al. "Effects of solution conditions on virus retention by the Viresolve® NFP filter". *Biotechnology Progress*, 2015, 31, 1280-1286.

45. J. N. Israelachvili, "Intermolecular and Surface Forces", Elsevier Science, 2015.

46. L. Gutierrez, et al. "Adsorption of rotavirus and bacteriophage MS2 using glass fiber coated with hematite nanoparticles". *Water Research*, 2009, 43, 5198-5208.

47. C. Dika, et al. "Impact of the virus purification protocol on aggregation and electrokinetics of MS2 phages and corresponding virus-like particles". *Phys Chem Chem Phys*, 2013, 15, 5691-5700.

48.   N. Boudaud, et al. "Removal of MS2, Qβ and GA bacteriophages during drinking water treatment at pilot scale". *Water Research*, 2012, 46, 2651-2664.

49.   J. Langlet, et al. "Efficiency of MS2 phage and Qβ phage removal by membrane filtration in water treatment: Applicability of real-time RT-PCR method". *Journal of Membrane Science*, 2009, 326, 111-116.

50.   B. Besser, et al. "A comparative experimental study on the deviation of the ideal selectivity in HDTMS-functionalized and untreated ceramic structures with pores in the upper mesoporous range". *Microporous and Mesoporous Materials*, 2015, 217, 253-261.

51.   B. N. Fields, et al., "Fields' Virology*"*, Wolters Kluwer Health/Lippincott Williams & Wilkins, 2007.

52.   A. Antony, et al. "Removal Efficiency and Integrity Monitoring Techniques for Virus Removal by Membrane Processes". *Crit Rev Env Sci Tec*, 2012, 42, 891-933.

53.   D. J. Cole, et al. "Development of a classical force field for the oxidized Si surface: Application to hydrophilic wafer bonding". *The Journal of Chemical Physics*, 2007, 127, 204704.

54.   A. Butenuth, et al. "Ab initio derived force-field parameters for molecular dynamics simulations of deprotonated amorphous-SiO2/water interfaces". *physica status solidi (b)*, 2012, 249, 292-305.

55.   J. Wang, et al. "Development and testing of a general amber force field". *Journal of Computational Chemistry*, 2004, 25, 1157-1174.

56.   A. Jakalian, et al. "Fast, efficient generation of high-quality atomic charges. AM1-BCC model: II. Parameterization and validation". *Journal of Computational Chemistry*, 2002, 23, 1623-1641.

57.   J. Wang, et al. "Automatic atom type and bond type perception in molecular mechanical calculations". *Journal of Molecular Graphics and Modelling*, 2006, 25, 247-260.

58.   D. A. Case, et al. "AMBER 14". *University of California, San Francisco*, 2014.

59.   W. L. Jorgensen, et al. "Comparison of simple potential functions for simulating liquid water". *The Journal of Chemical Physics*, 1983, 79, 926-935.

60.   P. Li, et al. "Rational Design of Particle Mesh Ewald Compatible Lennard-Jones Parameters for +2 Metal Cations in Explicit Solvent". *Journal of Chemical Theory and Computation*, 2013, 9, 2733-2748.

61.   N. Hildebrand, et al. "Adsorption Orientation and Binding Motifs of Lysozyme and Chymotrypsin on Amorphous Silica". *The Journal of Physical Chemistry C*, 2015, 119, 7295-7307.

62.   S. Páll, et al., in *Solving Software Challenges for Exascale: International Conference on Exascale Applications and Software, EASC 2014, Stockholm, Sweden, April 2-3, 2014, Revised Selected Papers*, eds. S. Markidis and E. Laure, Springer International Publishing, Cham, 2015, pp. 3-27.

63.   B. Hess, et al. "LINCS: A linear constraint solver for molecular simulations". *J. Comput. Chem.*, 1997, 18, 1463–1472.

64.   G. Bussi, et al. "Canonical sampling through velocity rescaling". *The Journal of Chemical Physics*, 2007, 126, 014101.

65.   U. Essmann, et al. "A smooth particle mesh Ewald method". *The Journal of Chemical Physics*, 1995, 103, 8577-8593.

66.   W. Humphrey, et al. "VMD: Visual molecular dynamics". *Journal of Molecular Graphics*, 1996, 14, 33-38.

67.   A. Barducci, et al. "Well-Tempered Metadynamics: A Smoothly Converging and Tunable Free-Energy Method". *Physical Review Letters*, 2008, 100, 020603.

68.   K. Minoukadeh, et al. "Potential of Mean Force Calculations: A Multiple-Walker Adaptive Biasing Force Approach". *Journal of Chemical Theory and Computation*, 2010, 6, 1008-1017.

69.   G. A. Tribello, et al. "PLUMED 2: New feathers for an old bird". *Computer Physics Communications*, 2014, 185, 604-613.

70.   M. Pham, et al. "Deposition kinetics of bacteriophage MS2 to natural organic matter: Role of divalent cations". *Journal of Colloid and Interface Science*, 2009, 338, 1-9.

7. Hydrophobic Ceramic Capillary Membranes for Versatile Virus Filtration

Authors

Julia Bartels[1], Artur Guedert Batista[1], Stephen Kroll[1,2], Michael Maas[1,3], Kurosch Rezwan[1,3]

[1]*Advanced Ceramics, University of Bremen, Am Biologischen Garten 2, 28359 Bremen, Germany*
[2] *IfBB – Institute for Bioplastics and Biocomposites, Hochschule Hannover, University of Applied Sciences and Arts, Heisterbergallee 10A, 30453 Hannover,Germany*
[3] *MAPEX Center for Materials and Processes, University of Bremen, Am Fallturm 1,28359 Bremen, Germany*

Abstract

In this study, we present hydrophobic yttria-stabilized zirconia capillary membranes (YSZ-90nm) conditioned for virus filtration. As amino-silanized capillary membranes can only adsorb viruses which are negatively charged due to their positively charged membrane surface as shown in chapter 5 and 6, positively charged viruses cannot be effectively removed from water samples. Hydrophobic macroporous ceramic filters (d_{50} = 150 nm) efficiently extract viruses regardless of their surface charge with high throughput rates. For hydrophobic functionalization of the ceramic membranes we used two different silanes, n-hexyltriethoxysilane (HTS, C6-chain) and n-octyltriethoxysilane (OTS, C8-chain), in three different molarities. The virus retention of the membranes is tested in dead-end mode by intracapillary virus feeding using two small bacteriophages as model species: MS2 and PhiX174. Virus retention increases most strongly for hydrophobic capillaries functionalized with 0.05 M OTS, showing a virtually complete retention with log-reduction values (LRVs) of ~9 for both bacteriophages compared to the non-functionalized membrane with LRVs of 0.3 ± 0.1 for MS2 and 3.4 ± 0.2 for PhiX174. The functionalized membranes allow a high membrane flux of ~150 L/(m²hbar), with throughput rates up to ~400 L/(m²h) while maintaining high filtration efficiency. Even under varying feed conditions using only mono- or divalent salt ions or pH values ranging from 3 to 9, retention capacities of the capillary membranes are high. Accordingly, such hydrophobic ceramic membranes offer a versatile alternative to conventional polymeric membranes for virus removal with greatly improved membrane flux.

7.1 Introduction

Designing versatile and highly effective filtration systems for a wide variety of viruses with both high membrane throughput rates and high retention capacities is very challenging. Due to the small size of virus particles ranging from 20 to 500 nm[1], decontamination via size exclusion is impeded by low water permeate fluxes as a result of the required mesopores.[2-5] Conventional filtration systems adsorb viruses at the membrane surface via electrostatic interactions, but this only works for viruses that are charged oppositely to the membrane surface. Since surface charge varies strongly between different types of viruses, it is crucial to control the interactions of pathogens independently of their electrostatic charge in respect to the material surface.

Tailoring virus-surface interactions has wide-ranging technological applications in purification processes of water[6, 7] and food products[8], where the membranes have to fulfill a log reduction value (LRV) of 4, which is given by the World Health Organization (WHO) as a standard for safe and clean water.[9, 10] Furthermore, virus filtration plays a major role in biopharmacy[11], where it is mainly used for virus clearance of plasma products and monoclonal antibodies and purification of viral vectors and vaccines.[12-14] Another application for virus filtration systems is the detection and quantification of small virus concentrations.[15]

Today, conventional membranes for virus filtration are mainly based on polymeric materials and rely on the size exclusion principle.[16, 17] Conventional polymeric filter systems only allow moderate fluxes due to limited pressure tolerances, which could be improved by using ceramic membranes with their characteristic high mechanical strength which allows high pressure loads. Compared to polymeric membranes, ceramic membranes furthermore do not show any swelling behavior during filtration and can be cleaned by back-flushing without affecting the porous structure.[18] Due to the structural diversity of viruses, virus-material interactions are complex and difficult to predict.[19] In the absence of a direct size exclusion effect, electrostatic interactions were demonstrated to play the dominant role in virus-material interactions.[13] E.g. at the pH of ~6, many viruses are negatively charged and readily adsorb to a positively charged membrane surface (isoelectric point (IEP) > 9).[20-23] In our own recent study, we demonstrated the functionalization of ceramic capillary membranes with n-(3-trimethoxysilylpropyl)diethylenetri-amine (TPDA, an aminosilane with three amino groups per silane, IEP > 9). Here, the log-reduction value (LRV) could be increased by a factor of ~9 to 9.6 ± 0.3 for the bacteriophage MS2 at a pH of 5.8.[20] In contrast, no MS2 adsorption was observed for capillaries functionalized with 3-(trihydroxysilyl)-1-propanesulfonic acid (HSPSA), which exhibit the same surface charge as the virus capsid.[20] Electrostatic double layer forces between the virus particle and the membrane surface, as described by the DLVO theory[24-29], are well-known to be central for the electrostatic adsorption and can be influenced by pH or salt concentration. Lukasik et al.[30] demonstrated that the effects of salt ions further depend on the filter type and the filtration conditions, as $MgCl_2$ promoted, inhibited or had no effect on virus adsorption under different circumstances. In our own work, we showed that the LRV for TPDA functionalized capillary membranes is higher in the presence of divalent salt ($MgCl_2$) when compared to monovalent salt (NaCl), as the electrostatic shielding between surface and amino groups by the adsorbed Mg^{2+} ions leads to an upright orientation of the TPDA molecules and thus to a better accessibility during filtration.[31]
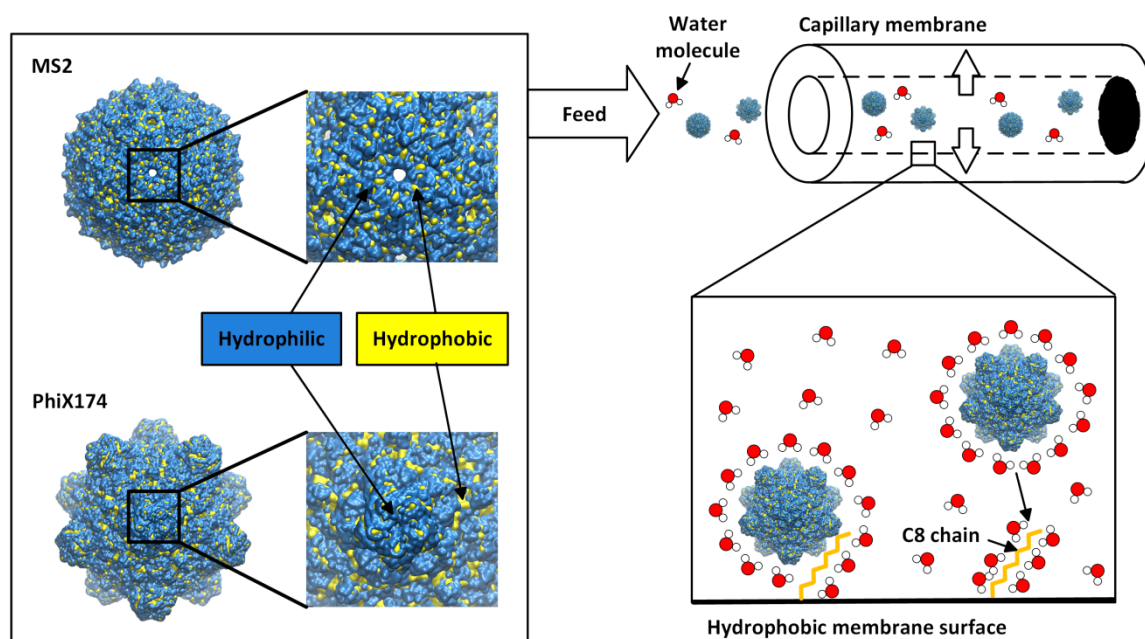
Figure 7.1. Illustration of the principle of dead-end filtration with hydrophobic ceramic capillary membranes.

Beyond the classic DLVO forces, hydrophobic interactions can significantly influence the adsorption of viruses to membranes. In water, hydrophobic surfaces have a preference to associate with each other, which is caused by the high free energy of the interfacial solute layer of polar water molecules which decreases with a reduction of the water-exposed surface area.[32] This effect is shown in Figure 7.1. Various studies reported hydrophobic interactions during virus filtration especially with regard to the removal of viruses by soil passage.[19, 33] The significance of hydrophobic interactions for the retention of the bacteriophage MS2 were shown for hydrophobic polymer membranes which were found to be a better barrier for MS2 than hydrophilic polymer membranes.[34-36] Even for relatively hydrophilic viruses the hydrophobic effect is important for adsorption as shown by Bales et al.[37] Additionally, some salts have a positive effect on virus removal by increasing the ordering of water molecules and the promotion of the sequestering of the hydrophobic entities.[24]

The aim of this work is to design a filtration system to remove various kinds of viruses independently of their IEP and their surface charge from liquids based on ceramic capillary membranes. Modern ceramic materials offer a platform of ultra-hard substrates with defined pore size, porosity and tailored surface chemistry, charge and wetting properties which can be engineered by chemical functionalization. In this respect, silanization, the well-known hydrolysis-condensation reaction with silanes, is a versatile and well-established tool[38], as the reaction can be performed in aqueous media[39, 40], organic solvents[41-44] or in the vapor phase[45, 46] with silanes consisting of different functional groups (e.g. alkyl-[47, 48], amino-[49, 50] or sulphonate-groups[40]) and spacer lengths[38]. In our previous work with ceramic capillary membranes, we investigated the retention behavior of the bacteriophage MS2 based on electrostatic interaction, while being very efficient, this filtration system is only working for specific viruses which have IEPs lower than the pH of the feed solution.[20]

Here, we hydrophobized our well established yttria-stabilized zirconia (YSZ) capillary membranes by silanization with 0.2 M, 0.05 M or 0.0125 M n-hexyltriethoxysilane (HTS) or n-octyltriethoxysilane (OTS). The capillaries are characterized by microstructure analysis with focus on the pore size, the open porosity and the specific surface area and mechanical stability. The functionalization of the filters is investigated

by water contact angle measurements, thermogravimetric analysis (TGA) and the long-term stability of the functionalization is evaluated for a period of three weeks. Virus filtration is carried out with the two model bacteriophages MS2 (IEP = 3.5) and PhiX174 (IEP = 6.2) which are selected for their strong differences in surface charge. Both virus species exhibit a fraction of hydrophobic moieties on the virus surface of around 10 %.[51] Virus retention capacities are determined by filtration experiments in dead-end mode under varying conditions, e.g. with filtration pressures ranging from 0.5 to 2.5 bar and at a pH range from 3 to 12. With this experimental design we demonstrate the performance of the hydrophobic ceramic membrane at throughput rates up to 400 L/(m²hbar) and with different surface charges of the virus particles.

7.2 Materials and Methods

7.2.1 Materials

We used the yttria stabilized zirconia powder TZ-3YS-E (YSZ-90nm, Lot. S305635P) from Krahn Chemie GmbH, Germany for the fabrication of the capillaries. The following reagents were purchased from Sigma-Aldrich Chemie GmbH, Germany: 3-aminopropyltriethoxysilane (APTES, 99 %, product number 440140, Lot. SHBD4935V), hydrogen peroxide solution (purum p.a. ≥ 35 %, product number 95299, Lot. BCBH5638V), magnesium chloride hexahydrate (MgCl$_2$, product number M2670, Lot. BCBJ4439V), polyvinyl alcohol (PVA, fully hydrolyzed, product number P1763, Lot. SLBC9027V), sodium chloride (NaCl, product number S7653, Lot. SZBF0350V), sulfuric acid (95 - 97 %, product number 30743, Lot. SZBF0330V), tryptic soy agar (TSA, product number 22091, Lot. BCBR8554V), culture media tryptic soy broth (TSB, product number T8907, Lot. SLBL1497V), N-(3-trimethoxysilylpropyl)diethylenetriamine (TPDA, product number 413348, Lot. MKBW1074V), hydrochloric acid solution (HCl,

product number 35328, Lot. SZBD2670V) and sodium hydroxide (NaOH, product number 71692, Lot. SZB82950). N-hexyltriethoxysilane (HTS, 95 %, product number AB174350, Lot. 1365286), n-octyltriethoxysilane (OTS, 97 %, product number AB110649, Lot. 1350285) and 3-(trihydroxysilyl)-1-propanesulfonic acid (HSPSA, 30 - 35 %, product number AB130830, Lot. 1246512) were obtained from abcr GmbH & Co. KG, Germany.

The bacteriophage MS2 (DSM Cat. No. 13767) and its host bacteria *E. coli* (DSM Cat. No. 5210) as well as the bacteriophage PhiX174 (DSM Cat. No. 4497) and its host bacteria *E. coli* (DSM Cat. No. 13127) were purchased from German Collection of Microorganisms and Cell Cultures (DSMZ), Germany.

Double-deionized water with an electrical resistance of 18.2 MΩ, which was obtained from a Synergy® apparatus (Millipore, Germany), was used for all experiments.

7.2.2 Fabrication of Hydrophobic YSZ Capillary Membranes

The tubular YSZ membranes were prepared by extrusion as described in detail in our previous studies.[2][20] The ceramic slurry consists of 132 g YSZ powder (YSZ-90nm) as ceramic material, 4 g APTES as dispersant, 20 g PVA-water solution (25 wt.%) as binder and 13.5 g double-deionized water. The ingredients were milled in a planetary ball mill (PM400, Retsch), using 50 alumina grinding balls with a diameter of 10 mm, for 3 h at 350 rpm while changing the rotation direction every 5 min. Afterwards, the slurry was shaped with a self-made laboratory extruder which was equipped with a nozzle of 2.0 mm in diameter and a pin of 1.0 mm in diameter with an extrusion speed of 50 cm/min. After drying for at least two days at room temperature (RT) (20 °C, relative humidity ~50 %) the capillaries were sintered for 2 h at 1050 °C with dwell times at 280 °C (0.5 h) and 500 °C (1 h) (HT40/17, Nabertherm, Lilienthal, Germany).
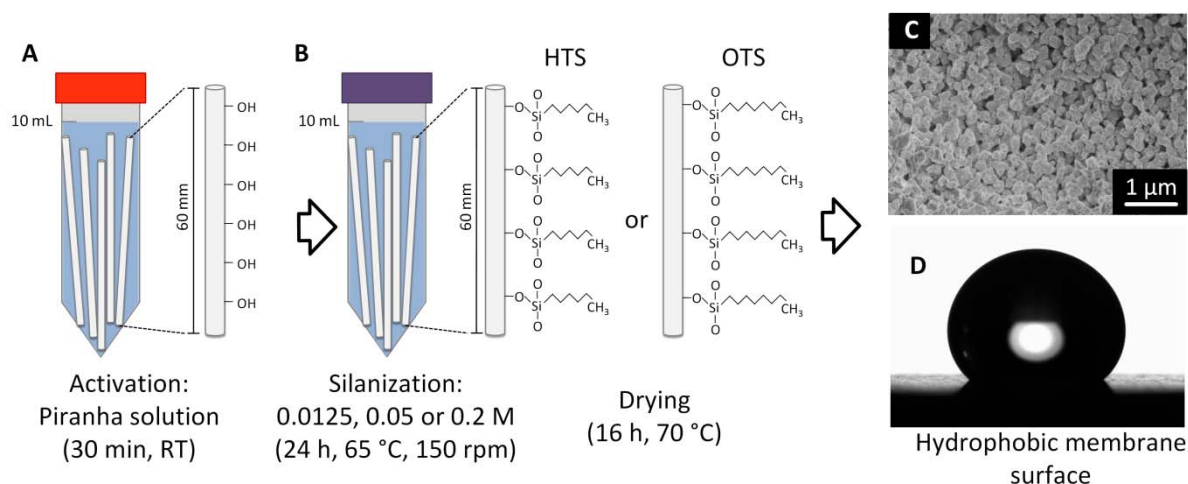
Figure 7.2. Functionalization strategy of sintered YSZ capillary membranes silanized with HTS or OTS (A, B), a SEM picture of a 0.05 M OTS functionalized membrane surface (C) and a photograph of a water contact angle measurement of a 0.05 M OTS functionalized flat membrane. HTS = n-hexyltriethoxysilane, OTS = n-octyltriethoxysilane.

To generate hydroxyl groups on the surfaces of the capillaries, the sintered YSZ capillary membranes were incubated in Piranha solution (97 % H_2SO_4 : 35 % H_2O_2, 3:1 (v/v)) for 30 min at RT (Figure 7.2A). As shown in our previous work, the membrane microstructure is not affected by an activation with Piranha solution.[20] Afterwards, the capillaries were washed with water until the effluents achieved a neutral pH and dried at 70 °C for 16 h (UT6120, Heraeus, Hanau, Germany). For hydrophobization, five activated capillaries with an individual length of 60 mm were incubated in 10 mL silane solution at 65 °C under slight shaking at 150 rpm (Inkubator 1000/Unimax 1010, Heidolph, Schwabach, Germany) for 24 h (Figure 7.2B). The silane solutions based on HTS or OTS were prepared by dilution with water (pH not adjusted) in three different molarities (0.2 M, 0.05 M and 0.0125 M). After functionalization, the hydrophobic capillaries (Figure 7.2C, 7.2D) were washed until the effluents had a neutral pH and dried at 70 °C for 16 h (UT6120, Heraeus, Hanau, Germany). The activated capillary membranes were silanized in the same way with 0.2 M HSPSA or 0.2 M TPDA to serve as references.

7.2.3 Characterization of Silanized Membranes

7.2.3.1 Capillary Properties

The determination of structural and mechanical properties of the silanized membranes was performed as described in detail in our previous studies.[2, 20] In short, Hg-porosimetry (Mercury Porosimeter Pascal 140 and 440, POROTEC GmbH) was used to obtain the pore size distribution, the average pore size (d_{50}) and the open porosity, the specific surface area was measured by nitrogen adsorption according to BET method (Gemini, Micromeritics) after degassing the capillaries at 120 °C for at least 3 h with argon and 3-point bending tests were used according to DIN EN 843-1 (Roell Z005, Zwick) to determine the flexural strength and the Weibull modulus. The microstructure of the outer capillary surface was analyzed by scanning electron microscopy (SEM, Field-emission SEM SUPRA 40, Zeiss). The zeta-potential of the capillary membranes was measured in the pH range between 3 and 9 with a SurPASS (Anton Paar) apparatus which is based on the streaming potential method. Water contact angle measurements were performed with filter platelets (diameter = 12 mm) which were produced with a hydraulic press. The YSZ-90nm powder was pressed at 10 kN for 30 seconds and sintered in the same way as the capillaries to have

Table 7.1.   Properties of the bacteriophages MS2 and PhiX174.

	MS2	PhiX174
Nucleic acid [1,2]	ssRNA, 3569 nucleotides	ssRNA, 5386 nucleotides
Morphology [1]	Non-enveloped, icosahedral, d= 25 - 27 nm	Non-enveloped, icosahedral, d= 26 - 32 nm
Host [3]	*E-Coli*; F-specific	*E-Coli, Salmonella typhimurium*; somatic
Multiplication rate (h^{-1}) [4]	669	697
Molecular weight (MDa) [5]	3.6	6.2
IEP [6]	3.5 ± 0.6	6.2 ± 1.6

[1], [2], [3], [4], [5], [6]

similar structural properties. The water contact angle (Dataphysics, OCA25) was measured with a needle size of 0.5 mm and a drop volume of 0.25 µL.

Thermogravimetric analysis (TGA; STA503, Bähr-Thermoanalyse GmbH, Hüllhorst, Germany) was performed with the capillary membranes in a temperature range between 40 °C and 900 °C with a heating rate of 10 K/min under 2 L/h flowing air.

7.2.3.2 Membrane Flux Measurements

Membrane flux measurements of the tubular filters were performed by intracapillary water feeding for 30 min with a peristaltic pump (BVP Standard, Ismatec) in dead-end mode where one end of the capillary was sealed with silicone (Wirosil Dublier-Silikon, Bego Medical GmbH, Bremen, Germany) using pressures between 250 and 1000 mbar (C9500, COMARK). For each capillary type, three individual capillaries in vertical orientation were tested and the membrane flux for 1 bar was calculated by linear regression in L/(m²hbar).

7.2.3.3 Virus Retention Test

The model bacteriophages MS2 and PhiX174 are not pathogenic for humans[17, 21, 52] and are therefore often used in virus inactivation and filtration tests. The bacteriophage properties are summarized in Table 7.1.

MS2 is a single-stranded RNA virus which is 25 - 27 nm in diameter and has an isoelectric point (IEP) of 3.5 ± 0.6 and PhiX174 is a single-stranded DNA virus with a diameter of 26 - 32 nm and an IEP of 6.2 ± 1.6.[3, 53] Both bacteriophages have an excess of positively

charged amino acids at pH 7.3, even if their zeta potential is negative which can be explained by the strong influence of the negatively charged nucleic acid in the capsid.[51, 54, 55] Both bacteriophages can be considered mainly hydrophillic with hydrophobic residues.[35, 51, 56, 57] Both virus species show a fraction of hydrophobic moieties on the virus surface of around 10 %.[51]

For the preparation of the bacteriophage solution the bacteria were grown in 50 mL of a sterile 30 g/L TSB medium at 37 °C in an incubator shaker (Inkubator 1000/Unimax 1010, Heidolph) at 150 rpm for 4 h to obtain bacteria in an exponential growth phase (4-h culture). Two different *E.coli* strains were used depending on the bacteriophage. For the propagation of the bacteriophage MS2 the host bacteria *E.coli* (DSM Cat. No. 5210) and for the bacteriophage PhiX174 the host bacteria *E.coli* (DSM Cat. No. 13127) were used. The bacteria culture was centrifuged at 3000 g for 10 min and the supernatant was removed while the bacteria were resuspended in 50 mL of a salt solution containing 0.02 M $MgCl_2$ and 0.15 M NaCl to remove the agents from the TSB medium. The pH of the salt solution was not adjusted (pH 5.8). At the pH of 5.8 the viruses are charged differently according to their IEPs. MS2 with an IEP of 3.5 is negatively charged and PhiX174 with an IEP of 6.2 is positively charged at these conditions. 1 mL of the bacteriophage stock suspension (prepared according to suppliers information) was added and the culture was incubated at 37 °C at 100 rpm for 20 h. After the incubation time, the bacteria are removed by centrifugation at 3000 g for 30 min at RT and the supernatant which contains the viruses was

cleared additionally of bacterial debris and organic matter through sterile 0.2 µm syringe filters.

The virus retention test of the bacteriophages MS2 and PhiX174 was performed by analyzing the feed solution and the permeate using the Plaque Forming Unit (PFU) method. The PFU method (plaque assay) is the most quantitative and useful biological assay for viruses which is based on the ability of a single virus to give rise to a macroscopic area of cytopathology on a monolayer of bacteria cells.[58] For the PFU method, dilution series of 10-fold steps were performed in 0.02 M MgCl$_2$/0.15 M NaCl solution. The diluted phage suspensions were mixed with the specific host bacteria (*E.Coli* 5210 for MS2 and *E.Coli* 13127 for PhiX174) and agar, poured on a Petri dish and incubated for 16 h at 37 °C (Memmert, Modell 100-800). The formed plaques were counted and the log reduction value (LRV) was calculated as shown by Kroll et al.[52] Retention of microorganisms is expressed in the LRV, which is defined as the logarithm to base 10 of the ratio of viral concentrations in the feed to those in the permeate.

The standard virus retention test was performed by intracapillary virus feeding in dead-end mode with a pressure of 500 mbar until a permeate volume of 15 mL was filtrated. The permeate was obtained after ~85 min of filtration through the active filtering area of 1.4 cm². After this time the influent and effluent samples were taken to determine the LRV. The used standard feed was based on 0.02 M MgCl$_2$/0.15 M NaCl (pH 5.8, not adjusted) showing initial virus concentrations of around 10^9 PFU/mL.

Additional to the standard virus retention test, the feed solution was varied by using only one salt component in the feed solution, namely 0.02 M MgCl$_2$ or 0.15 M NaCl or by adjusting the pH to 3 with HCl or to 9 and 12 with NaOH. Furthermore, the standard virus test was performed with increased pressure to up to 2.5 bar.

For each experiment, three individual capillary membranes with a length of 5 cm (active filter area = 1.4 cm²) were tested.

7.2.3.4 Leaching Test

To analyze wash-out effects of the silane on the capillaries, the capillaries were intracapillary fed in dead-end-mode with a saline solution (0.02 M MgCl$_2$/0.15 M NaCl) at 500 mbar at RT for 21 days. After each week a virus retention test was performed with MS2 and PhiX174 to analyze the LRV of the capillaries. For each time period, three individual capillary membranes with a filter length of 5 cm were tested.

7.3 Results and Discussion
7.3.1 Structural and Mechanical Properties

Before considering the performance of the ceramic membranes for virus removal, the material properties of the membrane need to be fully characterized. The membrane properties obtained by Hg-porosimetry (pore size range, average pore size and open porosity), BET method (specific surface area), 3-point bending tests (bending strength, Weibull modulus) and water contact angles of the capillary membranes are shown in Table 7.2. The non-functionalized capillary membranes show an average pore size of 144 nm and a pore size distribution in the range between 5 and 200 nm in combination with a relatively high open porosity of 49.3 % and homogeneously distributed pores. The mechanical stability of the capillaries is 29.0 ± 4.4 MPa, which makes them suitable for filtration experiments. The capillaries functionalized with HTS or OTS show the same structural and mechanical properties as the non-functionalized capillary membranes. Only for the capillaries silanized with 0.2 M HTS or OTS the average pore size is decreased to values of 126 nm and 122 nm, respectively.

Table 7.2. Membrane properties of capillary membranes functionalized with HTS and OTS.

| Membrane-functionalization | Hg-porosimetry | | | BET method | 3-point bending test | Water contact angle measurement |
	Pore size range in nm	d_{50} in nm	Open porosity in %	Specific surface area in m²/g	Bending strength in MPa	Water contact angle in °
Non-functionalized	5 - 200	144	49.3	5.4	29.0 ± 4.4	very hydrophilic
0.0125 M HTS	5 - 200	151	47.0	5.1	25.0 ± 6.3	133.1 ± 7.7
0.05 M HTS	5 - 200	148	46.6	4.9	22.7 ± 5.0	135.1 ± 6.9
0.2 M HTS	5 - 200	126	50.1	5.2	27.9 ± 6.7	135.9 ± 8.1
0.0125 M OTS	5 - 200	149	49.9	4.8	28.7 ±5.2	131.3 ± 6.6
0.05 M OTS	5 - 200	153	47.8	5.1	23.5 ± 6.0	140.5 ± 7.3
0.2 M OTS	5 - 180	122	50.1	4.9	22.4 ± 5.5	140.5 ± 3.0
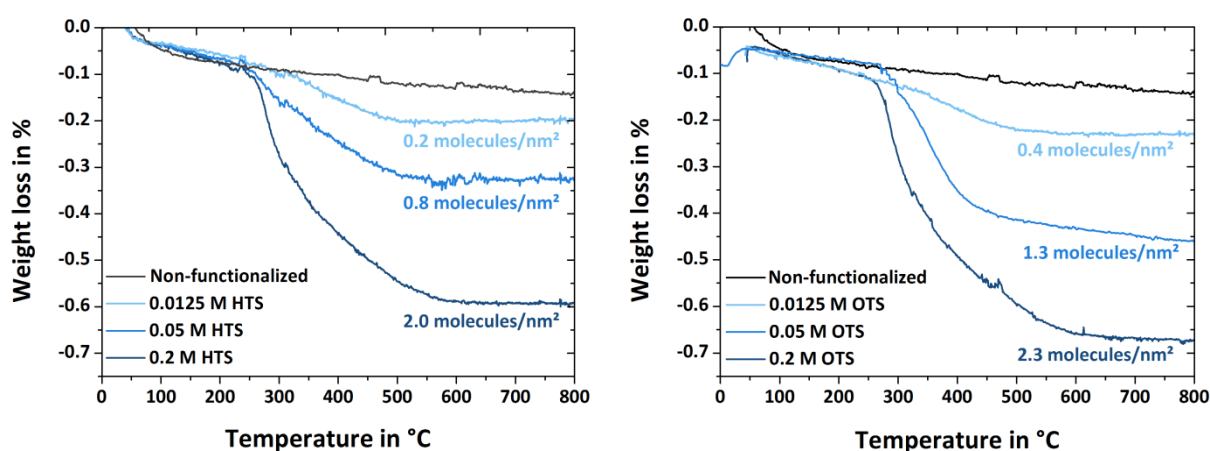
Figure 7.3. Weight loss determined by TGA measurements with the assessed loading capacities of the capillaries functionalized with HTS (left) and OTS (right) compared with non-functionalized capillary membranes.

The wettability of the functionalized material was determined by static water contact angle measurements on flat membrane surfaces. The water contact angle for the non-functionalized platelets could not be measured, as the platelets were too hydrophilic and the water was sucked into the highly porous structure by capillary forces. All samples functionalized with either HTS or OTS show a high static water contact angle between 131.3° and 140.5°. Accordingly, the membranes were successfully converted from hydrophilic to hydrophobic with the chosen functionalization approach.

TGA of the capillaries was performed measuring the mass of the samples during a temperature increase to 900°C. Figure 7.3 shows the weight loss of the functionalized HTS capillaries (left) and the OTS capillaries (right) compared to the non-functionalized membranes as a function of temperature. The non-functionalized membrane loses 0.14 % of its weight which is most likely related to water desorption. Below 200 °C, the same initial weight-loss observed for the functionalized samples. The two silane types show a nearly identical increased weight loss in the range between 250 °C and 600 °C at the respective molarities when compared to the non-functionalized sample. The weight loss increases with silane concentration used during functionalization. Accordingly, the highest weight loss is attributed to the 0.2 M samples. After 600 °C the 0.0125 M HTS samples have a weight loss of around 0.2 % which is attributed to 0.2 molecules/nm², the 0.05 M HTS samples show a weight loss of 0.33 % (0.9 molecules/nm²) and the highest weight loss
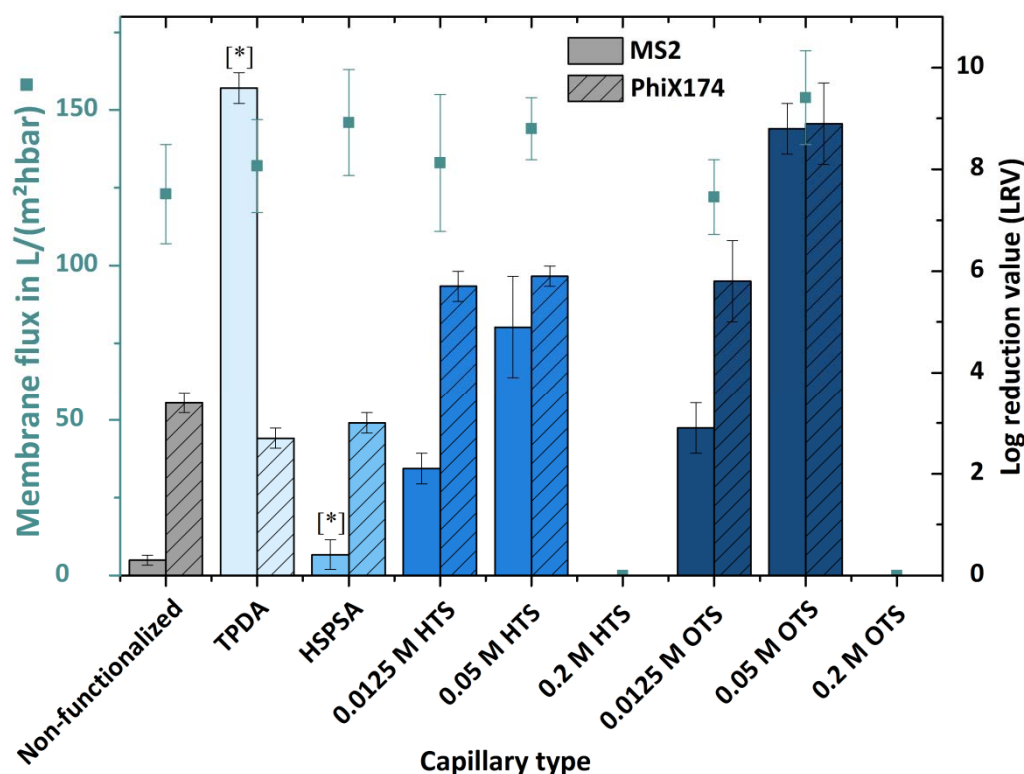
Figure 7.4. Membrane flux and virus retention of the bacteriophages MS2 and PhiX174 measured in dead-end mode with non-functionalized and functionalized ceramic capillary membranes. The feed was based on a saline solution (0.02 M MgCl$_2$, 0.15 M NaCl, pH 5.8) with a viral concentration of around 10^9-10^{10} PFU/mL. TPDA and HSPSA retention capacities and membrane fluxes tested under the same conditions were taken from our previous publication.[20]

was determined for 0.2 M HTS with 0.59 % (2.1 molecules/nm²). For the OTS samples the weight loss is slightly higher compared to the HTS samples with 0.22 % (0.4 molecules/nm²) for the 0.0125 M OTS membranes, 0.46 % (1.3 molecules/nm²) for the 0.05 M OTS membranes and 0.67 % (2.3 molecules/nm²) for the 0.2 M OTS membranes. The weight loss is not increasing any further after 600 °C for both capillary types.

The TGA results show that the silanization with HTS and OTS was successful for all used molarities and could confirm the hydrophobic functionalization also observed by water contact angle measurements. The contact angles are in the same range for all sample types as discussed previously (Table 7.2), in contrast to the clear differences in the TGA measurement. We assume that the outer membrane surface is fully silanized for all membrane types, but that the silanization of the internal pore structure is improved at higher molarities.

7.3.2 Membrane Flux and Virus Retention

Figure 7.4 shows the membrane flux and the virus retention capacity of the bacteriophages MS2 and PhiX174 for the non-functionalized and the silanized capillary membranes. The membrane flux of the non-functionalized, as well as the membranes silanized with 0.0125 M and 0.05 M HTS or OTS is around 150 L/(m²hbar). For comparison, membranes silanized with TPDA and the HSPSA, which were investigated in our previous work ,[31] show the same membrane flux. At concentrations of 0.0125 M and 0.05 M HTS or OTS, the hydrophobicity of the functionalized membranes is not significantly influencing the water flux. However, capillaries functionalized with 0.2 M HTS and OTS show no water permeate flux at 1 bar. Due to their high loading with ~ 2.0 silanes/nm² (Figure 7.3) and the slightly reduced pore diameters (Table 7.2), no water was capable to flow through the pores of the membranes in dead-end mode which

renders them unsuitable for filtration applications. The membrane flux should not be influenced even by a high organic carbon content in the feed which can adsorb onto the membrane and lead to membrane fouling as the pore size of 150 nm is much higher compared to the size of the DOCs.

The non-functionalized capillary membranes show relatively low virus retention capacities of LRV 0.3 ± 0.1 for MS2 and of 3.4 ± 0.2 for PhiX174. For MS2, poor retention is caused by repulsion between negatively charged viruses (IEP = 3.9) and negatively charged pore wall surfaces (IEP < 3)[20] at the applied pH of 5.8. PhiX174 (IEP = 6.6) is slightly positively charged at pH 5.8 and therefore adsorbs to the non-functionalized capillary surface. However, the retention is below LRV of 4, which is given by the World Health Organization (WHO) as a standard for safe and clean water.[9, 10]

As shown in our previous work, the virus retention capacity for MS2 can be strongly increased to LRVs of 9.6 ± 0.3 by using positively charged TPDA-silanized capillaries (IEP > 9). Here, the negatively charged MS2 viruses (at pH 5.8) can adsorb to the positively charged membrane during dead-end filtration.[20] In contrast, the retention capacity for PhiX174 viruses is decreased with the TPDA-functionalized membrane compared to the non-functionalized membrane, down to an LRV of 3.0 ± 0.2 for the TPDA capillaries, as the repulsion between the positively charged PhiX174 and the positively charged pore wall surfaces at the applied pH of 5.8 is hindering adsorption. Nevertheless, an adsorption occurs and we assume that the moderately high filtration efficiency for PhiX174 with the TPDA-functionalized membrane is a result of the complex surface chemistry of the virus membrane that also bears patches or domains with negative charge. The negatively charged HSPSA capillary (IEP < 3) shows a similar virus retention capacity as the non-functionalized capillary membrane at pH 5.8, which can be explained by the nearly identical zeta-potentials of virus and membrane.[20]

The virus retention capacities of the HTS functionalized capillaries is increased for both virus types and both used molarities compared to the non-functionalized membranes. The HTS capillaries retain MS2 with LRVs of 2.1 ± 0.3 (0.0125 M HTS) and 4.9 ± 1.0 (0.05 M HTS), which is much lower than the retention with TPDA capillaries. The PhiX174 retention shows an LRV of around 6 for both used molarities which is higher compared to the non-functionalized, the TPDA- and the HSPSA-silanized capillary membranes. Thus, the 0.05 M HTS membrane is fulfilling the virus filter criterion of LRV 4 required by the World Health Organization for clean water for both bacteriophage types.[9, 10] However, for the purification of biopharmaceutical products like monoclonal antibodies, a full removal of virus particles is desired.[59] Such a virtually complete virus removal is obtained by the ceramic capillary membranes functionalized with 0.05 M OTS, where LRVs of 8.8 ± 0.5 for MS2 and 8.9 ± 0.8 for PhiX174 are observed. The 0.0125 M OTS capillaries still show an LRV of 2.9 ± 0.5 for the MS2 bacteriophages and of 5.8 ± 0.8 for the PhiX174 bacteriophages. The OTS capillaries most likely have a higher virus retention as a result of the higher functionalization density (Figure 7.3) compared to the HTS capillaries.

Both bacteriophages are mainly hydrophilic with hydrophobic residues[35, 51, 56, 57], therefore, they attach to the hydrophobic regions of the capillary membranes. PhiX174 viruses have 11 % hydrophobic moieties, which is slightly higher compared to MS2 which have 8 % hydrophobic residues.[51] This might explain the stronger attraction of PhiX174 to the hydrophobic capillary surface resulting in higher LRVs compared to MS2, especially at low molarities of HTS and OTS. To a certain extent, electrostatic adsorption can also be used to explain the findings. The HTS and OTS functionalized membranes have IEPs around 4.5, therefore the PhiX174 viruses are positively charged at pH 5.8 and the functionalized membranes are negatively charged, which increases the removal effect when compared to MS2. For the 0.05 M OTS capillaries the electrostatic interactions seem to play only a minor role, as both virus types have
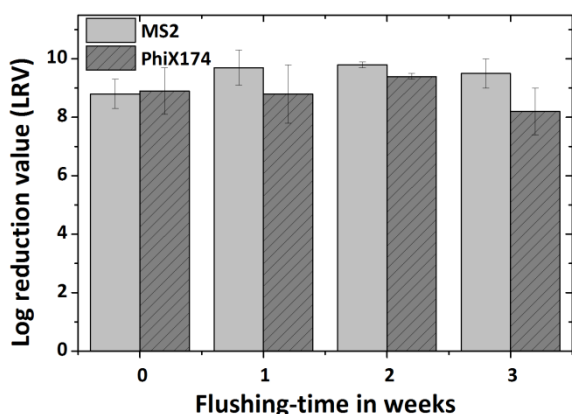
Figure 7.5. Virus retention of the bacteriophages MS2 and PhiX174 measured in dead-end mode with 0.05 M OTS capillary membranes after flushing with a salt solution (0.02 M MgCl$_2$, 0.15 M NaCl) to evaluate the stability of the immobilized silane. The stability test was performed over a period of 3 weeks.
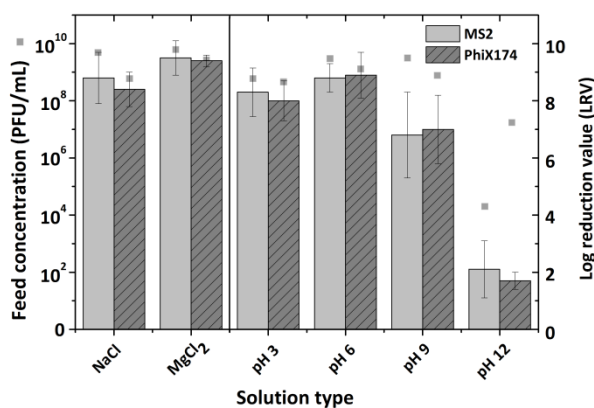
Figure 7.6. Virus retention of the bacteriophages MS2 and PhiX174 measured in dead-end mode with 0.05 M OTS capillary membranes in salt solutions varying in composition (NaCl and MgCl$_2$) and in pH.

nearly the same retention values.

In our previous as well as in the present study, the observed inactivation of viruses is not necessarily equal to virus absorption on the membrane surface. Based on the observed correlation between phage inactivation and surface properties, inactivation and retention occurs due to hydrophobic and electrostatic interactions between membrane surface and virus. Remaining organic material present in the feed solution is negligible and has no influence on the retention rate as the electrostatic and hydrophobic virus-membrane interactions play the mayor role in the interaction between virus and membrane.

Without post-chemical functionalization, such LRVs are otherwise only reachable by using membranes with significantly smaller pore sizes in the order of the viral target (d$_{50}$ = ~25 nm). As shown in our previous work, this pore size reduction is associated with a strong decrease in membrane flux from 150 L/(m²hbar) to values of around 3 L/(m²hbar).[2] Commercially available polymeric membranes obtained from Sartorius, Germany (Virosart CPV) reached the same high virus retention levels,[20] but, according to the manufacturer, with a moderate membrane flux of ~ 84 L/(m²hbar).

Stability and wash-out effects of the silane on the capillaries were evaluated under filtration conditions with capillary membranes functionalized with 0.05 M OTS as they show the best virus retention capacities (Figure 7.4). Therefore, the capillary membranes were intracapillarly fed with a saline solution (0.02 M MgCl$_2$, 0.15 M NaCl, pH 5.8) at 500 mbar for up to 3 weeks in dead-end mode. After each week a PFU test was performed as described above. As shown in Figure 7.5, the LRV for both bacteriophages was higher than 8 over the time period of 3 weeks. No wash-out effects are determined, which means that a stable bond of OTS on the hydroxyl-activated membrane surface was formed, which is suitable for virus filtration even under throughflow filtration conditions.

Furthermore, the virus retention of the bacteriophages MS2 and PhiX174 was analyzed in dead-end mode with 0.05 M OTS capillary membranes using varying feed solutions and the results are presented in Figure 7.6.

In our previous work, we showed that the LRV for TPDA functionalized capillary membranes is higher in the presence of divalent salt (MgCl$_2$) when compared to monovalent salt (NaCl), as the shielding between surface and amino groups by the adsorbed Mg^{2+} ions leads to an upright orientation of the TPDA molecules and thus to a better accessibility [31]. As shown by Gerba et al.,
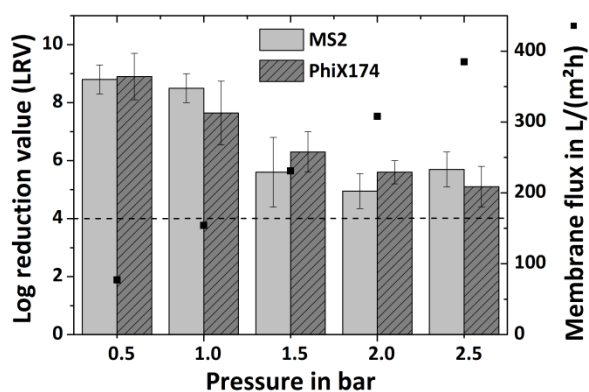
Figure 7.7. Virus retention of the bacteriophages MS2 and PhiX174 measured in dead-end mode with 0.05 M OTS capillary membranes with pressures ranging from 0.5 to 2.5 mbar.

some salts also have a positive effect on virus removal via the hydrophobic effect.[24] However, for the OTS functionalized capillary membranes no significant change in the retention capacity can be observed in the presence of divalent cations (0.02 M $MgCl_2$). Here, virus retention is 9.5 ± 0.6 for MS2 and 9.4 ± 0.2 for PhiX174. The LRV for a feed solution containing 0.15 M NaCl (pH 6.3) is still high with 8.8 ± 0.9 for MS2 and 8.4 ± 0.6 for PhiX174.

Furthermore, the pH stability of the ceramic filter system was analyzed by adjusting the feed solution (0.02 M $MgCl_2$, 0.15 M NaCl) to different pHs with HCl or NaOH. The virus retention for the feed in the acidic and neutral range show LRVs above 8 for both bacteriophages. At pH 9 the virus retention is decreased to around 7 for both bacteriophages. When using pH 12 the bacteriophage feed is reduced from a concentration of ~10^9 to ~10^4 even before filtration, which indicates that the viruses are inactivated in this pH regime. The retention of the reduced feed concentration is around 2 for both bacteriophages. To determine if the silane is removed due to the high pH, water contact angle measurements with membrane platelets, which were incubated in pH 9 or pH 12 over 1.5 h, were performed. The results show a slight decrease of the contact angle from 135.1° ± 6.9° to 124.8° ± 6.4° for the incubation in pH 9 and a further decrease to 115.0° ± 10.1° for the incubation in pH 12. Thus, the functionalization

100

is not stable at basic pH for longer periods of time.

The standard virus test, which was previously performed at 500 mbar, was tested with increased pressure to up to 2.5 bar, which is the overall practical limit of the testing setup (Figure 7.7). The retention is slightly decreased for experiments performed at 1.0 bar to retentions of around LRV 8 and further decreased for pressures of 1.5 bar to LRVs of around 6 for both bacteriophages. A further increase of the pressure to 2.0 and 2.5 bar only result in a slight decrease of the retention capacity. Thus, at a pressure of 2.5 bar a LRV of 5.7 ± 0.6 for MS2 and of 5.1 ± 0.7 for Phix174 is observed, which still fulfills the required LRV of 4 for clean water. The decrease of virus retention during pressure increase can be explained by the shorter contact time of the virus to react with the hydrophobic parts of the membrane surface. With a pressure of 2.5 bar, a water volume of nearly 400 L/(m²h) can be filtrated which showcases the promising properties of hydrophobic ceramic capillaries for filtration applications. Compared to a commercially available polymeric membrane obtained from Sartorius, Germany (Virosart CPV) a maximal water flux of 168 L/(m²h) can be reached as the working pressure of 2.0 bar should not be exceeded.

7.4 Conclusions

In our study, YSZ capillary membranes with pore sizes 6 times larger than the bacteriophages MS2 and PhiX174 are successfully hydrophobized with HTS and OTS. The functionalization with 0.05 M OTS with a resulting surface coverage of around 1.3 molecules/nm² can be beneficially utilized for virus retention as a result of hydrophobic interactions, which do not significantly affect the water permeate flux (~150 L/(m²hbar)). The hydrophobic membrane and the hydrophobic regions of the viral capsid preferentially associate to each other due to the high free energy of the interfacial solute layer of polar water molecules. At 0.5 bar, an almost complete virus removal is obtained with LRVs of 8.8 ± 0.5 for MS2 and 8.9 ± 0.8 for PhiX174, which is in the same range as commercially

available polymeric virus filtration membranes. The ceramic membranes surpass those polymeric membranes in the higher applicable pressures of up to 2.5 bar resulting in high throughput rates of nearly 400 L/(m²h), at which the retention of both viruses is still fulfilling the requirements for safe water of LRV 4. Combined with the general advantages of ceramic membranes like high mechanical stability of the porous structure and long-term stability of the functionalization, the hydrophobic ceramic capillary membranes open promising perspectives for filtration applications of diverse viruses and related biological entities.

Acknowledgements

References

1. M. Henry and L. Debarbieux. "Tools from viruses: Bacteriophage successes and beyond". *Virology*, 2012, 434, 151-161.
2. J. Werner, et al. "Production of ceramic membranes with different pore sizes for virus retention". *Journal of Water Process Engineering*, 2014, 4, 201-211.
3. A. Duek, et al. "New and conventional pore size tests in virus-removing membranes". *Water Research*, 2012, 46, 2505-2514.
4. I. Voigt. "Nanofiltration with ceramic membranes". *Chemie Ingenieur Technik*, 2005, 77, 559-564.
5. H. Leclerc, et al. "Bacteriophages as indicators of enteric viruses and public health risk in groundwaters". *Journal of Applied Microbiology*, 2000, 88, 5-21.
6. J. P. S. Cabral. "Water Microbiology: Bacterial Pathogens and Water". *International Journal of Environmental Research and Public Health*, 2010, 7, 3657-3703.
7. P. Reeve, et al. "Virus removal of new and aged UF membranes at full-scale in a wastewater reclamation plant". *Environmental Science: Water Research & Technology*, 2016, 2, 1014-1021.
8. M. Koopmans and E. Duizer. "Foodborne viruses: an emerging problem". *Int J Food Microbiol*, 2004, 90, 23-41.
9. A. Bennett. "Maintaining the integrity of filtration systems". *Filtration & Separation*, 2005, 42, 30-33.
10. J. J. Simonis, et al. "Removal of microbes to World Health Organization requirements using a locally developed, low cost, micro-porous, ceramic water filter". *Journal of Water, Sanitation and Hygiene for Development*, 2014, 4, 620-624.
11. G. Miesegaes, et al. "Analysis of viral clearance unit operations for monoclonal antibodies". *Biotechnology and Bioengineering*, 2010, 106, 238-246.
12. P. Nestola, et al. "Improved virus purification processes for vaccines and gene therapy". *Biotechnology and Bioengineering*, 2015, 112, 843-857.
13. J. A. Redman, et al. "Filtration of Recombinant Norwalk Virus Particles and Bacteriophage MS2 in Quartz Sand: Importance of Electrostatic Interactions". *Environmental Science & Technology*, 1997, 31, 3378-3383.
14. C. Charcosset, "Membrane Processes in Biotechnology and Pharmaceutics", Elsevier, 2012.
15. M. D. Sobsey and B. L. Jones. "Concentration of poliovirus from tap water using positively charged microporous filters". *Applied and Environmental Microbiology*, 1979, 37, 588-595.
16. J. Langlet, et al. "Efficiency of MS2 phage and Qβ phage removal by membrane filtration in water treatment: Applicability of real-time RT-PCR method". *Journal of Membrane Science*, 2009, 326, 111-116.
17. A. M. ElHadidy, et al. "An evaluation of virus removal mechanisms by ultrafiltration membranes using MS2 and φX174 bacteriophage". *Separation and Purification Technology*, 2013, 120, 215-223.
18. J. Finley. "Ceramic membranes: a robust filtration alternative". *Filtration & Separation*, 2005, 42, 34-37.
19. J. F. Schijven and S. M. Hassanizadeh. "Removal of Viruses by Soil Passage: Overview of Modeling, Processes, and Parameters". *Crit Rev Env Sci Tec*, 2000, 30, 49-127.
20. J. Bartels, et al. "Amino-Functionalized Ceramic Capillary Membranes for Controlled Virus Retention". *Environmental Science & Technology*, 2016.
21. B. Michen, et al. "Improved Virus Removal in Ceramic Depth Filters Modified with MgO". *Environmental Science & Technology*, 2013, 47, 1526-1533.
22. M. Wegmann, et al. "Nanostructured surface modification of microporous ceramics for efficient virus filtration". *Journal of the*

European Ceramic Society, 2008, 28, 1603-1612.

23. I. Bradley, et al. "Iron oxide amended biosand filters for virus removal". *Water Research*, 2011, 45, 4501-4510.

24. C. P. Gerba. "Applied and Theoretical Aspects of Virus Adsorption to Surfaces". *Advances in Applied Microbiology*, 1984, 30, 133-168.

25. H. Cao, et al. "Salinity and Soluble Organic Matter on Virus Sorption in Sand and Soil Columns". *Ground Water*, 2010, 48, 42-52.

26. S. K. Dishari, et al. "Effects of solution conditions on virus retention by the Viresolve® NFP filter". *Biotechnology Progress*, 2015, 31, 1280-1286.

27. I. C. Bourg and G. Sposito. "Molecular dynamics simulations of the electrical double layer on smectite surfaces contacting concentrated mixed electrolyte (NaCl–CaCl2) solutions". *Journal of Colloid and Interface Science*, 2011, 360, 701-715.

28. H. Yu, et al. "Simulating Monovalent and Divalent Ions in Aqueous Solution Using a Drude Polarizable Force Field". *Journal of Chemical Theory and Computation*, 2010, 6, 774-786.

29. C. Bergonzo, et al. "Divalent Ion Dependent Conformational Changes in an RNA Stem-Loop Observed by Molecular Dynamics". *Journal of Chemical Theory and Computation*, 2016, 12, 3382-3389.

30. J. Lukasik, et al. "Influence of Salts on Virus Adsorption to Microporous Filters". *Applied and Environmental Microbiology*, 2000, 66, 2914-2920.

31. J. Bartels, et al. "Effect of divalent versus monovalent cations on the MS2 retention capacity of amino-functionalized ceramic filters". *Phys Chem Chem Phys*, 2018, 11215-11223.

32. J. N. Israelachvili, "Intermolecular and Surface Forces*"*, Elsevier Science, 2015.

33. H. Zhang, et al. "Removal of bacteriophages MS2 and phiX174 from aqueous solutions using a red soil". *Journal of Hazardous Materials*, 2010, 180, 640-647.

34. E. Arkhangelsky and V. Gitis. "Effect of transmembrane pressure on rejection of viruses by ultrafiltration membranes". *Separation and Purification Technology*, 2008, 62, 619-628.

35. C. D. Lytle and L. B. Routson. "Minimized virus binding for tests of barrier materials". *Applied and Environmental Microbiology*, 1995, 61, 643-649.

36. E. M. van Voorthuizen, et al. "Role of hydrophobic and electrostatic interactions for initial enteric virus retention by MF membranes". *Journal of Membrane Science*, 2001, 194, 69-79.

37. R. C. Bales, et al. "Bacteriophage adsorption during transport through porous media: chemical perturbations and reversibility". *Environmental Science & Technology*, 1991, 25, 2088-2095.

38. L. Treccani, et al. "Review: Functionalized ceramics for biomedical, biotechnological and environmental applications". *Acta Biomaterialia*, 2013, 9, 7115-7150.

39. S. Kroll, et al. "Highly Efficient Enzyme-Functionalized Porous Zirconia Microtubes for Bacteria Filtration". *Environmental Science & Technology*, 2012, 46, 8739-8747.

40. F. Meder, et al. "Protein adsorption on colloidal alumina particles functionalized with amino, carboxyl, sulfonate and phosphate groups". *Acta Biomaterialia*, 2012, 8, 1221-1229.

41. S. Kroll, et al. "Colored ceramic foams with tailored pore size and surface functionalization used as spawning plates for fish breeding". *Ceramics International*, 2014, 40, 15763-15773.

42. H. J. Kim, et al. "Enhancement of mechanical properties of aluminium/epoxy composites with silane functionalization of aluminium powder". *Composites Part B: Engineering*, 2012, 43, 1743-1748.

43. M. Moritz and M. Łaniecki. "SBA-15 mesoporous material modified with APTES as the carrier for 2-(3-benzoylphenyl)propionic acid". *Applied Surface Science*, 2012, 258, 7523-7529.

44. L. A. S. A. Prado, et al. "Surface modification of alumina nanoparticles with silane coupling agents". *Journal of the Brazilian Chemical Society*, 2010, 21, 2238-2245.

45. H. Weetall. "Preparation of immobilized proteins covalently coupled through silane coupling agents to inorganic supports". *Applied Biochemistry and Biotechnology*, 1993, 41, 157-188.

46. S. Fiorilli, et al. "Vapor-phase self-assembled monolayers of aminosilane on plasma-activated silicon substrates". *Journal of Colloid and Interface Science*, 2008, 321, 235-241.

47. A. Y. Ku, et al. "Evidence of Ion Transport through Surface Conduction in Alkylsilane-Functionalized Nanoporous Ceramic Membranes". *Langmuir*, 2006, 22, 8277-8280.

48. J. R. Stephens, et al. "Diffusive flux of nanoparticles through chemically modified alumina membranes". *Analyst*, 2011, 136, 3797-3802.

102

49.   S. Kroll, et al. "Development and characterisation of functionalised ceramic microtubes for bacteria filtration". *Journal of Membrane Science*, 2010, 365, 447-455.

50.   J. A. Howarter and J. P. Youngblood. "Optimization of Silica Silanization by 3-Aminopropyltriethoxysilane". *Langmuir*, 2006, 22, 11142-11147.

51.   F. Meder, et al. "The role of surface functionalization of colloidal alumina particles on their controlled interactions with viruses". *Biomaterials*, 2013, 34, 4203-4213.

52.   S. Kroll, et al. "High virus retention mediated by zirconia microtubes with tailored porosity". *Journal of the European Ceramic Society*, 2012, 32, 4111-4120.

53.   B. Michen and T. Graule. "Isoelectric points of viruses". *Journal of Applied Microbiology*, 2010, 109, 388-397.

54.   C. Dika, et al. "Impact of Internal RNA on Aggregation and Electrokinetics of Viruses: Comparison between MS2 Phage and Corresponding Virus-Like Particles". *Applied and Environmental Microbiology*, 2011, 77, 4939-4948.

55.   C. M. Schaldach, et al. "The influence of ionic strength on the interaction of viruses with charged surfaces under environmental conditions". *Journal of Colloid and Interface Science*, 2006, 294, 1-10.

56.   R. Attinti, et al. "Virus' (MS2, ϕX174, and Aichi) Attachment on Sand Measured by Atomic Force Microscopy and Their Transport through Sand Columns". *Environmental Science & Technology*, 2010, 44, 2426-2432.

57.   R. M. Chaudhry, et al. "Impact of virus surface characteristics on removal mechanisms within membrane bioreactors". *Water Research*, 2015, 84, 144-152.

58.   B. N. Fields, et al., "Fields' Virology*"*, Wolters Kluwer Health/Lippincott Williams & Wilkins, 2007.

59.   S. R. Wickramasinghe, et al. "Understanding virus filtration membrane performance". *Journal of Membrane Science*, 2010, 365, 160-169.

8. Conclusion

The aim of this work is to develop effective virus filtration systems which offer both a high water membrane flux and a high virus retention rate. To achieve this, yttria-stabilized zirconia capillary membranes with adjustable pore sizes were prepared by extrusion, as the tubular shape of the membranes is advantageous, because of the high surface-to-volume ratio. Highly homogeneous membranes with a uniform microstructure were prepared. Sintering at moderate temperatures of 1050 °C for 2 h induced the formation of sintering necks between single YSZ particles which generates relatively high open porosities of ~45 %. The effect of the initial YSZ particle size on the capillary properties was analyzed in detail. Increasing the initial YSZ particle size led to an increased pore size of the capillary membrane, where average pore sizes in the meso- and lower macroporous range (25 nm - 150 nm) are produced. Increased pore sizes led to higher permeate fluxes, but at the same time to reduced virus retention capacities of the bacteriophages MS2 and PhiX174. Capillaries with an average pore size of 55 nm made of YSZ-40nm are fulfilling the virus filter criterion of at least 4 LRV level required by the WHO for safe water in combination with relatively high flow capacities of 30 L/m²hbar. The capillaries made of YSZ-90 nm with an average pore size of ~150 nm (approximately 6 times larger than MS2 with a diameter of ~25 nm), do not fulfil the virus filter criterion by simple size exclusion effects. With high membrane fluxes of ~150 L/(m²hbar) they are promising candidates for high flux filtration applications, if an adequate adsorption capacity for viruses by membrane surface functionalization is provided. Therefore, the YSZ-90nm capillaries were functionalized with different types of aminosilanes with one, two or three amino groups per silane molecule, namely 3-aminopropyltriethoxysilane (APTES), N-(2-aminoethyl)-3-aminopropyltriethoxysilane (AE-APTES) and N-(3-trimethoxysilylpropyl)diethylenetriamine (TPDA). Especially, the functionalization with TPDA resulted in around 1 accessible NH_2-

groups/nm^2 membrane, which can be used for virus adsorption, if the pH of the feed is correctly adjusted (IEP_{Virus} < pH < $IEP_{Membrane}$). Due to the positive membrane surface charge of around 20 mV at the applied pH of 5.8, negatively charged MS2 viruses (IEP = 3.9) can adsorb to the functionalized membrane surface under throughflow conditions at 0.5 bar resulting in a LRV of 9.6 ± 0.3 when using feed solutions based on divalent salts ($MgCl_2$). In contrast, a lesser LRV of 6.4 is observed for feed solutions based on monovalent salts as NaCl. The TPDA functionalized surface is simulated by using explicit-solvent molecular dynamics (MD) at the atomistic scale in the presence of either monovalent (Na^+) or divalent (Mg^{2+}) ions. The binding free energy of the Mg^{2+} ions are preferentially adsorbed to the surface of the membrane and Na^+ ions only form a weakly bound dissolved ionic layer. The charge shielding between the membrane surface and the amino groups of the TPDA molecule by the adsorbed Mg^{2+} ions leads to an upright orientation of the TPDA molecules. In contrast to that, a more tilted orientation of TPDA molecules in the presence of Na^+ ions is found. The better accessibility of the TPDA molecules is responsible for the increased virus retention capacity when using a feed solution based on divalent Mg^{2+} ions compared to the feed solution based on only monovalent Na^+ ions. Long-term dead-end filtration experiments show the high stability of immobilized TPDA. By iterative backflushing with desorption buffer at pH 3 MS2 fouled membranes can be regenerated and therefore are reusable for repeated filtration cycles.

The presented functionalization with TPDA is promising for controlled virus retention, but fouling by organic matter like humic and fulvic acids in water which are negatively charged and therefore are able to adsorb to the positively charged membrane surface are a disadvantage. Another disadvantage are repulsion forces between positively charged viruses like the bacteriophage PhiX174 (IEP = 6.6) and the

positively charged membrane.

To avoid this disadvantages the YSZ-90nm capillaries are successfully hydrophobized with n-hexyltriethoxysilane (HTS, C6-chain) and n-octyltriethoxysilane (OTS, C8-chain), in three different molarities to achieve a hydrophobic surface functionalization. With a 0.05 M OTS functionalization a resulting surface coverage of around 1.3 molecules/nm² is achieved, which does not significantly affect the water permeate flux of ~150 L/(m²hbar). The hydrophobic membrane and the hydrophobic regions of the viral capsid can associate to each other due to the high free energy of the interfacial solute layer of polar water molecules. At 0.5 bar, an almost complete virus removal is obtained with LRVs of 8.8 ± 0.5 for the negatively charged MS2 and 8.9 ± 0.8 for the positively charged PhiX174. The higher applicable pressures of up to 2.5 bar with throughput rates of nearly 400 L/(m²h) for ceramic compared to polymeric membranes resulted in higher flux values and a higher filter performance, potentially compensating their higher production costs. The hydrophobic ceramic capillary membranes open up promising perspectives for filtration applications of diverse viruses and related biological entities.

9. Outlook

The overall goal of this work was the development of an effective virus filtration system which show both a high membrane flux in combination with a high virus removal rate. In the first step the virus removal was based on the size exclusion effect. The further development steps of the membranes were based on functionalization to increase the electrostatic and hydrophobic interactions between the virus surface and the membrane surface.

The most successful membrane type which was generated in this work were the capillaries functionalized with 0.05 M n-octyltriethoxysilane (OTS, C8-chain), which show a water permeate flux of ~150 L/(m²hbar) and an almost complete virus removal at 0.5 bar for the viruses MS2 and PhiX174. In the presented study, the virus removal tests were just a first proof of principle to show that viruses adsorb to hydrophobic functionalized membranes and further investigations are necessary for specific applications. For the application of the membranes in drinking water processing, experiments with further constituents at more realistic concentrations are necessary. Next to different (pathogenic) virus types, bacteria, proteins and organic matter (e.g. humic and fulvic acid) could be used. In biopharmacy, virus filtration is mainly used for virus clearance of plasma products and monoclonal antibodies and purification of viral vectors and vaccines. To test the suitability of the membranes for this kind of approach further experiments with realistic biopharmaceutical products could be performed.

Additional questions arise due to the virus-material interactions which are complex and difficult to predict. Therefore, molecular dynamics simulations (MD) could be additionally performed to understand the hydrophobic and electrostatic interactions between virus and capillary surface better.

Membrane fouling may the main obstacle for wider implementations of the capillary membranes. Therefore, the fouling behavior of the 0.5 M OTS could be investigated and regeneration experiments could be performed for the re-usability of the capillary membranes. After the successful completion of the regeneration experiments, the long-term performance of the capillaries with repeated regenerations could be performed for the fundamental understanding of the capillary reusability.

A. Appendix

A.1 Additional Information for Chapter 4: Production of Ceramic Membranes with Different Pore Size for Virus Retention
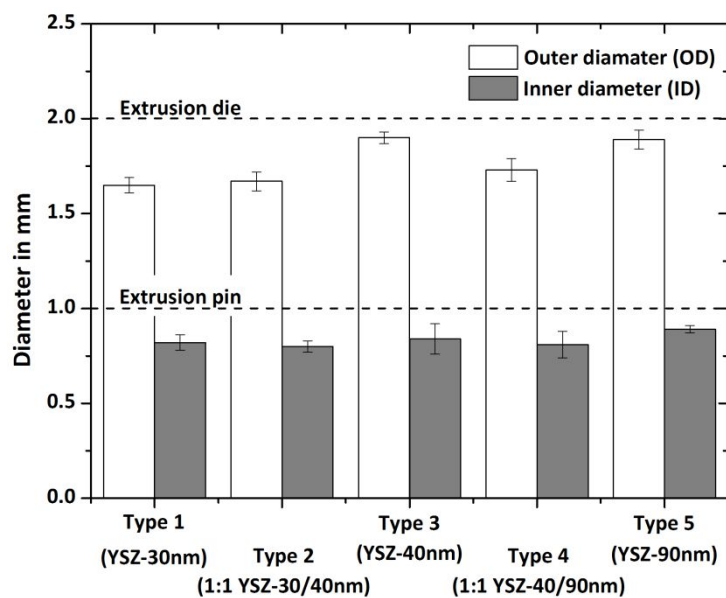

Figure S1.   Capillary outer diameters (OD) and inner diameters (ID) after sintering at 1050 °C for 2 h of YSZ membranes based on different initial YSZ powders.

A.2 Additional Information for Chapter 5: Production of Ceramic Membranes with Different Pore Size for Virus Retention
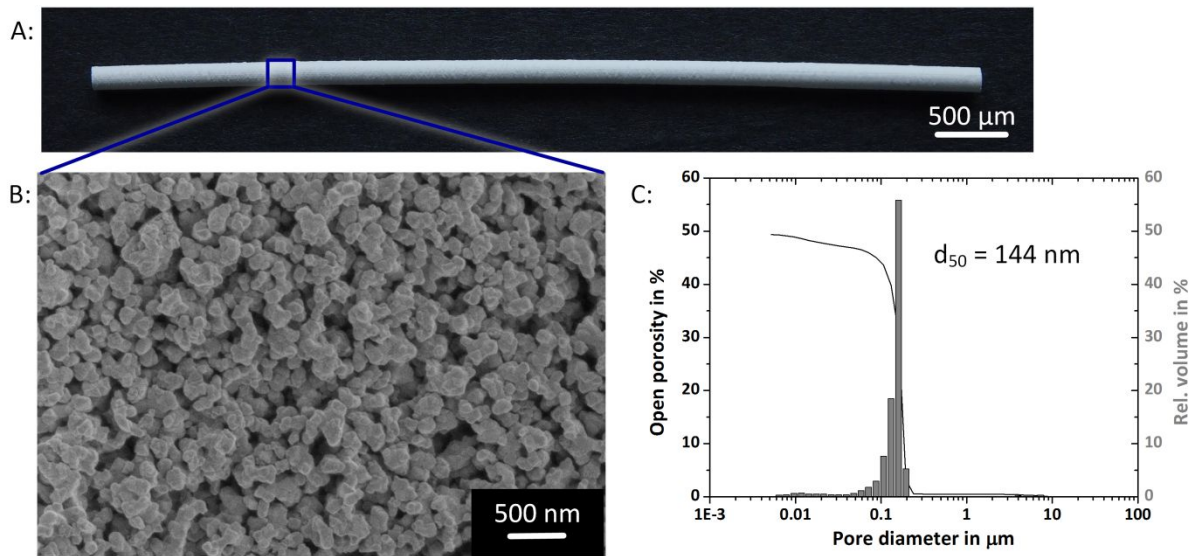

Figure S2. Non-functionalized YSZ capillary membrane. A: Photograph of a sintered (1050 °C for 2 h) capillary membrane showing a length of 6 cm, B: SEM micrograph of the microstructure (outer membrane surface), C: Pore size distribution, average pore size (d_{50}) and open porosity obtained by Hg-porosimetry.
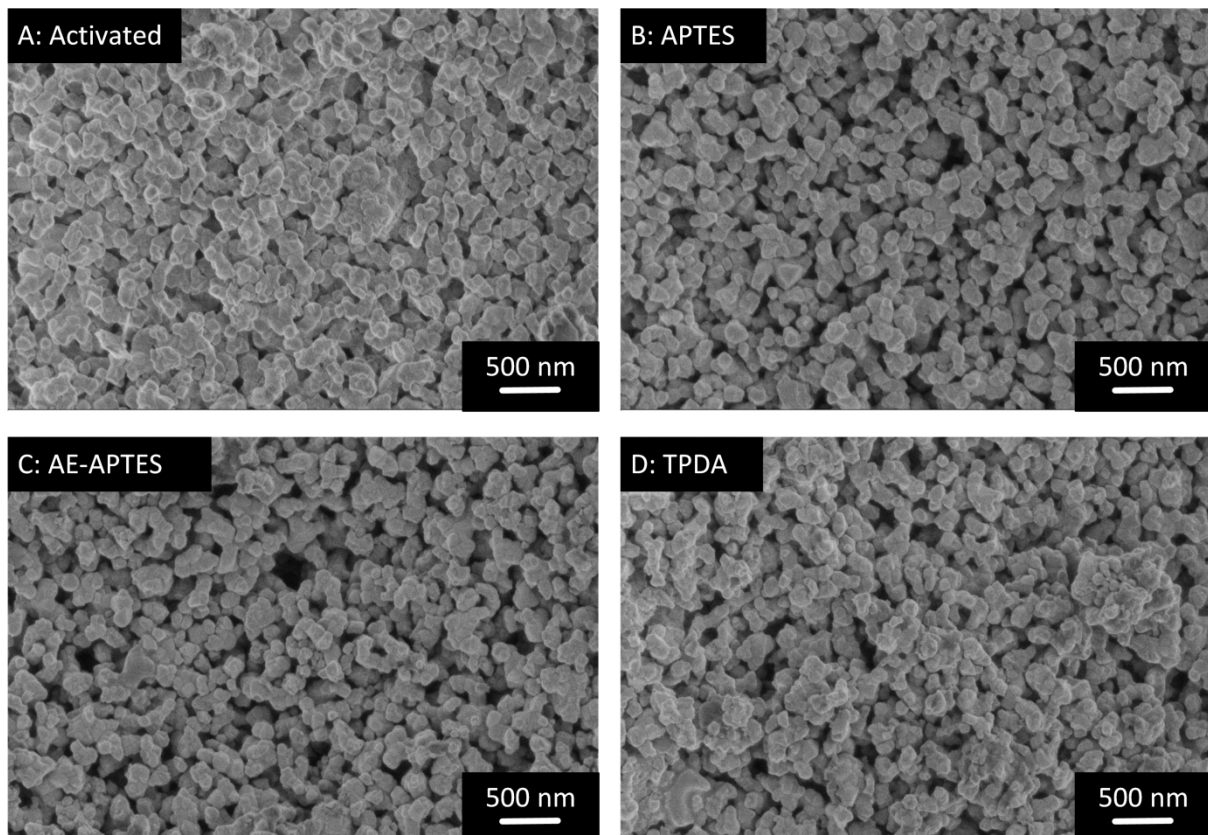

Figure S3. SEM micrographs of the outer membrane surface of the activated (A) and amino-functionalized capillaries (B = APTES, C = AE-APTES, D = TPDA).
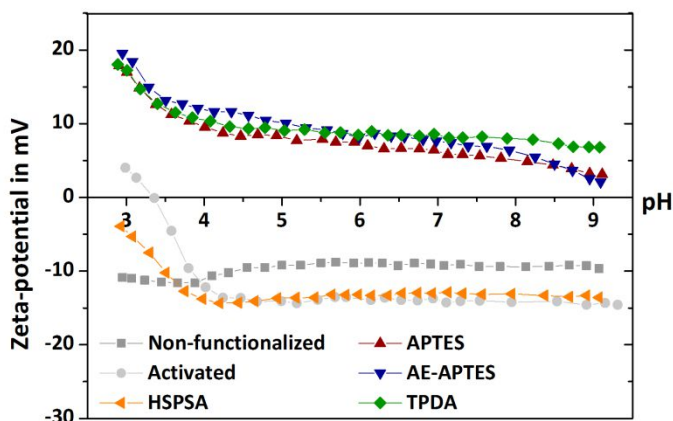
Figure S4. Zeta-potential of non-functionalized, activated, HSPSA-functionalized and aminosilanized YSZ capillaries measured in overflow mode..
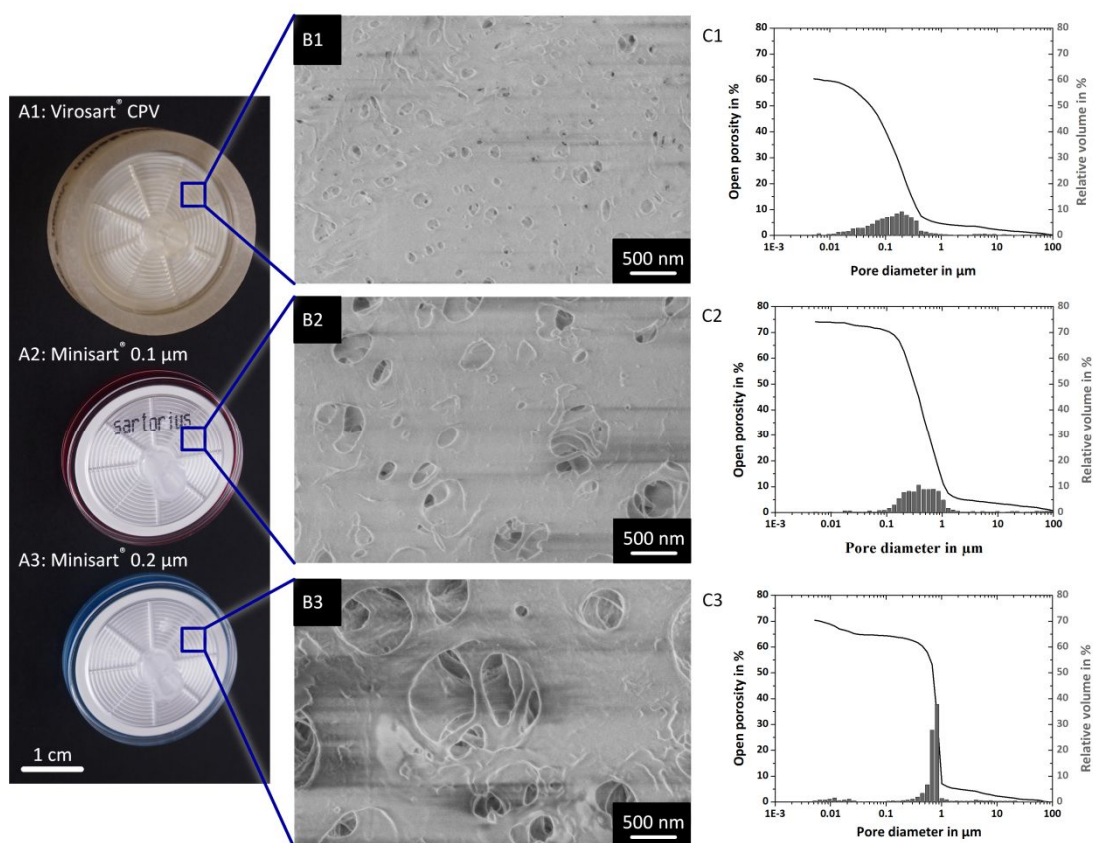

Figure S5. A: Photographs of commercial available polymeric filter devices obtained from Sartorius, Germany (Virosart[®] CPV, Minisart[®] 0.1 µm and Minisart[®] 0.2 µm), B: SEM micrographs of the membrane surface, C: Pore size distribution and open porosity of the polymeric membranes determined by Hg-porosimetry

111

Curriculum Vitae

Personal Information

Name	Julia Bartels, née Werner
Date/Place of birth	April, 8th 1987, Bremen, Germany

Education

09/2010 - 10/2012	Master of Science, Medical Engineering, University of Applied Sciences Bremerhaven, Germany
09/2006 - 09/2010	Diploma Engineer (FH) , Medical Engineering, University of Applied Sciences Bremerhaven, Germany
07/2006	Abitur (university-entracnce dipoma), KGS Leeste, Germany

Research Experience

02/2013 - 10/2018	Ph.D. student, University of Bremen, Department of Production Engineering, Advanced Ceramics Group, Germany Head: Prof. Dr.-Ing. Kurosch Rezwan, Bremen, Germany
10/2013 - 09/2016	Member of the research training group "Micro-, meso- and macroporous nonmetallic Materials: Fundamentals and Applications (MIMENIMA)", University of Bremen, Germany
02/2012 - 10/2012	Master thesis: "Herstellung und Charakterisierung von Alginat-Kügelchen als Wirkstoffträger in Hydroxylapatit/Protein Knochenersatzmaterialien", University of Bremen, Department of Production Engineering, Advanced Ceramics Group, Germany
03/2010 - 02/2009	Diploma thesis: "Untersuchungen generativ hergestellter, offenporöser Strukturen am Beispiel einer Hüft-Endoprothese", Fraunhofer IFAM, Bremen, Germany
09/2008 - 02/2009	Student research assistant, Klinikum Bremen Mitte, Medical Engineering, Germany

List of Publications (peer-reviewed)

J. Bartels, A. Batista, S. Kroll, M. Maas, K. Rezwan, "Hydrophobic ceramic capillary membranes for versatile virus filtration", Journal of Membrane Science, 2019, 570-571, 85-92, DOI: 10.1016/j.memsci.2018.10.022

M. Hoog Antink, L. Röpke, **J. Bartels**, C. Soltmann, A. Kunzmann, K. Rezwan, S. Kroll, "Porous ceramics with tailored pore size and morphology as substrates for coral larval settlement", Ceramics International, 2018, 44, 16561-16571, DOI: 10.1016/j.ceramint.2018.06.078

J. Kiefer, **J. Bartels**, S. Kroll, K. Rezwan, "Vibrational Spectroscopy as a Promising Toolbox for Analyzing Functionalized Ceramic Membranes", Applied Spectroscopy, 2018, 72, 947-955, DOI: 10.1177/0003702818769479

J. Bartels, N. Hildebrand, M. Nawrocki, S. Kroll, M. Maas, L. Colombi Ciacchi, K. Rezwan, "Effect of divalent versus monovalent cations on the MS2 retention capacity of amino-functionalized ceramic filters", Physical Chemistry Chemical Physics, 2018, 20, 11215-11223, DOI: 10.1039/c8cp01607k

W. Wesseling, M. Lohmeyer, S. Wittka, **J. Bartels**, S. Kroll, C. Soltmann, P. Kegler, A. Kunzmann, S. Neumann, B. Ramsch, B. Sellner, F. Meinhardt, "Adverse Effects of Immobilised Pseudoalteromonas on the Fish Pathogenic Vibrio anguillarum: An In Vitro Study", Journal of Marine Biology, 2016, Volume 2016, 11 pages, DOI: 10.1155/2016/3683809

J. Bartels, M. Souza, A. Schaper, P. Árki, S. Kroll, K. Rezwan, "Amino-functionalized Ceramic Capillary Membranes for Controlled Virus Retention", Environmental Science and Technology, 2016, 50, 1973-1981,DOI: 10.1021/acs.est.5b05124

B. Besser, T. Veltzke, J. A. H. Dreyer, **J. Bartels**, M. Baune, S. Kroll, J. Thöming, K. Rezwan, "A comparative experimental study on the deviation of the ideal selectivity in HDTMS-functionalized and untreated ceramic structures with pores in the upper mesoporous range", Microporous and Mesoporous Materials, 2015, 217, 253-261, DOI: 10.1016/j.micromeso.2015.06.042

J. Werner, B. Besser, C. Brandes, S. Kroll, K. Rezwan, "Production of ceramic membranes with different pore size for virus retention", Journal of Water Process Engineering, 2014, 4, 201-211, DOI: 10.1016/j.jwpe.2014.10.007

Author Contributions for the Publications Presented in this Work

Publication presented in chapter 4:

J. Werner, B. Besser, C. Brandes, S. Kroll, K. Rezwan, "Production of ceramic membranes with different pore size for virus retention", Journal of Water Process Engineering, 2014, 4, 201-211, DOI: 10.1016/j.jwpe.2014.10.007

Author	Contributions
Julia Werner	Concept and planning of work, fabrication of samples, preparation of samples, characterization of samples, data analysis and interpretation, manuscript preparation (design, editing, writing)
Benjamin Besser	Preparation of samples
Christoph Brandes	Data analysis
Stephen Kroll	Gave conceptual advice, discussed data, edited manuscript
Kurosch Rezwan	Gave conceptual advice, discussed data, edited manuscript

Publication presented in chapter 5:

J. Bartels, M. Souza, A. Schaper, P. Árki, S. Kroll, K. Rezwan, "Amino-functionalized Ceramic Capillary Membranes for Controlled Virus Retention", Environmental Science and Technology, 2016, 50, 1973-1981,DOI: 10.1021/acs.est.5b05124

Author	Contributions
Julia Bartels	Concept and planning of work, fabrication of samples, preparation of samples, characterization of samples, data analysis and interpretation, manuscript preparation (design, editing, writing)
Marina Souza	Preparation and characterization of samples
Amelie Schaper	Preparation and characterization of samples
Pál Árki	Streaming potential measurements
Stephen Kroll	Gave conceptual advice, discussed data, edited manuscript
Kurosch Rezwan	Gave conceptual advice, discussed data, edited manuscript

Publication presented in chapter 6:

J. Bartels, N. Hildebrand, M. Nawrocki, S. Kroll, M. Maas, L. Colombi Ciacchi, K. Rezwan, "Effect of divalent versus monovalent cations on the MS2 retention capacity of amino-functionalized ceramic filters", Physical Chemistry Chemical Physics, 2018, 20, 11215-11223, DOI: 10.1039/c8cp01607k

Author	Contributions
Julia Bartels	Concept and planning of work, fabrication of samples, preparation of samples, characterization of samples, data analysis and interpretation, manuscript preparation (design, editing, writing)
Nils Hildebrand	Molecular dynamics simulation and manuscript writing of regarding parts
Marcin Nawrocki	Preparation and characterization of samples
Stephen Kroll	Gave conceptual advice, discussed data, edited manuscript
Michael Maas	Gave conceptual advice, discussed data, co-wrote manuscript
Lucio Colombi Ciacchi	Gave conceptual advice, discussed data, edited manuscript
Kurosch Rezwan	Gave conceptual advice, discussed data, edited manuscript

Publication presented in chapter 7:

J. Bartels, A. Batista, S. Kroll, M. Maas, K. Rezwan, "Hydrophobic ceramic capillary membranes for versatile virus filtration", Journal of Membrane Science, 2019, 570-571, 85-92, DOI: 10.1016/j.memsci.2018.10.022

Author	Contributions
Julia Bartels	Concept and planning of work, fabrication of samples, preparation of samples, characterization of samples, data analysis and interpretation, manuscript preparation (design, editing, writing)
Artur Guedert Batista	Preparation and characterization of samples
Stephen Kroll	Gave conceptual advice, discussed data, edited manuscript
Michael Maas	Gave conceptual advice, discussed data, co-wrote manuscript
Kurosch Rezwan	Gave conceptual advice, discussed data, edited manuscript

List of Oral and Poster Presentations

J. Bartels, B. Besser, C. Brandes, S. Kroll and K. Rezwan, "Ceramic Capillary Membranes with Adjustable Pore Size for Controlled Virus Retention", Euromembrane 2015, Aachen, 07.09.2015 - 10.09.2015, Poster Presentation

J. Werner, B. Besser, S. Kroll and K. Rezwan, "Ceramic Capillary Membranes with Adjustable Pore Size for Controlled Virus Retention", CIMTEC 2014 Montecatini, 08.06.2014 - 13.06.2014, Oral Presentation

120

List of Student Projects

This work could not have been accomplished without the support of several motivated, hard-working students, which are gratefully acknowledged. In this dissertation the results from the supervision of the following students' works are included:

Batista, Artur	"Hydrophobic Functionalized Capillaries for Virus Filtration", 2018
Knape, Amelie	"Hydrophobe Keramikkapillaren für den Einsatz in der Virenfiltration", 2015
Masterprojekt Dunker, Tim Klebert, Erik Kretschmer, Martin Schmidt, Simon	"Poröse Keramiken für Umwelt- und Biotechnologische Anwendungen - Funktionalisierte Keramische Membranen für die Virenfiltration", 2016
Schaper, Amelie	"Amino-silanisierte Keramikmembranen für die Virenfiltration", 2015
Souza, Marina	"Amino-silanized Ceramic Membranes for Virus Filtration", 2015
Zilli, Marina	"Functionalized Ceramic Capillary Membranes for Virus Filtration", 2015